Sede Amministrativa: Università degli Studi di Padova

Dipartimento di Scienze Biomediche Sperimentali

SCUOLA DI DOTTORATO DI RICERCA IN BIOSCIENZE

INDIRIZZO NEUROBIOLOGIA

CICLO XXII

TITOLO TESI

Role of Autophagy in the control of muscle mass

Direttore della Scuola : Ch.mo Prof. Tullio Pozzan
Coordinatore d'indirizzo: Ch.ssa Prof.ssa Daniela Pietrobon
Supervisore :Ch.mo Prof. Stefano Schiaffino

Dottoranda : Eva Masiero

01 Febbraio 2010

INDEX

Supplemental data

RIASSUNTO

Nel muscolo scheletrico, la degradazione proteica è principalmente mediata da due sistemi altamente conservati: il sistema ubiquitina-proteasoma e il sistema autofagico-lisosomiale.

Nel sistema ubiquitina-proteasoma, le proteine destinate alla degradazione vengono poli-ubiquitinate e successivamente veicolate e degradate nel proteasoma. Tale sistema è costitutivamente attivo nel normale muscolo scheletrico ed è responsabile per il riciclo di proteine muscolari solubili e proteine miofibrillari (Lecker *et al.*, 2006; Mammucari *et al.*, 2007).

Nel sistema autofagico-lisosomiale, porzioni citoplasmatiche e organelli vengono sequestrati all'interno di vescicole (autofagosomi), i quali successivamente si fondono con i lisosomi (Lum *et al.*, 2005). Anche tale sistema è costitutivamente attivo nel muscolo scheletrico.

Il sistema ubiquitina-proteosoma è costitutivamente attivo nel muscolo, però la sua attività aumenta in maniera significativa durante l'atrofia muscolare, dovuto all'attivazione di due ubiquitine-ligasi: Atrogin-1/Mafbx e Murf1 (Gomes *et al.*, 2001). L'attivazione di questi due geni è regolata dal fattore di trascrizione FoxO3. Tale fattore è normalmente fosforilato e inattivo quando la via di segnale AKT/PKB è attiva; di contro quando tale via è repressa (ad esempio durante l'atrofia muscolare) il fattore di trascrizione può traslocare nel nucleo dove può attivare la trascrizione dei suoi geni target (Sandri *et al.*, 2004; Stitt *et al.*, 2004).

Durante l'atrofia muscolare indotta da diverse condizioni debilitanti (ad esempio: digiuno e diabete), vi è l'attivazione di diversi geni, comunemente chiamati "*Atrogenes*" e i più indotti sono le due ubiquitine-ligasi Atrogin-1 e Murf-1. Tra questi "*Atrogenes*" fanno parte anche geni correlati all'autofagia. Questi geni sono: *LC3*, *GABARAP* e *BNIP3*.

Durante la prima parte del mio dottorato di ricerca, ci siamo concentrati sulla regolazione trascrizionale dei geni dell'autofagia. La nostra ipotesi era che FoxO3 potesse regolare sia il sistema ubiquitina-proteasoma sia il sistama autofagico-lisosomiale a livello del muscolo scheletrico.

Per caratterizzare i meccanismi che regolano il sistema autofagico durante l'atrofia muscolare *in vivo*, abbiamo analizzato se la via di segnale Akt/mTOR fosse coinvolta nella regolazione di alcuni geni autofagici. Durante l'atrofia muscolare indotta dal digiuno e dalla denervazione, abbiamo osservato che tali geni sono indotti (Mammucari *et al*., 2007). Comunque l'induzione di questi geni sono inibiti quando la via di segnale Akt è attiva e inoltre l'attivazione acuta di tale sistema, mediante l'utilizzo dei topi transgenici per Akt, inibisce il sistema autofagico durante l'atrofia muscolare. Inoltre, abbiamo osservato che la via di segnale mTOR non sembra svolgere un ruolo significativo nella attivazione della via autofagica-lisosomiale durante l'atrofia muscolare. Infatti la regolazione di geni autofagici e la formazione delle vescicole autofagiche non erano indotte sia in seguito al trattamento degli animali con il farmaco rapamicina (inibitore di mTOR), sia abbattendo mTOR. Questi risultati sono in accordo con studi precedenti (Kochl *et al*., 2006; Mordier *et al*., 2000; Sarkar *et al*., 2007; Yamamoto *et al*., 2006).

Per capire il ruolo di FoxO3 nella regolazione del sistema autofagico-lisosomiale, ci siamo avvalsi di diverse metodiche sperimentali che consistevano nella *gain/loss function*. Tali esperimenti ci hanno permesso di identificare due nuovi geni bersaglio per Foxo3, i quali sono coinvolti nella regolazione dell'autofagia. Questi geni sono *LC3* e *Bnip3*. L'analisi dei promotori di LC3 e Bnip3 ha evidenziato alcuni potenziali siti per l'interazione con il fattore di trascrizione FoxO3. Mediante l'utilizzo della metodica ChIP (Chromatin–ImmunoPrecipitation) abbiamo dimostrato che FoxO3, durante condizioni di atrofia, si lega in siti specifici dei promotori. Per validare queste osservazioni abbiamo condotto degli studi funzionali e quindi le regioni di interazione FoxO3 sono state clonate a monte del gene della luciferasi. Questi studi funzionali hanno confermato che FoxO3 è in grado di indurre l'espressione dei geni *LC3* e *BNIP3*. Ulteriori esperimenti di *loss-function* hanno inoltre documentato che l'induzione di BNIP3 è necessaria per l'attivazione dell' autofagia nel muscolo scheletrico adulto.

Infine ci siamo chiesti se l'induzione del sistema autofagico fosse un evento secondario o no rispetto all'attivazione del sistema ubiquitina-proteasoma. L'inibizione del sistema ubiquitina-proteasoma, mediante approccio

farmacologico o genetico, non ha influenzato l'autofagia, suggerendo che le due vie di degradazione proteica siano controllate da FoxO3 in modo indipendente (Mammucari *et al.*, 2007). Questo ha dimostrato che il fattore di trascrizione FoxO3 è in grado di regolare due diversi sistemi proteolitici nel muscolo scheletrico.

Nella seconda parte del mio dottorato ci siamo concentrati sulla comprensione del ruolo del sistema autofagico basale nell'omeostasi del muscolo scheletrico.

E' noto che una eccessiva attivazione dell'autofagia induce una esacerbata atrofia muscolare, dovuta ad una sproporzionata eliminazione di porzioni citoplasmatiche, proteine ed organelli (Dobrowolny *et al.*, 2008; Mammucari *et al.*, 2007; Wang *et al.*, 2005; Zhao *et al.*, 2007). Di contro, l'inibizione del sistema, dovuto a difetti genetici degli enzimi lisosomiali o a farmaci che inibiscono la funzione lisosomiale, come la clorochina (Shintani e Klionsky, 2004), causa diverse miopatie come le malattie di Pompe e di Danon. Si pensa che l'inibizione del sistema autofagico giochi un ruolo in molte miopatie caratterizzate da inclusioni, o che presentano mitocondri anormali (Levine e Kroemer, 2008; Temiz *et al.*, 2009). In ogni caso il ruolo specifico del sistema autofagico nel muscolo scheletrico non è stato determinato.

Per comprendere il ruolo esatto del sistema autofagico nella fisiologia del muscolo scheletrico, abbiamo generato dei topi transgenici-condizionali, in cui è stato deleto il gene *Atg7* specificatamente a livello del muscolo scheletrico. Quindi per tale scopo, topi transgenici Atg7flox sono stati incrociati con dei topi esprimenti l'enzima Cre-recombinasi, regolata da un promotore muscolo-specifico (*Myosin Light Chain 1f*).

La proteina Atg7 è fondamentale per la formazione delle vescicole autofagiche, mediante l'attivazione di diverse proteine Atg, e per la formazione degli autofagosomi.

La delezione del gene *Atg7* induce una profonda atrofia muscolare, formazione di aggregati proteici che risultano essere positivi per la proteina p62/SQSTM1 e una diminuzione della forza muscolare che è correlata con l'età dell'animale. Inoltre mediante microscopia elettronica, abbiamo rilevato che tali animali presentano dei depositi di mitocondri anormali, distensione reticolo sarcoplasmatico, disorganizzazione del sarcomero, e la formazione di strutture membranose

aberranti e concentriche. Per di più, la perdita muscolare è più accentuata nei topi durante la denervazione ed il digiuno. Questi risultati suggeriscono che il sistema autofagico nel muscolo scheletrico è importante per evitare la perdita di massa muscolare e per mantenere l'integrità delle miofibre. Inoltre l'inibizione di Atg7 ha mostrato l'attivazione di proteine chaperonine associate al reticolo endoplasmatico, in particolare la proteina BIP, così come la fosforilazione di eIF2α, fattore d'inizio della traduzione, suggerendo una continua attivazione delle vie implicate nella regolazione delle proteine mal formate. La presenza di proteine alterate nei topi transgenici induce stress del reticolo endoplasmatico, che può generare ROS, e la soppressione della sintesi proteica, che possono contribuire ad atrofia muscolare (Masiero *et al.*, 2009).

Per confermare i dati ottenuti nei topi transgenici-condizionali, abbiamo generato un altro tipo di topo transgenico tamoxifen-inducibile per Atg7 muscolo specifico. In questo caso i topi Atg7flox sono stati incrociati con dei topi esprimenti la Cre-recombinasi fusa con un recettore degli estrogeni modificato, sotto il controllo di un promotore muscolo-specifico (*Human Skletal Muscle*). In condizioni normali il gene *Atg7* sarà espresso in tutti i tessuti perché, in assenza del ligando per gli estrogeni, la proteina di fusione è bloccata e inattivata a livello citoplasmatico da un complesso di *Heat Shock Protein*. Quando trattiamo gli animali con il Tamoxifen, un analogo degli estrogeni che presenta un'alta affinità per il recettore degli estrogeni modificato, il legame del composto determina il distacco del complesso delle *Heat Shock Protein* e la traslocazione della proteina di fusione nel nucleo, dove può esplicare la sua attività enzimatica. In questo modo, in seguito al trattamento con il Tamoxifen, si ottiene la delezione del gene *Atg7* solo a livello muscolare. Anche in questo tipo di transgenico si sono avuti gli stessi risultati ottenuti con i topi transgenici-condizionali per Atg7. Infatti si sono osservati aggregati proteici positivi per la proteina p62/SQSTM1, atrofia muscolare e riduzione della forza muscolare. Inoltre l'analisi morfologica, ha rilevato degli accumuli di mitocondri alterati nelle fibre atrofiche, ed un più abbondante numero di fibre con nuclei centrali dopo la delezione del gene *Atg7* in maniera acuta rispetto agli animali non-inducibili (Masiero *et al.*, 2009).

SUMMARY

Protein degradation in skeletal muscle cells is essentially mediated by the activity of two highly conserved pathways, the ubiquitin-proteasome and the autophagy-lysosome pathway.

In the ubiquitin-proteasome pathway, target proteins are conjugated to multiple ubiquitin moieties and ubiquitin-tagged proteins are degraded within the proteasome complex (Lecker *et al*., 2006; Mammucari *et al*., 2007). The ubiquitin-proteasome system is constitutively active in normal skeletal muscle and is responsible for the turnover of most soluble and myofibrillar muscle proteins.

In the autophagy-lysosome system, portions of cytoplasm and cell organelles are sequestered into vacuoles, called autophagosomes, that are delivered to the lysosomes for the degradation of their content by acidic hydrolases (Lum *et al*., 2005). Also the autophagy system is constitutively active in skeletal muscle.

The ubiquitin-proteasome system is constitutively active in muscle but its activity increases significantly during muscle atrophy due to activation of two ubiquitin-ligases: Atrogin-1/Mafbx and Murf1 (Gomes *et al*., 2001). The activation of these two genes is regulated by the transcription factor FoxO3. This factor is normally phosphorylated and inactivated by AKT / PKB. Conversely when this pathway is suppressed (eg during muscle atrophy), FoxO3 translocates into the nucleus where it can transactivate its target genes (Sandri *et al*., 2004; Stitt *et al*., 2004).

Alteration of autophagy has been observed in various myopathies caused by genetic defects of lysosomal components, e.g. Pompe's and Danon's disease, or by drugs that inhibit lysosomal function, such as chloroquine (Shintani and Klionsky, 2004).

During muscle atrophy induced by various debilitating conditions (such as fasting and diabetes), there is activation of several genes, named "*Atrophy-Related-Genes*" or "*Atrogenes*". Among the atrogenes, two most-induced are two ubiquitin-ligases, Atrogin-1 and Murf1. Several autophagy genes belong to the "Atrogenes". These genes are: *LC3*, *GABARAP* and *BNIP3*.

During the first part of my PhD we focused on the transcriptional regulation of the autophagy genes. Our hypothesis was that FoxO3 can coordinate the ubiquitin-proteasome and the autophagy-lysosome system.

To characterize the mechanisms that control the autophagic/lysosomal pathway during muscle atrophy *in vivo*, we first determined whether the Akt/mTOR pathway is involved in the regulation of some of autophagy-related genes.

During starvation and denervation, two different models of muscle wasting, the *Autophagy-Related-Genes* are induced. Moreover these autophagy-related genes are suppressed by Akt, and acute activation of Akt in transgenic mice inhibits autophagy in atrophying muscle. Importantly mTOR pathway did not appear to play a significant role in the activation of the autophagic/lysosomal pathway during muscle atrophy. Indeed the regulation of autophagy-related genes and the formation of autophagic vesicles are not induce either by rapamycin, an inhibitor of mTOR, or by knocking down of mTOR. These findings are in agreement with previous studies (Kochl *et al*., 2006; Mordier *et al*., 2000; Sarkar *et al*., 2007; Yamamoto *et al*., 2006).

We used gain- and loss-of-function experiments to determine the role of FoxO3 in the autophagic/lysosomal pathway. These experiments found two novel FoxO3 targets that regulate autophagy. LC3 and Bnip3 promoters contain several potential FoxO binding sites and ChIP (Chromatin-ImmunoPrecipitation) experiments on atrophying muscles showed that FoxO3 binds chromatin of their promoters in specific sites. The regions of FoxO3 interaction were cloned upstream luciferase gene and functional studies confirmed that FoxO3 transactivates LC3 and BNIP3 genes. Moreover, loss-function experiments showed that BNIP3 upregulation is necessary for autophagy induction in adult muscle.

Finally, we asked whether the induction of autophagy is secondary to the activation of the ubiquitin-proteasome system. Inhibition of ubiquitin-proteasome system by pharmacological or genetic approach, did not affect autophagy, suggesting that the two degradation pathways are independently controlled by FoxO3 (Mammucari *et al*., 2007). Thus, FoxO3 coordinates the two major proteolytic systems of the cell.

In the second part of my PhD I focused my studies on the role of basal autophagy in skeletal muscle homeostasis.

It is known that excessive activation of autophagy aggravates muscle wasting by removing portion of cytoplasm, proteins, and organelles (Dobrowolny *et al.*, 2008; Mammucari *et al.*, 2007; Wang *et al.*, 2005; Zhao *et al.*, 2007). Conversely, inhibition of lysosome-dependent degradation causes myopathies like Pompe and Danon diseases, and autophagy inhibition is thought to play a role in many myopathies with inclusions or with abnormal mitochondria (Levine and Kroemer, 2008; Temiz *et al.*, 2009).

To understand the exact role of autophagy in physiology of skeletal muscle we have generated conditional knockout for *Atg7* gene to block autophagy specifically in skeletal muscle.

The Atg7 protein is crucial for the formation of the autophagy vesicles by the activations of different Atg proteins and for the formation of the autophagosome.

To understand the role of the autophagy in adult skeletal muscle, Atg7 floxed mice were crossed with mice that express the Cre-recombinase under the muscle-specific promoter Myosin light chain 1f.

Muscle-specific deletion of Atg7, resulted in profound muscle atrophy, accumulation of protein aggregates that are positive for p62/SQSTM1 and age-dependent decrease in force. Moreover Atg7 null muscles showed accumulation of abnormal mitochondria, distension of sarcoplasmic reticulum, sarcomere disorganization, and formation of aberrant concentric membranous structures. Moreover, muscle loss is more exacerbated in autophagy knockout mice during denervation and fasting. These results suggest that the autophagy flux is important to preserve muscle mass and to maintain myofiber integrity. Moreover Atg7 null muscles showed activation of endoplasmic reticulum chaperones, such as BiP, as well as the phosphorylation of eIF2α, suggesting an ongoing unfolded protein response. The failure of protein-folding quality control in Atg7 null mice induces endoplasmic reticulum stress which can generate ROS, and suppression of protein synthesis which can contribute to muscle atrophy (Masiero *et al.*, 2009).

To further confirm our findings in adulthood, we generated a tamoxifen-inducible muscle-specific Atg7 knockout mice. In this case, the floxed Atg7 mice were crossed with mice expressing the Cre-recombinase fused with a modified estrogen

receptor, under the control of a muscle-specific promoter (Human Skletal Muscle). When animals are treated with tamoxifen (an estrogen analogue that has a high affinity for the modified estrogen receptor), the Cre-recombinase is stabilized and can recombinate the loxP site.

Identical results were obtained in inducible Atg7 null muscles. These mice showed p62/SQSTM1 accumulation, muscle atrophy and decrease in force generation. Morphological analyses revealed accumulation of abnormal mitochondria in small atrophic fibers and the number of centrally nucleated fibers were more abundant after acute Atg7 deletion than in non-inducible autophagy-deficient muscles (Masiero *et al*., 2009).

Our results suggest that inhibition/alteration of autophagy can contribute to myofiber degeneration and weakness in muscle disorders characterized by accumulation of abnormal mitochondria and inclusions.

INTRODUCTION

Skeletal muscle: structure and function

Skeletal muscle is constituted by cylindrical multinucleated cells, called muscle fibers, bundled together and wrapped by connective tissue. Each muscle is surrounded by a connective tissue sheath called the epimysium. Fascia, the connective tissue outside the epimysium, surrounds and separates the muscles. Portions of the epimysium project inside the muscle to divide compartments. Each compartment contains a bundle of muscle fibers. Each bundle of muscle fiber is called a fasciculus and is surrounded by a layer of connective tissue, called perimysium. Within the fasciculus, each individual muscle fiber is surrounded by connective tissue called the endomysium (Figure 1).

Skeletal muscles have an important vascularisation to provide nutrients and oxygen and are innervated. Generally, an artery and at least one vein accompany each nerve that penetrates the epimysium of a skeletal muscle. Branches of the nerve and blood vessels follow the connective tissue components of the muscle reaching the single myofibers together with the capillaries network.
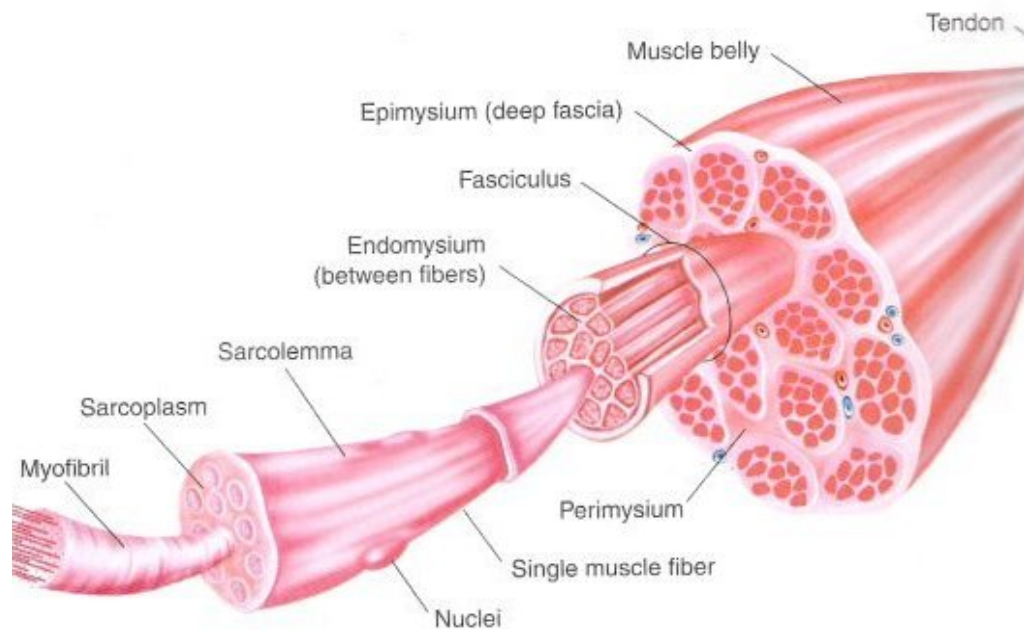
Figure 1: Schematic representation of skeletal muscle structure.

The nuclei of muscle cells are located at the periphery of the muscle cell, just under plasma membrane, the <u>sarcolemma</u>. Conversely, the presence of central-located nuclei is pathological and is consistent with a disease called centre nuclear myopathy. Mice have a peculiarity since regenerating muscles maintain the nuclei in a central position, therefore, only in mice the presence of central-nucleated myofibers reveal a precedent injury which was followed by regeneration.

Closed to muscle cell and surrounded by their own membrane located, the nuclei of satellite cell, the skeletal muscle stem cell.

The cytoplasm of muscle cell is filled by the contractile proteins organized in <u>myofibrils</u> (also called simply fibrils); they are all packed in a parallel arrangement. Each myofibril runs the entire length of the fibre In transversal section, myofibrils display a characteristic banding pattern of striated skeletal muscle. This aspect is due by the serial alignement of <u>sarcomeres</u>, which are the structural units. The sarcomere comprises two sets of filament: the thin ones, constituted by actin, and thick filaments, made by myosin. Several other important

proteins, like troponin and tropomyosin, titin, nebulin, and desmin, help to hold these units together.

The sarcomere is defined as the segment between two neighbour Z-lines. In electron micrographs the Z-line appears as a series of dark lines. Surrounding the Z-line, there is the region of the I-band (the light band). Following the I-band there is the A-band (the dark band). Within the A-band, there is a paler region called the H-band. The nomenclature of A- and I-band comes form their properties to reflect the polarized light under a polarization microscope. Finally, inside the H-band is a thin M-line (*middle* of the sarcomere).

Actin filaments are the major component of the I-band and extend into the A-band. *Myosin* filaments extend throughout the A-band and are thought to overlap in the M-band. The giant protein, *titin* (connectin), extends from the Z-line of the sarcomere, where it binds to the thin filament system, to the M-band, where it is thought to interact with the thick filaments. Several proteins important for the stability of the sarcomeric structure are found in the Z-line as well as in the M-band of the sarcomere. Actin filaments and titin molecules are cross-linked in the Z-disc via the Z-line protein alpha-actinin. The M-band myosin as well as the M-proteins bridge the thick filament system to the M-band part of titin (the elastic filaments) (Figure 2).
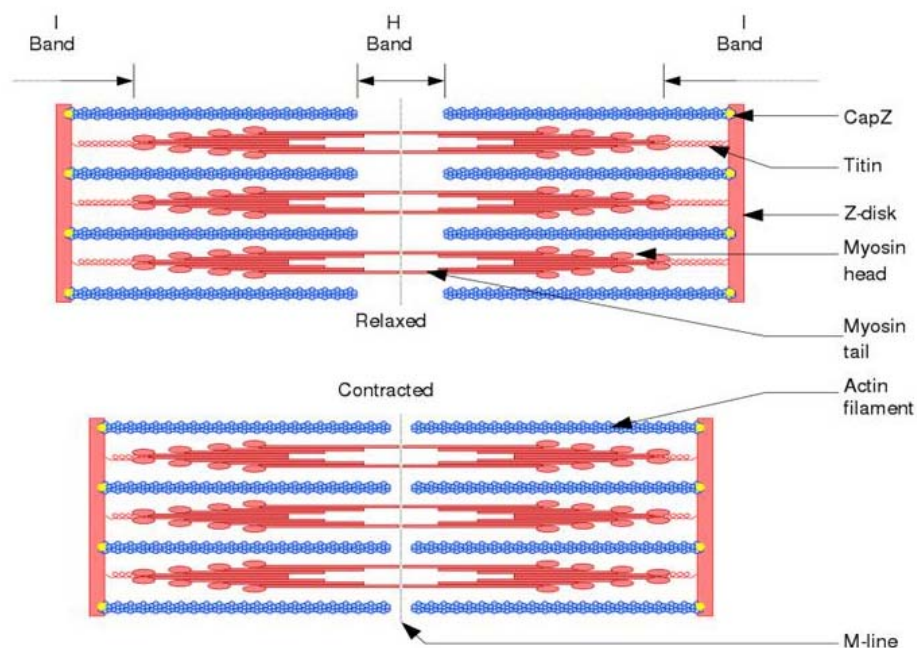

Figure 2: A scheme of muscle contraction.

The interaction between actin and myosin filaments in the A-band of the sarcomere is responsible for the muscle contraction (*sliding filament model*).

Upon muscle contraction, the A-bands do not change their length, whereas the I-bands and the H-zone shorten. This is called the *sliding filament hypothesis* which is now widely accepted. There are projections from the thick filaments, called *cross-bridges* which contain the part (head) of myosin linked to actin; able to hydrolyze ATP and convert chemical energy into mechanical energy. This process is quite efficient and 40-60% of energy is consumed for mechanical action while the remaining energy is lost as heat. These cross-bridges can be seen by electron microscopy. The cross bridges are mostly oriented transverse to the fibre axis in relaxed fibres and are angled at about 45 degrees in rigor. Contraction is a transient state, hard to capture because it is very fast, but it is assumed that these two states are representative of relaxed and contracted situations.

To allow the simultaneous contraction of all sarcomers, the sarcolemma penetrates into the cytoplasm of the muscle cell between myofibrils, forming membranous tubules called *t-tubules*. The t-tubules are electrically coupled with the terminal cisternae which continue into the sarpolasmic reticulum. Thus the sarcoplasmic reticulum, which is the enlargement of smooth Endoplasmic Reticulum and which contains the majority of calcium ions required for contraction, extends from both sides of t-tubules into the myofibrils. Anatomically the structure formed by t-tubules surrounded by two smooth ER cisternal is called the triad and it allows the transmission of membrane depolarization from the plasmalemma to the Endoplasmic Reticulum.

The contraction starts when an action potential diffuses from the motor neuron to the sarcolemma and then it travels along t-tubules until it reaches the sarcoplasmic reticulum. Here the action potential changes the permeability of the sarcoplasmic reticulum, allowing the flow of calcium ions into the cytosol between the myofibrils. The release of calcium ions induces the myosin heads to interact with the actin, allowing the muscle contraction. The contraction process is ATP-dependent. The energy is provided by mitochondria which are located closed to Z-line.

Skeletal muscles contains several fiber types which differ for structural and functional properties. Mammalian muscle fibers are divided into two distinct

classes: the type I, also called slow fibers, and type II, called fast fibers. This first classification considered only the mechanical properties. However the different fiber types show also peculiar myosin ATPase enzymes, metabolism (oxidative or glycolitic), mitochondrial content revealed by succinate dehydrogenase (SDH) staining, resistance to fatigue (Pette and Heilmann, 1979; Pette *et al.*, 1979; Schiaffino *et al.*, 2007). Altogether these biochemical and molecular properties explain the contraction properties.

Since in most cases different fiber types coexist in one muscle, the type of contraction (slow or fast) results form the percentage of the fiber types present in the muscle. In this way, the skeletal muscle can be classified either in <u>slow</u>, if it contains more type I fibers, or in <u>fast</u>, if type II fibers are more abundant. The different fiber types contain also peculiar Myosin Heavy Chain (MHC) which are coded by different genes. The fiber type I expresses the slow isoform of MHC (MHCβ or MHC1), and shows a great content of mitochondria, high levels of myoglobin, high capillary densities and high oxidative enzyme capacity. Muscles containing many type I fibers display red colour for the great vascularisation and for the high myoglobin content.

The type II, fast, myofibers are divided in three groups depending on which myosin is expressed. In fact distinct genes encode for MHC IIa, IIx (also called IId) and IIb. Type IIa myofibers are faster than type I, but they are still relatively fatigue-resistant. IIa fibers are relatively slower than IIx and IIb and have an oxidative metabolism due to the rich content of mitochondria (Schiaffino and Reggiani, 1996). Given all these characteristics, IIa fibers are also termed fast-oxidative fibers. They exhibit fast contraction, high oxidative capacity and a relative fatigue resistance. The IIx and IIb fiber types are called fast-glycolitic fibers and they show a prominent glycolitic metabolism containing few mitochondria of a small size, high myosin ATPase activity, expression of MHC IIb and MHC IIx proteins, the fastest rate of contraction and the highest level of fatigability.

The fiber type profile of different muscles is initially established, during development, independently of nerve influence. Nerve activity has a major role in maintenance and modulation of fiber type properties in adult muscle (Schiaffino *et al.*, 2007). Indeed type I fibers start to appear only after innervation and the

absence of the nerve maintains a fast program and blocks the expression of slow isoform of myosin.

Plasticity of skeletal muscle: hypertrophy versus atrophy

Skeletal muscle comprise 40-50% of total body mass, and it is the major protein storage for the body. Being the largest protein reservoir, muscle serves as a source of amino acids to be utilized for energy production by various organs during catabolic periods (Lecker *et al*., 2006a). For instance, amino acids generated from muscle protein breakdown are utilized by the liver to produce glucose and to support acute phase protein synthesis (Lecker *et al*., 2006a). Skeletal muscle is a dynamic tissue continuously adapting its size in response to a variety of external stimuli including mechanical load, nerve activity, presence of hormones/growth factors, and nutritional status (Waddell *et al*., 2008b). For instance, exercise stimulates protein synthesis that leads to increase of muscle mass and force. This process is named hypertrophy.

Conversely muscle disuse causes a rapid loss of myofibrillar proteins that results in a decrease of fiber size and in general a decrease of muscle mass and force. This condition is called atrophy.

Muscle Hypertrophy

The growth of skeletal muscle mass, like the mass of any other tissue, depends on protein turnover and cell turnover (Sartorelli and Fulco, 2004). Cellular turnover plays a major role during muscle development in embryo. Moreover satellite cell incorporation into the growing fibers takes place during post-natal muscle growth (Moss and Leblond, 1971) concomitantly with increased protein synthesis. The activation of satellite cells is important for maintaining a constant size of each nuclear domain (quantity of cytoplasm/number of nuclei within that cytoplasm). Unlike young muscle, the contribution of cellular turnover to homeostasis of adult fibers is minor and its role in hypertrophy has even been recently debated (McCarthy and Esser, 2007; Rehfeldt, 2007). In adult muscle the physiological

conditions promoting muscle growth, therefore, do so mainly by increasing protein synthesis and decreasing protein degradation. The IGF-1-AKT signaling is the major pathway which controls muscle growth. In addition to circulating IGF-1, mainly synthesized by the liver under GH control, local production by skeletal muscle of distinct IGF-1 splicing products has recently raised considerable interest. A specific IGF-1 splicing product is important for load- and stretch-induced adaptations in skeletal muscle (Goldspink, 1999) Muscle-specific over-expression in transgenic mice of an IGF-1 isoform, locally expressed in skeletal muscle, results in muscle hypertrophy and, importantly, the growth of muscle mass matches with a physiological increase of muscle strength. Furthermore, the over-expression of a constitutively active form of Akt, a downstream target of IGF-1, in adult skeletal muscle induced muscle hypertrophy. Similar results were obtained by the generation of conditional transgenic mice in which Akt is expressed in adult skeletal muscles only after tamoxifen or tetracycline treatment. Taken together with other observations, these results suggest that IGF-1-Akt1 axis is a major mediator of skeletal muscle hypertrophy. While it has been established that Akt plays a crucial role in muscle growth, the downstream targets involved in muscle hypertrophy remain to be defined.

Muscle Atrophy

Atrophy is a decrease in cell size mainly caused by loss of organelles, cytoplasm and proteins. A general loss of skeletal muscle mass occurs in many debilitating diseases including sepsis, burn injury, cancer, AIDS, diabetes, heart and renal failure.

In most types of muscle atrophy overall rates of protein synthesis are suppressed and rates of protein degradation are consistently elevated; this response accounts for the majority of rapid loss of muscular proteins. The identification of precise signaling cascade, that directs muscle wasting, is only at the beginning, although in recent years several pathways have emerged to be critical for the maintenance of muscle mass. A major contribution in understanding muscle atrophy comes from the pioneering studies on gene expression profiling performed independently by groups of Goldberg AL and Glass DJ. The idea to compare gene expression in

different models of muscle atrophy leads to the identification of a subset of genes that are commonly up- or down-regulated in atrophying muscle. Since all the diseases used for the experiments of microarray (i.e. Diabetes, Cancer cachexia, chronic renal failure, fasting and denervation) have muscle atrophy in common, the commonly up- or down-genes are believed to regulate the loss of muscle components and are called *Atrophy-Related Genes* or *Atrogenes*. Together these findings indicate that muscle atrophy is an active process controlled by specific signaling pathways and transcriptional programs. These genes encode for proteins involved in different cellular processes like energy production, transcription factors, regulators or protein synthesis and enzymes of metabolic pathways. Among the upregulated atrophy-related genes there is a subset of transcripts related to protein degradation pathways. The major proteolytic systems responsible for protein breakdown in eukaryotic cells are the ubiquitin-proteasome system and the autophagy lysosome pathways. In diverse types of muscle wasting, the ubiquitin-proteasome pathway is activated, as shown by increased sensitivity to proteasome inhibitors; increased levels of ubiquitin conjugates; enhanced rates of ubiquitin conjugation; and induction of genes for ubiquitin, several proteasomal subunits, and two critical ubiquitin ligases (E3s), atrogin-1/MAFbx and MuRF1 (Bodine *et al*., 2001a; Lecker *et al*., 2004). An increased capacity for lysosomal autophagic proteolysis has been demonstrated in various types of atrophy (Bechet *et al*., 2005). Electron microscopic studies have previously shown that autophagy is activated in denervation atrophy (Schiaffino and Hanzlikova, 1972b) and this system is stimulated in different conditions leading to muscle atrophy (Bechet *et al*., 2005).

Protein degradation system

The Ubiquitin-Proteasome System

Several evidences strongly support a major role of ubiquitin proteasome system (UPS) during muscle loss. Decrease in muscle mass is associates with: I) increase conjugation of ubiquitin to muscle proteins, II) increase of proteasomal ATP-dependent activity, III) increase protein breakdown which can be efficiently blocked by proteasome inhibitors and IV) up-regulation of mRNA for ubiquitin, some ubiquitin-conjugating enzymes (E2), few ubiquitin-protein ligases (E3) and several proteasome subunits. The rate limiting enzyme of UPS is the E3 which catalyzes the transfer of ubiquitin from the E2 to the lysine in the substrate. This reaction is highly specific and the proteins, committed to ubiquitination and to proteasomal degradation, are recognized by the E3 (Figure 3). Thus the amount and the type of proteins degraded by the proteasome is largely determined by which E3 ligases are activated in the cell (Gomes *et al*., 2001).

Among the atrogenes, the two most induced genes are two novel ubiquitin ligases E3, atrogin-1 (muscle atrophy F-box-MAFbx) and MuRF1 (muscle ring finger1). These enzymes are up regulated in different models of muscle atrophy and are responsible for the increased protein degradation through the ubiquitin proteasome system (Sacheck *et al*., 2004).

Atrogin-1, also known as MAFbx, contains an F-box domain, a characteristic motif seen in a family of E3 ubiquitin ligases belonging to SCF complex (for Skp1, Cullin, F-box) (Gomes *et al*., 2001; Jackson and Eldridge, 2002). The F-box protein interacts with the substrates, while Cul1-Roc1 components associate with the E2 Ub-conjugating enzymes. Skp1 is an adaptor that brings F-box protein to the Cul1-Roc1-E2 complex. Most substrates require the phosphorylation to interact with the F-box protein in an SCF complex (Jackson and Eldridge, 2002).
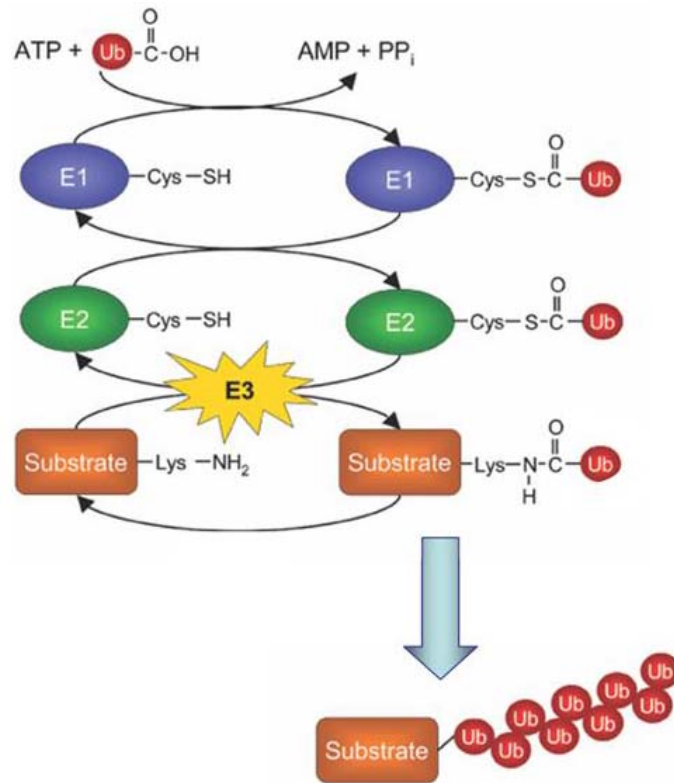
Figure 3: Ubiquitin –proteasome pathway: Ubiquitin (Ub) is covalently attached to substrate proteins via a three-step mechanism involving the sequential actions of E1 (ubiquitin-activating enzyme), E2 (ubiquitin-conjugating enzyme) and E3 (ubiquitin ligase) enzymes. The attachment of multiple ubiquitin moieties by E3 is the rate limiting step. Modified from Lori A. Passmore1 and David Barford Biochem. J 2004.

MuRF1 belongs to the RING finger E3 ligase subfamily, characterized by three RING-finger domains (Borden, *et al* 1996) which are required for ubiquitin-ligase activity (Kamura *et al*., 1999). Those domains include a B-box, whose function is still unknown, and a coiled-coil domain, which may be required for the formation of heterodimers between MuRF1 and a related protein, MuRF2 The precise substrates of atrogin-1and MuRF1 have not been identified, but their expression is increased in many diseases (Price, 2003), even before the loss of muscle mass become evident, underling their important role. The strong induction of atrogin-1 and MuRF1 at early stage of muscle wasting and their high expression suggests the role of both E3s in initiation and maintenance of accelerated proteolysis. Knockout animals lacking either MuRF1 or atrogin-1 show a reduced rate of muscle atrophy after denervation (Bodine *et al*., 2001a), confirming that these

liagases are necessary for the atrophy program. Up to now atrogin-1 and MuRF1 are actually the best markers for muscle atrophy and could be consider as master genes for muscle wasting.

Signaling Pathways Controlling Muscle Atrophic Program

Given the important role of muscle loss in prognosis of many diseases, a subsequent crucial step was the identification of the signaling pathways which regulate the expression of the *Atrophy-Related-Genes* (Sandri, 2008). The insulin/IGF-1 signaling cascade was the first example of a pathway which promotes protein synthesis and at the same time suppresses protein breakdown, indicating that the dynamic regulation of skeletal muscle mass is the result of a balance between hypertrophic and atrophic programs (Figure 4).
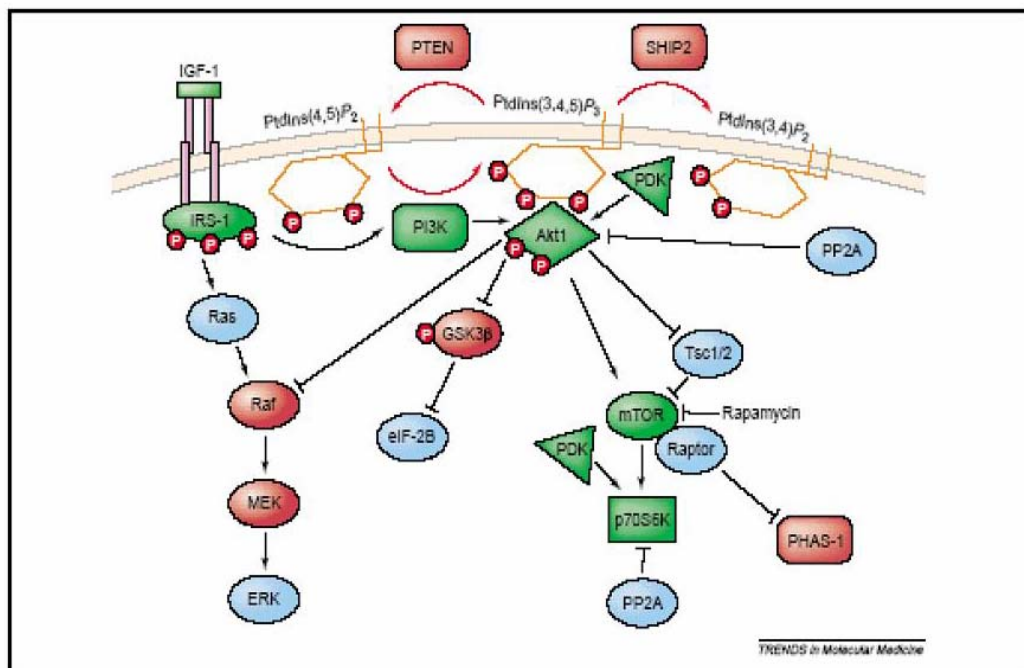
Figure 4: Insulin-like growth factor 1 (IGF-1)-mediated signalling pathways. Signalling molecules, that have been shown to have a negative effect on hypertrophy are red coloured, and the proteins, whose activation induces hypertrophy are green. Protein that have not been dissected their role are blue (Glass, 2003).

The binding of IGF-1 or insulin to their membrane receptors activates two major signalling pathways: the Ras-Raf-MEK-ERK pathway and the PI3K/AKT pathway. The Ras-Raf-MEK-ERK is involved in controlling fiber type by promoting, *in vivo*, a nerve-dependent slow phenotype. Conversely the activation of PIK3/ AKT pathway induces muscle growth. Once AKT is activated, it initiates a cascade of phosphorylation events targeting mammalian target of rapamycin (mTOR) and glycogen synthases kinase 3β (GSK3β). GSK3β is inhibited by Akt and, in turn, blocks the eukaryotic translation initiation factor 2B (eIF-2B), which is involved in protein synthesis. mTOR is part of two complexes: TORC1, which contains Raptor and is rapamycin sensitive and while TORC2, which contains Rictor. TORC1 signals to S6K1 and 4EBP1 and it controls proteins synthesis, while TORC2 phosphorylates, in a retrograde way, AKT, affecting also FoxO signalling. TORC2 complex is rapamycin insensitive and it does not affect protein synthesis (Figure 5).
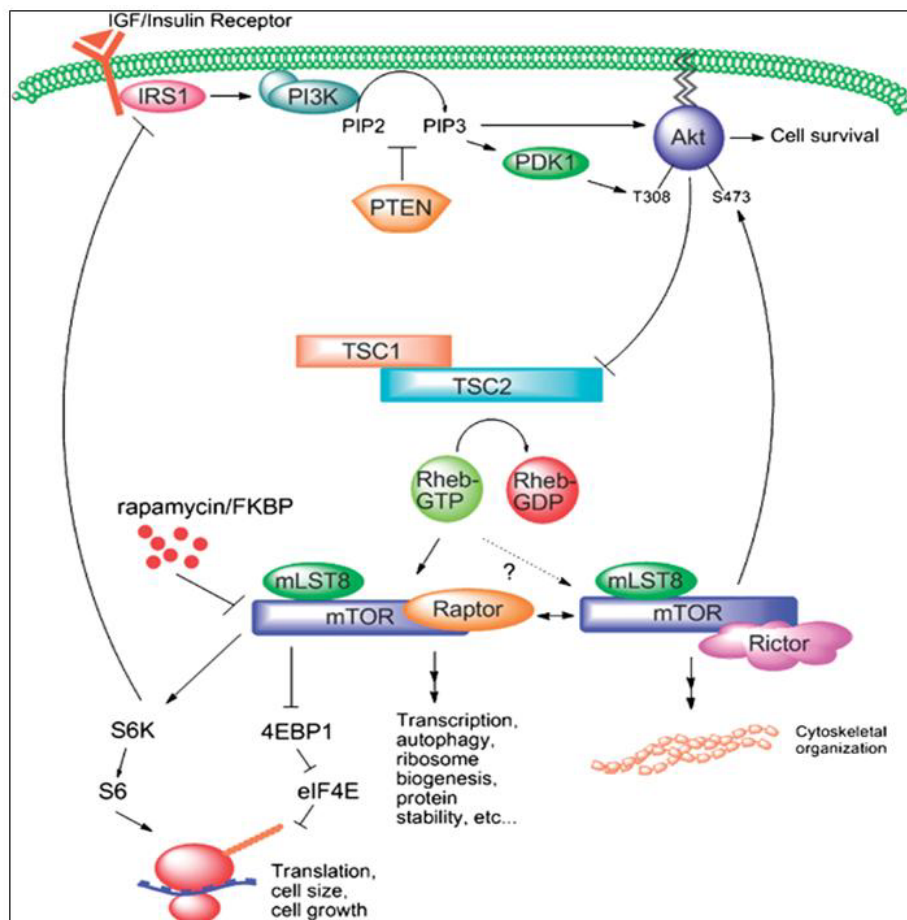
Figure 5: IGF-1 AKT m-TOR pathway.

Several finding suggest that the decrease activity of IGF-1 /PI3K /AKT signalling pathway can regulate the muscle atrophy program. In fact, the inhibition of PI3K activity and the expression of dominant negative of AKT reduces the mean size of myotubes and increases protein degradation and atrogin-1 expression. Conversely, both IGF1 transgenic mice and overexpression of constitutively active AKT in adult myofibers suppress protein degradation and muscle atrophy induced by denervation. Moreover the up regulation of MuRF1 and atrogin-1 is blocked by IGF1 treatment or AKT activation. The up-regulation of atrogin-1/MAFbx and MuRF1 is normally blocked by Akt functioning through negative regulation of the family of transcription factors FoxO The FoxO family in skeletal muscle is comprised of three isoforms: FoxO1, FoxO3 and FoxO4. Akt phosphorylates FoxOs, promoting the export of FoxOs from the nucleus to the cytoplasm. AKT blocks FoxO activity by phosphorylation of three conserved residues leading to 14-3-3 binding (Figure 6).
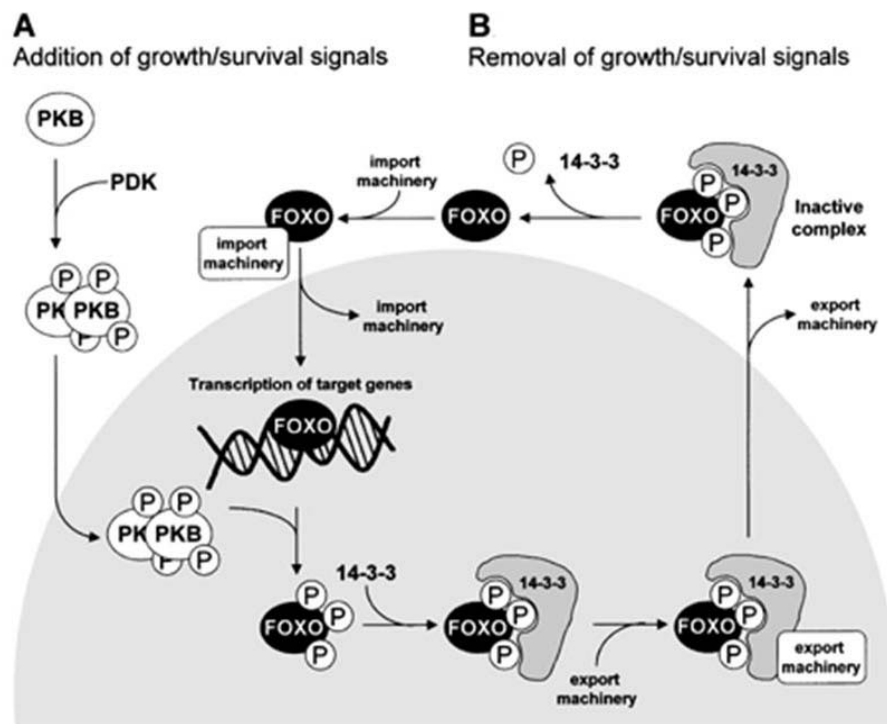
Figure 6: **Regulation of FOXO transcriptional activity.** (**A**) Growth/survival signals activate AKT/PKB, which then translocates into the nucleus. Phosphorylation of FOXO by AKT/PKB results in release from DNA and in binding to 14-3-3 proteins. This complex is then transported out of the nucleus, where it remains inactive in the cytoplasm. (**B**) Upon removal of growth/survival signals, FOXO is dephosphorylated, 14-3-3 is released and FOXO is transported back into the nucleus where it can bind target promoters and transcribe them (Birkenkamp *et al.*, 2003).

The resulting complex prevents re-entry of FoxOs into the nucleus. As predicted, the reduction in the activity of the Akt pathway, observed in different models of muscle atrophy, results in decreased levels of phosphorylated FoxO in the cytoplasm and a marked increase of nuclear FoxO protein. The translocation and activity of FoxO members is required for the up-regulation of atrogin-1/ MAFbx and MuRF1, and FoxO3 was found to be sufficient to promote atrogin-1/MAFbx expression and muscle atrophy when transfected in skeletal muscles *in vivo* (Figure 7).
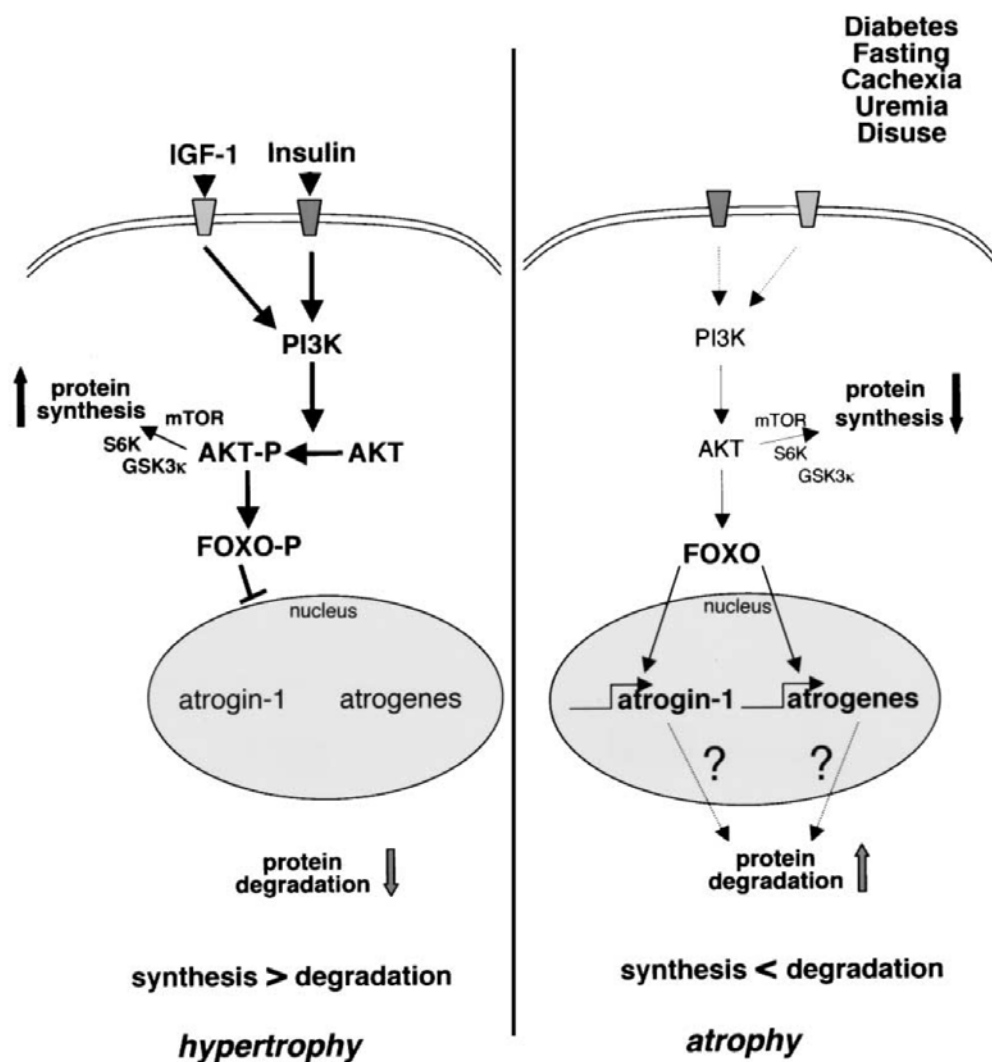
Figure 7: IGF-1/ AKT pathway and FoxO action during muscle atrophy (on the right) and hypertrophy (on the left) (Sandri *et al*. 2004).

Recently the NF-kB signaling cascade, beside the IGF-1/PI3K/Akt/FoxO pathway, emerged to play an important role in the control of muscle mass. First

hints on involvement of NF-kB in muscle wasting came from the up-regulation of this gene during disuse atrophy (Hunter *et al*., 2002) or sepsis (Penner *et al*., 2001). In the inactive state NF-κB is sequestered in the cytoplasm by a family of inhibitory proteins called IκB. In response to tumour necrosis factor-α (TNFα), the IκB kinase (IKK) complex phosphorylates IκB, resulting in its ubiquitination and proteasomal degradation; this leads to nuclear translocation of NF-κB and activation of NF-κB mediated gene transcription.

Experiments in cultured myotubes demonstrated that the inhibition of NF-κB by over-expression of a mutant form of IκBα, that is insensitive to degradation by the proteasome, inhibits protein loss induced by TNFα (Li and Reid, 2000). Interestingly, treatments with TNFα attenuates insulin stimulated protein synthesis (Williamson *et al*., 2005).

To further study the role of NF-kB in muscle wasting, Cai and co-workers created two transgenic mice in which the NF-κB pathway was activated or inhibited, through the muscle-specific expression of IKKα or a dominant inhibitory form of IκBα respectively (Cai *et al*., 2004). In these animals the activation of the NF-κB pathway is sufficient to induce significant muscle atrophy, marked by muscle weight loss, and the expression of the E3 ubiquitin ligase MuRF-1, but not atrogin-1, providing the first functional dissection of the roles of the two E3 ligases. On the other hand, while muscle-specific inhibition of NF-κB by transgenic expression of a constitutively active IκB mutant leads to no obvious phenotype, but denervation atrophy is substantially reduced. Similarly in another study, transgenic animals lacking NF-κB, undergo less atrophy induced by hind limb unloading than control littermates (Hunter and Kandarian, 2004). Finally conditional knockout mice for IKKβ are resistant to muscle atrophy confirming the role of this pathway in regulating muscle mass. However, despite the indirect evidence from genetic studies, up to now there is no evidence of a direct NFkB recruitment on MuRF1 promoter or on any other promoter of the atrophy-related genes.

Autophagic-Lysosomal System

Autophagy-Lysosome System involves dynamic rearrangements of membranes which engulf a portion of cytoplasm for its degradation into the lysosome. This system allows cell survival during starvation through the bulk degradation of proteins and organelles by lysosomal enzymes.

Autophagy is an evolutionarily conserved process whose primary task in lower organisms is the maintenance of metabolic homeostasis in the face of changing nutrient availability. This role in recycling is complementary to that of the ubiquitin-proteasome system, which degrades proteins to generate oligopeptides that are subsequently degraded into amino acids.

The autophagy system is highly regulated through the action of various kinases, phosphatases, and guanosine Triphosphatases (GTPases). The core protein machinery that is necessary to commit membranes to become vesicles includes two ubiquitin-like protein conjugation systems. Moreover there is another set of proteins, that regulates the vesicle formation and their docking and fusion with lysosome .

The autophagy pathway includes: **(1) <u>chaperone-mediated autophagy:</u>** it degrades proteins that contain the amino acid sequence Lys-Phe-Glu-Arg-Gln (KFERQ) (Chiang and Dice, 1988). Proteins containing this motif are recognized by the cytosolic form of heat shock cognate protein of 70 kDa (Hsc-70), a molecular chaperone (Terlecky and Dice, 1993; Cuervo *et al*., 1994). The complex binds by lgp-96 (or lamp-2a), a lysosomal integral membrane receptor of 96 kDa (Cuervo and Dice, 1996), and this binding facilitates the transport of the targeted protein into the lysosome. Transport of the complex requires the assistance of a second chaperone protein, the lysosomal form of hsc-73 (Agarraberes *et al*., 1997; Cuervo *et al*., 1997) (Figure 8). The list of the substrates for chaperone-mediated autophagy include annexins, transcription factors, glycolytic enzymes, and cytosolic protease subunits (Cuervo *et al*., 2000). Importantly, nearly 30% of cytosolic proteins contain the KFERQ-related motif (Dice, 1992).

(2) <u>microautophagy</u>: the direct engulfment of cytoplasmic proteins and small particles into the lysosome (Figure 8). In this pathway, proteins are internalized

via direct uptake by the lysosomal membrane; this is accomplished by invagination of the membrane at multiple locations, forming a multivesicular body (Ahlberg, 1982; Dice, 1987). The microautophagy appeared to be responsible for the gradual, continuous turnover of cytosolic proteins and is not induced by stresses or lack of nutrients.

(3) **macroautophagy** (hereafter referred as to autophagy): cytosolic components are engulfed by double membranes into vesicles and are delivered to the lysosomes (Figure 8). This process appears to be selective and can target to degradation different organelles including: mitochondria (*mitophagy*), portions of the nucleus (*nucleophagy*), peroxisomes (*pexophagy*), endoplasmic reticulum (*reticulophagy*), microorganisms (*xenophagy*), ribosomes (*ribophagy*) or protein aggregates (*aggrephagy*).
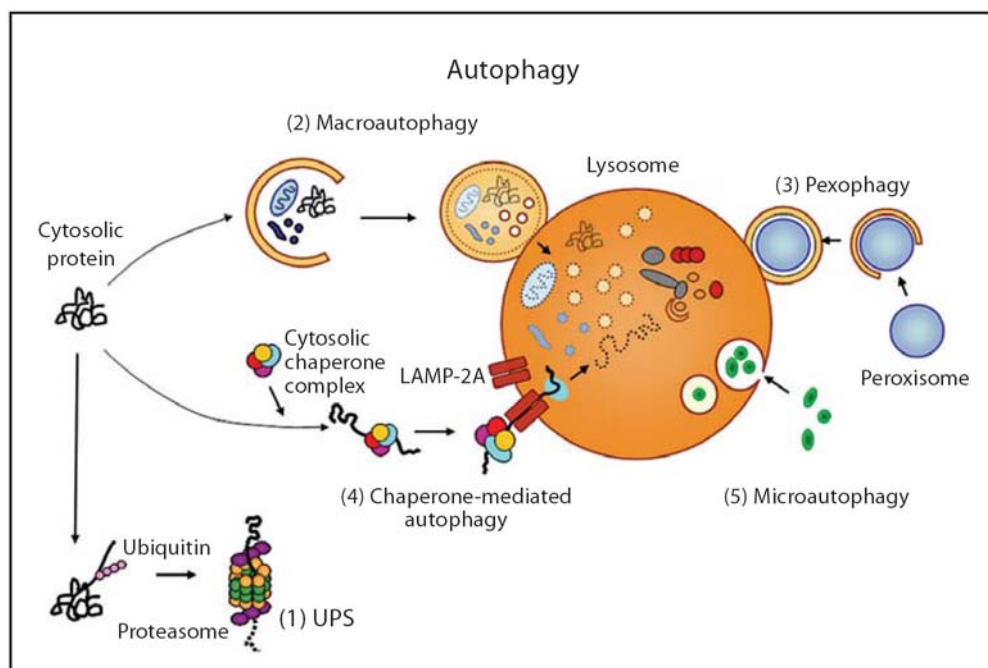
Figure 8: Intracellular protein degradation pathways. Cytosolic proteins can be degraded by the UPS or autophagy-lysosome system. Multiple forms of autophagy involve distinct routes by which cytoplasmic components are delivered for lysosome-mediated degradation. (1) Proteasome-mediated degradation involves covalent addition of ubiquitin chains to target proteins followed by proteolytic cleavage within the catalytic barrel of the proteasome. (2) Macroautophagy is a multistep process by which cytosolic components are engulfed by an isolation membrane to form autophagosomes that are delivered to lysosomes. (3) In pexophagy, peroxisomes are surrounded by autophagic membranes and delivered to lysosomes. (4) Chaperone-mediated autophagy involves recognition of a peptide signal that induces receptor-mediated translocation into the lysosome. (5) In microautophagy, cytosolic contents are directly engulfed by lysosomes. (Figure by Brett A. McCray, J. Paul Taylor 2008).

In mammalian cells, microautophagy has not been well characterized, and chaperone-mediated autophagy is a secondary response that temporally follows macroautophagy.

Nutrient deprivation is a potent stimulus that induces autophagy. In yeast, nitrogen starvation is the most potent stimulus, but withdrawal of other essential factors such as carbon, auxotrophic amino acids and nucleic acids, and even sulfate can induce autophagy, albeit less efficiently (Takeshige *et al*., 1992). Nitrogen or carbon starvation also triggers autophagy in plant cells (Moriyasu and Ohsumi 1996; Yoshimoto *et al*., 2004).

In mammals, regulation of autophagy appears to be highly complicated. Depletion of total amino acids strongly induces autophagy in many types of cultured cells. However, such profiles depend on cell type because amino acid metabolism differs greatly among tissues. In mammals the autophagy is essential for survival after birth, when nutrients supply falls acutely since the newborn shifts its dependence to an external source of food (Kuma *et al*., 2004).

Amino acid and insulin/growth factor signals converge on mTOR kinase (Mammalian Target of Rapamycin), which is the master regulator of nutrient signaling. Indeed, treatment with inhibitors of mTOR such as rapamycin and CCI-779 induces autophagy in yeast (Noda and Ohsumi 1998) and mammals (Ravikumar *et al*., 2004).

Moreover the involvement of many other factors in autophagy regulation has recently been found (Codogno and Meijer 2005). These include Bcl-2, reactive oxygen species (ROS) (Djavaheri-Mergny *et al*., 2006; Scherz-Shouval *et al*., 2007; Xiong *et al*., 2007b), calcium (Hoyer-Hansen *et al*., 2007), AMP-activated protein kinase (AMPK) (Meley *et al*., 2006; Hoyer-Hansen *et al*., 2007; Liang *et al*., 2007), BNIP3 (Daido *et al*., 2004), p19 ARF (Reef *et al*., 2006), DRAM (Crighton *et al*., 2006), calpain (Demarchi *et al*., 2006), TRAIL (Mills *et al*., 2004), FADD (Pyo *et al*., 2005; Thorburn *et al*., 2005), and myo-inositol-1,4,5-triphosphate (IP$_3$) (Sarkar *et al*., 2005; Criollo *et al*., 2007). The process of macroautophagy can be divided down into at least three steps: formation of the autophagosome, autophagosome docking and fusion with the lysosome.

The formation of autophagy vesicles

Membrane dynamics during autophagy are highly conserved from yeast to plants and animals. Autophagosome formation proceeds in distinct phases that can be morphologically and biochemically characterized and are referred as the initiation, execution, and maturation phases. These steps require energy (Kim and Klionsky 2000; Klionsky and Emr 2000).

The process begins with the generation of a double membranes, the isolation membrane or <u>phagophore</u>, that sequester portion of cytoplasm and organelles (Mizushima *et al*., 2002). The expansion of the double membranes and its closure result in a vesicle named <u>autophagosome</u> (Figure 9). The origins of the double-membrane bilayers are difficult to determine because autophagosomes contain a mixture of markers from the ER, endosomes and mitochondrial (Kirkegaard *et al*., 2004; Mitchener *et al*., 1976). Autophagosomes can be large, ranging between 0.5 and 1.5 μm in diameter in mammalian cells (Dunn 1990). Maturation of these vesicles involves docking and fusion with lysosomes which results in the degradation of sequestered contents and recycling of amminoacids, lipids and glucose (Punnonen *et al*., 1992). The endosomal fusion step may provide the "intermediate" autophagosomes with factors that enable them to fuse with lysosomes. Intermediate filament proteins, cytokeratin and vimentin, are required for sequestration, while fusion with lysosomes requires the micotubular system.
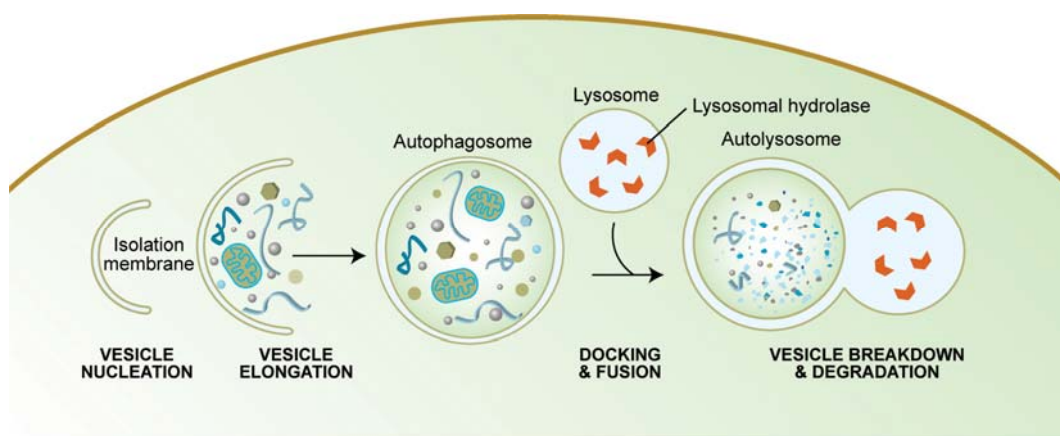
Figure 9: The process of macroautophagy in mammalian cells. A portion of cytoplasm, including organelles, is enclosed by a phagophore or isolation membrane to form an autophagosome. The outer membrane of the autophagosome subsequently fuses with the endosome and then the lysosome, and the internal material is degraded. In yeast, autophagosomes are generated from the PAS (pre-autophagosomal structure), which has not yet been identified in mammalian cells. The nomenclature for various autophagic structures is indicated .

The autophagy genes

Genetic screens in *S. cerevisiae* and other fungi have led to the identification of a number of molecular factors essential for autophagy. There are currently over 30 genes that are primarily involved in bulk and selective types of autophagy and they have been named autophagy-related genes (ATG) (Klionsky *et al*., 2003). Fifteen of them constitute the basic core machinery required for the formation of double-membrane vesicles in all eukaryotes (Levine and Klionsky, 2004; Reggiori, 2006) (Table 1).

Protein	Role	Interactions
Atg1	Serine/threonine protein kinase	Atg13, Atg11, Atg17
Atg2	Atg9 recycling	Atg9, Atg18
Atg3	Atg8 conjugation system (E2)	Atg7, Atg8, Atg12
Atg4	Cysteine protease	Atg8
Atg5	Atg12 conjugation system	Atg12, Atg16
Atg6	PtdIns-3-P synthesis	Atg14, Vps15, Vps34
Atg7	Atg8 and Atg12 conjugation systems (E1)	Atg3, Atg8, Atg10, Atg12
Atg8	Ubiquitin-like protein	Atg3, Atg4, Atg7, Atg19
Atg9	Transmembrane protein	Atg2, Atg18, Atg23, Atg27
Atg10	Atg12 conjugation system (E2)	Atg12
Atg12	Ubiquitin-like protein	Atg3, Atg5, Atg7, Atg10, Atg16
Atg13	Modulates Atg1 activity	Atg1, Atg17, Vac8
Atg14	PtsIns-3-P synthesis	Atg6, Vps15, Vps34
Atg16	Associates with the Atg12–Atg5 conjugate	Atg5, Atg12, Atg16
Atg18	PtdIns-3-P binding protein	Atg2, Atg9

PtdIns-3-P, phosphatidylinositol 3-phosphate; Vps, vacuolar protein sorting.

Table 1: The 15 conserved autophagy-related gene (Atg) proteins involved in double-membrane vesicle formation (adapted from Reggiori, 2006).

Two protein conjugation systems are necessary for autophagosome formation, the Atg12-Atg5 and the Atg8-phosphatidyl ethanolamine systems (Ohsumi *et al.*, 2001). The mechanism of both conjugation systems closely resemble ubiquitination reaction. In fact both systems require energy to activate small molecules, i.e. ubiquitin and ubiquitin-like proteins. Different classes of enzymes catalyze the reaction of activation (E1 protein) and the transfer of the small ubiquitins to the conjugation system (E2 proteins). In the ubiquitin-proteasome system, the final step, regulated by enzymes called E3 or ubiquitin ligases, is the transfer of ubiquitin from the conjugation system to the protein leading to polyubiquitination and targeting to the proteasome for degradation (Lecker *et al.*, 2006). In the autophagy system, small ubiqutin-like molecules (LC3, GABARAP, GATE 16, Atg12) are transferred from the conjugation system to membranes for their growth and commitment to become a double membrane vesicle (autophagosome) that engulfs portions of cytoplasm (Levine and Kroemer 2008; Mizushima *et al.*, 2008). This reaction requires the recruitment and assembly of different components of the autophagy machinery on phospholipids but only the ubiquitin-like components, LC3, GABARAP and GATE16, are covalently bound to phosphatidylethanolamine (Tanida *et al.*, 2004a; Tanida *et al.*, 2004b). This covalent bound occurs both on the outer and inner membranes of the autophagosome. Sequestered organelles and proteins are then docked to the lysosomes for their degradation. The fusion of the outer membrane of the autophagosome with the lysosomal membrane also determines the degradation of the innermembrane and of the proteins that are associated with it. Because of the transient nature of the autophagosomes, the lifetime of LC3 and its homologs is rather short. Thus, the main difference between the two systems is related to the fate of the ubiquitin and ubiquitin-like proteins. While the ubiquitin proteasome pathway recycles ubiquitin molecules, the autophagy-lysosome system progressively loses the ubiquitin-like proteins, forcing the cell to replenish them in order to maintain the autophagic flux.

Atg12-Atg5 conjugate assists the formation, but is not present in mature autophagosomes (Mizushima *et al.*, 2001). Instead Atg8 (called MAP-LC3 (microtubule-associated protein light chain 3 in mammals) is present in mature

vesicles and it may enhance membrane fusion with lysosome (Nakatogawa *et al*., 2007).

Atg8 and Atg12 shows similarities to ubiquitin and their crystal structures reveal a conserved ubiquitin-fold region (Sugawara *et al*, 2004; Suzuki *et al*, 2005) (Figure 10).
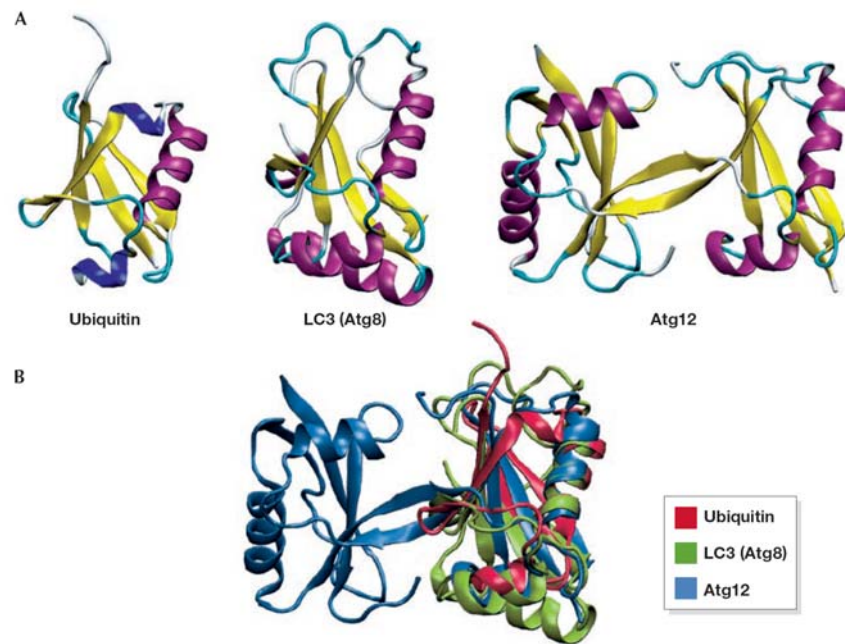
Figure 10: Structural comparisons of ubiquitin, LC3 and AtAtg12. (A) Ribbon diagrams of ubiquitin; Protein Data Bank (PDB) code 1UBQ), LC3 (Sugawara *et al*, 2004; PDB code 1UGM) and AtAtg12 (Suzuki *et al*, 2005; PDB code 1WZ3) are shown in the same orientation; α-helices are shown in purple, 310 helices in blue, β-strands in yellow, β-turns in cyan and unstructured loops in white. (B) Superimposition of ubiquitin (red), LC3 (blue) and AtAtg12 (green). A multiple structural alignment was constructed using MAMMOTH-mult (http://ub.cbm.uam.es/mammoth/mul) and the structures were visualized with the Visual Molecular Dynamics (VMD) program (http://www.ks.uiuc.edu/Research/vmd). At, Arabidopsis thaliana; Atg, autophagy-related; LC3, microtubule-associated protein 1 light chain 3.

Atg12 conjugation system

Atg12 was the first ubiquitin-like Atg protein to be identified. In the canonical system, ubiquitin is synthesized as a precursor and is processed by a specific protease to expose the carboxy-terminal glycine residue. Activated by an E1 enzyme, ubiquitin is then transferred to an E2 enzyme, forming a thioester bond. An E3 ubiquitin ligase recognizes the target protein and transfers ubiquitin from the E2 to a lysine residue on the target. The amino-acid sequence of Atg12 ends with a glycine residue and there is no protease involved in Atg12 conjugation.

Analogous to ubiquitination, there is an E1-like enzyme, Atg7, and Atg12 is activated by forming a thioester bond between the C-terminal Gly 186 of Atg12 and the Cys 507 of Atg7 (Tanida *et al.*, 1999). After activation, Atg12 is transferred to Atg10, which is an E2 enzyme (Shintani *et al.*, 1999), and is eventually conjugated to the target protein Atg5 at Lys 149 through an isopeptide bond (Mizushima *et al.*, 1998a) (Figure 11). There is no typical E3 enzyme involved in Atg12–Atg5 conjugation. Atg5 interacts further with a small coiled-coil protein, Atg16, and Atg12–Atg5-Atg16 forms a multimeric complex through the homo-oligomerization of Atg16 (Mizushima *et al.*, 1999). The molecular weight of this multimeric complex is approximately 350 kDa and it probably represents a tetramer of Atg12–Atg5-Atg16 (Kuma *et al.*, 2002). Although the overall sequence of Atg7 shows little similarity to E1 enzymes in yeast, and so far only Atg7 has been shown to function as E1 (Komatsu *et al.*, 2001). Atg7 shares a conserved metal-binding motif and a downstream active-site cysteine residue with other E1 enzymes such as Uba2, Uba3, Uba4 and Uba5. The ATP -binding domain of Atg7 is also homologous to the corresponding region in other E1 enzymes and is essential for the formation of the Atg12–Atg5 conjugate. In contrast to ubiquitin, which is conjugated to multiple targets in an inducible and reversible manner, Atg5 seems to be the only target of Atg12 and the conjugation of Atg12–Atg5 occurs constitutively (Mizushima *et al.*, 1998a). In addition, no processing enzyme has been identified that cleaves the isopeptide bond between Atg12 and Atg5, suggesting that this conjugation is irreversible. Orthologues of each component of the Atg12 system have been found in mice and humans, and they function similarly to their yeast counterparts (Mizushima *et al.*, 1998b; Mizushima *et al.*, 2002; Tanida *et al.*, 2001). There is also a mammalian Atg16-like protein (ATG 16L) that mediates the formation of an ATG12–ATG5-ATG16L complex of approximately 800 kDa (Mizushima *et al.*, 2003).

Atg8 conjugation system

Rather than conjugating to another protein, the Ubl protein Atg8 is attached to phosphatidylethanolamine (PE). The C-terminal Arg 117 residue of Atg8 is initially proteolytically removed by a cysteine protease, Atg4, to expose Gly 116

(Kirisako *et al.*, 2000). This exposed glycine forms a thioester bond with Cys 507 of Atg7, which is also the site that participates in the Atg12–Atg5 conjugation (Ichimura *et al.*, 2000). This feature differentiates Atg7 from most other E1 enzymes, which activate single Ubl proteins. Activated Atg8 is then transferred to the E2-like enzyme Atg3, also through a thioester bond (Ichimura *et al.*, 2000). In the final step of Atg8 lipidation, Gly 116 of Atg8 is conjugated to PE through an amide bond (Ichimura *et al.*, 2000) (Figure 11); Atg8–PE exists in a tightly membrane-associated form. Although Atg3 shares little sequence homology with other E2 enzymes, structural comparison shows that the head moiety of Atg3 is similar to that of canonical E2 enzymes (Yamada *et al.*, 2007). The amino-acid sequence around the active-site cysteine residue of Atg3 (Cys 234) is also homologous to the corresponding region (Cys 133) in Atg10. Unlike Atg12–Atg5 conjugation, lipidation of Atg8 is reversible. Atg8–PE can be cleaved by Atg4 to release free Atg8 and it can still be used for another processes (Kirisako *et al.*, 2000).
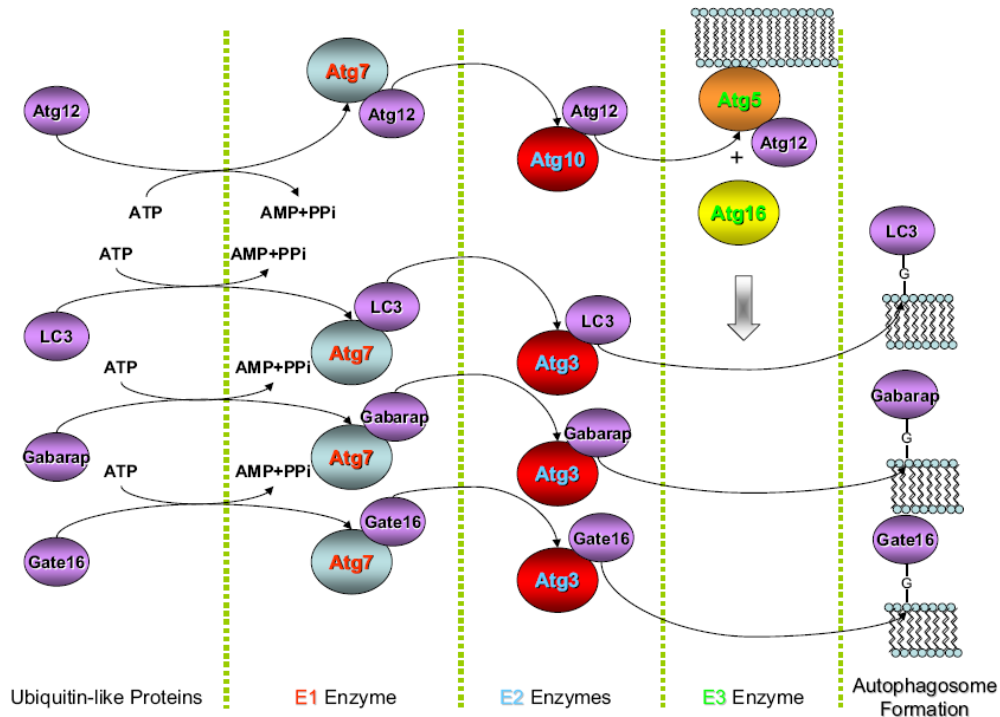
Figure 11: Schematic representation of the autophagic conjugation system. The conjugation system of autophgay-related genes (Atg) in mammals. In yeast, the ubiquitin like proteins are Atg12 and Atg8. Mammals have three Atg8 family homologs, which are LC3, Gabarap and Gate16, while Atg12 is conserved. The ubiquitin-like proteins are activated by Atg7, theE1 enzyme, and transferred to the E2 enzymes. There are two E2 enzymes for Atg12 and for the Atg8 family homologs. In subsequent steps Atg12 is transferred to Atg10, while LC3, Gabarap and Gate 16 are transferred to Atg3. Finally Atg12 is conjugated to a specific lysine residue of Atg5 and the Atg5-Atg12 complex interacts with Atg16 and forms oligomers that associate with membranes. The Atg5-Atg12-Atg16 complex exerts an E3 enzyme-like function on LC3, Gabarap and Gate16 and catalyzes the transfer reaction from the E2 (Atg3) to the phospholipid, phosphatidylethanolamine (PE). The conjugation between the ubiquitin-like protein and PE involves a covalent binding that can be hydrolyzed by the Atg4 protein to recycle the ubiquitin-like proteins (Sandri 2010).

In mammalian cells, several homologues of yeast Atg8 have been identified: MAP-LC3 (microtubule-associated protein light chain 3), GATE-16 (Golgi-associated ATPase enhancer of 16 kDa), GABARAP (γ-aminobutyric-acid-type-A-receptor-associated protein). All of these undergo a modification process similar to that of their yeast counterpart, which is also catalysed by ATG4, ATG3 and ATG7 (Kabeya *et al.*, 2004; Tanida *et al.*, 2003; Tanida *et al.*, 2006; Tanida *et al*., 2002; Tanida *et al.*, 2001). Among them, MAP-LC3 (typically abbreviated LC3) has been best characterized as an autophagosome marker in mammalian cells. LC3 is synthesized as proLC3, and ATG4B processes this precursor into LC3-I with an exposed C-terminal glycine (Kabeya *et al.*, 2004). Catalysed by ATG7 and ATG3, cytosolic LC3-I is transformed to a membrane-bound form,

LC3-II, which corresponds to Atg8–PE in yeast. Further analysis shows that LC3 is also attached to PE, and the conjugate can be cleaved by ATG4B. In mammalian cells, the formation of LC3-II can be induced by nutrient depletion or in response to hormone (Kabeya *et al.*, 2000), although the induction level is usually cell line-dependent and tissue-dependent (Mizushima *et al.*, 2004). Consequently, the generation and turnover of LC3-II is used as an index of autophagy induction and/or flux (Klionsky *et al.*, 2008). LC3-II staining is also used as a primary histological marker of autophagosomes. Because LC3-II remains on the inner membrane of autophagosomes until lysosomal enzymes degrade it, increased steady-state levels of LC3-II may be due to induction of autophagosome formation, a blockade in their maturation, or both.

Although many Atg proteins are conserved between yeast and mammals, several mammalian-specific factors that modulate the functions of Atg proteins have been identified.

Atg1 is a serine–threonine kinase that functions in the signaling pathway activating autophagy (Kamada *et al.*, 2000; Young *et al.*, 2006). Atg1 interacts with Atg13 in a manner that is regulated by phosphorylation. During autophagy induction, the phosphorylation of Atg13 is decreased, which increases the assembly of Atg1-Atg13 complexes (Kamada *et al.*, 2000). The mammalian homolog of Atg1 is called ULK1 (Chan *et al.*, 2007).

The most well studied is Beclin 1, which is a mammalian Atg6/Vps30 (vacuolar protein sorting 30) ortholog and a subunit of the class III PI3-kinase complex. Beclin 1 was originally identified as an interaction partner of Bcl-2, an anti-apoptotic protein (Liang *et al.*, 1998). This Bcl-2–Beclin 1 interaction is mediated through a BH3 domain in Beclin 1 (Maiuri *et al.*, 2007; Oberstein *et al.*, 2007) and is reduced upon starvation, increasing the level of free Beclin 1 that activates autophagy (Pattingre *et al.*, 2005; Maiuri *et al.*, 2007). The Endoplasmic Reticulum (ER)-targeted but not mitochondrial-targeted Bcl-2 effectively suppresses autophagy (Pattingre *et al.*, 2005; Criollo *et al.*, 2007). The starvation-induced dissociation of Beclin 1 and Bcl-2 (or Bcl-X_L) could be one way in which nutrient starvation induces autophagy. Therefore, it is proposed that Bcl-2 is not only an anti-apoptotic but also an anti-autophagic protein. Alternatively, Bcl-2 is reported to suppress autophagy by inhibiting cytosolic calcium elevation, which

can induce autophagy (Hoyer-Hansen *et al*., 2007). Another Beclin 1 partner is UVRAG (UV irradiation resistance-associated gene) (Liang *et al*., 2006), which interacts via the coiled-coil region of Beclin 1. UVRAG is shown to be a member of the class III PI3-kinase complex and a positive regulator of autophagy. Recently, a WD-40 domain-containing protein named Ambra1, which was identified by a gene trap experiment, is shown to be a Beclin 1-interacting protein (Maria Fimia *et al*., 2007) and is shown to positively regulate Beclin 1-dependent autophagy. Ambra1 is primarily expressed in neural tissues and is indispensable for normal neural tube development. Therefore, mammalian Beclin 1 is likely to be regulated by its binding partners, which may not be present in yeast.
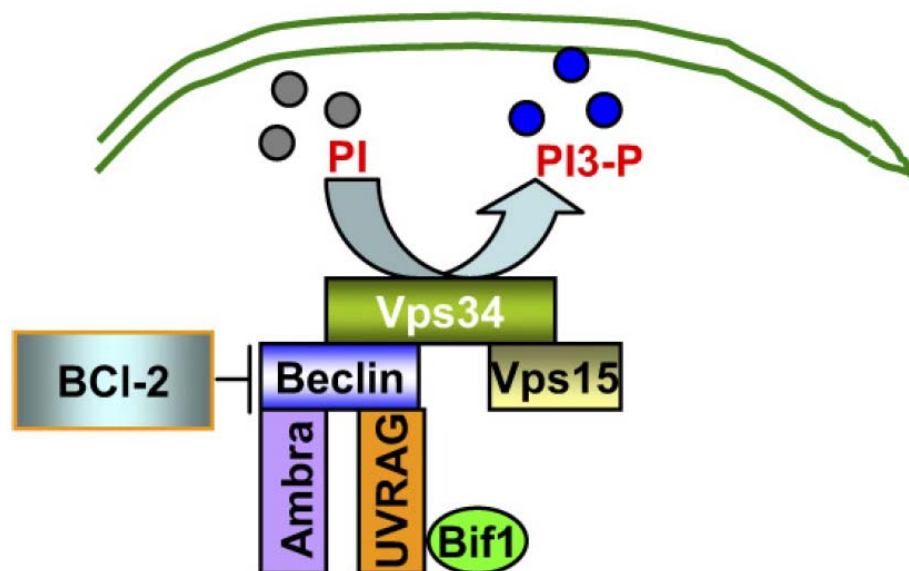
Figure 12: **The class III phosphatidylinositol 3-kinase (PI3-kinase) complex**. Vps34, a class III PI3-kinase, phosphorylates phosphatidylinositol (PI) to produce phosphatidylinositol 3-hosphate (PI3P), a docking lipid that promotes protein complex formation, membrane enclosing, and the consequent sequestration of cytoplasmic components in autophagic vacuoles. Vps34 forms complexes with and is regulated by beclin-1 and Vps15. Beclin-1 further interacts with and is regulated by Bcl-2, Ambra, and UVRAG. (Figure by Periyasamy *et al*., 2009).

Molecular signaling in Autophagy

The complex molecular machinery of autophagy suggests that its regulation can be extremely complicated and may involve multiple signaling inputs. These different signaling pathways may cross talk and regulate at different levels in the autophagic cascade, including induction and expansion of the isolation membrane,

enclosure of the isolation membrane to form autophagosome, and fusion with lysosome.

One of the key regulators of autophagy is the target of rapamycin, TOR kinase, which is the major inhibitory signal that shuts off autophagy in the presence of growth factors and abundant nutrients. The class I PI3K/Akt signaling molecules link receptor tyrosine kinases to TOR activation and thereby repress autophagy in response to insulin-like and other growth factor signals (Lum *et al.*, 2005).

TOR activity prevents the formation of Atg complexes including the Atg1-Atg13-Atg17 serine/threonine protein kinase complex and the Vps34-Atg6-Vps15 lipid kinase complex (Kim *et al.*, 2002; Mizushima *et al.*, 2001; Suzuki *et al.*, 2001) (Figure 13). It also interferes with the two ubiquitin-like conjugation systems of autophagy (Atg12-5 and Atg8). As a result, induction and expansion of the isolation membrane is abrogated. Conversely, TOR is inhibited during nutrient deprivation, inducing the autophagy machinery. Therefore, inhibition of TOR has been suggested to be necessary for the autophagy activation (Abeliovich *et al.*, 2000). However it remains to be determined whether TOR inhibition is a universal mechanism for autophagy regulation.

Some of the other regulatory molecules that control autophagy include 5′-AMP-activated protein kinase (AMPK), which responds to low energy, the eukaryotic initiation factor 2α (eIF2α), which responds to nutrient starvation, double-stranded RNA, and Endoplasmic Reticulum (ER) stress (Kouroku *et al.*, 2007); BH3-only proteins that contain a Bcl-2 homology-3 (BH3) domain and disrupt Bcl-2/Bcl-XL inhibition of the Beclin 1/class III PI3K complex; the tumor suppressor protein, p53; death-associated protein kinases (DAPk); the ER-membrane-associated protein, Ire-1; the stress-activated kinase, c-Jun-N-terminal kinase; the inositol-trisphosphate (IP3) receptor (IP3R); GTPases; Erk1/2; ceramide; and calcium (Figure 13) (Criollo *et al.*, 2007; Maiuri *et al.*, 2007a; Meijer and Codogno, 2006; Rubinsztein *et al.*, 2007).
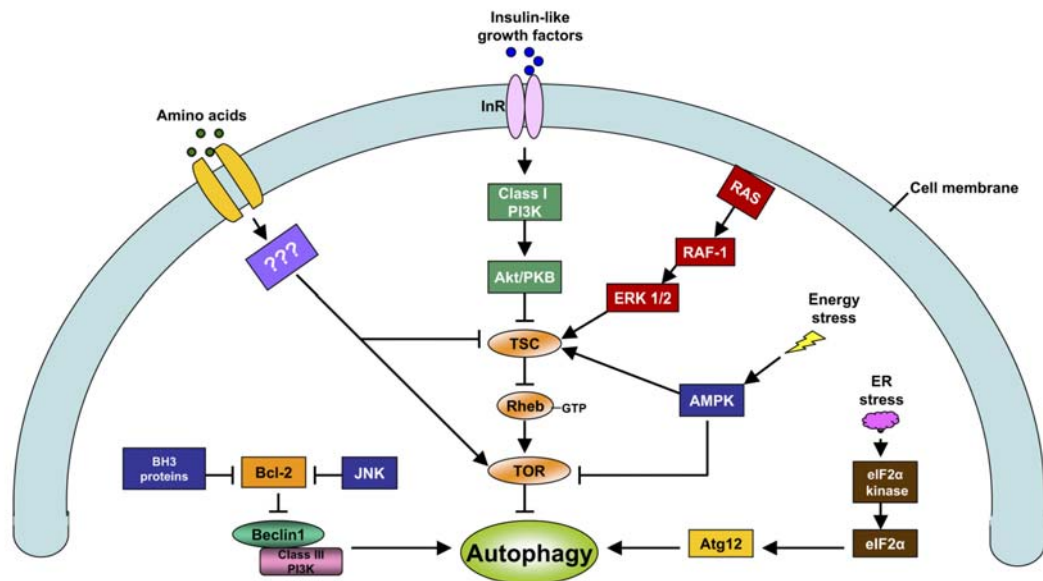
Figure 13: Major regulatory mechanisms of autophagy. The major signaling pathways of autophagy regulation under conditions of nutrient (amino acids, growth factors) deprivation, Endoplasmic Reticulum (ER) stress, energetic stress or depletion The pathways may cross talk and regulate autophagy at different levels, including induction and expansion of the isolation membrane, enclosure of the isolation membrane to form autophagosome, and fusion with lysosome. PI3K, PI3-kinase; AMPK, AMP-dependent protein kinase; TSC, tuberous sclerosis complex; eIF-2α, eukaryotic initiation factor-2α; InR, insulin receptor; RAS, rat sarcoma (a protein encoded by rat sarcoma virus oncogene). (Figure by Periyasamy *et al*., 2009).

Autophagy and Muscle

Autophagy is constitutively active in skeletal muscle, as shown by the accumulation of autophagosomes seen in human myopathies caused by genetic deficiency of lysosomal proteins, e.g. Pompe's and Danon's disease, or by pharmacological inhibition of lysosomal function, as in chloroquine myopathy (Shintani and Klionsky, 2004). Electron microscopic studies previously showed that autophagy is activated in denervation atrophy (Schiaffino and Hanzlikova, 1972b) and the lysosomal proteolytic system is stimulated in different atrophic conditions (Bechet *et al*., 2005). Autophagy is also induced in skeletal muscle in the immediate postnatal period when glycogen-filled autophagosomes are abundant (Schiaffino and Hanzlikova, 1972a). The crucial role of autophagy in the newborn is demonstrated by the finding that mice deficient in autophagy genes Atg5 or Atg7 die soon after birth during the critical starvation period when transplacental nutrient supply is suddenly interrupted (Komatsu *et al*., 2005; Kuma *et al*., 2004).

p62/SQSTM1

The autopaghy system is a important process to prevent accumulation of protein aggregates, which are the cause of different degeneration diseases (see below). These aggregates can be selectively degraded by autophagy system via p62 protein, also called sequestosome 1 (SQSTM1).

p62 protein has been found in inclusion bodies present in different human disorders such as in liver injuries (e.g., alcoholic hepatitis, steatohepatitis, and α1-antitrypsin deficiency) and neurodegenerative diseases (e.g. Alzheimer Disease (AD), Parkinson's Disease (PD), and Amyotrophic lateral sclerosis (ALS).

p62/SQSTM1, originally identified as an ubiquitin-associated protein, provides a link between autophagy and selective protein degradation. This protein can bind a large number of proteins through its multiple protein–protein interaction motifs.

Structural analysis reveals that p62/SQSTM1 N-terminal Phox and Bem1 (PB1) domain exhibits self-oligomerization, and that the C-terminal ubiquitin-associated (UBA) domain can bind ubiquitinated proteins (Figure 14).

p62/SQSTM1 is linked more to the autophagy-lysosome system than to the ubiquitin-proteasome system. In fact inhibition of lysosome but not proteasome, results in important accumulation of p62 (Bjørkøy *et al.*, 2005; Pankiv *et al.*, 2007). Accumulation of p62 results in self-oligomerization and formation of aggregates that contains polyubiquitinated proteins. Moreover, tissue specific inhibition of autophagy leads to a rapid and robust increase in p62 protein levels (Komatsu *et al.*, 2007). Mice double knockout for p62 and autophagy reduces the formation of ubiquitin positive aggregates in mice and fly (Nezis *et al.*, 2008).

Recent studies have identified the LC3 recognition sequence (LRS) in murine p62, that is located between the zinc finger and UBA domains (Figure 14). The LRS is comprised of 11 amino acids (Ser334–Ser344), which include an acidic cluster and hydrophobic residues (DDD or DEE and WXXL or WXXV).
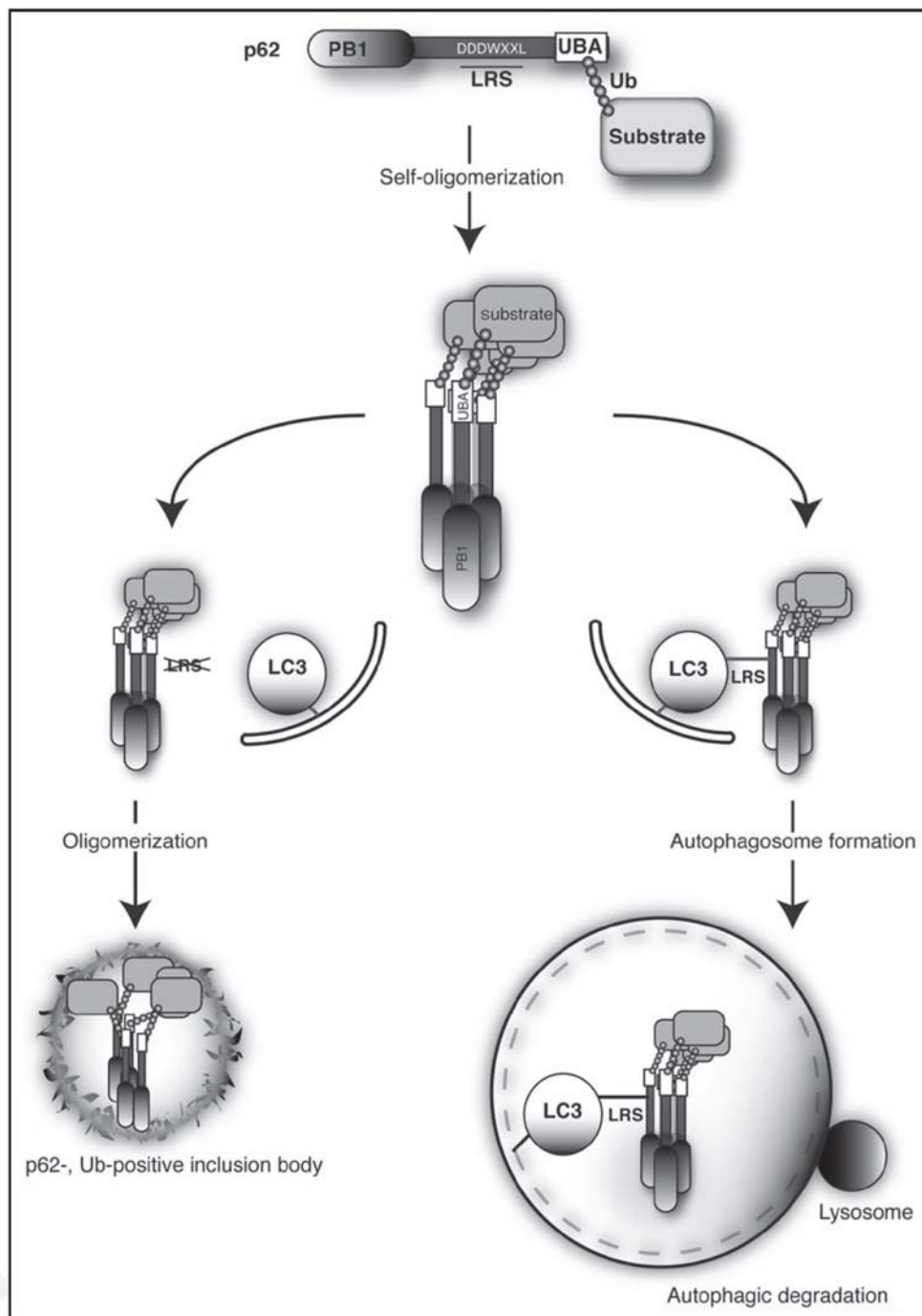
Figure 14: Selective autophagy mediated by p62-LC3 interaction. Ubiquitinated proteins interact with the ubiquitin-associated (UBA) domain of p62, and are selectively sequestered in autophagosomes through the LC3-recognition sequence (LRS)-LC3 interaction. This process is achieved efficiently by selfoligomerization of p62 via the Phox and Bem1 (PB1) domains. Finally, the ubiquitinated protein, p62, and LC3 are degraded by lysosomal hydrolysis. On the other hand, the impaired turnover of p62 (e.g., through the genetic loss of autophagy, or mutation of the LRS in p62) causes the accumulation of p62 associated with ubiquitinated proteins, resulting in high cytoplasmic levels of oligomerized p62. Subsequently, these oligomeric complexes form inclusions. (Figure by Ichimura *et al.*, 2008).

The crystal structure of the LC3-LRS complex, solved at 1.56 Å resolution, reveals that the acidic cluster of Asp337–Asp339 in LRS interacts with basic residues in the N terminus of LC3, and that the Trp-340 and Leu-343 residues are inserted into two hydrophobic pockets, exposed on the ubiquitin domain of LC3. LC3 has basic residues at its N-terminal α-helix surface, and these residues are involved in the interaction with the acidic cluster of LRS, whereas the other two Atg8 mammalian homologues, GATE-16 and GABARAP, have acidic residues in their respective N-terminal α-helical surfaces (Ichimura *et al.*, 2008). It is thus conceivable that p62 is a more favorable target for LC3 than GATE-16 or GABARAP.

Autophagy in disease

Autophagy occurs at basal levels in most tissues and contributes to the routine turnover of cytoplasmic components. In contrast, the dramatic enhancement of autophagy can be triggered by some conditions such as starvation and hormonal stimulation. Moreover, autophagy is also involved in development, differentiation, and tissue remodeling in various organisms (Levine and Klionsky *et al.*, 2004). In addition, the increase in autophagy is a characteristic of type II programmed cell death (also known as autophagic cell death), which differs from apoptosis (type I programmed cell death) (Gozuacik *et al.*, 2004). Furthermore autophagy may not cause cell death, but it may precede apoptosis as a defensive mechanism. Autophagy is also implicated in wide range of diverse human diseases (Table 2): cancer, neurodegeneration, muscular disorders, liver diseases and pathogen infection (Kalimo *et al.*, 1998).

1. *Cancer*
2. *Neurodegeneration*
    Polyglutamine diseases
    Alzheimer's disease
    Parkinson's disease
    Prion disease
3. *Muscular disorders*
    Acid maltase deficiency
    Danon disease
    Rimmed vacuolar myopathies
4. *Liver diseases*
    α1-antitrypsin deficiency
5. *Pathogen infection*

Table 2: Summary of autophagy in diseases

Autophagy in muscular disorders

The lysosome is the major site of organelle and long-lived protein degradation. When the function of the lysosome is altered, excessive levels of undigested materials accumulate within the lysosome and ultimately become toxic to the cell. This phenotype is seen with certain lysosomal storage diseases (Danon's disease and Pompe's disease), which typically effect heart and skeletal muscle (Terman *et al*., 2005; Eskelinen *et al*., 2006). Interestingly, autophagy often correlates with these diseases, which are also named autophagic vacuolar myopathies. These autophagic vacuoles show several morphological and biochemical properties of sarcolemma, and characterize this group of diseases (Nishino *et al*., 2006).

Danon's disease, one of the lysosomal glycogen storage diseases, is the best-studied example of autophagy-linked myopathies. It is caused by the genetic deficiency of LAMP-2 gene.

Studies of LAMP-2-deficient mice, which provide a mouse model of Danon's disease, suggest that fusion of autophagosomes with the endosome/lysosome is impaired (Tanaka *et al*., 2000). It is not known how mutated LAMP-2 alters autophagy, but mutation or deletion of this lysosomal membrane protein may result in abnormal lysosomal membrane structure, which probably directly or indirectly hinders fusion between the autophagosome outer membrane and the

lysosomal membrane. LAMP-2 mutations also impair the Chaperone-Mediated-Autophagy.

Another example of autophagic vacuolar myopathy, similar to Danon's disease is the Pompe disease (glycogen storage disease type II, GSDII), a deficiency of the glycogen-degrading lysosomal enzyme acidalpha glucosidase (GAA). The deficiency of this enzyme results in the failure to metabolize lysosomal glycogen to glucose leading to progressive accumulation of glycogen and the enlargement of lysosomes in multiple tissues cardiac and skeletal muscles are the major tissues affected by this storage. Transcription of several autophagy genes, such as BECLIN 1, ATG12 and ATG8/LC3 are significantly upregulated in the muscle cells of acid α-glucosidase-knockout mice, suggesting the induction of autophagy (Fukuda *et al*., 2006).

Muscle-specific autophagy-deficient mice were crossed with the Pompe mice and the resulting mice show an improvement of Pompe phenotype suggesting that autophagy is not required for glycogen transport to lysosomes in skeletal muscle. (Raben *et al*., 2008).

Other muscle diseases, in which autophagy impairment may contribute to the desease progression include: sporadic inclusion body myositis, limb girdle muscular dystrophy type 2B, and Miyoshi myopathy.

Sporadic inclusion body myositis, the most common acquired muscle disease in patients above 50 years of age, is characterized by accumulation of amyloid precursor protein (APP) and its proteolytic fragment β-amyloid in vacuolated cells (Askanas and Engel, 2006). Both APP and β-amyloid colocalize with LC3 in cultured human muscle cells and in degenerating muscle fibers of human biopsies, suggesting that these proteins are cleared by autophagy (Lunemann *et al*., 2007).

Limb girdle muscular dystrophy type 2B and Miyoshi myopathy are both caused by mutations of the gene encoding dysferlin, a type II transmembrane protein expressed primarily in muscle sarcolemma. Although wild-type dysferlin in the ER is degraded primarily by the ubiquitin-proteasome system, mutant dysferlin spontaneously aggregates in the Endoplasmic Reticulum and is primarily degraded by the autophagy/lysosomal system (Askanas and Engel, 2006). In cells expressing mutant dysferlin autophagy inhibition increases protein aggregation

whereas activation autophagy by rapamycin treatment decreases protein aggregation.

The autophagy system play a central role in the clearance of aggregate-prone proteins, which are toxic in neurons as well as in liver and muscle. Moreover the role of basal autophagy in homeostasis of muscle has never been addressed.

Neurodegeneration

Several human diseases are associated with increased autophagy, particularly in nondividing cells like nervous or muscle tissue where turnover of intracellular proteins may be critical.

Autophagy is crucial for neuronal homeostasis, predominantly as housekeeping process to prevent accumulation of protein aggregates, which affect the function of neurons.

Elevated levels of autophagy are also associated with neurodegenerative diseases such as Parkinson's (PD), Huntington's (HD), and Alzheimer's (AD) diseases, (Anglade *et al*., 1997; Okamoto *et al*., 1991) and transmissible spongiform encephalopathies (prion diseases) (Liberski *et al*., 2004) The occurrence of intracellular protein aggregates and altered activity of proteolytic systems is characteristic of neurodegenerative diseases. An accumulation of autophagosomes is observed in samples from the brains of patients, cell lines or mouse models of these diseases, which represents both an upregulation of autophagic activity and a deficiency in autophagosome-lysosome fusion (Cuervo *et al*., 2004; Ravikumar *et al*., 2002; Yu *et al*., 2005).

Mice lacking Atg7 gene specifically in the central nervous system, showed features of neurodegeneration. Moreover the knockout mice showed behavioural defects, including abnormal limb-clasping reflexes and a reduction in coordinated movement, and died within 28 weeks of birth. Atg7 deficiency caused massive neuronal loss in the cerebral and cerebellar cortices. Notably, polyubiquitinated proteins accumulated in autophagy-deficient neurons as inclusion bodies, which increased in size and number with ageing. These results indicate that autophagy is essential for the survival of neural cells, and that impairment of autophagy is

implicated in the pathogenesis of neurodegenerative disorders involving ubiquitin-containing inclusion bodies (Komatsu *et al*., 2006).

In Parkinson disease, death of dopaminergic neurons in the substantia nigra is associated with accumulation of α-synuclein, a cytosolic protein that has synaptic functions, within inclusions called Lewy bodies.

The pathology is complex, having features of apoptosis and necrosis in addition to accumulations of autophagosome-like structures (Stefanis, 2005). Both macroautophagy and proteasome pathways might be involved in a-synuclein turnover (Webb *et al*., 2003; Stefanis *et al*., 2001); however, CMA has been identified as the rate-limiting degradative mechanism in neuronal cells (Cuervo *et al*., 2004). Mutation in α-Synuclein causes familial Parkinson's disease and which shows impairment of translocation into lysosomal membrane, LAMP-2a mediated. Interesting the binding of mutant α-synuclein to LAMP-2a also blocks the uptake and the degradation of other CMA substrates (Cuervo, 2004). Cell death induced by the overexpression of α-synuclein is associated with accumulations of Autophagic Vacuoles (AVs) that are not completely acidified, suggesting that autophagosome–lysosome fusion is impaired when macroautophagy is induced to compensate the CMA defect.

Alzheimer's disease is characterized by the accumulation of aggregated tau protein in neurons and excessive extracellular deposit of β-amyloid (Aβ).

Aβ peptide is a 40 to 42 amino acid cleavage product of the amyloid precursor protein. The generation of Aβ peptide occurs in intracellular compartments including the Endoplasmic Reticulum, Golgi complex, endosomes and lysosome. A recent study shows that autophagy is another site for Aβ peptide production (Yu *et al*., 2005). Enrichment of Aβ in autophagosomes is observed in brains from AD patients and in the AD mouse model, and a marked accumulation of autophagosomes is also detected (Yu *et al*., 2005). Although most Aβ formed during autophagy is normally degraded within lysosomes, in the Alzheimer's disease brain, Aβ accumulates within the large pool of autophagic vacuoles in dystrophic neuritis and becomes a major intracellular reservoir of the toxic peptide (Yu *et al*., 2005). Aβ within lysosomal compartments is known to destabilize autophagic vacuoles membranes and trigger release of hydrolytic enzymes into the cytoplasm (Glabe, 2001). Inefficient maturation of autophagic

vacuoles to lysosomes possibly leaves the accumulated compartments vulnerable to many other destabilizing factors over long periods.

In Huntington's disease the autophagy system play a important role . This disease is caused by gene mutations that encode abnormally long sequences of polyglutamine in the mutant protein. Polyglutamine sequences are poor substrates for the proteasome, and a dependence on autophagy is evidenced by the accumulation of highly ubiquitinated aggregates of huntingtin (htt), the causative gene product, in the endosomal–lysosomal organelles of affected neurons (Sapp *et al*., 1997) and lymphoblasts (Nagata *et al*., 2004) of Huntington's disease patients.

I PART

FoxO3 Controls Autophagy in Skeletal Muscle In Vivo

Cristina Mammucari,[1,2] Giulia Milan,[1,3] Vanina Romanello,[1,3] Eva Masiero,[1] Ruediger Rudolf,[1,4]
Paola Del Piccolo,[1] Steven J. Burden,[5] Raffaella Di Lisi,[1] Claudia Sandri,[1,3] Jinghui Zhao,[6] Alfred L. Goldberg,[6]
Stefano Schiaffino,[1,2,7] and Marco Sandri[1,2,3,*]
[1]Venetian Institute of Molecular Medicine, 35129 Padova, Italy
[2]Department of Biomedical Sciences, University of Padova, 35121 Padova, Italy
[3]Dulbecco Telethon Institute, 35129 Padova, Italy
[4]Institute of Toxicology and Genetics, Forschungszentrum Karlsruhe, 76021 Karlsruhe, Germany
[5]Skirball Institute of Biomolecular Medicine, New York University School of Medicine, New York, NY 10016, USA
[6]Department of Cell Biology, Harvard Medical School, Boston, MA 02115, USA
[7]Institute of Neuroscience, Consiglio Nazionale delle Ricerche, 35121 Padova, Italy
*Correspondence: marco.sandri@unipd.it
DOI 10.1016/j.cmet.2007.11.001

SUMMARY

Autophagy allows cell survival during starvation through the bulk degradation of proteins and organelles by lysosomal enzymes. However, the mechanisms responsible for the induction and regulation of the autophagy program are poorly understood. Here we show that the FoxO3 transcription factor, which plays a critical role in muscle atrophy, is necessary and sufficient for the induction of autophagy in skeletal muscle in vivo. Akt/PKB activation blocks FoxO3 activation and autophagy, and this effect is not prevented by rapamycin. FoxO3 controls the transcription of autophagy-related genes, including *LC3* and *Bnip3,* and Bnip3 appears to mediate the effect of FoxO3 on autophagy. This effect is not prevented by proteasome inhibitors. Thus, FoxO3 controls the two major systems of protein breakdown in skeletal muscle, the ubiquitin-proteasomal and autophagic/lysosomal pathways, independently. These findings point to FoxO3 and Bnip3 as potential therapeutic targets in muscle wasting disorders and other degenerative and neoplastic diseases in which autophagy is involved.

INTRODUCTION

Protein degradation in skeletal muscle cells is essentially mediated by the activity of two highly conserved pathways, the ubiquitin-proteasomal pathway and the autophagic/lysosomal pathway. In the first, target proteins are conjugated to multiple ubiquitin moieties and ubiquitin-tagged proteins are degraded within the proteasome complex (Lecker et al., 2006). In the second, portions of cytoplasm and cell organelles are sequestered into vacuoles, called autophagosomes, with subsequent fusion of autophagosomes with lysosomes and digestion of the content of the vacuoles by lysosomal hydrolases (Lum et al., 2005). The molecular components of these pathways have been extensively characterized, but the regulatory networks that control their function are still incompletely defined.

The ubiquitin-proteasomal pathway is constitutively operative in normal skeletal muscle and is responsible for the turnover of most soluble and myofibrillar muscle proteins (Lecker et al., 2006). The activity of this pathway is markedly increased in atrophying muscle due to transcriptional activation of ubiquitin; several proteasomal subunit genes; and two muscle-specific ubiquitin ligases, *atrogin-1/MAFbx* and *MuRF1*, which are induced severalfold during early stages of muscle atrophy (Gomes et al., 2001). Importantly, the rate of muscle atrophy is markedly reduced by targeted inactivation of these genes (Bodine et al., 2001a). Two major signaling pathways appear to control the activation of muscle ubiquitin ligases. One is mediated by the forkhead box O (FoxO) transcription factors, which are normally phosphorylated and inactivated by Akt/PKB but translocate to the nucleus and induce the transcription of both *atrogin-1* and *MuRF1* in the absence of Akt repression (Sandri et al., 2004; Stitt et al., 2004). The second regulatory pathway involves the transcription factor NF-κB, which is known to mediate the effect of the cytokine TNF-α in the inflammatory response and which in turn is able to induce the activation of *MuRF1* (Cai et al., 2004).

Autophagy is also constitutively active in skeletal muscle, as shown by the accumulation of autophagosomes seen in human myopathies caused by genetic deficiency of lysosomal proteins, e.g., Pompe's and Danon's diseases, or by pharmacological inhibition of lysosomal function, as in chloroquine myopathy (Shintani and Klionsky, 2004). Electron microscopic studies have previously shown that autophagy is activated in denervation atrophy (Schiaffino and Hanzlikova, 1972b) and that the lysosomal proteolytic system is stimulated in different conditions leading to muscle atrophy (Bechet et al., 2005). Autophagy is also induced in skeletal muscle in the immediate postnatal period, when glycogen-filled autophagosomes are

especially abundant (Schiaffino and Hanzlikova, 1972a). The crucial role of autophagy in newborns is demonstrated by the finding that mice deficient in the autophagy genes *Atg5* or *Atg7* die soon after birth during the critical starvation period when the transplacental nutrient supply is interrupted (Komatsu et al., 2005; Kuma et al., 2004).

Recently, a fusion protein of GFP with the autophagy protein LC3, the mammalian homolog of the yeast *Atg8* gene, has been introduced as a specific marker for autophagosomes (Mizushima et al., 2004). Food deprivation was found to induce the rapid appearance of cytoplasmic fluorescent dots, corresponding to autophagosomes, in fast skeletal muscle of transgenic mice expressing GFP-LC3 (Mizushima et al., 2004). In different cell systems, autophagy is activated by depletion of nutrients or lack of growth factors and, according to current views, this is mediated by the kinase mTOR (Lum et al., 2005). Autophagy is suppressed by mTOR, which is in turn controlled directly by the level of intracellular amino acids and indirectly by growth factors via Akt/PKB and cell energy status via AMPK. Accordingly, rapamycin, a specific inhibitor of mTOR, activates autophagy. However, autophagy can also be induced by mTOR-independent mechanisms: leucine starvation has been reported to induce mTOR-independent autophagy in cultured myotubes (Mordier et al., 2000), and mTOR has also been found to be dispensable in other cell systems (Kochl et al., 2006; Sarkar et al., 2007; Yamamoto et al., 2006).

Upregulation of autophagy and lysosomal genes has been documented at the transcript and protein level in different settings, but the mechanisms controlling this transcriptional regulation and their physiological relevance have not been characterized. The lysosomal proteinase cathepsin L is induced in muscle wasting (Sacheck et al., 2007), and microarray analyses suggest that this is also true for the autophagy-related genes *LC3* and *Gabarapl1* (Lecker et al., 2004). Several studies point to upregulation of autophagy genes in other cell systems and in different experimental conditions (Juhasz et al., 2007). However, the factors involved in the transcriptional regulation of autophagy genes have not yet been identified.

To characterize the mechanisms that control the autophagic/lysosomal pathway during muscle atrophy in vivo, we first identified autophagy-related genes induced in atrophying muscle and determined whether the Akt-mTOR pathway is involved in the upregulation of some of these genes. Having found that Akt is essential but mTOR is dispensable in suppressing autophagy, we tested the hypothesis that FoxO transcription factors, which play a major role in the activation of the ubiquitin-proteasome system, are also involved in the activation of the autophagic/lysosomal pathway. Gain- and loss-of-function experiments strongly supported a major role of FoxO3, and two targets and mediators of FoxO3, LC3 and Bnip3, were identified. Finally, we addressed the question of whether the induction of autophagy by FoxO3 is secondary to the activation of the ubiquitin-proteasome system and found that the two protein degradation pathways are independently controlled by FoxO3.

RESULTS

Autophagy-Related Genes and Genes Involved in the Regulation of Autophagy Are Induced during Muscle Atrophy

The key ubiquitin ligases *atrogin-1* and *MuRF1* and several other genes of the ubiquitin-proteasome system are upregulated in different models of muscle wasting (Bodine et al., 2001a; Sacheck et al., 2007). We asked whether the induction of atrophy in skeletal muscle is also accompanied by the upregulation of autophagy-related genes. As shown in Figure 1, 1 day of fasting induces the transcription of several autophagy-related genes, including two members of the *Atg8* family, *LC3* and *Gabarapl1*, as well as *Atg4b* and some genes involved in the regulation of autophagy, including *Vps34* (a class III PI3K), *Bnip3*, and *Bnip3l*. Similar changes were observed after 3-day denervation; in this case, two additional autophagy-related genes, *Beclin1* and *Atg12*, were found to be induced (see Figure S1 in the Supplemental Data available with this article online). In agreement with previous studies (Sacheck et al., 2007), fasting and denervation also induced the lysosomal proteinase *cathepsin L* (data not shown). Thus, two different models of muscle atrophy led to increased expression of different genes of the autophagic/lysosomal pathway or genes involved in the regulation of autophagy. Interestingly, four of the most upregulated genes in these models, *LC3*, *Gabarapl1*, *Bnip3*, and *Bnip3l*, are among the atrophy-related genes ("atrogenes") induced in other types of muscle wasting (Lecker et al., 2004).

Autophagy-Related Gene Induction and Autophagosome Formation Are Suppressed by Akt

To identify the signaling pathways responsible for the upregulation of autophagy-related genes, we focused on the role of Akt/PKB, since activation of Akt by growth factors is known to inhibit autophagy in different cell types (Lum et al., 2005). In skeletal muscle, Akt promotes muscle growth by inducing protein synthesis via mTOR (Bodine et al., 2001b; Pallafacchina et al., 2002) and prevents muscle wasting by blocking proteasome protein breakdown through inhibition of FoxO transcription factors (Sandri et al., 2004). To assess the effect of Akt activation on autophagy, we generated a transgenic mouse line in which an Akt-estrogen receptor (Akt-ER) fusion protein can be activated in an inducible manner by tamoxifen specifically in skeletal muscle (Figure S2). In control mice, 1 day of fasting caused dephosphorylation of Akt. In contrast, tamoxifen injection caused Akt-ER phosphorylation, as well as phosphorylation of different Akt targets, including FoxOs and the mTOR effectors 4E-BP1 and S6, even during fasting (Figure 1B). Adult skeletal muscles were transfected with the GFP-LC3 plasmid to monitor autophagosome formation. In agreement with a previous report (Mizushima et al., 2004), GFP-LC3-positive vesicles were rare in adult muscle of fed mice but increased significantly during fasting (Figure 1C; Figure S3). It has been reported that LC3-positive dots sometimes represent protein
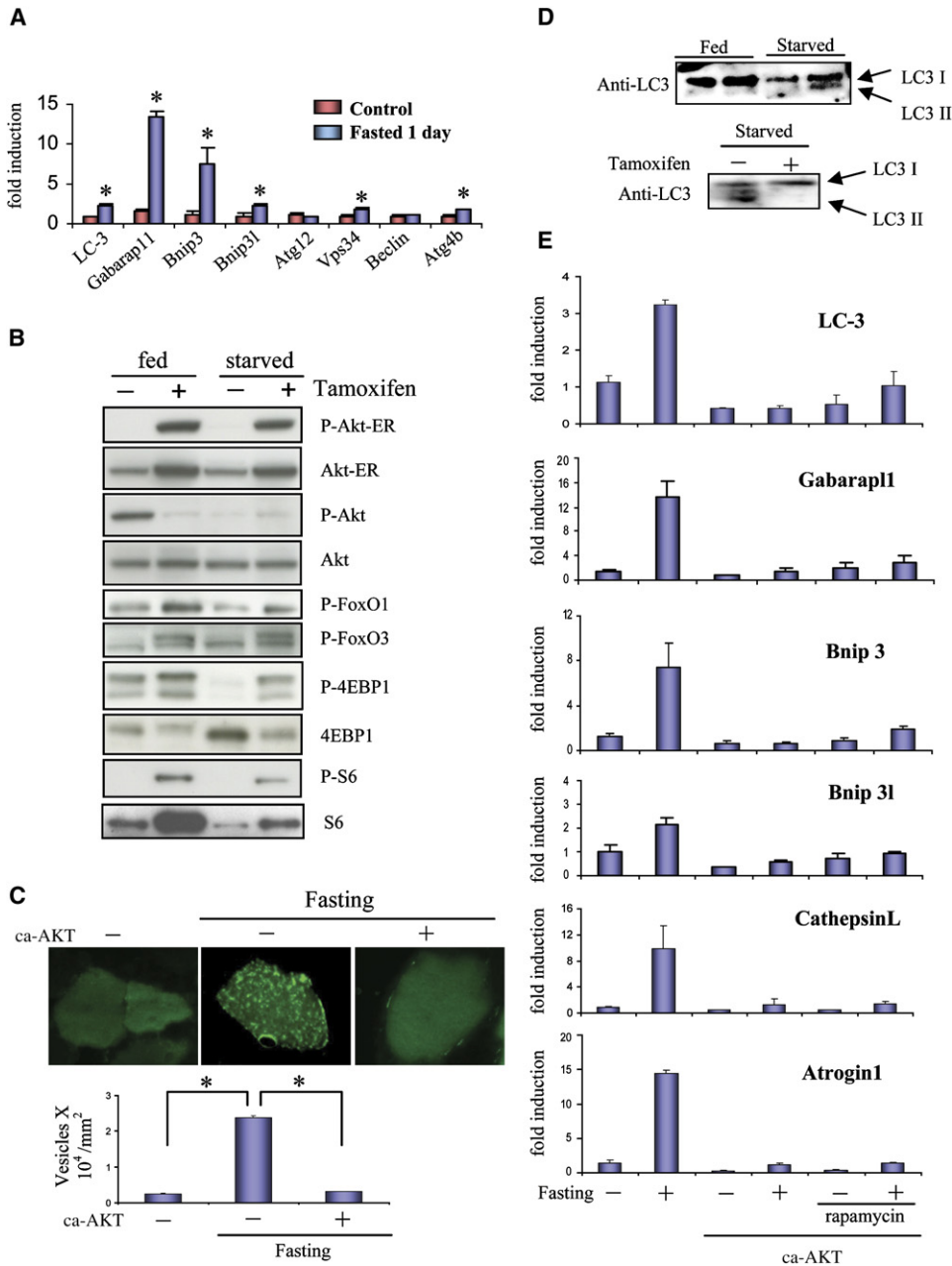
Figure 1. Regulation of Autophagy Genes and Autophagosome Formation in Skeletal Muscle Is Dependent on Akt but Independent of mTOR

(A) Upregulation of autophagy genes in adult tibialis anterior muscle induced by 1 day of fasting. Quantitative PCR analysis was performed in triplicate using specific oligonucleotides (see Table S1). The differences in gene expression levels in control versus fasted animals were statistically significant (*p < 0.001) except for Atg12 and beclin1. Error bars represent SD.

(B) Immunoblotting analysis shows that Akt activation induced by tamoxifen in extensor digitorum longus muscles from *Akt* transgenic mice (described in Figure S2) causes phosphorylation of the Akt targets 4E-BP1, FoxO1, FoxO3, and S6 in muscles from both fed and starved mice.

(C) Autophagosome formation induced by fasting is suppressed by tamoxifen-inducible activated Akt. Adult muscles from *Akt* transgenic mice were transfected by electroporation with a plasmid expressing GFP-LC3. Eight days later, mice were treated with tamoxifen or vehicle and fasted for 24 hr before sacrifice. Myofibers expressing GFP-LC3 were analyzed by fluorescence microscopy. Autophagosomes were quantified by counting GFP-LC3-positive dots and normalizing for cross-sectional area. Values represent means of four different experiments; error bars represent SEM. *p < 0.001.

(D) Immunoblotting for LC3 shows that the amount of LC3-I (upper band) is decreased and conversion of LC3-I to LC3-II is induced in starved muscles (upper panel). LC3 lipidation is blocked by tamoxifen treatment (lower panel).

(E) Akt blocks the induction of LC3, Gabarapl1, Bnip3, Bnip3l, cathepsin L, and atrogin-1 transcripts by fasting, and this effect is not reversed by rapamycin treatment. Error bars represent SD.

aggregation rather than autophagy (Kuma et al., 2007). However, we did not observe such structures in muscles from fed animals, even in highly transfected muscle fibers (Figure 1C; Figure S3). Overexpression of activated Akt in fasting muscle completely abolished the formation of GFP-LC3-positive autophagosomes (Figure 1C; Figure S4) and the conversion of LC3 from the unlipidated species (LC3-I) to the lipidated species (LC3-II) (Figure 1D). Furthermore, Akt prevented the increase in transcript levels of *LC3*, *Gabarapl1*, *Bnip3*, *Bnip3l*, *cathepsin L*, and *atrogin-1* induced by fasting (Figure 1E) or denervation (Figure S5). These results support the conclusion that Akt has a major role in the transcriptional control of the autophagy program in skeletal muscle in vivo and raise the question of which downstream pathways mediate the effect of Akt. To address this issue, we first examined the role of a major Akt effector, the kinase mTOR, which is known to suppress autophagy in different cell systems.

Autophagy-Related Genes and Autophagic Vesicles Are Not Induced by Rapamycin in Skeletal Muscle

To determine whether the repressive effect of Akt on the fasting-dependent upregulation of autophagy-related genes is mediated by mTOR, we examined the effect of the mTOR inhibitor rapamycin on these genes' expression. As shown in Figure 1E, rapamycin did not reverse the effect of Akt on autophagy-related genes or on *cathepsin L* and *atrogin-1* gene expression. Accordingly, rapamycin did not induce autophagosome formation in *Akt* transgenic mice or control mice (Figure 2A). In our system, rapamycin caused complete dephosphorylation of S6K and S6, as well as 4E-BP1, confirming efficient mTOR inhibition (Figure 2B). Moreover, rapamycin induced LC3 lipidation in liver, but not in skeletal muscle (Figure S6). To confirm the rapamycin results, we transfected adult muscles with vectors producing shRNAs specific for mTOR. Two different shRNAs effectively knocked down mTOR expression (Figure 2C) and caused dephosphorylation of S6, without altering the level of Akt phosphorylation, in transfected muscle fibers of *Akt* transgenic mice (Figure 2D; Figure S7). However, autophagosome formation was not induced by RNAi-mediated knockdown of mTOR (Figure 2E; Figure S7), thus confirming the results with rapamycin.

mTOR Controls Autophagy via the mTORC2 Complex

The mTOR kinase is part of two signaling complexes, referred to as mTOR complex 1 (mTORC1), which is rapamycin sensitive and contains raptor, and mTOR complex 2 (mTORC2), which is rapamycin insensitive and contains rictor. Inactivation of mTORC2 induced by rictor knockout has revealed that mTORC2 is required for signaling to Akt-FoxO but not to S6K1, which is a target of mTORC1 (Guertin et al., 2006). To explore the role of the mTORC2 pathway in skeletal muscle, we used two plasmid vectors producing shRNAs specific for rictor. Both shRNAs knocked down rictor expression (Figure 2F) and, when

cotransfected in vivo with plasmids coding for FoxO3, induced FoxO3 nuclear translocation in transfected myofibers, supporting the notion that mTORC2 affects FoxO signaling (Figure 2G). Accordingly, we observed that RNAi-mediated knockdown of rictor induced a significant increase in autophagosome formation in skeletal muscle (Figure 2H) and that this effect was abrogated by constitutively active Akt (ca-Akt) in both the absence (Figure S8) and the presence of rapamycin (Figure 2I). Taken together, these results indicate that fasting-induced autophagosome formation and autophagy-gene upregulation are independent of mTORC1 but partially dependent on mTORC2 and suggest that the Akt-FoxO pathway may be involved in the control of autophagy.

FoxO3 Induces Autophagy and Lysosomal Protein Breakdown in Muscle Fibers

To directly determine the role of FoxO transcription factors in autophagy, we first examined the effect of constitutively active FoxO3 (ca-FoxO3) on autophagosome formation, as we had previously shown that ca-FoxO3 causes dramatic muscle atrophy in vivo (Sandri et al., 2004). Cotransfection with ca-FoxO3 and GFP-LC3 was found to induce a large number of fluorescent puncta in single cultured fibers isolated from adult skeletal muscle, in myofibers of fed live mice as shown by two-photon microscopy, and in muscle sections (Figures 3A–3C). Induction of autophagy by ca-FoxO3 was confirmed by electron microscopy of muscles cotransfected with ca-FoxO3 and GFP. By applying a fixation-embedding procedure that allows preservation of GFP fluorescence, we found that transfected fibers were filled with autophagic vacuoles (Figure 3D). Atrophic muscle fibers containing accumulations of large autophagosomes were also seen frequently in transfected muscles processed by conventional fixation-embedding procedures (Figure 3E), whereas they were not observed in control muscles transfected with GFP plasmids (data not shown). The notion that FoxO3 activates the autophagic/lysosomal system in skeletal muscle cells is supported by studies on cultured C2C12 muscle cells showing that FoxO3 overexpression markedly increases LC3 lipidation (Figure 3F) and that a major fraction (about 70%) of the protein breakdown induced by FoxO3 is lysosomal dependent because it is blocked by concanamycin A, a specific inhibitor of the lysosomal proton pump (Figure 3G).

FoxO3 Is Required for Fasting-Induced Autophagy

To determine whether FoxO3 is required for the induction of autophagy by fasting, we used a dominant-negative *FoxO3* mutant (dn-FoxO3) that was previously found to prevent the upregulation of *atrogin-1* and muscle cell atrophy induced by dexamethasone (Sandri et al., 2004). As shown in Figure 4A, dn-FoxO3 markedly inhibits autophagosome formation induced by fasting in adult skeletal muscle. Similar results were obtained using two different siRNA sequences against FoxO3 (Figure 4B). The result of the RNAi experiments was validated by a rescue experiment in which we used a human *FoxO3* cDNA. There are
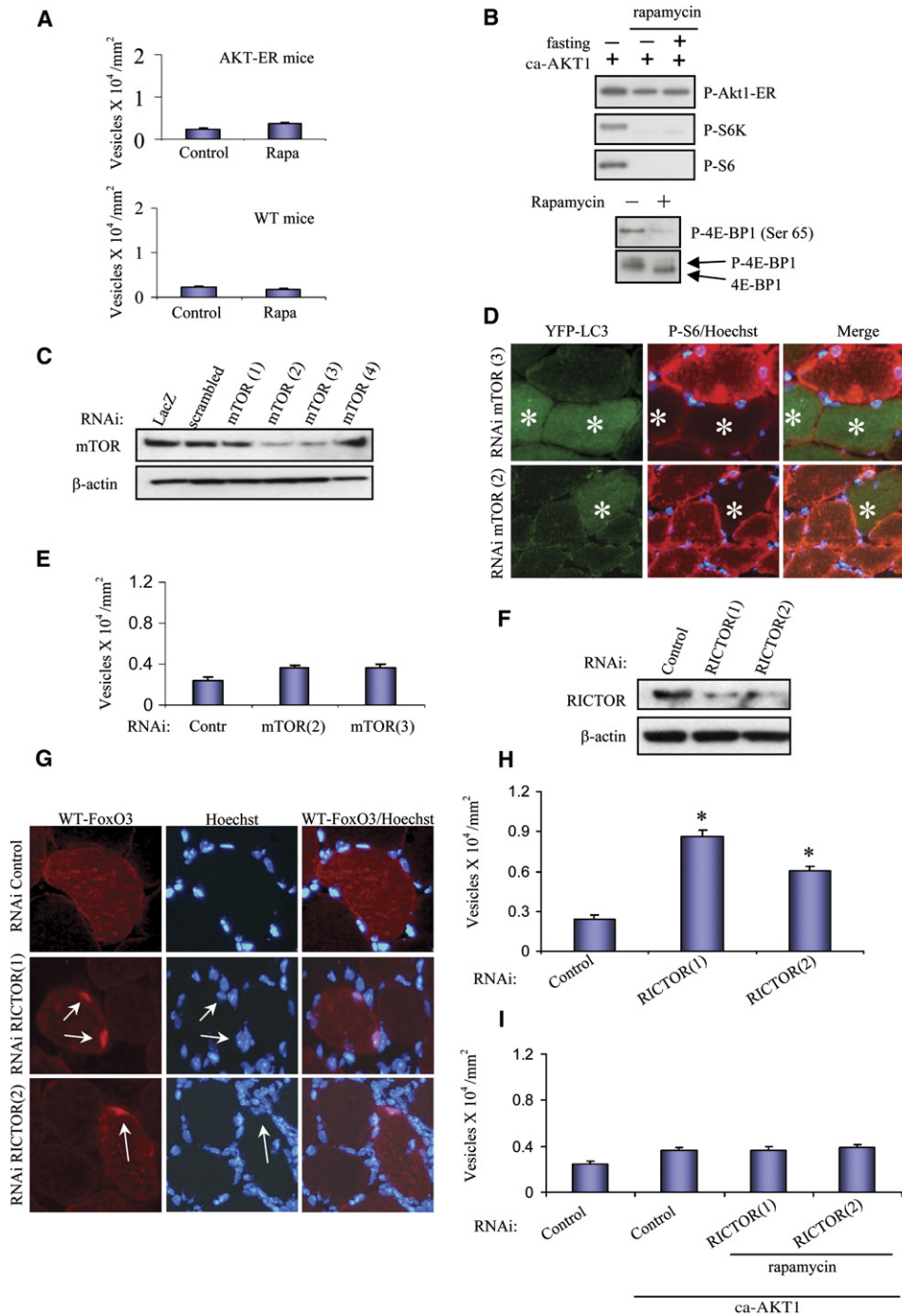
Figure 2. mTOR Regulates Autophagy via the mTORC2 Complex

(A) Autophagosome formation is not induced by rapamycin in skeletal muscle. Muscles from *Akt* transgenic mice (AKT-ER) (upper panel) and wild-type mice (lower panel) were transfected with GFP-LC3, and 7 days later, mice were treated with rapamycin for 4 days as described in Experimental Procedures. Fluorescent autophagosomal vesicles were counted as in Figure 1C.

(B) Rapamycin causes suppression of mTOR activity in *Akt* transgenic mice (upper panel) and control mice (lower panel) as shown by complete dephosphorylation of the Akt targets S6K, S6, and 4E-BP1.

(C) RNAi-mediated knockdown of mTOR revealed by immunoblotting. Murine embryonic fibroblasts (MEFs) were transfected with vectors expressing four different mTOR shRNAs.

(D) Immunostaining for anti-phospho-S6 shows that the mTOR downstream target S6 is dephosphorylated in muscle fibers in which mTOR is knocked down. Skeletal muscles of adult *Akt* transgenic mice were cotransfected with YFP-LC3 and mTOR shRNAs 2 and 3.

(E) Autophagosome formation is not induced by mTOR knockdown. Adult skeletal muscles were transfected with YFP-LC3 and mTOR shRNAs 2 or 3. Vesicles were counted as in Figure 1C.

FoxO3 Regulates *LC3* Gene Expression in Skeletal Muscle

Having shown that FoxO3 is necessary and sufficient for the induction of autophagy, we asked whether FoxO3 is directly involved in the transcriptional regulation of autophagy-related genes and first focused on *LC3*, a typical autophagy-related gene of the *Atg8* family. We identified three putative FoxO binding sites in the promoter region of the *LC3* gene. The ability of FoxO3 to bind to the most proximal FoxO site in the *LC3* promoter was tested by chromatin immunoprecipitation (ChIP) assays in skeletal muscle nuclei. Overexpressed ca-FoxO3 and endogenous FoxO3 were found to interact with the *LC3* promoter (Figure 5A; Figure S11). Furthermore, fasting increased FoxO3 binding and histone acetylation at this site. To determine the functional role of FoxO3 binding, the region of the *LC3* promoter containing the proximal FoxO site was cloned upstream of a minimal *SV40* promoter into a luciferase reporter vector and used for in vivo transfection in skeletal muscle. ca-FoxO3 activates the *LC3* promoter in transfected muscles, but not the promoter in which the FoxO site was mutated (Figure 5B). In contrast, dn-FoxO3 strongly inhibited the *LC3* promoter (Figure 5C), and FoxO3 inhibition by either dn-FoxO3 or RNAi decreased LC3 protein in transfected cells (Figure 5D). To determine whether the transcriptional regulation of *LC3* by FoxO3 is physiologically relevant, we cotransfected skeletal muscles with ca-FoxO3 and LC3 shRNAs. Muscle atrophy induced by ca-FoxO3 was significantly decreased, but not completely abolished, by LC3 knockdown (Figure 5E).

FoxO3-Induced Autophagy Is Modulated by Bnip3

We subsequently focused on *Bnip3* and *Bnip3l*, which are among the most induced atrogenes in different types of muscle wasting and have been shown to control autophagy in other cell systems (Hamacher-Brady et al., 2007; Tracy et al., 2007). We observed that several potential binding sites for FoxO transcription factors are present in the *Bnip3* and *Bnip3l* promoters and found that FoxO3 binding to *Bnip3* and *Bnip3l* promoters increased in fasting muscle as determined by ChIP experiments (Figure 6A). The notion that FoxO3 may control the expression of Bnip3 was strongly supported by the finding that ca-FoxO3 induced Bnip3 and Bnip3l expression (Figure 6B). Conversely, FoxO3 inhibition by dn-FoxO3 or shRNAs reduced Bnip3 protein level (Figure 6C). Importantly, overexpression of Bnip3 or Bnip3l was sufficient to induce autophagosome formation in normal skeletal muscle (Figure 6D). Next, we examined whether Bnip3, which is strongly upregulated in fasting muscle, is required for the induction of the autophagy process. Two siRNA sequences, one of which is shown in Figure 6E and the other of which was reported in a previous study (Hamacher-Brady et al., 2007), were used in these experiments. Bnip3 knockdown strongly reduced both the formation of GFP-LC3-positive autophagosomes and LC3 lipidation (Figures 6F and 6G) induced by ca-FoxO3 in skeletal muscle. In addition, autophagosome formation induced by fasting was also markedly reduced, though not completely abolished, by Bnip3 knockdown (Figure 6H). Thus, Bnip3 induction by FoxO3 appears to play a major role in autophagosome formation during muscle atrophy.

Autophagy Is Not Impaired by Inhibition of the Ubiquitin-Proteasome System

FoxO transcription factors are known to control the expression of the ubiquitin ligases atrogin-1 and MuRF1 and the activation of the ubiquitin-proteasome system, a major pathway involved in muscle protein degradation and muscle atrophy (Stitt et al., 2004). We therefore asked whether the induction of autophagy by FoxO3 is due to a direct effect or is secondary to the activation of the ubiquitin-proteasomal pathway. To determine whether autophagy is dependent on the activity of the muscle-specific ubiquitin ligases, skeletal muscles of *atrogin-1* and *MuRF1* knockout mice were transfected with GFP-LC3, and 7 days later, the mice were fasted for 24 hr. As shown in Figures 7A and 7B, autophagosome formation was unaffected by loss of these genes. To determine whether autophagy is dependent on proteasome function, we used the proteasome inhibitor MG262. The induction of GFP-LC3-positive autophagosomes by ca-FoxO3 was unaffected by treatment with MG262 (Figure 7C). To demonstrate the efficacy of MG262 treatment in blocking proteasome function in vivo, skeletal muscles of control and MG262-treated mice were transfected with the

three mismatches between the mouse FoxO3(2) siRNA sequence and the corresponding human sequence; therefore, human FoxO3 should not be silenced by the mouse siRNA. In fact, cotransfection of human *FoxO3* cDNA restored autophagy in muscle fibers in which mouse FoxO3 was knocked down (Figure 4C). Since FoxO1 has been reported to inhibit mTOR signaling in skeletal muscle (Southgate et al., 2007), we explored whether the same is true for FoxO3. However, phosphorylation of S6 was not affected by ca-FoxO3 or dn-FoxO3 (Figures S9 and S10).

(F) RNAi-mediated knockdown of rictor revealed by immunoblotting. MEFs were transfected with vectors expressing two different shRNAs against rictor.

(G) Anti-HA immunostaining shows that FoxO3 is dephosphorylated and is translocated into the nucleus of myofibers of adult muscles transfected with wild-type HA-FoxO3 and pSUPER vectors expressing shRNAs against rictor.

(H) Knockdown of rictor activates autophagy in mice. Adult skeletal muscles were cotransfected with YFP-LC3 and shRNAs against rictor. Seven days later, YFP-positive vesicles were quantified. *p < 0.001.

(I) Overexpression of constitutively active Akt (ca-Akt) blocks autophagosome formation induced by mTORC2 inhibition. Skeletal muscles of adult transgenic mice were cotransfected with YFP-LC3 and RNAi vectors against rictor. Mice were treated with tamoxifen and with rapamycin as described in Figure 1D.
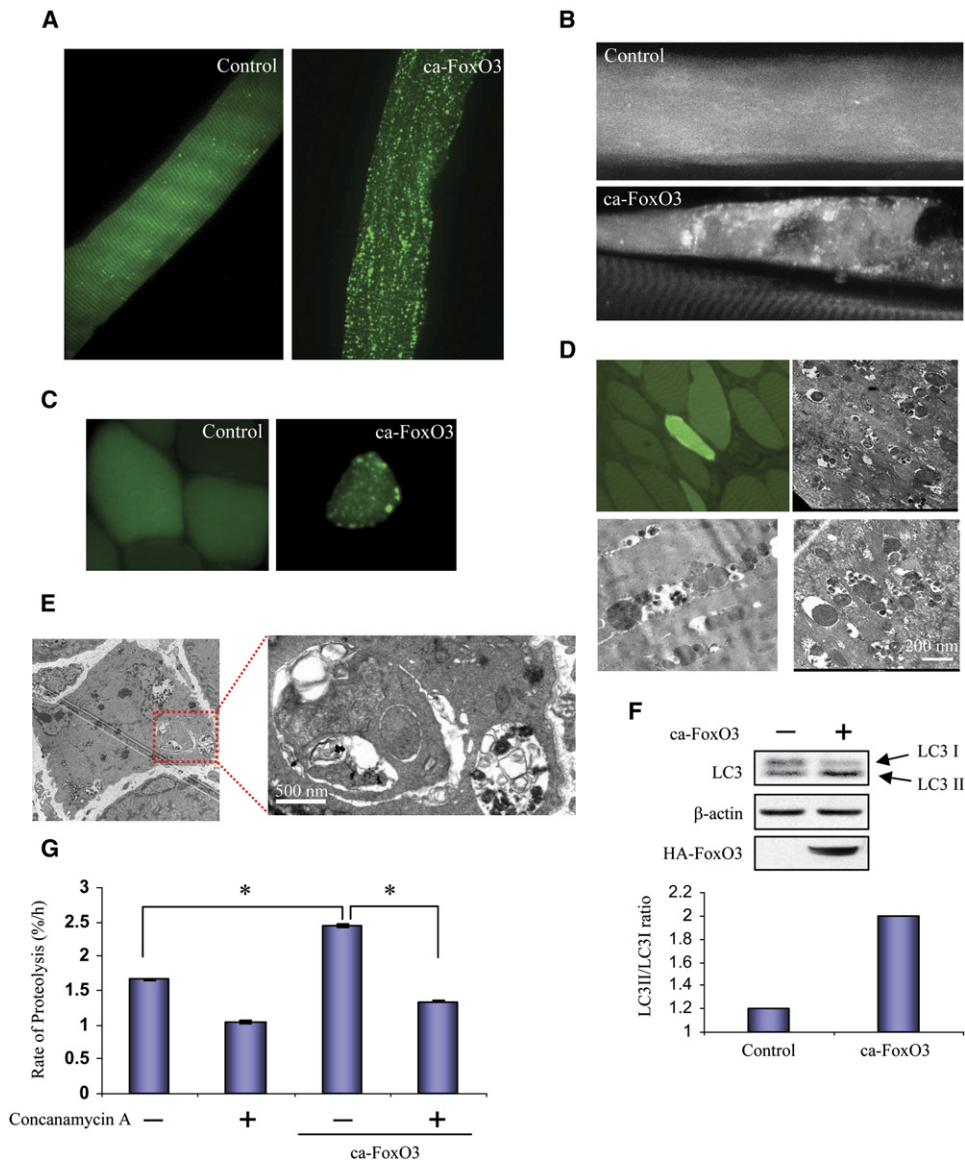
Error bars represent SEM.

Figure 3. Autophagosome Formation Is Induced in Adult Skeletal Muscle by Constitutively Active FoxO3

(A) Isolated single myofibers were transfected with GFP-LC3 and either constitutively active FoxO3 (ca-FoxO3) or mock vector and placed in cell culture. Forty-eight hours later, GFP-positive fibers were analyzed for autophagosome formation by confocal microscopy.

(B) Imaging of FoxO3-mediated autophagosome formation in muscles of live mice. Adult tibialis anterior muscle was transfected with GFP-LC3 and either ca-FoxO3 or mock vector. Two weeks later, muscle was exposed and observed in situ using two-photon microscopy as described in Experimental Procedures.

(C) Adult muscles were transfected with GFP-LC3 and either ca-FoxO3 or mock vector (control). Two weeks later, muscles were collected and analyzed for fluorescent vesicle formation.

(D) Electron micrographs of ca-FoxO3-transfected fibers. Adult muscles were cotransfected with GFP and ca-FoxO3. Atrophic GFP-positive fibers identified in the semithin section (upper left panel) show numerous autophagosomes when analyzed by electron microscopy (upper right and lower panels).

(E) Electron micrograph from a muscle transfected with ca-FoxO3 processed using standard fixation-embedding procedures. Note the large autophagosomes in an atrophic myofiber. The boxed area in the left panel is shown at higher magnification in the right panel.

(F) C2C12 myotubes were infected with control or ca-FoxO3 adenoviruses. Twenty-four hours later, cells were treated with concanamycin A (0.1 μM) to prevent LC3-II degradation. FoxO3 induces an increase in conversion of LC3-I to LC3-II (upper panel). Quantification of the LC3 conversion ratio (LC3-II/LC3-I) is shown in the lower panel.

(G) ca-FoxO3 increases lysosomal proteolysis in C2C12 cells, and this increase is almost completely abolished by the lysosomal inhibitor concanamycin A. *p < 0.001. Error bars represent SEM.
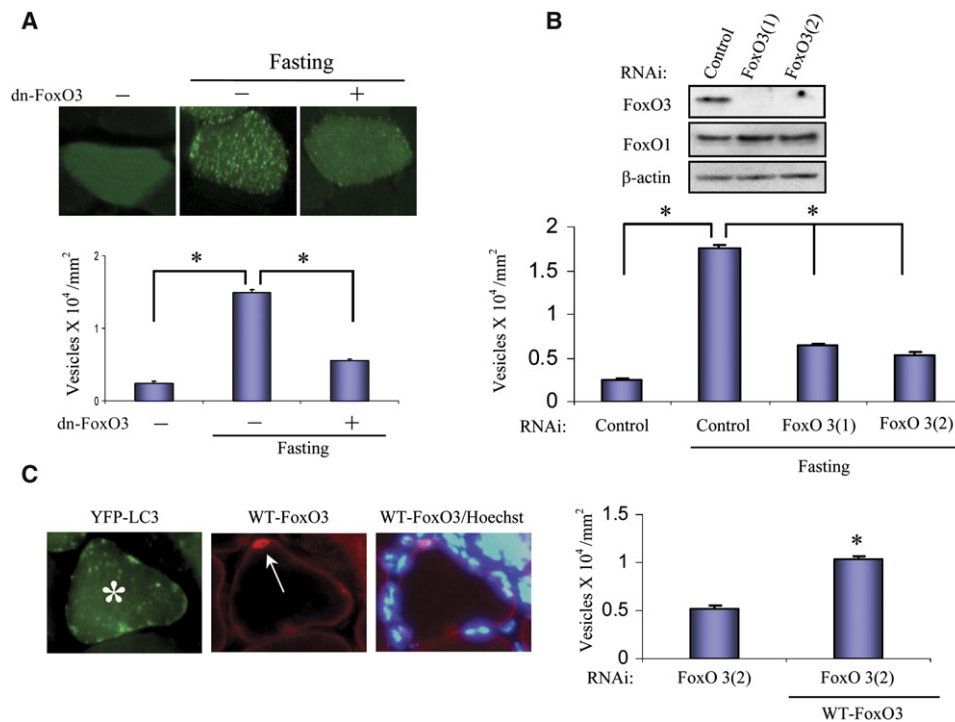
Figure 4. Fasting-Induced Autophagy Is Blocked by Dominant-Negative FoxO3 and by RNAi-Mediated FoxO3 Knockdown
(A) Autophagosome formation induced by fasting is blocked by dominant-negative FoxO3 (dn-FoxO3). Adult muscles were cotransfected with GFP-LC3 and dn-FoxO3 or control vector, and GFP-positive vesicles were quantified. *p < 0.001.
(B) RNAi-mediated knockdown of FoxO3 inhibits autophagosome formation during fasting. Upper panel: immunoblotting analyses confirmed that pSUPER vectors expressing shRNA against FoxO3 were effective in blocking FoxO3 but not FoxO1. Lower panel: adult muscles were transfected with YFP-LC3 together with control shRNA or two different FoxO3-specific shRNAs. One week later, mice were fasted for 24 hr, and fluorescent vesicles were quantified as in Figure 1C. *p < 0.001.
(C) Inhibition of autophagosome formation induced by FoxO3 RNAi is rescued by overexpression of human FoxO3. Adult skeletal muscles were cotransfected with YFP-LC3, wild-type human FoxO3, and a shRNA specific for mouse FoxO3. Seven days later, mice were fasted for 24 hr. Vesicle formation is detected only in a myofiber positive for FoxO3 (asterisk). Anti-FoxO3 immunofluorescence confirms FoxO3 nuclear translocation during fasting (arrow). Quantification of rescued fibers (shown at right) was performed as described above. *p < 0.001.
Error bars represent SEM.

short-lived UbG76V-GFP reporter, using cotransfection with histone 2B-RFP to identify transfected fibers (Lindsten et al., 2003). As shown in Figure 7D, GFP fluorescence was detected in transfected fibers of MG262-treated mice, but not in transfected fibers of control mice, thus confirming that proteasome function is effectively repressed by the inhibitor in vivo. These findings indicate that FoxO3 controls the ubiquitin-proteasomal and autophagic/lysosomal pathways independently.

DISCUSSION

Autophagy is a fundamental mechanism essential for cell survival in all eukaryotic organisms. Cultured mammalian cells die rapidly if autophagy is inhibited following nutrient deprivation or growth-factor withdrawal (Lum et al., 2005), and mice deficient in the *Atg5* or *Atg7* autophagy genes do not survive the early neonatal starvation period (Komatsu et al., 2005; Kuma et al., 2004). However, the mechanisms responsible for the induction and regulation of the autophagy program are poorly understood. In particular,

although there is evidence that autophagy genes are upregulated during the activation of the autophagic/lysosomal pathway in different species (see Introduction), the transcription factors responsible for the induction of these genes are unknown. The present study, based primarily on in vivo analyses in skeletal muscle, identifies a FoxO3-Bnip3 pathway as a major player in the transcriptional regulation of autophagy-related genes. The starting point of this investigation was the demonstration that several autophagy-related genes and genes involved in the regulation of autophagy are upregulated in two models of muscle atrophy, fasting and denervation.

The results presented here, based on gain- and loss-of-function approaches, show that FoxO3 controls the activation of the autophagic/lysosomal pathway during muscle atrophy in vivo. This conclusion is supported by studies in cultured muscle cells showing that FoxO3 stimulates lysosomal proteolysis by inducing autophagy (Zhao et al., 2007 [this issue of *Cell Metabolism*]). A role of FoxO transcription factors in autophagy is also supported by evidence from studies in *C. elegans* and *Drosophila*. In
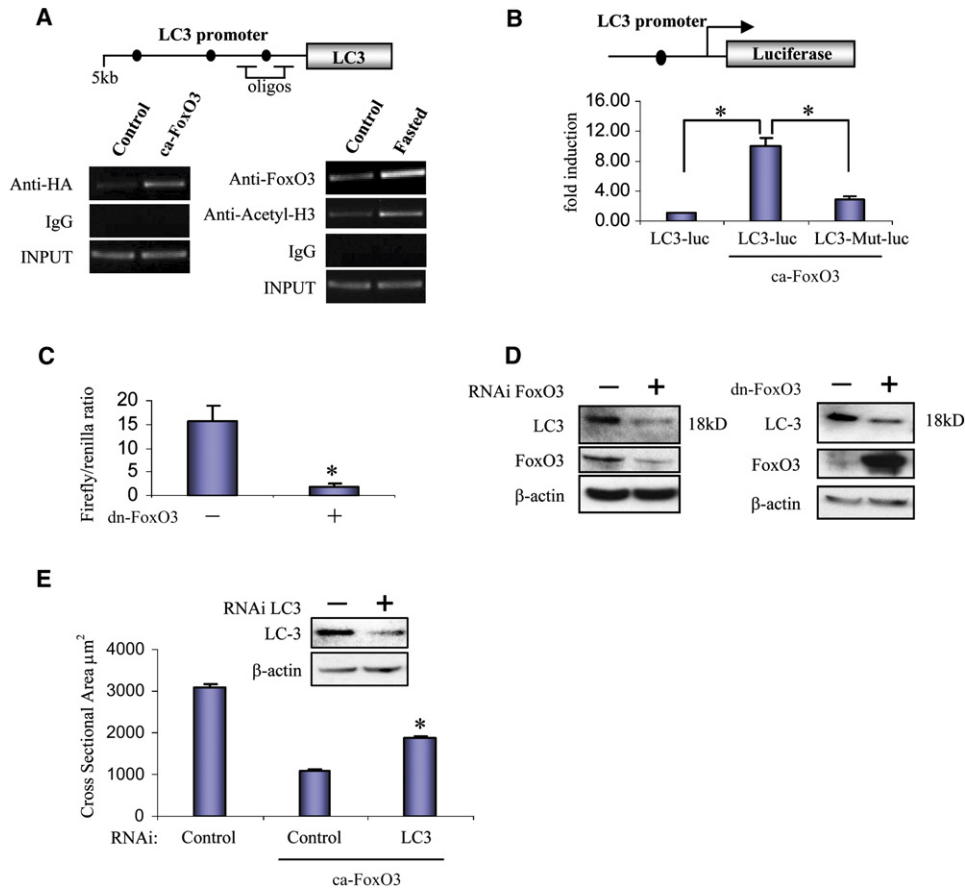
Figure 5. Upregulation of LC3 Is Under FoxO3 Control and Is Required for Muscle Wasting

(A) FoxO3 binds to a FoxO response element in the *LC3* promoter as determined by ChIP, and this binding is increased in skeletal muscle by fasting.
(B) ca-FoxO3 activates an *LC3* promoter-reporter construct, but not a construct in which the FoxO binding site is mutated. A plasmid coding for the region of the *LC3* promoter containing the proximal FoxO site or the mutated one linked to a minimal *SV40* promoter and a luciferase reporter was transfected into adult tibialis anterior muscle in the presence or absence of ca-FoxO3. A renilla luciferase construct was cotransfected to normalize for transfection efficiency. Eight days later, firefly/renilla luciferase activity was determined. *p < 0.001. Error bars represent SD.
(C) The activity of the LC3 reporter is suppressed by dn-FoxO3. Experimental conditions were as in (B). Error bars represent SD.
(D) FoxO3 inhibition by RNAi against FoxO3 or by dn-FoxO3 reduces LC3 protein level. MEFs were transfected with either shRNA specific for mouse FoxO3 or a vector expressing dn-FoxO3 and analyzed by immunoblotting against LC3 and FoxO3. Note that the signal with FoxO3 antibodies is decreased by FoxO3 RNAi and increased by overexpression of dn-FoxO3.
(E) Muscle atrophy induced by FoxO3 is reduced by LC3 RNAi. Adult skeletal muscles were transfected with shRNA specific for mouse LC3 or GFP with or without HA-tagged ca-FoxO3 and examined after 2 weeks. Cross-sectional area of transfected fibers, identified by anti-HA immunofluorescence, was measured as described previously (Sandri et al., 2004). *p < 0.001. Error bars represent SEM.

response to nutrient deprivation, nematodes undergo dauer formation, a stage of development arrest, and autophagy genes are essential for dauer formation, which is controlled positively by daf-16 (the *C. elegans* homolog of FoxO) and negatively by Akt (Melendez et al., 2003). Accordingly, a recent study has shown that flies that have mutated *DFoxO* cannot activate autophagy in response to starvation, while *DFoxO* overexpression is sufficient to activate autophagy (Juhasz et al., 2007).

FoxO3 was previously shown to control the ubiquitin-proteasome pathway by upregulating two crucial ubiquitin ligases, *atrogin-1* and *MuRF1* (Sandri et al., 2004; Stitt et al., 2004). We show here that the effect of FoxO3 on autophagy is not affected by deficiency of these two genes

or by inhibition of proteasome function, suggesting that FoxO3 controls the two major cellular catabolic pathways, the ubiquitin-proteasomal pathway and the autophagic/lysosomal pathway, independently. This interpretation is consistent with the finding that proteasome function is not affected by loss of autophagy in the brain (Komatsu et al., 2006). On the other hand, protein breakdown via the proteasome and lysosome is likely to proceed in a coordinated manner in different models of muscle atrophy, in which the degradation of myofibrillar proteins via the proteasome proceeds in parallel with the disposal of mitochondria and sarcoplasmic reticulum membranes via the autophagic/lysosomal pathway. This could well be explained by the existence of a common transcription factor
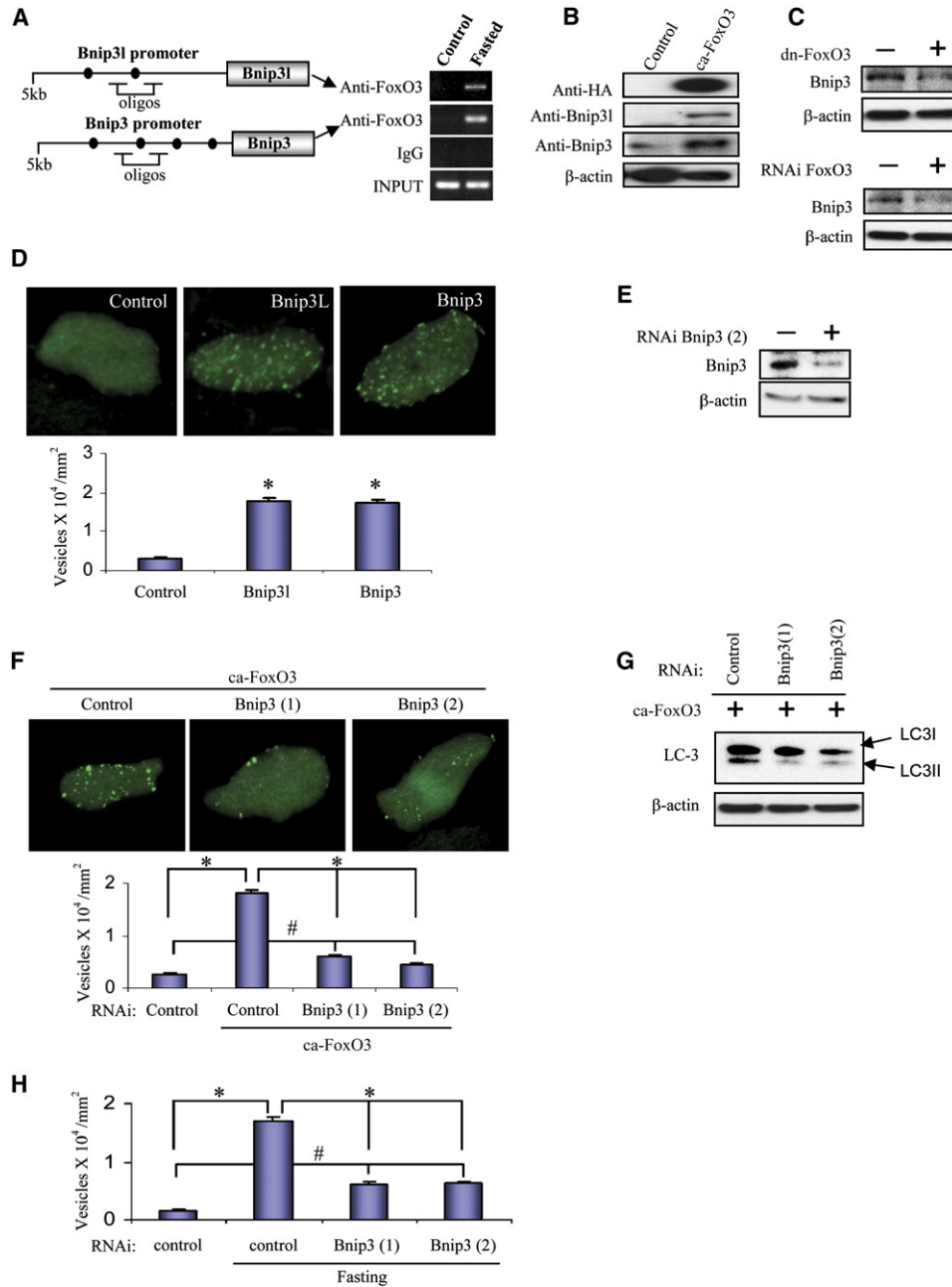
Figure 6. *Bnip3* Genes Are Controlled by FoxO3 and Mediate the Effect of FoxO3 on Autophagy
(A) FoxO3 binding to a FoxO response element in the *Bnip3l* and *Bnip3* promoters, as determined by ChIP, is increased by fasting.
(B) ca-FoxO3 induces Bnip3 and Bnip3l protein expression in HEK293 cells as determined by western blotting.
(C) FoxO3 inhibition by RNAi or by d.nFoxO3 reduces Bnip3 protein detected by immunoblotting.
(D) Bnip3 and Bnip3l induce the formation of autophagic vesicles in skeletal muscle. Adult muscles were cotransfected with GFP-LC3 and Bnip3 or Bnip3l expression plasmids, and LC3-positive vesicles were quantified as in Figure 1C. *p < 0.001.
(E) Immunoblotting analysis shows reduced Bnip3 protein levels after transfection of MEFs with a pSUPER vector expressing shRNA against Bnip3.
(F) Bnip3 inhibition by RNAi blocks FoxO3-mediated autophagosome formation. Adult skeletal muscles were cotransfected with vectors expressing YFP-LC3, ca-FoxO3, and shRNAs against Bnip3, and YFP-positive vesicles were quantified. *p < 0.001; #p < 0.001.
(G) Conversion of LC3-I to LC3-II induced by ca-FoxO3 is prevented by RNAi against Bnip3 in MEFs.
(H) RNAi-mediated knockdown of Bnip3 inhibits autophagosome formation during fasting. Adult skeletal muscles were cotransfected with YFP-LC3 and vectors expressing shRNA against Bnip3. Seven days later, mice were fasted for 24 hr and YFP-positive vesicles were quantified. *p < 0.001; #p < 0.001.
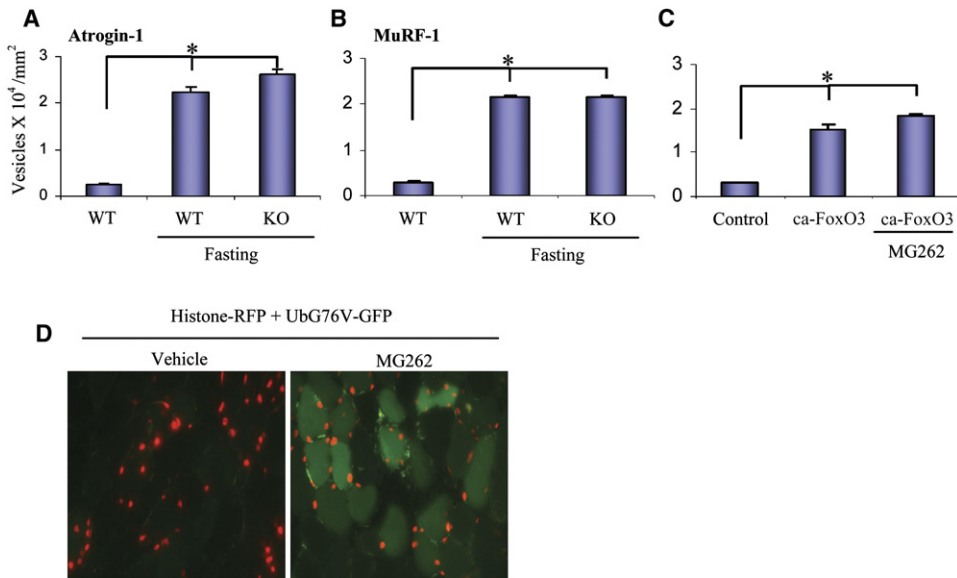Error bars represent SEM.

Figure 7. Autophagosome Formation Is Not Impaired by Loss of Muscle-Specific Ubiquitin Ligases or Blockade of the Proteasome
(A and B) Fasting-induced autophagy is not impaired in adult skeletal muscle of *atrogin-1* null (A) or *MuRF1* null (B) mice. Mice were transfected with GFP-LC3. Seven days later, mice were fasted for 24 hr and GFP-positive vesicles were quantified. *p < 0.001.
(C) FoxO3-induced autophagosome formation is not impaired by proteasome inhibition with MG262. Muscles of wild-type mice were transfected with GFP-LC3 and ca-FoxO3. MG262 was injected daily for the last 4 days before sacrifice, and GFP-positive vesicles were counted. *p < 0.001.
(D) Validation of the efficacy of the proteasome inhibitor MG262. Adult skeletal muscles were cotransfected with histone 2B-RFP and UbG76V-GFP. Transfected myofibers are revealed by the presence of red nuclei. The mutated ubiquitin is targeted to proteasomal degradation, and the GFP fluorescence is not detected in transfected myofibers but is revealed when proteasome function is inhibited by MG262 treatment.
Error bars represent SEM.

that orchestrates muscle atrophy by controlling both pathways, although other possible mechanisms of interaction between the two pathways remain to be established. Autophagy is a fundamental mechanism of survival during starvation, and the results reported here support a role of FoxO factors as master regulators of the transcriptional adaptations of the organism to starvation. In fact, the increased muscle protein catabolism induced by FoxO3 contributes amino acids that are used for glucose production by the liver, where FoxO1 has been shown to control gluconeogenesis gene expression (Puigserver et al., 2003).

A surprising finding of this study is that mTOR does not appear to play a significant role in the activation of the autophagic/lysosomal pathway during muscle atrophy. Previous studies have shown that the mTOR inhibitor rapamycin induces autophagy in many cell types (Lum et al., 2005). However, mTOR-independent autophagy has also been reported in different cell systems, including cultured muscle cells (Kochl et al., 2006; Mordier et al., 2000; Sarkar et al., 2007; Yamamoto et al., 2006). We found that autophagy is unaffected in skeletal muscle when mTOR activity is blocked by rapamycin or by mTOR knockdown, conditions in which S6 phosphorylation is completely blocked. Furthermore, rapamycin was not able to reverse the inhibitory effect of activated Akt in preventing the upregulation of autophagy-related genes induced by fasting. mTOR is part of two multiprotein complexes: mTORC1, which contains

raptor and is rapamycin sensitive, is required for signaling to S6K and 4E-BP1, while mTORC2, which contains rictor, is required for signaling to Akt-FoxO (Guertin et al., 2006). Our finding that mTORC2 inhibition by RNAi against rictor results in FoxO3 translocation and autophagy induction is consistent with the role of FoxO. The finding that autophagy can be induced by rictor knockdown but not by mTOR knockdown could be explained by the existence of a negative feedback effect of S6K on Akt activity (Aguilar et al., 2007). Thus, the two mTOR complexes may have opposite effects on Akt activity.

An additional factor that complicates the interpretation of the effect of rapamycin is that long-term rapamycin treatment in vitro can also inhibit the mTORC2 complex in some cell types and thus potentially affect the Akt-FoxO pathway (Sarbassov et al., 2006). This raises the possibility that, under certain circumstances, rapamycin may induce autophagy not through a direct effect—e.g., by blocking mTOR phosphorylation of specific components of the autophagy machinery—but through an indirect transcriptional effect by inhibiting Akt and thus derepressing FoxO. However, in our in vivo system, rapamycin treatment did not affect Akt phosphorylation (Figure 2B) but blocked mTORC1, as revealed by S6K and S6 dephosphorylation. The discrepancy between the results presented here and previous studies with respect to the role of mTOR in autophagy might also reflect the slower pace of autophagy in vivo, based on

transcription-dependent regulation via FoxO3, compared to the rapid pace of autophagy in some in vitro systems, based on transcription-independent regulation via mTOR. The complexity of the regulatory networks controlling autophagy is also illustrated by the paradoxical and still unexplained finding that Vps34 has been suggested to be a positive effector in both autophagy and mTORC1 signaling (Nobukuni et al., 2007).

The mechanism of FoxO3 effect on autophagy remains to be determined; however, our results on the transcriptional regulation of the autophagy-related gene *LC3* and the autophagy-regulatory genes *Bnip3* and *Bnip3l* suggest that FoxO3 could act in two ways. The upregulation of LC3 is unlikely to be relevant to the induction of autophagy but is likely to be important for the maintenance of this process. In agreement with previous studies (Mizushima et al., 2004), we found that autophagosome formation is not induced by overexpression of GFP-LC3 in fed mice; therefore, LC3 induction per se is not sufficient to trigger autophagy. On the other hand, since LC3 is continuously consumed during the activation of the autophagic/lysosomal pathway that occurs in muscle atrophy, it is likely that the upregulation of LC3 is required to replenish the LC3 protein pool and thus allow the progression of autophagy. LC3 inhibition by RNAi partially blocks muscle atrophy, confirming that autophagy contributes to muscle atrophy and that upregulation of LC3 is physiologically important. In contrast, the upregulation of Bnip3 has a major role in mediating the effect of FoxO3, as shown by the findings that (1) the binding of FoxO3 to the *Bnip3* and *Bnip3l* promoters is increased in fasted muscle, (2) autophagosome formation is induced in normal muscle in vivo by Bnip3 or Bnip3l overexpression, and (3) the induction of autophagy by ca-FoxO3 is markedly decreased by Bnip3 knockdown. The fact that autophagosome formation is not completely abolished by Bnip3 RNAi could be due to the presence of Bnip3l. Bnip3 is a Bcl-2-related BH3-only protein that is induced by hypoxia in cultured cardiomyocytes (Kubasiak et al., 2002) and ischemic regions of tumors (Okami et al., 2004) and was initially implicated in cell death. However, Bnip3 is now emerging as a central player in autophagy signaling. Bnip3 inhibition using a dominant-negative *Bnip3* mutant blocks autophagy in cardiomyocytes during ischemia-reperfusion injury (Hamacher-Brady et al., 2007), and knockdown of Bnip3 blocks autophagy in hypoxic tumor cells (Tracy et al., 2007). Conversely, overexpression of Bnip3 increases autophagy in these same cell systems (Hamacher-Brady et al., 2007; Tracy et al., 2007). In agreement with the results presented here, Bnip3l has been shown to be under the control of FoxO3 in breast cancer cell lines (Real et al., 2005).

In conclusion, our results point to a FoxO3-Bnip3 pathway as a major regulatory pathway of autophagy in skeletal muscle in vivo. Since autophagy is implicated in a variety of pathological processes, a better understanding of the regulatory role of FoxO3 and Bnip3 in autophagy in different cell systems will be important for the treatment of not only muscle wasting disorders but also other diseases, including cancer and neurodegenerative diseases.

EXPERIMENTAL PROCEDURES

Animals and In Vivo Transfection Experiments
Experiments were performed on adult CD1 mice. The inducible transgenic mice are described in Figure S2. In vivo transfection experiments were performed as described previously (Sandri et al., 2004). In some experiments, mice were injected intraperitoneally (i.p.) with 4 mg/kg rapamycin as described previously (Pallafacchina et al., 2002). Mice transfected with the UbG76V-GFP reporter were treated for 4 days with a daily i.p. injection of 150 μl of MG262 (5 μmol/kg) or vehicle only (30% DMSO in 0.9% NaCl).

Plasmids and Antibodies
See Supplemental Experimental Procedures.

Gene Expression Analyses
Total RNA was prepared from skeletal muscle using the Promega SV Total RNA Isolation kit. Complementary DNA generated with Invitrogen SuperScript III reverse transcriptase was analyzed by quantitative real-time RT-PCR using the QIAGEN QuantiTect SYBR Green PCR kit. All data were normalized to β-actin or GAPDH expression. Oligonucleotide primers used are listed in Table S1.

Immunoblotting
Frozen skeletal muscle was pulverized by pestle and mortar, lysed, and immunoblotted as described previously (Sandri et al., 2004). Blots were stripped using Restore western blotting stripping buffer (Pierce) and reprobed if necessary. Antibodies used are listed in Supplemental Experimental Procedures.

Fluorescence Microscopy and Electron Microscopy
Cryosections of muscle transfected with GFP-LC3 were examined using a fluorescence microscope, and fluorescent dots were counted as described previously, normalizing for cross-sectional area (Mizushima et al., 2004). For electron microscopy, we used both conventional fixation-embedding procedures and another procedure based on fixation in paraformaldehyde-glutaraldehyde without osmium and embedding in LR White resin, which allows preservation of GFP fluorescence in semithin 1 μm sections and subsequent analysis of serial thin sections by electron microscopy (Luby-Phelps et al., 2003).

In Vivo Imaging via Two-Photon Microscopy
To monitor autophagosome formation in situ in living animals, muscles were transfected with GFP-LC3 probe, and two-photon microscopy was performed 2 weeks later upon in situ exposure of transfected muscles as described previously (Tothova et al., 2006).

Single-Fiber Analyses
Flexor digitorum brevis muscles from adult mice were digested in type I collagenase at 4°C for 1 hr, at 37°C for 2 hr, and dissociated into single fibers. The fibers were electroporated using a BTX porator (50 volts/4 mm, 3 pulses, 200 ms intervals) to transfer plasmid DNA and then plated on glass coverslips coated with laminin and cultured in Tyrode's salt solution (pH 7.3) containing 10% fetal bovine serum, 50 U/ml penicillin, 50 μg/ml streptomycin, and 5% CO_2 (37°C).

Protein Breakdown Assay
C2C12 myotubes were incubated with [³H]tyrosine 24 hr before infection and then infected with control or ca-FoxO3 virus for 24 hr. After the chase period, new medium containing concanamycin A (0.1 μM) was added, and proteolysis was measured starting 1 hr later (Sacheck et al., 2004). Each point is the average of four plates.

In Vivo RNAi
In vivo RNAi experiments were performed as described previously (Sandri et al., 2004) using at least two difference sequences for each gene. Sequences and plasmids used are listed in Supplemental Experimental Procedures and Table S2. For the validation of shRNA

constructs, murine embryonic fibroblasts (MEFs) were maintained in DMEM/10% FBS and transfected with shRNA constructs using Lipofectamine 2000 (Invitrogen). Cells were lysed 72 hr later, and immunoblotting was performed as described above.

ChIP Assays and Promoter Analyses

We performed ChIP assays on adult skeletal muscle using the Chromatin Immunoprecipitation (ChIP) assay kit (Upstate). Oligonucleotide primers used are listed in Table S3. The LC3 mouse genomic DNA fragment (−1608 to −1379) was amplified by PCR with the same primers and inserted into the KpnI and XhoI sites of pGL3-Promoter vector (Promega). Mutations in the FoxO binding site were generated by PCR using the QuikChange technique (Stratagene) with the primers listed in Table S3. These constructs were transfected into tibialis anterior muscles together with a renilla luciferase vector (pRLTK) to normalize for transfection efficiency as described previously (Sandri et al., 2004).

Supplemental Data

Supplemental Data include Supplemental Experimental Procedures, three tables, and eleven figures and can be found with this article online at http://www.cellmetabolism.org/cgi/content/full/6/6/458/DC1/.

REFERENCES

Aguilar, V., Alliouachene, S., Sotiropoulos, A., Sobering, A., Athea, Y., Djouadi, F., Miraux, S., Thiaudiere, E., Foretz, M., Viollet, B., et al. (2007). S6 kinase deletion suppresses muscle growth adaptations to nutrient availability by activating AMP kinase. Cell Metab. 5, 476–487.

Bechet, D., Tassa, A., Taillandier, D., Combaret, L., and Attaix, D. (2005). Lysosomal proteolysis in skeletal muscle. Int. J. Biochem. Cell Biol. 37, 2098–2114.

Bodine, S.C., Latres, E., Baumhueter, S., Lai, V.K., Nunez, L., Clarke, B.A., Poueymirou, W.T., Panaro, F.J., Na, E., Dharmarajan, K., et al. (2001a). Identification of ubiquitin ligases required for skeletal muscle atrophy. Science 294, 1704–1708.

Bodine, S.C., Stitt, T.N., Gonzalez, M., Kline, W.O., Stover, G.L., Bauerlein, R., Zlotchenko, E., Scrimgeour, A., Lawrence, J.C., Glass, D.J., et al. (2001b). Akt/mTOR pathway is a crucial regulator of skeletal muscle hypertrophy and can prevent muscle atrophy in vivo. Nat. Cell Biol. 3, 1014–1019.

Cai, D., Frantz, J.D., Tawa, N.E., Jr., Melendez, P.A., Oh, B.C., Lidov, H.G., Hasselgren, P.O., Frontera, W.R., Lee, J., Glass, D.J., et al.

(2004). IKKbeta/NF-kappaB activation causes severe muscle wasting in mice. Cell 119, 285–298.

Gomes, M.D., Lecker, S.H., Jagoe, R.T., Navon, A., and Goldberg, A.L. (2001). Atrogin-1, a muscle-specific F-box protein highly expressed during muscle atrophy. Proc. Natl. Acad. Sci. USA 98, 14440–14445.

Guertin, D.A., Stevens, D.M., Thoreen, C.C., Burds, A.A., Kalaany, N.Y., Moffat, J., Brown, M., Fitzgerald, K.J., and Sabatini, D.M. (2006). Ablation in mice of the mTORC components raptor, rictor, or mLST8 reveals that mmTORC2 is required for signaling to Akt-FOXO and PKCalpha, but not S6K1. Dev. Cell 11, 859–871.

Hamacher-Brady, A., Brady, N.R., Logue, S.E., Sayen, M.R., Jinno, M., Kirshenbaum, L.A., Gottlieb, R.A., and Gustafsson, A.B. (2007). Response to myocardial ischemia/reperfusion injury involves Bnip3 and autophagy. Cell Death Differ. 14, 146–157.

Juhasz, G., Puskas, L.G., Komonyi, O., Erdi, B., Maroy, P., Neufeld, T.P., and Sass, M. (2007). Gene expression profiling identifies FKBP39 as an inhibitor of autophagy in larval Drosophila fat body. Cell Death Differ. 14, 1181–1190.

Kochl, R., Hu, X.W., Chan, E.Y., and Tooze, S.A. (2006). Microtubules facilitate autophagosome formation and fusion of autophagosomes with endosomes. Traffic 7, 129–145.

Komatsu, M., Waguri, S., Ueno, T., Iwata, J., Murata, S., Tanida, I., Ezaki, J., Mizushima, N., Ohsumi, Y., Uchiyama, Y., et al. (2005). Impairment of starvation-induced and constitutive autophagy in Atg7-deficient mice. J. Cell Biol. 169, 425–434.

Komatsu, M., Waguri, S., Chiba, T., Murata, S., Iwata, J., Tanida, I., Ueno, T., Koike, M., Uchiyama, Y., Kominami, E., et al. (2006). Loss of autophagy in the central nervous system causes neurodegeneration in mice. Nature 441, 880–884.

Kubasiak, L.A., Hernandez, O.M., Bishopric, N.H., and Webster, K.A. (2002). Hypoxia and acidosis activate cardiac myocyte death through the Bcl-2 family protein BNIP3. Proc. Natl. Acad. Sci. USA 99, 12825–12830.

Kuma, A., Hatano, M., Matsui, M., Yamamoto, A., Nakaya, H., Yoshimori, T., Ohsumi, Y., Tokuhisa, T., and Mizushima, N. (2004). The role of autophagy during the early neonatal starvation period. Nature 432, 1032–1036.

Kuma, A., Matsui, M., and Mizushima, N. (2007). LC3, an autophagosome marker, can be incorporated into protein aggregates independent of autophagy: caution in the interpretation of LC3 localization. Autophagy 3, 323–328.

Lecker, S.H., Jagoe, R.T., Gilbert, A., Gomes, M., Baracos, V., Bailey, J., Price, S.R., Mitch, W.E., and Goldberg, A.L. (2004). Multiple types of skeletal muscle atrophy involve a common program of changes in gene expression. FASEB J. 18, 39–51.

Lecker, S.H., Goldberg, A.L., and Mitch, W.E. (2006). Protein degradation by the ubiquitin-proteasome pathway in normal and disease states. J. Am. Soc. Nephrol. 17, 1807–1819.

Lindsten, K., Menendez-Benito, V., Masucci, M.G., and Dantuma, N.P. (2003). A transgenic mouse model of the ubiquitin/proteasome system. Nat. Biotechnol. 21, 897–902.

Luby-Phelps, K., Ning, G., Fogerty, J., and Besharse, J.C. (2003). Visualization of identified GFP-expressing cells by light and electron microscopy. J. Histochem. Cytochem. 51, 271–274.

Lum, J.J., DeBerardinis, R.J., and Thompson, C.B. (2005). Autophagy in metazoans: cell survival in the land of plenty. Nat. Rev. Mol. Cell Biol. 6, 439–448.

Melendez, A., Talloczy, Z., Seaman, M., Eskelinen, E.L., Hall, D.H., and Levine, B. (2003). Autophagy genes are essential for dauer development and life-span extension in C. elegans. Science 301, 1387–1391.

Mizushima, N., Yamamoto, A., Matsui, M., Yoshimori, T., and Ohsumi, Y. (2004). In vivo analysis of autophagy in response to nutrient starvation using transgenic mice expressing a fluorescent autophagosome marker. Mol. Biol. Cell 15, 1101–1111.

Mordier, S., Deval, C., Bechet, D., Tassa, A., and Ferrara, M. (2000). Leucine limitation induces autophagy and activation of lysosome-dependent proteolysis in C2C12 myotubes through a mammalian target of rapamycin-independent signaling pathway. J. Biol. Chem. *275*, 29900–29906.

Nobukuni, T., Kozma, S.C., and Thomas, G. (2007). hvps34, an ancient player, enters a growing game: mTOR Complex1/S6K1 signaling. Curr. Opin. Cell Biol. *19*, 135–141.

Okami, J., Simeone, D.M., and Logsdon, C.D. (2004). Silencing of the hypoxia-inducible cell death protein BNIP3 in pancreatic cancer. Cancer Res. *64*, 5338–5346.

Pallafacchina, G., Calabria, E., Serrano, A.L., Kalhovde, J.M., and Schiaffino, S. (2002). A protein kinase B-dependent and rapamycin-sensitive pathway controls skeletal muscle growth but not fiber type specification. Proc. Natl. Acad. Sci. USA *99*, 9213–9218.

Puigserver, P., Rhee, J., Donovan, J., Walkey, C.J., Yoon, J.C., Oriente, F., Kitamura, Y., Altomonte, J., Dong, H., Accili, D., et al. (2003). Insulin-regulated hepatic gluconeogenesis through FOXO1-PGC-1alpha interaction. Nature *423*, 550–555.

Real, P.J., Benito, A., Cuevas, J., Berciano, M.T., de Juan, A., Coffer, P., Gomez-Roman, J., Lafarga, M., Lopez-Vega, J.M., and Fernandez-Luna, J.L. (2005). Blockade of epidermal growth factor receptors chemosensitizes breast cancer cells through up-regulation of Bnip3L. Cancer Res. *65*, 8151–8157.

Sacheck, J.M., Ohtsuka, A., McLary, S.C., and Goldberg, A.L. (2004). IGF-I stimulates muscle growth by suppressing protein breakdown and expression of atrophy-related ubiquitin ligases, atrogin-1 and MuRF1. Am. J. Physiol. Endocrinol. Metab. *287*, E591–E601.

Sacheck, J.M., Hyatt, J.P., Raffaello, A., Jagoe, R.T., Roy, R.R., Edgerton, V.R., Lecker, S.H., and Goldberg, A.L. (2007). Rapid disuse and denervation atrophy involve transcriptional changes similar to those of muscle wasting during systemic diseases. FASEB J. *21*, 140–155.

Sandri, M., Sandri, C., Gilbert, A., Skurk, C., Calabria, E., Picard, A., Walsh, K., Schiaffino, S., Lecker, S.H., and Goldberg, A.L. (2004). Foxo transcription factors induce the atrophy-related ubiquitin ligase atrogin-1 and cause skeletal muscle atrophy. Cell *117*, 399–412.

Sarbassov, D.D., Ali, S.M., Sengupta, S., Sheen, J.H., Hsu, P.P., Bagley, A.F., Markhard, A.L., and Sabatini, D.M. (2006). Prolonged rapa-mycin treatment inhibits mmTORC2 assembly and Akt/PKB. Mol. Cell *22*, 159–168.

Sarkar, S., Davies, J.E., Huang, Z., Tunnacliffe, A., and Rubinsztein, D.C. (2007). Trehalose, a novel mTOR-independent autophagy enhancer, accelerates the clearance of mutant huntingtin and alpha-synuclein. J. Biol. Chem. *282*, 5641–5652.

Schiaffino, S., and Hanzlikova, V. (1972a). Autophagic degradation of glycogen in skeletal muscles of the newborn rat. J. Cell Biol. *52*, 41–51.

Schiaffino, S., and Hanzlikova, V. (1972b). Studies on the effect of denervation in developing muscle. II. The lysosomal system. J. Ultrastruct. Res. *39*, 1–14.

Shintani, T., and Klionsky, D.J. (2004). Autophagy in health and disease: a double-edged sword. Science *306*, 990–995.

Stitt, T.N., Drujan, D., Clarke, B.A., Panaro, F., Timofeyva, Y., Kline, W.O., Gonzalez, M., Yancopoulos, G.D., and Glass, D.J. (2004). The IGF-1/PI3K/Akt pathway prevents expression of muscle atrophy-induced ubiquitin ligases by inhibiting FOXO transcription factors. Mol. Cell *14*, 395–403.

Southgate, R.J., Neill, B., Prelovsek, O., El-Osta, A., Kamei, Y., Miura, S., Ezaki, O., McLoughlin, T.J., Zhang, W., Unterman, T.G., and Febbraio, M.A. (2007). FOXO1 regulates the expression of 4E-BP1 and inhibits mTOR signaling in mammalian skeletal muscle. J. Biol. Chem. *282*, 21176–21186.

Tothova, J., Blaauw, B., Pallafacchina, G., Rudolf, R., Argentini, C., Reggiani, C., and Schiaffino, S. (2006). NFATc1 nucleocytoplasmic shuttling is controlled by nerve activity in skeletal muscle. J. Cell Sci. *119*, 1604–1611.

Tracy, K., Dibling, B.C., Spike, B.T., Knabb, J.R., Schumacker, P., and Macleod, K.F. (2007). BNIP3 is an RB/E2F target gene required for hypoxia-induced autophagy. Mol. Cell. Biol. *27*, 6229–6242.

Yamamoto, A., Cremona, M.L., and Rothman, J.E. (2006). Autophagy-mediated clearance of huntingtin aggregates triggered by the insulin-signaling pathway. J. Cell Biol. *172*, 719–731.

Zhao, J., Brault, J.J., Schild, A., Cao, P., Sandri, M., Schiaffino, S., Lecker, S.H., and Goldberg, A.L. (2007). FoxO3 coordinately activates protein degradation by the autophagic/lysosomal and proteasomal pathways in atrophying muscle cells. Cell Metab. *6*, this issue, 472–483.

Supplemental Data

Article

FoxO3 Controls Autophagy

in Skeletal Muscle In Vivo

Cristina Mammucari, Giulia Milan, Vanina Romanello, Eva Masiero, Ruediger Rudolf, Paola Del Piccolo, Steven J. Burden, Raffaella Di Lisi, Claudia Sandri, Jinghui Zhao, Alfred L. Goldberg, Stefano Schiaffino, and Marco Sandri

Supplemental Experimental Procedures

Plasmids
The following plasmids were used for transfection experiments: ca-FoxO3 (Brunet et al., 1999); dn-FoxO3 (Shin et al., 2001); YFP-LC3 (Tanida et al., 2004), GFP-LC3 (Kabeya et al., 2000); Ub^{G76V}-GFP (Dantuma et al., 2000). Bnip3 (GenBank accession U15174) and HA tagged Bnip3l (GenBank accession AB004788) were amplified from human cDNA by PCR using the following primers:

BNIP3 Fw: 5'-AAAGAATTCTTGCCCTCTGGCGCCATGT-3'.

BNIP3 Rv: 5'AAAGCGGCCGCCTTCATCAAAAGGTGCTGGTGGA-3'.

HA-BNIP3l Fw: 5'AAAGAATTCATGTACCCATACGATGTTCCAGATTACGCTTCGTCCCACCTAGTCGAGC3'.

HA-BNIP3l Rv: 5'AAAGCGGCCGCGGTCACACGCATTTCCAGG3'.

The PCR fragments were cloned into EcoRI and NotI sites of pCI vector (Promega).

Antibodies
The following antibodies from Cell Signalling were used: anti-Akt, anti-phospho-Akt (Ser473), anti-phospho-FKHR (Thr24)/FKRL1 (Thr32), anti-phospho-FKHRL1 (Ser253), anti-phospho-4EBP1 (Thr37/46), anti-phospho-4EBP1 (Ser65), anti-4EBP1, anti-phospho-p70 S6 Kinase (Thr389), anti-p70 S6 Kinase, anti phospho-S6 (Ser240/244), anti-S6, anti-mTOR, anti-RICTOR. Bnip3 antibody (clone ANa40) was from Sigma, Bnip3l antibody from Calbiochem and HA antibody was from Santa Cruz Biotechnology, mouse LC3 antibody was from MBL International. Soluble chromatin was coimmunoprecipitated with anti-FoxO3 antiserum (Santa Cruz), anti-HA antiserum (Santa Cruz), anti-Acetyl-Histone3 (Upstate), or an equal amount of IgG.

In Vivo RNAi
Oligos were cloned into the pSUPER vector (Brummelkamp et al., 2002. A system for stable expression of short interfering RNAs in mammalian cells. Science *296*, 550-553.) or into Invitrogen BLOCK-IT Pol II miR RNAi Expression Vectors. For validation of shRNA constructs, MEF cells were maintained in DMEM/10%FBS and transfected with shRNA constructs using Lipofectamine 2000 (Invitrogen) according to manufacturer's protocols. Cells were lysed 72 hr later, and immunoblotting was performed as described above.

Table S1. Primers used for Quantitative PCR Analyses

	Forward primer	Reverse primer
MAP1-LC3b	cactgctctgtcttgtgtaggttg	tcgttgtgcctttattagtgcatc
Cathepsin L	gtggactgttctcacgctcaag	tccgtccttcgcttcatagg
Atrogin 1	gcaaacactgccacattctctc	cttgaggggaaagtgagacg
Gabarapl1	catcgtggagaaggctccta	atacagctggcccatggtag
Bnip3	ttccactagcaccttctgatga	gaacaccgcatttacagaacaa
Bnip3l	ttggggcattttactaaccttg	tgcaggtgactggtggtactaa
Atg12	tccgtgccatcacatacaca	taagactgctgtggggctga
Vps34	tgtcagatgaggaggctgtg	ccaggcacgacgtaacttct
Beclin	tgaatgaggatgacagtgagca	cacctggttctccacactcttg
Atg4b	attgctgtggggttttttctg	aaccccaggattttcagagg
Gapdh	caccatcttccaggagcgag	ccttctccatggtggtgaagac
β-actin	ctggctcctagcaccatgaagat	ggtggacagtgaggccaggat

Table S2. Oligos Used for siRNA Production

TARGET GENE	TARGET SEQUENCE	EFFICIENCY OF KNOCKDOWN
FoxO3(1)	tgaaggcacgggcaagagc	95%
FoxO3(2)	ggaaatgctcctcgcggcg	95%
Bnip3(1)	cagcctccgtctctattta (reference: Hamacher-Brady, A. et al.)	90%
Bnip3(2)	taccaacagagctgaaata	80%
mTOR(1)	Invitrogen BLOCK-iT™ miR RNAi Select Mmi552324	40%
mTOR(2)	Invitrogen BLOCK-iT™ miR RNAi Select Mmi552325	90%
mTOR(3)	Invitrogen BLOCK-iT™ miR RNAi Select Mmi552326	90%
mTOR(4)	Invitrogen BLOCK-iT™ miR RNAi Select Mmi552327	12%
Rictor (1)	ctgtgaactagcacttcag	90%
Rictor(2)	cacgatttctagccagtaa	95%
LC3	actctgatgcactaataaa	85%
LacZ	gactacacaaatcagcgattt	-
Control (scrambled)	gtctccacgcgcagtacattt	-

Hamacher-Brady, A. et al. Response to myocardial ischemia/reperfusion injury involves Bnip3 and autophagy. Cell death and Differentiation 14, 146-157 (2006)

Quantification of knockdown was performed considering the efficiency of transfection and the percentage of target protein decrease.

Table S3. Primers Used in ChIP Experiments and Oligos Used in Mutation Experiments

Primers used in ChIP experiments

LC3 Fw	-1608	5'- CATGCCTTGGGACACCAGAT
LC3 Rv	-1379	5'- ACCTTCTTCAAGTGCTGTTTGT
Atrogin1 Fw	-3228	5'-CTGGCAGGGAGGAGCCTAATGAATC
Atrogin1 Rv	-2966	5'-GGGAGTGGCAAAGCCGTCTC
Bnip3l Fw	-3177	5'-GAATGAAAAGAAACACGCCTCA
Bnip3l Rv	-3010	5'-GCACA CACATACACGCAAATAA
Bnip3 Fw -1	-4772	5'-GCTGTAGGTCAGAGCCAAAA
Bnip3 Rv -1	-4413	5'-CTCCACGACACCAGGATTAC
Bnip3 Fw-2	-1236	5'-GCCCTCGTATAACCTTAGCA
Bnip3 Rv-2	-1029	5'-TGGGTCAGGTCACTAGAAGC
MHCβ/slow Fw	-2949	5'-GGGAGTACTGTTTGGACAAGG
MHCβ/slow Rv	-2745	5'-ATGCTCAGAGCCAGACCTG

Oligos used in mutation experiments

LC3	5'-AACAATGCAAAGCAAGCAACCCAAGGAAAGTAACCAGCC-3'
LC3 Mutated	5'-GGCTGGTTACTTTCCTTGGGTTGCTTGCTTTGCATTGTT-3'

Upper panel: Primers used for chromatin immunoprecipitation (ChIP) analyses. These regions of amplification contain the FoxO binding sites for the *LC3*, *Atrogin-1*, *Bnip3* and *Bnip3l* promoters but not for the *MHC*β promoter. Lower panel: primers used to mutate FoxO binding site (mutations are underlined).
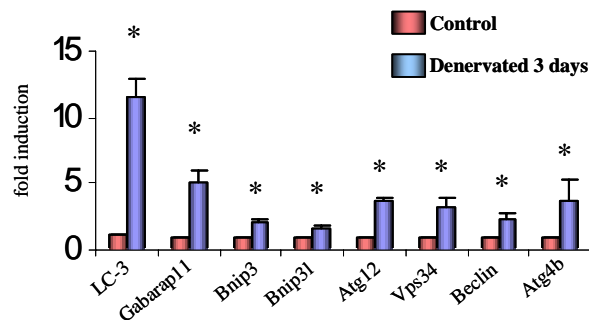

Figure S1. Upregulation of Autophagy Genes Induced by 3D Denervation in Adult Skeletal Muscle

Quantitative PCR analysis was performed in triplicates using specific oligonucleotides (see Table S1). The differences in gene expression levels in control vs. denervated were all statistically significant. *p < 0.001.
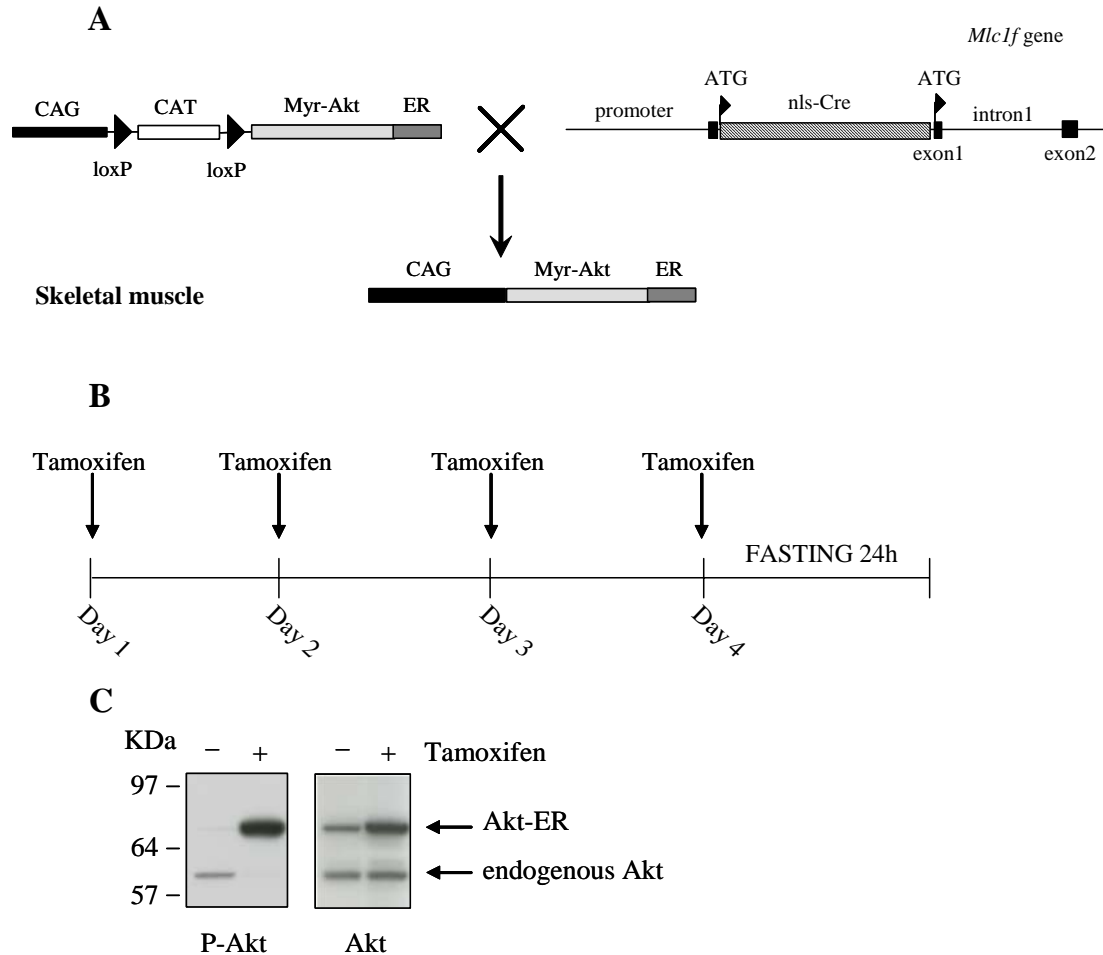
A

Skeletal muscle

B

C

Figure S2.

(A) Scheme of the generation of a transgenic mouse line in which the expression of Akt1 is muscle-specific and inducible. This line was obtained by crossing a transgenic line expressing a silent Akt-ER (Kroll, J., Cobo, P., and Sato, T.N. (2003). Versatile inducible activation system of Akt/PKB signaling pathway in mice. Genesis *35*, 160-163.) with a line expressing Cre under the control of a myosin light chain 1 fast promoter (Bothe, G.W., Haspel, J.A., Smith, C.L., Wiener, H.H., and Burden, S.J. (2000). Selective expression of Cre recombinase in skeletal muscle fibers. Genesis *26*, 165-166). The *Akt-ER* sequence contains the *Akt1* coding sequence fused to a modified estrogen receptor hormone binding domain. As a consequence, treatment with tamoxifen, which binds the estrogen receptor hormone binding domain, induces Akt1 phosphorylation and activation. The mice were injected with 1.5 mg/day of tamoxifen in sunflower oil for four days to induce the expression of the transgene, while control received only oil vehicle. CAG: chicken β-actin promoter and CMV enhancer; CAT: chloramphenicol acetyltransferase; myr-Akt: Akt fused to src myristoylation signal; ER: mutated hormone binding domain of estrogen receptor. nls-Cre: Cre recombinase fused to a nuclear localization signal.

(B) Scheme of tamoxifen treatment.

(C) Immunoblot analysis of protein extracts from EDL muscles of *Akt-Cre* mice treated with tamoxifen as described in (B). Tamoxifen treatment induces phosphorylation and protein stabilization of Akt-ER while the amount of endogenous Akt protein is unaffected.
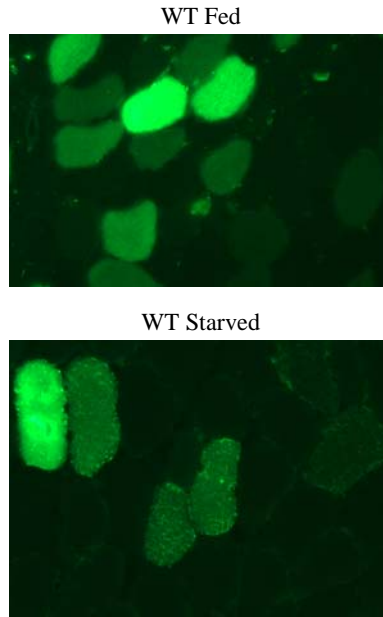
WT Fed

WT Starved

Figure S3.

Adult muscles from wild-type mice were transfected by electroporation with a plasmid expressing GFP-LC3. Eight days later mice were fasted for 24 hours before sacrifice. Myofibers expressing GFP-LC3 were analysed by fluorescent microscopy. Representative images are shown.

FASTING

AKT-ER

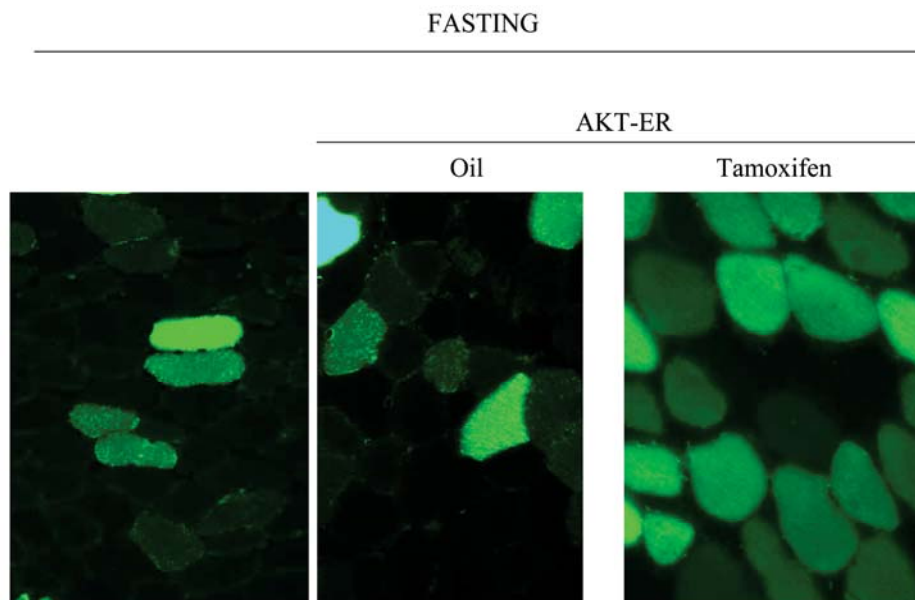Oil   Tamoxifen

Figure S4.

Adult muscles from *Akt* transgenic mice were transfected by electroporation with a plasmid expressing GFP-LC3. Eight days later mice were treated with tamoxifen or vehicle and fasted for 24 hours before sacrifice. Myofibers expressing GFP-LC3 were analysed by fluorescent microscopy. Representative images are shown.
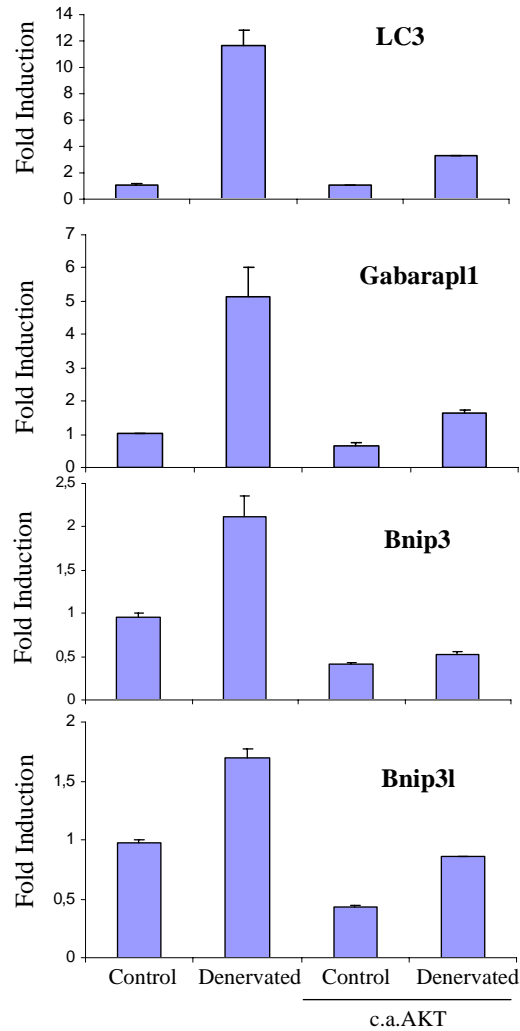
Figure S5. Upregulation of *LC3*, *Gabarapl1*, *Bnip3*, and *Bnip3l* Induced by Denervation Is Blocked by Akt

Mice were treated with tamoxifen for four days and muscles were removed one day later. Denervation was performed by sciatic nerve section three days before sacrifice. Levels of transcripts were determined by qPCR as described in Experimental Procedures.
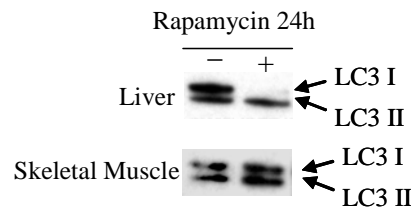
Figure S6.

Immunoblotting for LC3 shows that the amount of LC3-I (upper band) is decreased and conversion of LC3-I to LC3-II is induced in liver after 24 hours from rapamycin treatment (upper panel). However no significant change in LC3 lipidation is induced in skeletal muscle by rapamycin treatment (lower panel).

Figure S7.

Adult skeletal muscles of *Akt* transgenic mice were cotransfected with YFP-LC3 and mTOR shRNA3. Immunostaining for anti-phospho-S6 (P-S6) revealed that mTOR downstream target S6 is dephosphorylated in muscle fibers in which mTOR is knocked down. However the level of S473 phosphorylation of Akt is unchanged.
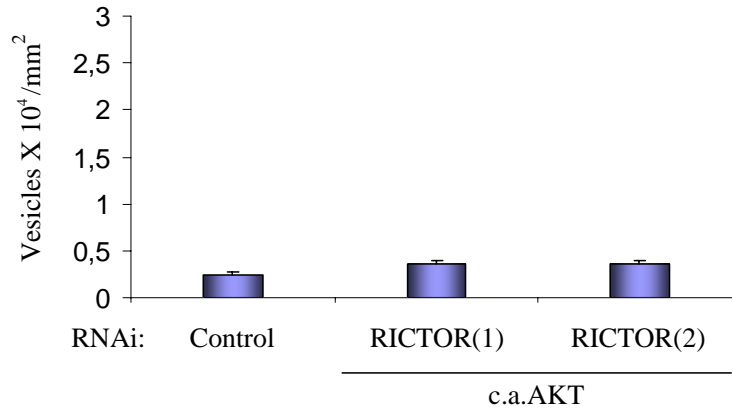
Figure S8. Overexpression of ca-Akt Blocks Autophagosome Formation Induced by mTORC2 Inhibition Also in the Absence of Rapamycin
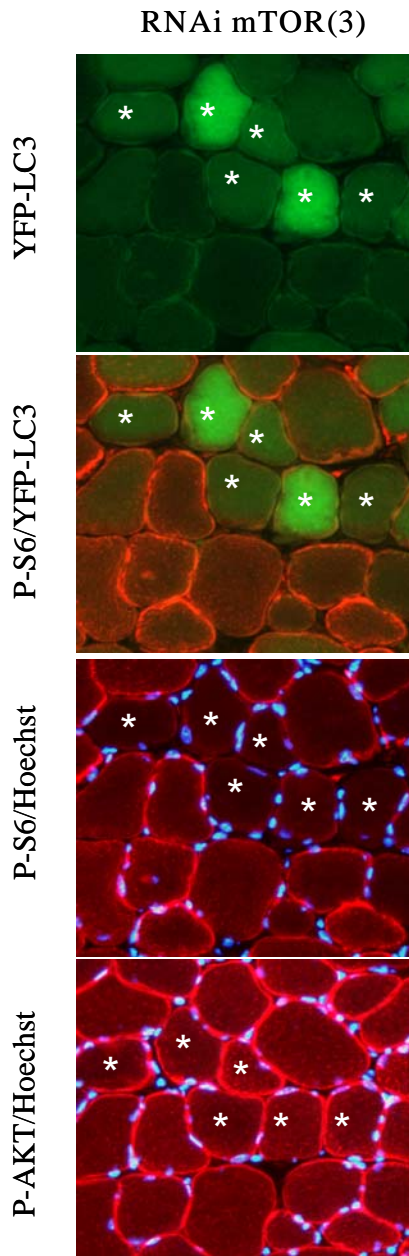
Adult skeletal muscles of transgenic mice were cotransfected with YFP-LC3 and RNAi vectors against Rictor. Mice were treated with tamoxifen and vesicles were quantified as above described.
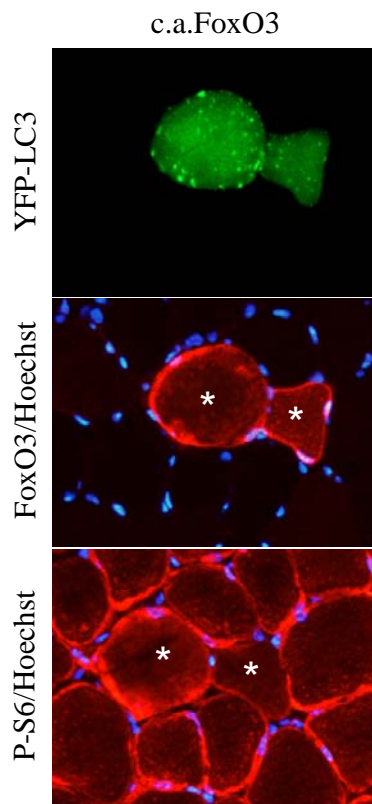
Figure S9.

Adult skeletal muscles of *Akt* transgenic mice were cotransfected with YFP-LC3 and ca-FoxO3. Immunostaining for anti-phospho-S6 (P-S6) revealed that mTOR downstream target S6 is maintained phosphorylated in muscle fibers in which ca-FoxO3 is expressed.
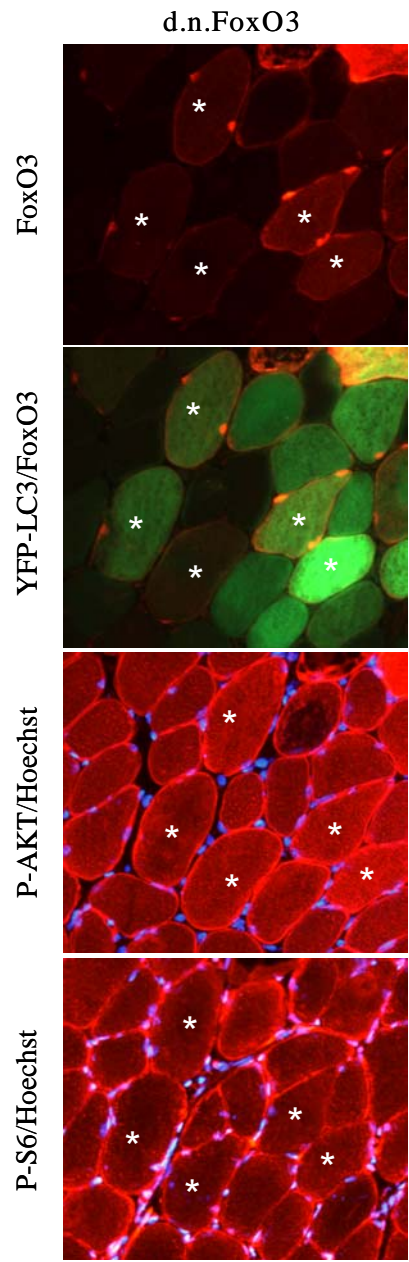
Figure S10.

Adult skeletal muscles of *Akt* transgenic mice were cotransfected with YFP-LC3 and dn-FoxO3. Immunostaining for anti-phospho-S6 (P-S6) revealed that mTOR downstream target S6 is maintained phosphorylated in muscle fibers in which FoxO3 is inhibited.

A

	Control	Fasted
Anti-FoxO3		
Anti-Acetyl-H3		
IgG		
INPUT		

B

MHCβ promoter

MHCβ

5kb

oligos

	Control	Fasted
Anti-FoxO3		
Anti-FoxO1		
IgG		
INPUT		

Figure S11.

(A) FoxO3 binds to a FoxO response element in the *atrogin-1* promoter and this binding, as well as histone acetylation at this site, is increased by fasting.

(B) *MHCβ* promoter does not contain FoxO binding sites and was used as control for ChIP.

MATERIALS AND METHODS (I PART)

Generation of muscle specific Akt-MLC1f mice

The generation of the inducible transgenic model was achieved by crossing a transgenic line which expresses the Cre-recombinase under a muscle-specific promoter (Bothe *et al.*, 2000) with a second line which expresses Akt1 only after the deletion of an upstream DNA sequence by the Cre-recombinase (Figure 1) (Kroll *et al.*, 2003).
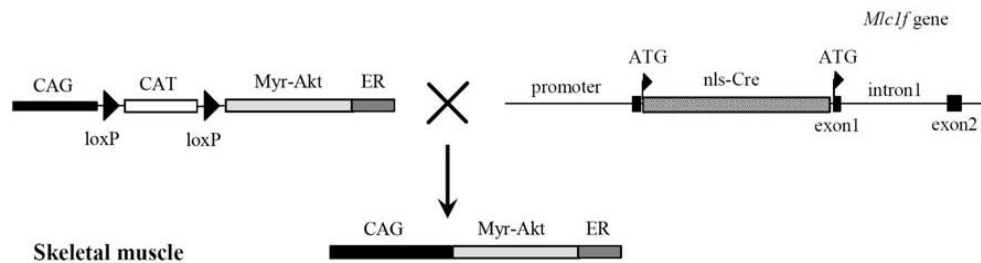
Figure 1: Scheme of the generation of a transgenic mouse line where the expression of Akt1 is muscle-specific and inducible.

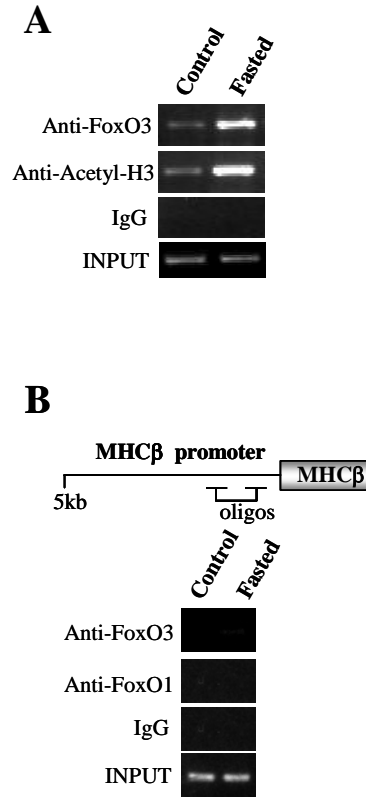The myr-Akt is expressed in skeletal muscle before treatment with tamoxifen, but since it has a heat shock protein complex bound to a modified estrogen receptor domain, it cannot be phosphorylated and is therefore degraded rapidly. Akt1 phosphorylation, activation and stabilization was induced only by exogenous treatment with tamoxifen, which binds the estrogen receptor (Kroll *et al.*, 2003). Transgenic mice were injected with 1.5 mg/day of tamoxifen in sunflower oil for four days to induce the expression of the transgene, while control mice received only oil vehicle.

Transgenic mice were injected intraperitoneally (i.p.) with 4 mg/kg rapamycin as described previously (Pallafacchina *et al.*, 2002). Mice transfected with the UbG76V-GFP reporter were treated for 4 days with a daily i.p. injection of 150 µl of MG262 (5 µmol/kg) or vehicle only (30% DMSO in 0.9% NaCl).

Mouse tibialis anterior muscle electroporation

Experiments were performed on adult CD1 and inducible transgenic Akt-Cre mice (28–30g) tibialis anterior (TA). The animals were anesthetized by an intraperitoneal injection of ketamine (75 mg/Kg) and xylazine (20 mg/Kg). The tibialis anterior muscle was isolated through a small surgical incision, and 25 μg of plasmid DNA were injected along the muscle length. Electric pulses were then applied by two stainless steel spatula electrodes placed on each side of the isolated muscle belly (50 Volts/cm, 5 pulses, 200 ms intervals). Muscles were analyzed 4, 8, or 14 days later. No gross or microscopic evidence for necrosis or inflammation as a result of the transfection procedure was noted (Sandri *et al*., 2004 and Dona *et al*., 2003).

Tibialis Anterior muscles were transfected with different plasmids:

- ca-FoxO3 (Brunet *et al*., 1999);

- dn-FoxO3 (Sandri *et al*., 2004);

- YFP-LC3 (Tanida *et al*., 2004),

- GFP-LC3 (Kabeya *et al*., 2000);

- UbG76V-GFP (Dantuma *et al*., 2000).

- Bnip3 (GenBank accession U15174)

HA tagged Bnip3l (GenBank accession AB004788) was amplified from human cDNA by PCR using the following primers:

BNIP3 Fw: 5'-AAAGAATTCTTGCCCTCTGGCGCCATGT-3'.

BNIP3 Rv: 5'AAAGCGGCCGCCTTCATCAAAAGGTGCTGGTGGA-3'.

HA-BNIP3l Fw:

5'AAAGAATTCATGTACCCATACGATGTTCCAGATTACGCTTCGTCCCACCTAGTCGAGC3'.

HA-BNIP3l Rv: 5'AAAGCGGCCGCGGTCACACGCATTTCCAGG3'.

The PCR fragments were cloned into EcoRI and NotI sites of pCI vector (Promega).

Cut of the sciatic nerve

The right hindlimbs of 3 months old Akt-MLC1f transgenic mice were denervated cutting the sciatic nerve unilaterally. The animals were anesthetized by an intraperitoneal injection of ketamine (75 mg/Kg) and xylazine (20 mg/Kg). The sciatic nerve was unilaterally cut at the level of trochanter. About 0.5-1 cm of the peripheral nerve stump was removed and the proximal stump was sutured into a superficial muscle to avoid reinnervation and obtain a permanent denervation of the lower hindlimb. The mice was sacrificed 3 days after operation for gene expression analyses, or after 14 days for biochemestry analyses.

Single-Fiber Analyses

Flexor digitorum brevis muscles from adult mice were digested in type I collagenase at 4°C for 1 hour, at 37°C for 2 hours, and mechanically dissociated into single fibers. The fibers were electroporated using a BTX porator (50 volts/4 mm, 3 pulses, 200 ms intervals) to transfer plasmid DNA and then plated onto glass coverslips coated with laminin and cultured in Tyrode's salt solution (pH 7.3) containing 10% fetal bovine serum, 50 U/ml penicillin, 50 μg/ml streptomycin, and 5% CO_2 (37°C).

In Vivo RNAi

Oligos were cloned into the pSUPER vector (Brummelkamp *et al*., 2002.) or into Invitrogen BLOCK-IT Pol II miR RNAi Expression Vectors. For validation of shRNA constructs, MEF cells were maintained in DMEM/10%FBS and transfected with shRNA constructs using Lipofectamine 2000 (Invitrogen) according to manufacturer's instructions. Cells were lysed 72 hours later, and immunoblotting was performed as described below.

The sequences of the Oligos Used for siRNA Production are listed in the Table 1:

TARGET GENE	TARGET SEQUENCE	EFFICIENCY OF KNOCKDOWN
FoxO3(1)	tgaaggcacgggcaagagc	95%
FoxO3(2)	ggaaatgctcctcgcggcg	95%
Bnip3(1)	cagcctccgtctctattta (reference: Hamacher-Brady, A. et al.)	90%
Bnip3(2)	taccaacagagctgaaata	80%
mTOR(1)	Invitrogen BLOCK-iT™ miR RNAi Select Mmi552324	40%
mTOR(2)	Invitrogen BLOCK-iT™ miR RNAi Select Mmi552325	90%
mTOR(3)	Invitrogen BLOCK-iT™ miR RNAi Select Mmi552326	90%
mTOR(4)	Invitrogen BLOCK-iT™ miR RNAi Select Mmi552327	12%
Rictor (1)	ctgtgaactagcacttcag	90%
Rictor(2)	cacgatttctagccagtaa	95%
LC3	actctgatgcactaataaa	85%
LacZ	gactacacaaatcagcgattt	-
Control (scrambled)	gtctccacgcgcagtacattt	-

Hamacher-Brady, A. et al. Response to myocardial ischemia/reperfusion injury involves Bnip3 and autophagy. Cell death and Differentiation 14, 146-157 (2006)

Table 1: Oligos Used for siRNA Production

Fluorescence Microscopy and Electron Microscopy

Cryosections of muscle transfected with GFP-LC3 were examined using an epifluorescence Leica DM5000B microscope equipped with a Leica DFC300-FX digital charge-coupled device camera by using Leica DC Viewer software. The fluorescent dots were counted as described by Mizushima (Mizushima *et al.*, 2004), normalizing for cross-sectional area. For electron microscopy, we used both conventional fixation-embedding procedures and another procedure based on fixation in paraformaldehyde-glutaraldehyde without osmium and embedding in LR White resin, which allows preservation of GFP fluorescence in semithin 1 μm sections and subsequent analysis of serial thin sections by electron microscopy (Luby-Phelps *et al.*, 2003).

In Vivo Imaging via Two-Photon Microscopy

To monitor in situ autophagosome formation in living animals, muscles were transfected with GFP-LC3 probe, and two-photon microscopy was performed 2 weeks later upon in situ exposure of transfected muscles as described previously (Tothova *et al.*, 2006).

Gene expression analyses

Quantitative Real-time PCR was performed with SYBR Green chemistry (Applied Biosystems). SYBR green is a fluorescent dye that intercalates into double-stranded DNA and produces a fluorescent signal. The Real-Time PCR Instrument allows real time detection of PCR products as they accumulate during PCR cycles and create an amplification plot, which is the plot of fluorescence signal versus cycle number. In the initial cycles of PCR, there is little change in fluorescence signal. This defines the baseline for the amplification plot. An increase in fluorescence above the baseline indicates the detection of accumulated PCR products. A fixed fluorescence threshold can be set above the baseline. The parameter Ct (threshold cycle) is defined as the fractional cycle number at which the fluorescence passes the fixed threshold. So the higher the initial amount of the sample, the sooner is the accumulated product detected in the PCR process as a significant increase in fluorescence, and the lower is the Ct value.

Quantification of the PCR products and determination of the level of expression

A relative quantification method was used to evaluate the differences in gene expression, as described by Pfaffl (Pfaffl, 2001). In this method, the expression of a gene is determined by the ratio between a test sample and a housekeeping gene. The relative expression ratio of a target gene is calculated on the PCR efficiency (E) and the threshold cycle deviation (ΔCt) of unknown samples versus control ones, expressed in comparison to a reference gene.

The mathematical model used for relative expression is represented in this equation:

$$Ratio = \frac{(E_{target})^{\Delta Ct}}{(E_{reference})^{\Delta Ct}}$$

The internal gene reference used in our real time PCR was β-actin or GAPDH, whose abundance did not change under different experimental conditions.

Primer pairs design

Gene-specific primer pairs were selected with Primer3 software (http://frodo.wi.mit.edu/cgi-bin/primer3/primer3_www.cgi); sequences of distinct exons were chosen to avoid amplifying contaminant genomic DNA. Primer pairs were selected in a region close to the 3'-end of the transcript, and amplified fragments of 150-250bp in length. To avoid the amplification of contaminant genomic DNA, the target sequences were chosen on distinct exons, separated by a long intron (more than 1000bp). The melting temperature was chosen to be about 58-60° C.

The sequences of the primer pairs are listed in the Table 2:

	Forward primer	Reverse primer
MAP1-LC3b	cactgctctgtcttgtgtaggttg	tcgttgtgcctttattagtgcatc
Cathepsin L	gtggactgttctcacgctcaag	tccgtccttcgcttcatagg
Atrogin 1	gcaaacactgccacattctctc	cttgaggggaaagtgagacg
Gabarapl1	catcgtggagaaggctccta	atacagctggcccatggtag
Bnip3	ttccactagcaccttctgatga	gaacaccgcatttacagaacaa
Bnip3l	ttggggcattttactaaccttg	tgcaggtgactggtggtactaa
Atg12	tccgtgccatcacatacaca	taagactgctgtggggctga
Vps34	tgtcagatgaggaggctgtg	ccaggcacgacgtaacttct
Beclin	tgaatgaggatgacagtgagca	cacctggttctccacactcttg
Atg4b	attgctgtggggttttctg	aaccccaggattttcagagg
Gapdh	caccatcttccaggagcgag	ccttctccatggtggtgaagac
β-actin	ctggctcctagcaccatgaagat	ggtggacagtgaggccaggat

Table 2: Primers used for Quantitative PCR Analyses

Extraction of total RNA

Total RNA was isolated from TA using the *Promega SV Total Isolation kit.*

Synthesis of the first strand of cDNA

400ng of total RNA was reverse transcribed with SuperScript^{TM} III (Invitrogen) in the following reaction mix:

Random primer hexamers (50ng/μl random)	1μl
dNTPs 10 mM	1μl
H$_2$O Rnase-free	8.5μl

The samples were mixed by vortexing and briefly centrifuged and denaturated by incubation for 5 minutes at 65° C to prevent secondary structures of RNA.
Samples were incubated on ice for 2 minutes to allow the primers to align to the RNA; and the following components were added sequentially:

First strand buffer 5× (Invitrogen)	5μl DTT 100mM 2μl
RNase Out (Invitrogen)	1μl
SuperScript^{TM} III (Invitrogen)	0.5μl

The volume was adjusted with water up to 20ul.

The reaction program was:

step1:	25°C for 10 minutes
step2:	42°C for 50 minutes
step3:	70°C for 15 minutes

At the end of the reaction, the volume of each samples was adjusted to 50ul with RNase free water.

Real-Time PCR reaction

1μl of diluted cDNAs were amplified in 10μl PCR reactions in an ABI Prism 7000 (Applied Biosystem) thermocycler, coupled with an ABI Prism 7000

Sequence Detection System (Applied Biosystems) in 96-wells plates (Micro Amp Optical, Applied Biosystems).

In each well 10ul Sample mix + 10ul reaction mix were added.

Sample mix was prepared as follows:

Template cDNA	1μl
H$_2$O Rnase-free	9μl
Total volume	10μl

The SYBR$^®$ Green qPCR (Qiagen) was used for the Real-Time PCR reaction as follows:

SYBR$^®$ Green qPCR (Qiagen)	10μl
Mix Primer forward /reverse 50 mM	0.4μl
Total volume	10μl

The PCR cycle for the Real-Time PCR was:

step 1:	95° C for 15 minutes
step2:	95° C for 25 seconds
step3	58° C for 1 minute
step4:	go to step2 for 40 times

Chromatin immunoprecipitation (ChIP) assay

The chromatin immunoprecipitation (ChIP) technique is the best tool to identify specific proteins associated with a region of the genome or, conversely, to find regions of the genome associated with specific proteins. Chromatin Immunoprecipitation experiments were performed using *ChIP assay kit* (UpState).

The principal phases of this procedure are the following:

1. Cross-linking of the protein to the chromatin, and lysis

2. Sonication of DNA

3. Immunoprecipitation (IP) of cross-linked Protein/DNA

4. Elution of Protein/DNA complexes

5. Reverse cross-linking of Protein/DNA complexes to free DNA

6. DNA extraction with phenol/chloroform

7. PCR chromatin immunoprecipitation

Extraction and lysis of nuclei

We used 4 tibialis anterior muscles of 2 month old CD1 mice for each ChIP experiment. The muscles were frozen in liquid nitrogen and powdered with pestle and mortar in liquid nitrogen and resuspended in 4ml <u>Homogenization Buffer</u> (18M Surcose, 10mM HEPES,1mM EDTA, 50mM KCl, 5% glycerol in distilled pure water). Muscles were then homogenized with mini-Polytron for 5 seconds. The homogenization procedure was repeated 3 times. The efficiency of extraction was analyzed by spotting 20ul of homogenized sample together with 20ul of Trypan Blue 1X (Sigma-Aldrich) on a slide and by observing the released nuclei at light microscope. The volume of homogenized solution was brought to 18ml with cold <u>Lysis Buffer</u> (10mM HEPES pH 7.5, 1mM EDTA, 50mM KCl, 12.5mM NaCl, 5mM $MgCa_2$, 0.1mM EGTA in distilled and pure water).

Cross-linking of the protein to the chromatin and lysis

The myonuclei were precipitated by centrifuging at 900 rpm for 10 minutes at 4°C, and then resuspended in 5ml of <u>Lysis Buffer</u> and treated with 1% formaldehyde for 10 minutes at room temperature. 0.02M glycine was added to the samples to quench the formaldehyde action. Then myonuclei are centrifuged at 900 rpm for 10 minutes and resuspended in 600ul of <u>Resuspention Buffer</u> (10mM HEPES pH 7.5, 1mM EDTA,0.5% SDS, 1mM PMSF).

Chromatin sonication

An efficient chromatin fragmentation was obtained by using 10 seconds pulse of a sonicator "Sonic Vibracell" at 4°C repeated 10 times. After sonication the samples were centrifuged at 13000 rpm for 10 min at 4°C.

Immunoprecipitation (IP) of cross-linked Protein/DNA

The supernatant was collected and brought to final volume of 2.2ml with <u>Dilution Buffer</u> (Upstate Millipore). 1ml of sheared chromatin was transferred in a 1.5ml tube for each immunoprecipitation experiment. An aliquot of fragmented chromatin (200ul) was stored at -80°C. This sample is called the "input" and is the control sample for PCR analyses. The remaining volume is used for the immunoprecipitation reaction. To remove proteins or DNA that could un-specifically bind to either the immunoglobulins or to Protein A-Agarose beads, the samples were pre-cleaned by 1 hour incubation at 4°C in rotation with 75ul of Protein A Agarose/Salmon Sperm DNA (Upstate Millipore). The beads were removed by centrifuging at 13000 rpm for 5 minutes, at 4°C. Then 5ug of specific antibody or general IgG was added to supernatant and was incubated overnight at 4°C in rotation. 60ul of Protein A Agarose/Salmon Sperm DNA was added to the antibody/protein/DNA complex and was incubated for 1 hour at 4°C in rotation. The agarose beads were collected by centrifugation at 1000 rpm for 1 minute at 4°C and the supernatant fraction was removed. Then the beads were washed three times with increasing ionic-strength cold buffers (Low Salt Immune Complex Wash Buffer, High Salt Immune Complex Wash Buffer, LiCl- Immune Complex

Wash Buffer Upstate Millipore). Finally the beads were washed with 1ml of TE (Tris EDTA) buffer for two times.

Elution and Reverse cross-linking of Protein/DNA complexes to free DNA

The samples were briefly centrifuged for 1 min at 13000 rpm and the supernatants were discarded. The beads were resuspended in 250ul of fresh Elution Buffer (1% SDS, 0.1M NaHCO$_3$) and incubated for 15 minutes at room temperature under rotation. The samples were briefly centrifuged for 1 minute at 13000 rpm and the supernatants were collected. The same procedure was repeated another time to reach the final volume of 500ul for each sample. The "input" control was thawed and brought to 500ul with Elution Buffer. To reverse the formaldehyde cross-linking, 24ul of 5M NaCl was added to the samples and to the "input" control and was further incubated for 6 hours at 65°C. At this stage the samples could be used either for biochemical studies, including western blotting analysis to confirm the efficient immunoprecipitation, or molecular approaches to reveal which part of the genome was pulled down.

For PCR analysis 10ul of 0.5M EDTA, 20ul of 1M Tris-HCl and 20ug of proteinase K (Gibco) were added to the samples for 1 hour at 45° C to remove the proteins. The genomic DNA was purified by Phenol/Chloroform:/Isoamyl Alcohol 25:24:1 extraction (Sigma-Aldrich). Briefly the samples were mixed by vortexing and centrifuged at 13000 rpm for 5 minutes at room temperature. The aqueous phases were collected in new tubes. DNA was precipitated by adding 50ul of 3M NaOAc, 20ug glycogen (Ambion), 1ml of 100% EtOH (Sigma-Aldrich) and incubated overnight at -20°C. To collect the DNA, the samples were centrifuged at 12000 g for 30 minutes at 4° C and the pellet were resuspended in 50μl of H$_2$O (GIBCO).

PCR chromatin immunoprecipitated DNA

To avoid unspecific amplification of the DNA the primers were designed to amplify regions around 200-300bp. The quality of primers was checked by

Primer3 software (http://frodo.wi.mit.edu/cgi-bin/primer3/primer3_www.cgi).
Oligonucleotide primers are listed in Table 3.

PCR reaction was prepared as follows:

Template DNA	2 μl
PCR buffer 10X (Invitrogen)	2.5μl
dNTPs 10mM	0.5 μl
MgCl2 1.5mM	0.75 μl
Primer forward 10μM	1.25 μl
Primer reverse 10μM	1.25μl
Taq DNA Polymerase 5U/μl (Invitrogen)	0.25 μl
H2O pure (Gibco)	16.75 μl
Total volume	25 μl

The following PCR reaction program was used:

step1:	94°C for 3 minutes
step2:	94°C for 30 seconds
step3:	58°C for 30 seconds
step4:	go to step 2 for 29 times
step5:	72°C for 45 seconds
step6:	94°C for 30 seconds
step7:	58°C for 30 seconds
step8:	72°C for 10 minutes

10ul of each PCR reaction was analyzed by electrophoresis in 2% agarose gel. The size of the PCR products was determined by using 1 Kb DNA molecular marker (Invitrogen).

LC3 Fw	-1608	5'- CATGCCTTGGGACACCAGAT
LC3 Rv	-1379	5'- ACCTTCTTCAAGTGCTGTTTGT
Atrogin1 Fw	-3228	5'-CTGGCAGGGAGGAGCCTAATGAATC
Atrogin1 Rv	-2966	5'-GGGAGTGGCAAAGCCGTCTC
Bnip3l Fw	-3177	5'-GAATGAAAAGAAACACGCCTCA
Bnip3l Rv	-3010	5'-GCACA CACATACACGCAAATAA
Bnip3 Fw -1	-4772	5'-GCTGTAGGTCAGAGCCAAAA
Bnip3 Rv -1	-4413	5'-CTCCACGACACCAGGATTAC
Bnip3 Fw-2	-1236	5'-GCCCTCGTATAACCTTAGCA
Bnip3 Rv-2	-1029	5'-TGGGTCAGGTCACTAGAAGC
MHCβ/slow Fw	-2949	5'-GGGAGTACTGTTTGGACAAGG
MHCβ/slow Rv	-2745	5'-ATGCTCAGAGCCAGACCTG

Table 3: Primers Used in ChIP Experiments. Primers used for chromatin immunoprecipitation (ChIP) analyses. These regions of amplification contain the FoxO binding sites for the LC3, Atrogin-1, Bnip3 and Bnip3l promoters but not for the MHCβ promoter.

Promoter Analyses and Mutagenesis

Promoter activity can be studied by using the luciferase firefly gene. In our experiments we used Dual-Luciferase®Reporter Assay Chemistry (Promega), that includes "dual reporters". The promoter region of interest is cloned upstream the firefly luciferase. Renilla luciferase expression is under the control of a minimal TK promoter and it is used to normalize the firefly data for the efficiency of transfection (which can vary from animal to animal).

The LC3 mouse genomic DNA fragment (1608 to 1379) was amplified by PCR with the same primers used for ChiP experiments, and inserted into the KpnI and XhoI sites of pGL3-Promoter vector (Promega).

Mutations in the FoxO binding site were generated by PCR using the QuikChange technique (Stratagene) with the primers listed in Table 4.

The technique consists of a PCR amplification with a primer mutated at the nucleotide sites that we wanted to change. The PCR reaction amplifies only one DNA strand of the template.

These constructs were transfected into tibialis anterior muscles together with a renilla luciferase vector (pRLTK) to normalize the transfection efficiency as described previously (Sandri *et al*., 2004).

| LC3 | 5'-AACAATGCAAAGCAAGCAACCCAAGGAAAGTAACCAGCC-3' |
| LC3 Mutated | 5'-GGCTGGTTACTTTCCTTGGGTTGCTTGCTTTGCATTGTT-3' |

Table 4: **Oligos used in mutation experiments**. Primers used to mutate FoxO binding site (mutations are underlined).

Protein Breakdown Assay

C2C12 myotubes were incubated with [3H]tyrosine 24 hours before infection and then infected with control or ca-FoxO3 virus for 24 hours. Upon the chase period, new medium containing concanamycin A (0.1 μM) was added, and proteolysis was measured starting 1 hour later (Sacheck *et al*., 2004). Each point is the average of four plates.

Gel Electrophoresis And Western Blot

Lysis and Protein extraction from transfected MEFs

The transfected cells were mechanically scraped from the plate and collected by centrifugation at 1250 rpm for 5 minutes. The pellet was resuspended in 200ul of the following lysis buffer:

5 mM Tris, pH 7.5

100 mM NaCl

5 mM MgCl2

1 mM DTT

10% glycerol (Sigma)

0.5% Triton (Sigma)

1X Cocktail di inibitori di proteasi (Complete, Roche)

After centrifugation at 10000 rpm for 5 minutes at 4°C, surnatant protein concentration was measured using BradFord assay kit (PIRCE) according to manufacturer's instructions.

Lysis and Protein extraction from skeletal muscle

Frozen skeletal muscles were shattered with a ceramic pestle in liquid nitrogen and lysed with 100μl of Lysis Buffer containing:

Solution	Final Concentration
Tris pH 7.5	50 mM
NaCl	150mM
$MgCl_2$	10mM
DTT	0.5mM
EDTA	1mM
Glycerol	10%
SDS	2%
Triton X100	1%
Cocktail di inibitori di proteasi (Complete, Roche)	1X
PMSF	1mM
$NaVO_3$	1mM
NaF	5mM
β-glycerophosphate	3mM

After a incubation at 70°C for 10 minutes and centrifugation at 13000 rpm for 10 minutes at 4°C we measured the protein concentration of the surnatant using BCA^{TM} protein assay kit (PIRCE) following the manufacture protocol.

Electrophoretic run of proteins

The proteins extracted from skeletal muscles or MEFs cells were solubizated in <u>Loading buffer</u> which was prepared as follows:

1X NuPAGE® LDS Sample Buffer (Invitrogen)   4μl

1X NuPAGE® Reducing Agent (Invitrogen)   2μl

The volume of each sample was brought to 20μl with 1% SDS. The samples were denaturated at 70 °C for 10 minutes. Samples were loaded on SDS 4-12 % precast

polyacrylamide gels (NuPAGE Novex-Bis-tris-gels, Invitrogen). The electrophoresis was run in 1X MES Running buffer (Invitrogen) for 1 hour and 30 minutes at 150V constant.

Transfer of the protein to the PVDF membrane

After electrophoretic run, proteins were transferred from gels to PDVF membranes. The gel and the membrane were equilibrated in Transfer Buffer. The Transfer Buffer was prepared as follows:

20X NuPAGE® Transfer buffer(Invitogen)	50ml
10X NuPAGE® Antioxidant (Invitogen)	1ml
20% Methanol (Sigma-Aldrich)	200ml

The volume was brought to 1l with distilled water. The transfer was obtained by applying a current of 400mA for 1 hour and 30 minutes at 4°C. To evaluate the efficiency of the transfer, proteins were stained with Red Ponceau 1x (Sigma). The staining was easily reversed by washing with distilled water.

Incubation of the membrane with antibodies

Once the proteins were transferred on PVDF membranes, the membranes were saturated with Blocking Buffer (5% no fat milk powder solubilizated in TBS 1X with 0.1% TWEEN) for 1 hour at room temperature, and then incubated overnight with various primary antibodies at 4°C. The membranes were then washed 3 times with TBS 1X with 0.1% TWEEN at room temperature and incubated with secondary antibody-HRP Conjugate (Bio-Rad), for 1 hour at room temperature. Immunoreaction was revealed by ECL (Pierce) and followed by exposure to X-ray film (KODAK Sigma-Aldrich).

The following antibodies were used for immunoblotting analyses:

Antibody	Company
anti-Akt	Cell Signalling
anti-phospho-Akt (Ser473)	Cell Signalling
anti-phospho-FKHR (Thr24)/FKRL1 (Thr32)	Cell Signalling
anti-phospho-FKHRL1 (Ser253)	Cell Signalling
anti-phospho-4EBP1 (Thr37/46)	Cell Signalling
anti-phospho-4EBP1 (Ser65)	Cell Signalling
anti-4EBP1	Cell Signalling
anti-phosphop70 S6 Kinase (Thr389)	Cell Signalling
anti-p70 S6 Kinase	Cell Signalling
anti phospho-S6 (Ser240/244)	Cell Signalling
anti-S6	Cell Signalling
AntimTOR	Cell Signalling
anti-RICTOR	Cell Signalling
Bnip3 (clone ANa40)	Sigma
Bnip3l	Calbiochem
HA	Santa-Cruz
anti-LC3	MBL International.
Soluble chromatin was coimmunoprecipitated	
anti-FoxO3 antiserum	Santa Cruz
anti-HA antiserum	Santa Cruz
anti-Acetyl-Histone3	Upstate

All the peroxidase-conjugated secondary antibodies were from Bio-Rad.

Blots were stripped using Restore Western Blotting Stripping Buffer (Pierce) according to the manufacturer's instructions and reprobed if necessary.

Statistical analysis

All data are expressed as means ± standard error (se). Differences between groups were assessed using Student's t test. Significance was defined as a value of $P < 0.05$ (95% confidence).

II PART

Autophagy Is Required to Maintain Muscle Mass

Eva Masiero,[1,2,4] Lisa Agatea,[2] Cristina Mammucari,[4] Bert Blaauw,[2,3] Emanuele Loro,[2] Masaaki Komatsu,[5] Daniel Metzger,[6] Carlo Reggiani,[3] Stefano Schiaffino,[2,4] and Marco Sandri[1,2,4,*]
[1]Dulbecco Telethon Institute, via Orus 2, 35129 Padova, Italy
[2]Venetian Institute of Molecular Medicine, via Orus 2, 35129 Padova, Italy
[3]Department of Human Anatomy and Physiology
[4]Department of Biomedical Science
University of Padova, viale Colombo 3, Padova, Italy
[5]Tokyo Metropolitan Institute of Medical Science, Tokyo, Japan
[6]Centre National de la Recherche Scientifique, INSERM, Illkirch-Cedex, France
*Correspondence: marco.sandri@unipd.it
DOI 10.1016/j.cmet.2009.10.008

SUMMARY

The ubiquitin-proteasome and autophagy-lysosome pathways are the two major routes for protein and organelle clearance. In skeletal muscle, both systems are under FoxO regulation and their excessive activation induces severe muscle loss. Although altered autophagy has been observed in various myopathies, the specific role of autophagy in skeletal muscle has not been determined by loss-of-function approaches. Here, we report that muscle-specific deletion of a crucial autophagy gene, *Atg7*, resulted in profound muscle atrophy and age-dependent decrease in force. *Atg7* null muscles showed accumulation of abnormal mitochondria, sarcoplasmic reticulum distension, disorganization of sarcomere, and formation of aberrant concentric membranous structures. Autophagy inhibition exacerbated muscle loss during denervation and fasting. Thus, autophagy flux is important to preserve muscle mass and to maintain myofiber integrity. Our results suggest that inhibition/alteration of autophagy can contribute to myofiber degeneration and weakness in muscle disorders characterized by accumulation of abnormal mitochondria and inclusions.

INTRODUCTION

Macroautophagy, hereafter referred to as autophagy, is a highly conserved homeostatic process carrying out degradation of cytoplasmic components including damaged organelles, toxic protein aggregates and intracellular pathogens (Mizushima et al., 2008). Autophagy takes place at basal levels in all eukaryotic cells, turning over long-lived macromolecules and large supramolecular structures including whole organelles to rejuvenate their function. In addition, autophagy can be upregulated during metabolic, genotoxic, or hypoxic stress conditions and acts as an adaptive mechanism essential for cell survival. Skeletal muscle is a major site of metabolic activity—and the most abundant tissue in the human body, accounting for about 40% of the total body mass. Being the largest protein reservoir, muscle serves as a source of amino acids to be utilized for energy production by various organs during catabolic periods (Lecker et al., 2006). For instance, amino acids generated from muscle protein breakdown are utilized by the liver to produce glucose and to support acute phase protein synthesis (Lecker et al., 2006). Protein degradation in skeletal muscle, like in all the mammalian cells, is controlled by the two major proteolytic systems, the ubiquitin proteasome and the autophagy lysosome. Both degradation pathways are activated in a number of catabolic disease states, including cancer, AIDS, diabetes, and heart and renal failure and contribute to muscle loss and weakness. The two systems are controlled by a transcriptional program that upregulates few critical and rate-limiting enzymes (Sandri, 2008). We have recently identified FoxO transcription factors as the main coordinators of the two proteolytic pathways by inducing several autophagy-related genes as well as the two muscle-specific ubiquitin ligases *atrogin-1* and *MuRF1* (Mammucari et al., 2007; Sandri et al., 2004). While ubiquitin-preoteasome dependent degradation has been deeply investigated and its contribution to muscle loss has been already well documented, the role of autophagy in regulating muscle mass has just started to be studied. Excessive activation of autophagy aggravates muscle wasting (Dobrowolny et al., 2008; Mammucari et al., 2007; Wang et al., 2005; Zhao et al., 2007) by removing portion of cytoplasm, proteins, and organelles. Conversely, inhibition of lysosome-dependent degradation causes myopathies like Pompe and Danon diseases, and autophagy inhibition is thought to play a role in many myopathies with inclusions or with abnormal mitochondria (Levine and Kroemer, 2008; Temiz et al., 2009). However, the exact role of autophagy in physiology of skeletal muscle has never been addressed. Thus, defining the role of autophagy in skeletal muscle homeostasis is critical for understanding the pathogenesis of different diseases and for developing new therapies against muscle loss. To clarify this issue we have generated conditional knockout for *Atg7* gene to block autophagy specifically in skeletal muscle.

RESULTS

Generation of Muscle-Specific Atg7 Knockout Mice

We crossed *Atg7*-floxed mice (*Atg7^f/f^*) with a transgenic line expressing Cre recombinase under the control of a myosin light chain 1 fast promoter to generate muscle-specific *Atg7*-knockout mice, which are hereafter referred to as Atg7$^{-/-}$. PCR analysis
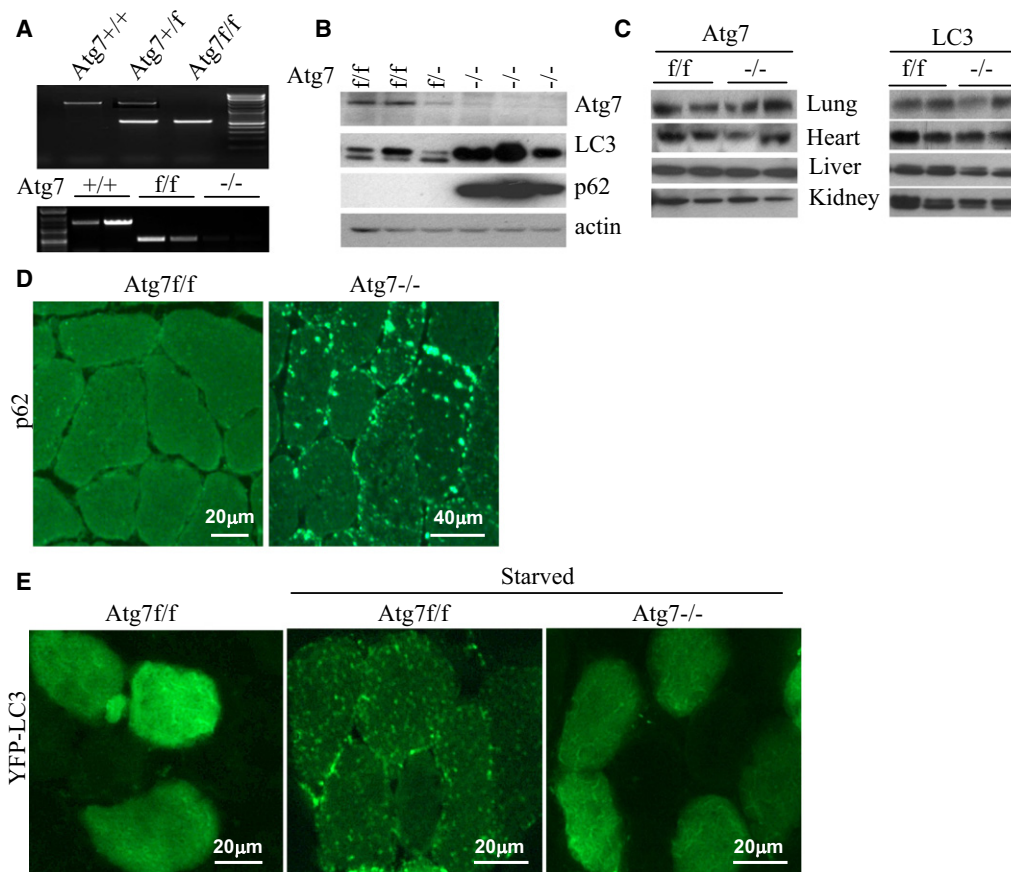
Figure 1. Generation of Muscle-Specific Atg7-Knockout (Atg7$^{-/-}$) Mice

(A) Upper panel, genotyping of the *Atg7$^{f/f}$* mice. Lower panel, PCR analysis with genomic DNA from gastrocnemius muscle. One of the two PCR primers is inside the floxed region. Absence of a PCR product revealed an efficient Cre-mediated recombination of lox-P sites.

(B) Impaired LC3 lipidation and accumulation of p62 protein in Atg7$^{-/-}$ muscles. Muscle homogenates were immunoblotted with antibodies against Atg7, LC3, and p62.

(C) Immunoblot analysis of Atg7 and LC3 in homogenates from different tissues.

(D) Immunohistochemistry for p62 showed aggregates in Atg7$^{-/-}$ muscles but not in Atg7$^{f/f}$ mice.

(E) Autophagosome formation induced by fasting is suppressed in Atg7$^{-/-}$ mice. Muscles of Atg7$^{f/f}$ and Atg7$^{-/-}$ were transfected by electroporation with plasmid coding for YFP-LC3. Eight days later, mice were fasted for 24 hr before sacrifice. Myofibers expressing YFP-LC3 were analyzed by fluorescent microscopy.

confirmed deletion of floxed sequence in genomic DNA from skeletal muscle (Figure 1A). Accordingly, Atg7 protein was almost undetectable in muscles of homozygous mice and considerably reduced in heterozygous animals (Figure 1B). Traces of persistent Atg7 protein are due to endothelial cells, fibroblasts, macrophages, and blood cells. Efficient inhibition of autophagy in skeletal muscles was confirmed by suppression of LC3 lipidation and accumulation of p62 and LC3 proteins in extracts of adult fast and slow muscles (Figures 1B and S1A). LC3 exists in two forms: the free mature form (LC3I) and the faster lipidated LC3 (LC3II). The absence of LC3II band confirms that the reaction of LC3 conjugation to phospholipids was completely blocked. LC3 and p62 proteins are known to be sequestered into the autophagosomes and lost when autophagosomes fuse with lysosomes. Thus, their increase indicates an efficient inhibition of autophagy. Conversely, Atg7 protein was detected and LC3I to LC3II conversion was unaffected in other tissues including heart (Figure 1C). Moreover, immunohistochemical analyses showed the presence of p62 aggregates in myofibers of Atg 7$^{-/-}$ mice (Figure 1D). To

further confirm that autophagic vesicles formation was blocked, we transfected adult skeletal muscle with YFP-LC3, and 1 week later we starved the mice (Mammucari et al., 2007). Ablation of *Atg7* in fasted muscle completely abolished the formation of YFP-LC3 positive autophagosomes in myofibers (Figure 1E). Altogether, these findings validate our genetic mouse model of muscle-specific inhibition of the autophagy system.

Autophagy Inhibition Induces Muscle Atrophy, Loss-of-Force Production, and Morphological Features of Myopathy

The resulting Atg7$^{-/-}$ mice were indistinguishable in appearance from age-matched control Atg7$^{+/+}$ mice. However, the growth curve showed a slight reduction of body growth, which started to differ from control after about 40 days from birth (Figure S2). Morphological analysis of adult muscles revealed degenerative changes, including vacuolated and centrally nucleated myofiber, and a general decrease in myofiber size at 2 months of age (Figures 2A and 2B). A few fibers were positive for immunoglobulin
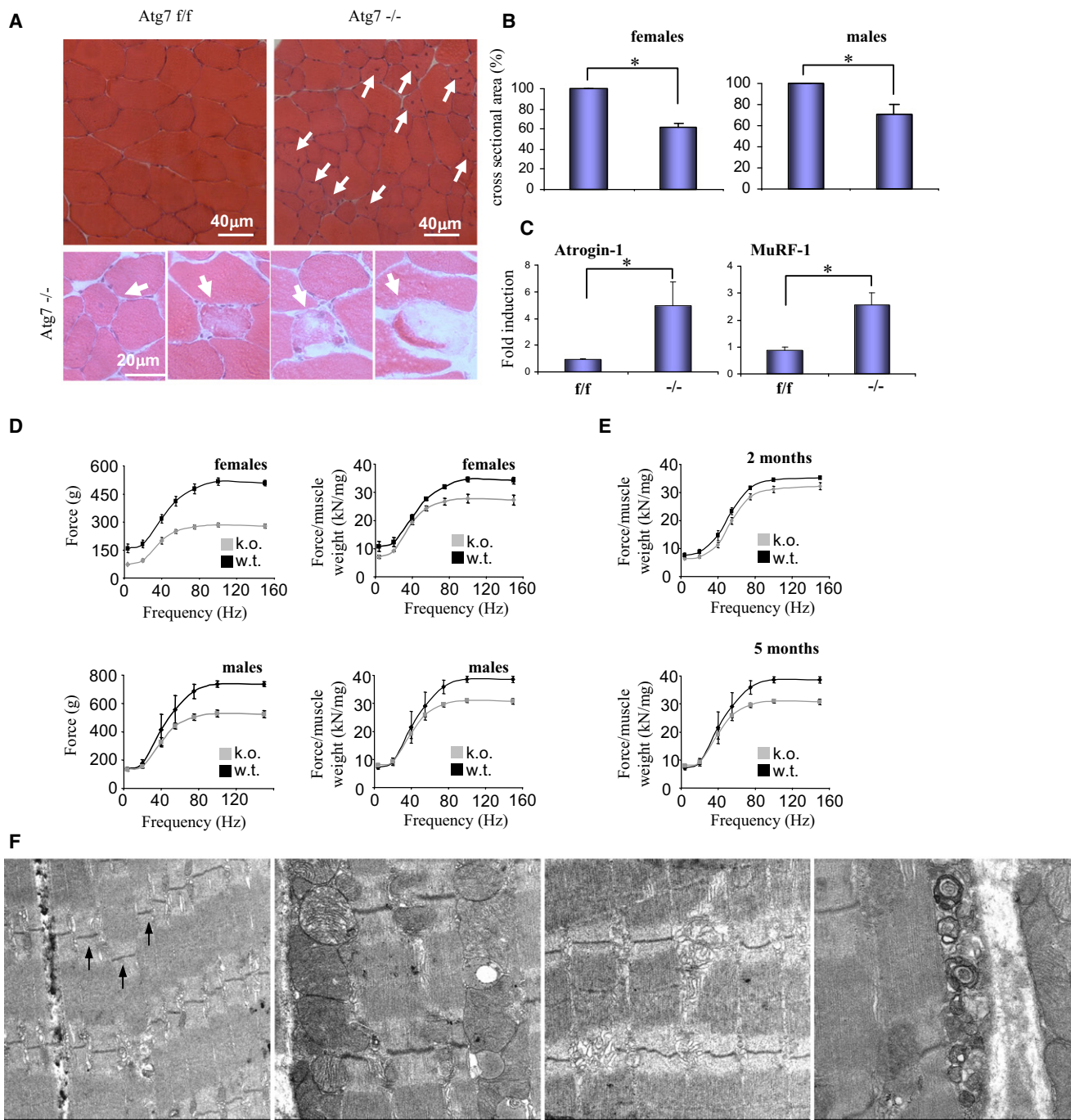
Figure 2. Morphological and Functional Changes in Muscles of Atg7$^{-/-}$ Mice Reveal Muscle Dysfunction and Features of Myopathy

(A) H&E staining showing a general decrease in myofibers size and different features of muscle degeneration (white arrows), including central nuclei and vacu-olated fibers.

(B) Quantification of cross-sectional area (CSA) of myofibers. Values are mean ± SEM of data from five mice in each group.

(C) Upregulation of the critical atrophy-related and muscle specific genes in adult skeletal muscle of Atg7$^{-/-}$. RNA was extracted from TA muscles, and quan-titative PCR analysis was performed in triplicates using specific oligonucleotides (see Table S1). Data were normalized to the β-actin content and expressed as fold increase over levels of Atg7$^{f/f}$ muscles, data are mean ± SEM. (*p < 0.001).

(D) Force measurements performed in vivo showed that Atg7$^{-/-}$ led to a profound decrease in force generation especially of maximal force generated during tetanic contraction. The force is still significantly reduced even when the absolute tetanic force is normalized for the muscle weight (n = 5); data are mean ± SEM.

(E) Age aggravated the impairment of force production.

(F) Electron micrographs of Atg7$^{-/-}$ EDL muscles.

staining as a consequence of membrane permeabilization, suggesting the presence of rare necrotic events, which, however do not modify creatine kinase blood levels. Myosin composition was not affected in Atg7$^{-/-}$ muscles (Figures S3 and S4). The frequency of centrally nucleated fibers slowly increased with age (Figure S5A). Importantly myofiber degeneration is not caused by alteration in dystrophin expression and localization (Figure S6). Quantification of cross-sectional area showed a 40% decrease in myofiber size both in females and males (Figures 2B and S7). Further characterization displayed no difference between fiber types; both glycolitic and oxidative fibers undergo muscle atrophy (Figure S8). The muscle-to-body weight ratio was also decreased, suggesting an important waste of muscle tissue (Figure S9). Loss of muscle mass is controlled by a transcriptional program that requires activation of a subset of genes named atrophy-related genes or atrogenes (Lecker et al., 2004). Thus, we monitored the level of expression of atrogenes involved in the ubiquitin proteasome. Indeed, the two atrophy-related ubiquitin ligases atrogin-1 and MuRF1, as well as genes involved in different catabolic pathways, were upregulated in Atg7$^{-/-}$ muscles at basal state (Figures 2C and S10). The upregulation of the ubiquitin ligases is associated with FoxO1 dephosphorylation and activation (Figure S11). Interestingly, proteasomal function is not impaired in Atg7 null muscles but instead is increased (Figure S12). Inhibition of autophagy led also to induction of apoptosis (Figure S12). Altogether, these results suggest that deletion of Atg7 triggers compensatory upregulation of ubiquitin proteasome system and activation of apoptosis, which contribute, at least partially, to muscle loss.

Next, we asked whether muscle atrophy is accompanied by changes of muscle force in living animals. Physiological analyses showed a marked reduction in absolute force independently of gender (Figure 2D). Importantly, when the absolute force was normalized for the muscle mass, the resulting specific force was still significantly decreased. Thus, not only do the muscles become smaller but there is a general impairment in force transmission that leads to profound weakness. Importantly, force drop was age dependent since 5-month-old males showed a more important decrease in specific force, when compared to age-matched control littermates, than 2-month-old mice (Figure 2E). To understand the important impairment in force generation, we performed electron-microscopy studies. Several changes were detected in Atg7$^{-/-}$ muscles including misalignment of Z-line, accumulation of big abnormal mitochondria which in some cases span from one to the next Z line, presence of swollen mitochondria, sarcoplasmic reticulum distension, and formation of aberrant concentric membranous structure (Figures 2F and S13) similar to those observed in Atg7-deficient livers and Atg5-deficient hearts (Komatsu et al., 2005; Nakai et al., 2007). The alteration of mitochondrial morphology is associated with oxidative stress, as revealed by increased protein carbonylation and expression of antioxidant genes, but apparently not to energy unbalance, since AMPK was not activated (Figures S14A–S14C). In addition, the changes of sarcoplasmic reticulum are related with a markedly increased phosphorylation, and therefore inhibition, of the translation initiation factor eIF2α, which is known to lead to suppression of ribosome assembly and protein synthesis. Altogether, the phosphorylation of eIF2α and the increase of the endoplasmic reticulum (ER) chaperone,

BiP/GRP78, are consistent with an unfolding protein response (Figure S15).

Inhibition of Autophagy Exacerbates Muscle Loss and Degeneration in Catabolic Conditions

Next, we wanted to clarify the contribution and the role of autophagy under conditions of muscle wasting. We used two models of muscle atrophy, fasting and denervation, and we compared Atg7 null muscles with controls. Inhibition of autophagy did not prevent muscle loss and activation of the atrophy-related program in denervated muscles. On the contrary, autophagy-deficient animals lost significantly more muscle mass than control ones (Figure 3A). Expression of several atrophy-related genes, including MuRF1, cathepsin L, and Bnip3l, were more upregulated in atrophying muscles of Atg7$^{-/-}$ muscles, which suggest a more important activation of the atrophy program (Figures 3B and S16). Morphological observations showed different features of myopathy in denervated Atg7$^{-/-}$ muscles, including presence of abnormal myonuclei, accumulation of hematoxylin-positive inclusions, and vacuolated area, which were present only in autophagy-deficient muscles (Figures 3C and S17). Electron microscopy revealed the presence of concentric membranous structures embedded into an electron-opaque amorphous material (Figure 3D). Interestingly, p62 aggregates were increased in size and number in denervated myofibers of Atg7$^{-/-}$ mice compared to innervated muscles (Figure 3E). The p62-positive aggregates were also positive for ubiquitin (Figures 3F and S18). Accordingly, p62 and ubiquitinated proteins greatly accumulate in detergent soluble and insoluble fractions of autophagy-deficient denervated muscles (Figures 3G and S19). Thus, autophagy inhibition does not preserve muscle mass during catabolic conditions and, surprisingly, exacerbates muscle loss during denervation.

We next examined muscle atrophy induced by fasting. Atg7$^{-/-}$ and Atg7$^{+/+}$ muscles showed similar upregulation of atrophy-related genes, which reflects no major difference in the changes of Akt phosphorylation and downstream targets (Figures 4A and 4B). However, the morphological features of muscle degeneration were more evident. Many small flattened or irregularly shaped fibers containing hematoxylin-positive inclusions as well as fibers with fragmented and vacuolated cytosol appeared in Atg7$^{-/-}$ muscles during fasting (Figure 4C). Electron microscopy revealed an increase of the concentric membranous structures (Figure 4D). However, fasted muscles never showed the amorphous material detected in denervated muscles. Interestingly, p62 aggregates were similar or smaller than the ones found in fed Atg7$^{-/-}$ muscles and certainly never reached the size of those observed in denervated muscles (Figure 4E). Indeed, p62 did not accumulate in detergent-soluble and -insoluble fractions of starved muscles (Figure S20). Thus, autophagy plays different roles and importance in different conditions of muscle loss but seems to be always crucial for maintaining normal homeostasis of muscle mass in physiological and pathological conditions.

Deletion of *Atg7* Gene in Adulthood Triggers Muscle Loss and Weakness

To further check the role of autophagy in adulthood, we generated tamoxifen-inducible muscle-specific Atg7 knockout mice.
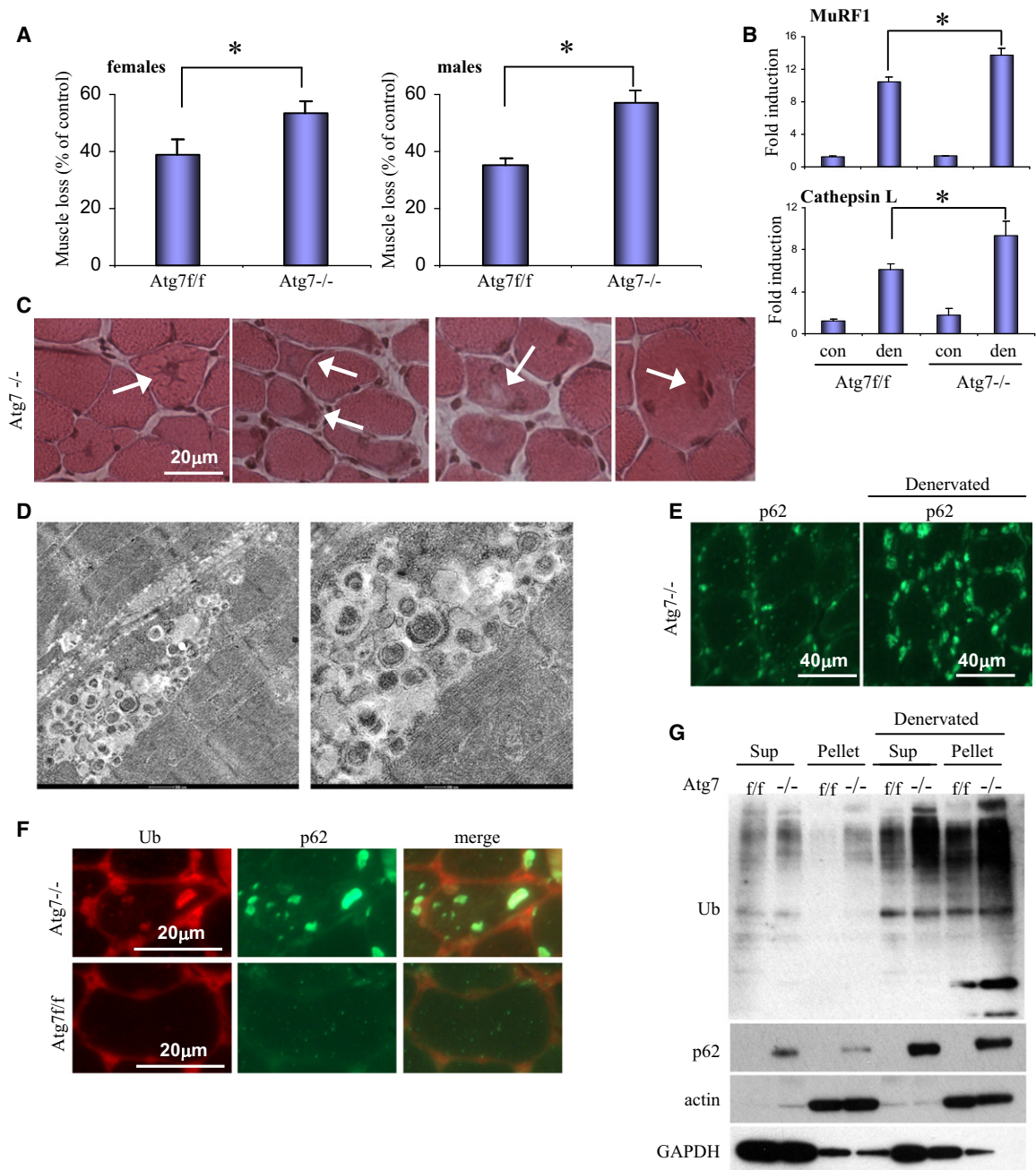
Figure 3. Denervation Aggravates Morphological Abnormalities and Muscle Loss in Atg7$^{-/-}$ Muscles

(A) Quantification of muscle loss after 2 weeks from denervation. CSA of innervated and denervated fibers was measured. Muscle loss is expressed as percentage of decrease of cross-sectional areas of denervated fibers versus innervated ones. More than 1000 fibers per each muscle were counted (n = 4); data are mean ± SEM (*p < 0.001).

(B) Enhanced upregulation of the atrophy-related genes in denervated skeletal muscles of Atg7$^{-/-}$ mice. Data are mean ± SEM (*p < 0.01).

(C) H&E staining showing accumulation of hematoxylin-positive structures, vacuolated areas, and abnormal nuclei (white arrows) in denervated Atg7$^{-/-}$.

(D) Electron micrographs of denervated Atg7$^{-/-}$ showing aberrant concentric membranous structures dispersed between amorphous electron opaque material.

(E) Immunostaining for anti-p62 showed that p62 aggregates increased in size and number in denervated muscle of Atg7$^{-/-}$.

(F) Double imunofluorescence staining reveals the colocalization of p62 and ubiquitin.

(G) Increase of ubiquitinated proteins and of p62 in Atg7$^{-/-}$ muscles during denervation. Detergent-soluble (Sup) and -insoluble (Pellet) fractions of control and denervated muscles were immunoblotted against ubiquitin and p62. Data are representative of three different experiments.
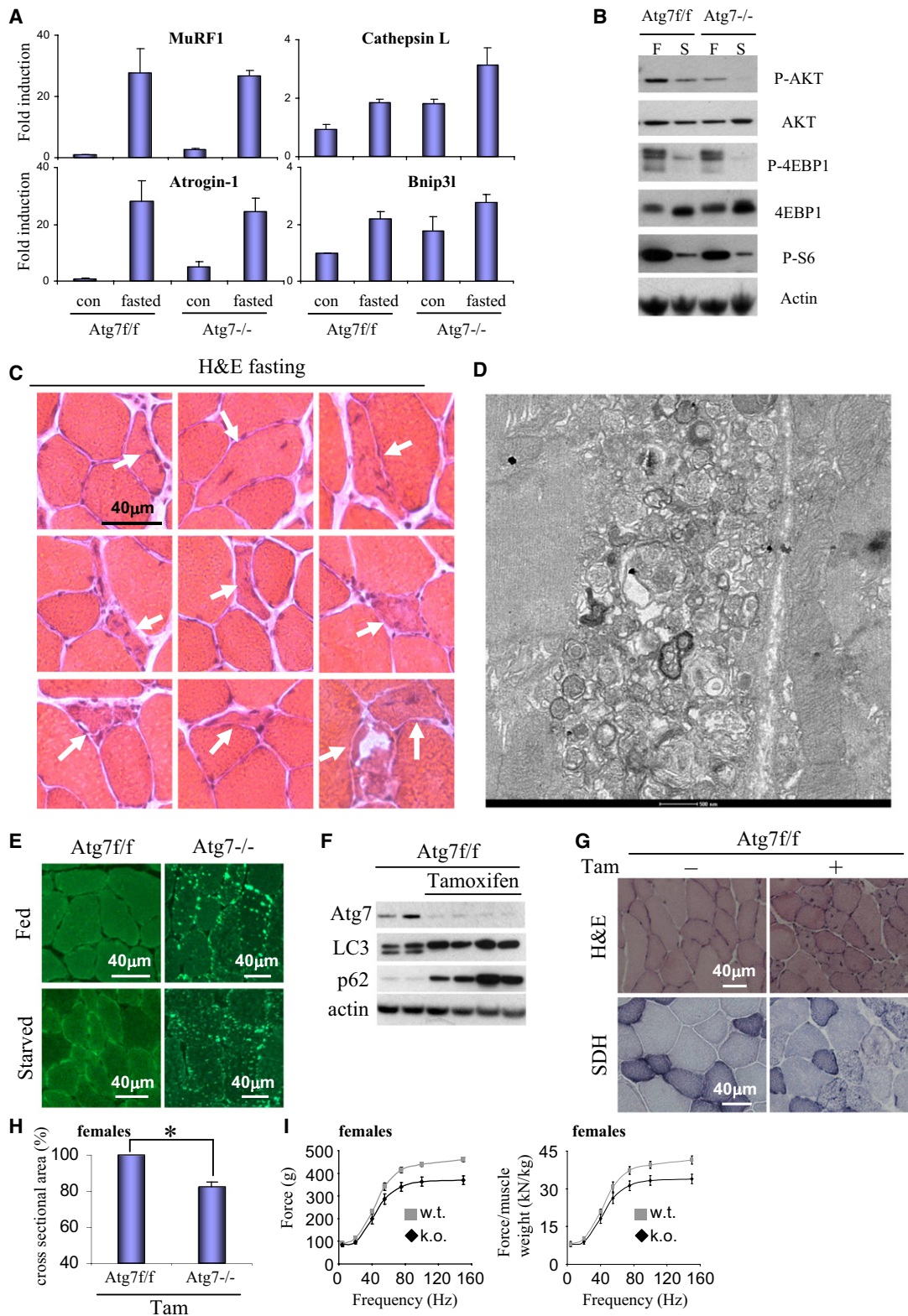
Figure 4. Atg7 Deficiency in Fasting and in a Tamoxifen-Inducible Muscle-Specific Atg7-Knockout Mice

(A) Upregulation of the atrophy-related genes in fasted skeletal muscles of Atg7$^{-/-}$ mice.

(B) Immunoblotting for insulin-dependent pathway in fed (F) and starved (S) muscles of Atg7$^{f/f}$ and Atg7$^{-/-}$ mice.

(C) H&E staining showing different features of muscle degeneration including small flattened or angulated atrophic fibers containing hematoxylin inclusion, central nuclei, vacuoles, and loss of plasma membrane integrity.

Immunoblotting analyses confirmed the *Atg7* deletion and the concomitant block of autophagy revealed by p62 accumulation and by inhibition of LC3 lipidation in glycolytic and oxidative muscles (Figures 4F and S1B). Morphological analyses showed the presence of structural alterations that are identical to those observed in non-inducible Atg7$^{-/-}$ muscle. Succinate dehydrogenase staining revealed accumulation of abnormal mitochondria in small atrophic fibers (Figure 4G). However, centrally nucleated fibers were more abundant after acute Atg7 deletion than in non-inducible autophagy-deficient muscles (Figure S5B). Indeed, when we measured muscle mass we found that autophagy inhibition triggered muscle wasting. Quantification of cross-sectional area showed a 20% decrease in myofiber size (Figure 4H), which was accompanied by a decrease in absolute and specific force (Figure 4I).

DISCUSSION

Our results indicate that basal autophagy plays a beneficial role in controlling muscle mass. Lack of autophagy affects the organelle shaping machinery and leads to accumulation of atypical giant mitochondria and dilated sarcoplasmic reticulum. However, accumulation of abnormal organelles is not always harmful for cellular function. In fact, ablation of *p62* in liver-specific autophagy-deficient mice suppresses pathological phenotypes including severe hepatomegaly, inflammation, and leakage of hepatic enzymes despite accumulation of abnormal organelles in the mice (Komatsu et al., 2007). Therefore, at least in autophagy-deficient liver, the presence of degenerated mitochondria might be hardly attributed to the phenotypes. Conversely, loss of p62 in neural-specific Atg7$^{-/-}$ mice does not suppress the pathology. Neurons from both single Atg7$^{-/-}$ and Atg7/p62 double knockout accumulate large number of abnormal organelles in the axon terminals, suggesting that an appropriate turnover of organelles in axon terminal is essential for neuronal homeostasis (Komatsu et al., 2007). Therefore, we can conclude that pathogenesis of cellular dysfunction and degeneration during autophagy inhibition differs among tissues and cell types.

In muscle, the persistence of dysfunctional organelle seems to be important for the activation of catabolic pathways, which results in muscle atrophy and weakness. In our model, alteration in sarcoplamic reticulum reflects an unfolding protein response that suppresses protein synthesis while mitochondrial damage generates oxidative stress and apoptosis. Also, the induction of Bnip3, which promotes mitochondrial fragmentation and mitophagy, in Atg7$^{-/-}$ muscles might contribute to caspase activation and apoptosis by affecting permeability transition pore opening. The control of mitochondrial function seems to be crucial for preventing a cascade of signals that lead to muscle

atrophy (Sandri et al., 2006). The accumulation of aged and dysfunctional mitochondria and their potential negative role for cell survival has been recently underlined by different genetic evidences. For instance, it has been shown that dysfunctional mitochondria contribute to the pathogenesis of Ullirich and Bethlem dystrophies (Angelin et al., 2007; Irwin et al., 2003; Merlini et al., 2008). Similarly, erythroid cells lacking Bnip3l show persistence of mitochondria, due to a block of autophagy, which causes premature cell death and anemia (Sandoval et al., 2008). It is unclear whether our data of oxidative stress in Atg7$^{-/-}$ muscle is mainly caused by accumulation of dysfunctional mitochondria due to a defect in mitophagy, as recently described in autophagy-deficient cells (Tal et al., 2009), or whether it is secondary to p62 aggregates (Mathew et al., 2009). Moreover Atg7$^{-/-}$ muscles showed activation of ER chaperones, such as BiP, as well as the phosphorylation of eIF2α, suggesting an ongoing unfolded protein response. The failure of protein-folding quality control in Atg7$^{-/-}$ mice induces endoplasmic reticulum stress, which can generate ROS, and suppression of protein synthesis, which can contribute to muscle atrophy.

Recently muscle-specific Atg5$^{-/-}$ mice have been generated (Raben et al., 2008), and their phenotype is similar though not identical to that of Atg7$^{-/-}$ mice. Both knockouts show muscle loss, protein aggregates, and accumulation of abnormal membranous structures. The main difference between the two studies is related to the lack-of-force impairment reported in Atg5$^{-/-}$ animals. However, muscle force in Atg5$^{-/-}$ mice was evaluated by an indirect test, the wire-hang test, which can be affected by many variables including fatigue, whereas we performed a direct physiological analysis of force measurement on gastrocnemius muscles. In conclusion, our results suggest that in skeletal muscle defects in organelle removal generate a signaling cascade, which induces profound muscle loss and weakness. It has been shown that the efficiency of autophagic degradation declines during aging, leading to accumulation of intracellular waste products (Salminen and Kaarniranta, 2009). Our results suggest that impaired autophagy may contribute to aging sarcopenia. Thus, to combat sarcopenia, it is important to maintain autophagy flux to rejuvenate organelles and to prevent accumulation of dysfunctional mitochondria and ER membranes, as well as to block excessive protein breakdown.

EXPERIMENTAL PROCEDURES

Generation of Muscle-Specific Atg7$^{-/-}$ Mice and In Vivo Transfection Experiments
Generation of muscle-specific Atg7$^{-/-}$ mice is described in Supplemental Data. In vivo transfection experiments were performed by intramuscular injection of plasmid DNA in tibialis anterior (TA) muscle followed by electroporation

---

(D) Electron micrograph of fasted Atg7$^{-/-}$ muscles.

(E) Immunostaining for p62 showed positive aggregates in Atg7$^{-/-}$ muscles.

(F) Immunoblotting for Atg7, LC3, and p62 proteins on muscle extracts from inducible Atg7$^{-/-}$ mice. Two weeks after the last tamoxifen injection, skeletal muscles were collected and analyzed.

(G) H&E staining showing a general decrease in myofiber size and accumulation of hematoxylin positive inclusions. SDH staining on serial sections showed an accumulation of abnormal mitochondria.

(H) Quantification of CSA of myofibers. Values are mean ± SEM of data from five mice in each group, at least 1000 fibers for each muscles were measured (*p < 0.001).

(I) Force measurements performed in vivo, data are mean ± SEM (n = 5).

as described (Mammucari et al., 2007). Muscles were removed at 8 days after transfection and frozen in liquid nitrogen for subsequent analyses. Denervation was performed by cutting the sciatic nerve of left limb while right limb was used as control. Muscles were collected 3 days after denervation for gene-expression studies and 14 days after denervation for morphological analyses.

Gene-Expression Analyses

Total RNA was prepared from TA muscles using Promega SV Total RNA Isolation Kit. Complementary DNA generated with Invitrogen SuperScript III Reverse Transcriptase was analyzed by quantitative real-time RT-PCR using QIAGEN QuantiTect SYBR Green PCR Kit. All data were normalized to β-actin. The oligonucleotide primers used are shown in Table S1.

Immunoblotting

Frozen gastrocnemius muscles were powdered by pestle and mortar and lysed in a buffer containing 50 mM Tris pH 7.5, 150 mM NaCl, 10 mM $MgCl_2$, 0.5 mM DTT, 1 mM EDTA, 10% glycerol, 2% SDS, 1% Triton X-100, Roche Complete Protease Inhibitor Cocktail, 1 mM PMSF, 1 mM $NaVO_3$, 5 mM NaF and 3 mM β-glycerophosphate. The samples were immunoblotted as previously described (Sandri et al., 2004) and visualized with SuperSignal West Pico Chemiluminescent substrate (Pierce). Blots were stripped using Restore Western Blotting Stripping Buffer (Pierce) according to the manufacturer's instructions and reprobed if necessary. Detergent-soluble and -insoluble fractions were obtained according to (Hara et al., 2006). A list of antibodies is shown in Supplemental Data.

Histology, Fluorescence Microscopy, and Electron Microscopy

Cryosections of TA muscles transfected with YFP-LC3 were examined in a fluorescence microscope as described (Mizushima et al., 2004). Cryosections of TA were stained for H&E, for SDH, PAS, anti-ubiquitin, and anti-p62. CSA was performed on TA as described (Blaauw et al., 2008; Mammucari et al., 2007). For electron microscopy, we used conventional fixation-embedding procedures based on glutaraldehyde-osmium fixation and Epon embedding.

Measurements of Muscle Force In Vivo

Muscle force was measured in a living animal as previously described (Blaauw et al., 2008). Briefly gastrocnemius muscle contractile performance was measured in vivo in anaesthetized mice using a 305B muscle lever system (Aurora Scientific, Inc.). Contraction was elicited by electrical stimulation of the sciatic nerve. Force developed by plantar flexor muscles was calculated by dividing torque by the lever arm length (taken as 2.1 mm).

SUPPLEMENTAL DATA

The Supplemental Data include 20 figures, Supplemental Experimental Procedures, and Supplemental References and can be found with this article online at http://www.cell.com/cellmetabolism/supplemental/S1550-4131(09)00310-6.

REFERENCES

Angelin, A., Tiepolo, T., Sabatelli, P., Grumati, P., Bergamin, N., Golfieri, C., Mattioli, E., Gualandi, F., Ferlini, A., Merlini, L., et al. (2007). Mitochondrial dysfunction in the pathogenesis of Ullrich congenital muscular dystrophy and prospective therapy with cyclosporins. Proc. Natl. Acad. Sci. USA 104, 991–996.

Blaauw, B., Mammucari, C., Toniolo, L., Agatea, L., Abraham, R., Sandri, M., Reggiani, C., and Schiaffino, S. (2008). Akt activation prevents the force drop induced by eccentric contractions in dystrophin-deficient skeletal muscle. Hum. Mol. Genet. 17, 3686–3696.

Dobrowolny, G., Aucello, M., Rizzuto, E., Beccafico, S., Mammucari, C., Bonconpagni, S., Belia, S., Wannenes, F., Nicoletti, C., Del Prete, Z., et al. (2008). Skeletal muscle is a primary target of SOD1G93A-mediated toxicity. Cell Metab. 8, 425–436.

Hara, T., Nakamura, K., Matsui, M., Yamamoto, A., Nakahara, Y., Suzuki-Migishima, R., Yokoyama, M., Mishima, K., Saito, I., Okano, H., and Mizushima, N. (2006). Suppression of basal autophagy in neural cells causes neurodegenerative disease in mice. Nature 441, 885–889.

Irwin, W.A., Bergamin, N., Sabatelli, P., Reggiani, C., Megighian, A., Merlini, L., Braghetta, P., Columbaro, M., Volpin, D., Bressan, G.M., et al. (2003). Mitochondrial dysfunction and apoptosis in myopathic mice with collagen VI deficiency. Nat. Genet. 35, 367–371.

Komatsu, M., Waguri, S., Ueno, T., Iwata, J., Murata, S., Tanida, I., Ezaki, J., Mizushima, N., Ohsumi, Y., Uchiyama, Y., et al. (2005). Impairment of starvation-induced and constitutive autophagy in Atg7-deficient mice. J. Cell Biol. 169, 425–434.

Komatsu, M., Waguri, S., Koike, M., Sou, Y.S., Ueno, T., Hara, T., Mizushima, N., Iwata, J., Ezaki, J., Murata, S., et al. (2007). Homeostatic levels of p62 control cytoplasmic inclusion body formation in autophagy-deficient mice. Cell 131, 1149–1163.

Lecker, S.H., Jagoe, R.T., Gilbert, A., Gomes, M., Baracos, V., Bailey, J., Price, S.R., Mitch, W.E., and Goldberg, A.L. (2004). Multiple types of skeletal muscle atrophy involve a common program of changes in gene expression. FASEB J. 18, 39–51.

Lecker, S.H., Goldberg, A.L., and Mitch, W.E. (2006). Protein degradation by the ubiquitin-proteasome pathway in normal and disease states. J. Am. Soc. Nephrol. 17, 1807–1819.

Levine, B., and Kroemer, G. (2008). Autophagy in the pathogenesis of disease. Cell 132, 27–42.

Mammucari, C., Milan, G., Romanello, V., Masiero, E., Rudolf, R., Del Piccolo, P., Burden, S.J., Di Lisi, R., Sandri, C., Zhao, J., et al. (2007). FoxO3 Controls Autophagy in Skeletal Muscle In Vivo. Cell Metab. 6, 458–471.

Mathew, R., Karp, C.M., Beaudoin, B., Vuong, N., Chen, G., Chen, H.Y., Bray, K., Reddy, A., Bhanot, G., Gelinas, C., et al. (2009). Autophagy suppresses tumorigenesis through elimination of p62. Cell 137, 1062–1075.

Merlini, L., Angelin, A., Tiepolo, T., Braghetta, P., Sabatelli, P., Zamparelli, A., Ferlini, A., Maraldi, N.M., Bonaldo, P., and Bernardi, P. (2008). Cyclosporin A corrects mitochondrial dysfunction and muscle apoptosis in patients with collagen VI myopathies. Proc. Natl. Acad. Sci. USA 105, 5225–5229.

Mizushima, N., Yamamoto, A., Matsui, M., Yoshimori, T., and Ohsumi, Y. (2004). In vivo analysis of autophagy in response to nutrient starvation using transgenic mice expressing a fluorescent autophagosome marker. Mol. Biol. Cell 15, 1101–1111.

Mizushima, N., Levine, B., Cuervo, A.M., and Klionsky, D.J. (2008). Autophagy fights disease through cellular self-digestion. Nature 451, 1069–1075.

Nakai, A., Yamaguchi, O., Takeda, T., Higuchi, Y., Hikoso, S., Taniike, M., Omiya, S., Mizote, I., Matsumura, Y., Asahi, M., et al. (2007). The role of autophagy in cardiomyocytes in the basal state and in response to hemodynamic stress. Nat. Med. 13, 619–624.

Raben, N., Hill, V., Shea, L., Takikita, S., Baum, R., Mizushima, N., Ralston, E., and Plotz, P. (2008). Suppression of autophagy in skeletal muscle uncovers the accumulation of ubiquitinated proteins and their potential role in muscle damage in Pompe disease. Hum. Mol. Genet. 17, 3897–3908.

Salminen, A., and Kaarniranta, K. (2009). Regulation of the aging process by autophagy. Trends Mol. Med. 15, 217–224.

Sandoval, H., Thiagarajan, P., Dasgupta, S.K., Schumacher, A., Prchal, J.T., Chen, M., and Wang, J. (2008). Essential role for Nix in autophagic maturation of erythroid cells. Nature *454*, 232–235.

Sandri, M. (2008). Signaling in muscle atrophy and hypertrophy. Physiology (Bethesda) *23*, 160–170.

Sandri, M., Sandri, C., Gilbert, A., Skurk, C., Calabria, E., Picard, A., Walsh, K., Schiaffino, S., Lecker, S.H., and Goldberg, A.L. (2004). Foxo transcription factors induce the atrophy-related ubiquitin ligase atrogin-1 and cause skeletal muscle atrophy. Cell *117*, 399–412.

Sandri, M., Lin, J., Handschin, C., Yang, W., Arany, Z.P., Lecker, S.H., Goldberg, A.L., and Spiegelman, B.M. (2006). PGC-1alpha protects skeletal muscle from atrophy by suppressing FoxO3 action and atrophy-specific gene transcription. Proc. Natl. Acad. Sci. USA *103*, 16260–16265.

Tal, M.C., Sasai, M., Lee, H.K., Yordy, B., Shadel, G.S., and Iwasaki, A. (2009). Absence of autophagy results in reactive oxygen species-dependent amplification of RLR signaling. Proc. Natl. Acad. Sci. USA *106*, 2770–2775.

Temiz, P., Weihl, C.C., and Pestronk, A. (2009). Inflammatory myopathies with mitochondrial pathology and protein aggregates. J. Neurol. Sci. *278*, 25–29.

Wang, X., Blagden, C., Fan, J., Nowak, S.J., Taniuchi, I., Littman, D.R., and Burden, S.J. (2005). Runx1 prevents wasting, myofibrillar disorganization, and autophagy of skeletal muscle. Genes Dev. *19*, 1715–1722.

Zhao, J., Brault, J.J., Schild, A., Cao, P., Sandri, M., Schiaffino, S., Lecker, S.H., and Goldberg, A.L. (2007). FoxO3 coordinately activates protein degradation by the autophagic/lysosomal and proteasomal pathways in atrophying muscle cells. Cell Metab. *6*, 472–483.

Autophagy Is Required to Maintain Muscle Mass

Eva Masiero, Lisa Agatea, Cristina Mammucari, Bert Blaauw, Emanuele Loro, Masaaki Komatsu, Daniel Metzger, Carlo Reggiani, Stefano Schiaffino, and Marco Sandri

SUPPLEMENTAL EXPERIMENTAL PROCEDURES

Generation of muscle specific Atg7 knockout mice

Mice bearing an *Atg7* Flox allele (Komatsu et al., 2005) (*Atg7$^{f/f}$*) were crossed with transgenic expressing *Cre* under the control of a *Myosin Light Chain 1 fast* promoter (*MLC1f-Atg7*) (Bothe et al., 2000; Mammucari et al., 2007) or with transgenic expressing a *Cre-ER* driven by *human skeletal actin* promoter (*HAS-Atg7*) (Schuler et al., 2005). Genomic DNA isolated from mice containing an *Atg7$^{f/f}$* was subjected to PCR analysis. *Cre*-mediated recombination was confirmed by PCR with genomic DNA from gastrocnemius muscles. The primers used are described in (Komatsu et al., 2005). Tamoxifen-inducible *Cre-ER* was activated by Intra Peritoneum injection of 5 μg Tamoxifen (Sigma) to 2 months old mice daily for one week. *Atg7$^{f/f}$* but *Cre-ER* negative mice have been treated with Tamoxifen as above described and have been used as controls. Muscles were collected two weeks after the last Tamoxifen injection.

Antibodies

The following antibodies from Cell Signalling were used: anti-Akt, anti-phospho-Akt (Ser473), anti-phospho-4EBP1 (Thr37/46), anti-phospho-4EBP1 (Ser65), anti-4EBP1, anti-phospho-S6 (Ser240/244), anti-S6, anti-P-AMPKα (Thr 172) and anti-AMPKα . LC3 antibody was from NanoTools, p62 antibody from PROGEN. Atg 7 antibody was a generous gift of Dr. T. Ueno. Anti-P-eIF2α (S51)and anti-eIF2α from ABCAM; monoclonal anti-Actin (clone AC40), monoclonal anti-GAPDH and monoclonal anti-dystrophin (clone MANDRA1) from Sigma-Aldrich; anti-dystrophin antibody for immunhistochemistry from ABCAM; anti-BIP from BD (Becton Dickinson and Company) and anti-mono- and polyubiquinylated conjugates (clone FK2) from BIOMOL international.

Oxidative stress.

Carbonylation of muscle proteins were detected by using the OxyBlot Protein Oxidation Detection Kit from Millipore.

Creatine kinase assay

To evaluate the amount of creatine kinase present in the blood, samples of blood were obtained by peri-orbital bleeding in anaesthetized mice. Serum creatine kinase content was measured by an indirect colorimetric assay (Sentinel Diagnostics kit).

In vivo proteasome function assay

Adult skeletal muscles of Atg7$^{-/-}$ and Atg7$^{f/f}$ were cotransfected with Histone2B-RFP and Ub^{G76V}-GFP as previously described (Mammucari et al., 2007). Transfected myofibers are revealed by the presence of red nuclei.

SUPPLEMENTAL TABLES

Table S1

Primers used in Q-RT-PCR analyses

	Forward primer	Reverse primer
MAP1-LC3b	cactgctctgtcttgtgtaggttg	tcgttgtgcctttattagtgcatc
Cathepsin L	gtggactgttctcacgctcaag	tccgtccttcgcttcatagg
Atrogin 1	gcaaacactgccacattctctc	cttgaggggaaagtgagacg
Murf1	acctgctggtggaaaacatc	cttcgtgttccttgcacatc
Bnip3	ttccactagcaccttctgatga	gaacaccgcatttacagaacaa
Bnip3l	ttggggcattttactaaccttg	tgcaggtgactggtggtactaa
p62	Cccagtgtcttggcattctt	agggaaagcagaggaagctc
b-actin	ctggctcctagcaccatgaagat	ggtggacagtgaggccaggat

Table S1

Table S1. Primers used for quantitative PCR (qPCR) analyses.

SUPPLEMENTAL FIGURE LEGENDS

Figure S1
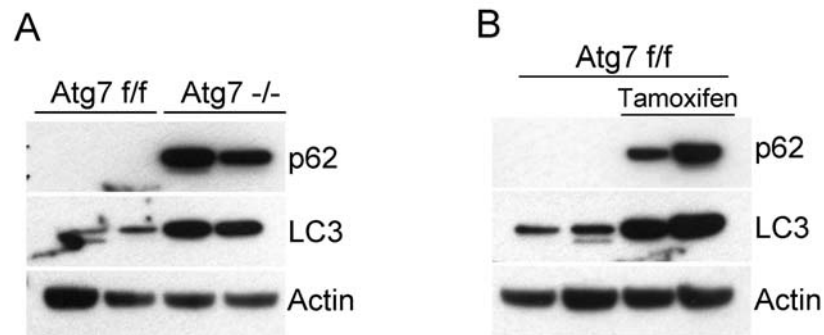
Figure S1.

(A) Impairment of LC3 lipidation and accumulation of p62 protein in Atg7-deficient soleus. Muscle homogenates from soleus of MLC1f-Atg7 mice were immunoblotted with antibodies against LC3 and p62. It is known that so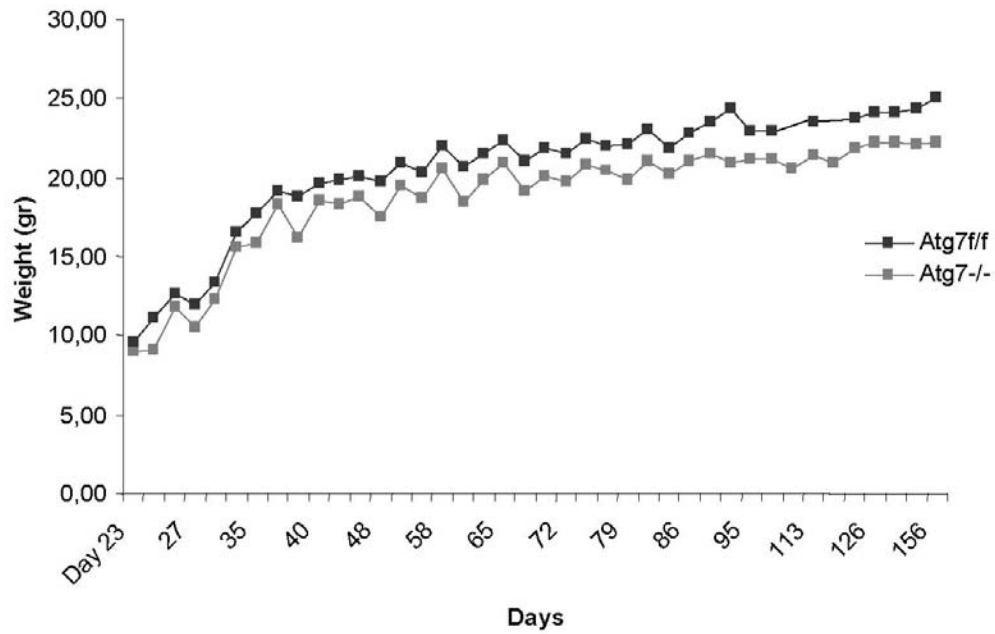leus muscle has a low rate of autophagy flux (Mizushima et al., 2004). Therefore, LC3 exists mainly in the unlipidated form. **(B)** Impairment of LC3 lipidation and accumulation of p62 protein in Tamoxifen-inducible Atg7-deficient soleus. Muscle homogenates from soleus of tamoxifen treated mice were immunoblotted with antibodies against LC3 and p62.

Figure S2

Figure S2. Growth curve of Atg7$^{f/f}$ and Atg7$^{-/-}$ mice. Female and Male mice were weighted every 3 days and plotted together. A significant difference between Atg7 deficient and control mice (* p<0.05) was observed after the age of 40 days.
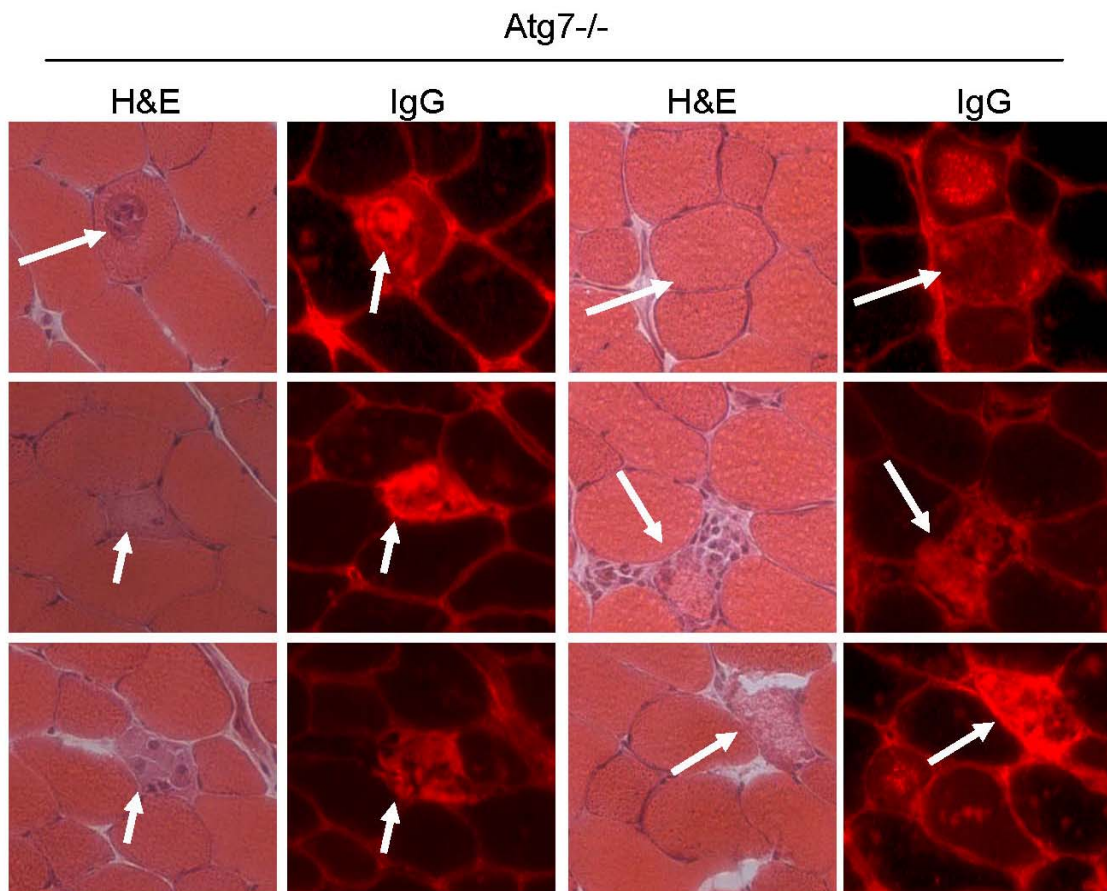
Figure S3

Figure S3. Morphology of Atg7$^{-/-}$ revealed myopathic phenotype. H&E staining showed different degrees of myofiber degeneration with macrophages infiltrations and foci of inflamamtion. Serial sections were stained for anti-IgG to confirm the plasma membrane permeabilization. However the necrotic fibers in Atg7 deficient muscles were rare and scattered between normal myofibers.
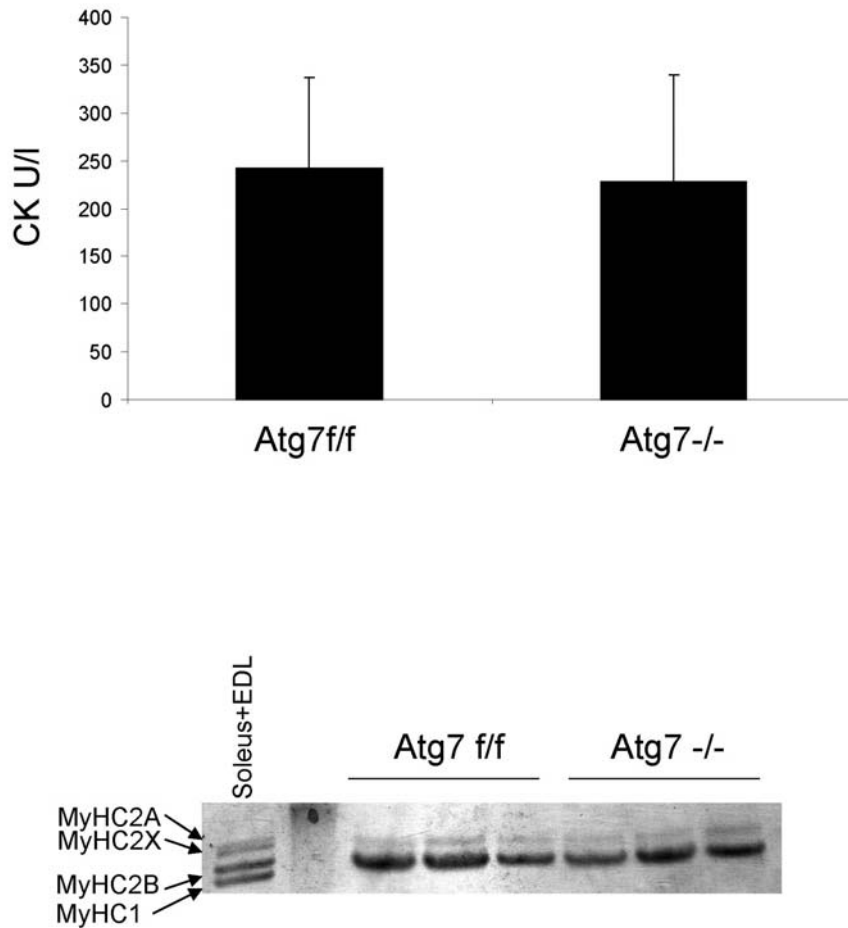
Figure S4. Upper panel: serum creatine kinase is not different between autophagy knockout mice and control animals. Lower panel: silver staining of SDS-PAGE for Myosin Heavy Chains (MyHC) extracted from gastrocnemius muscle of Atg7[f/f] and Atg7^{-/-}. No major differences in myosin composition have been revealed between controls and autophagy deficient muscles.
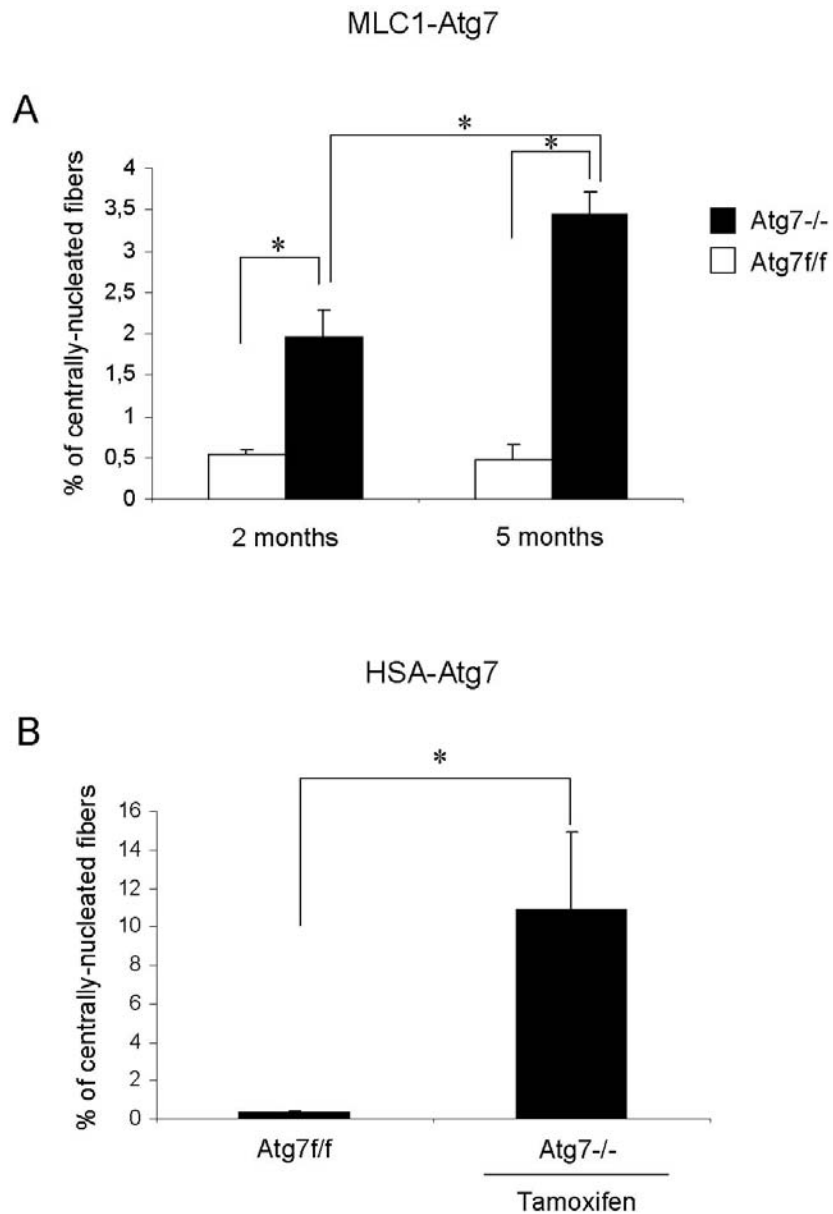
Figure S5

MLC1-Atg7

A

HSA-Atg7

B

Figure S5. (A) The proportion of fibers with central nuclei is higher in conditional autophagy knockout mice than in controls and increases with age. TA muscles were used for the quantification of central nuclei, n=5 (* p<0.05), data are mean +/-s.e.m. **(B)** Centrally-nucleated fibers in TA muscle of Tamoxifen-inducible autophagy knockout were quantified, n=5 (* p<0.05), data are mean +/-s.e.m. Acute deletion of Atg7 in adulthood induces ten fold more abundant myofibers with abnormal nuclei.
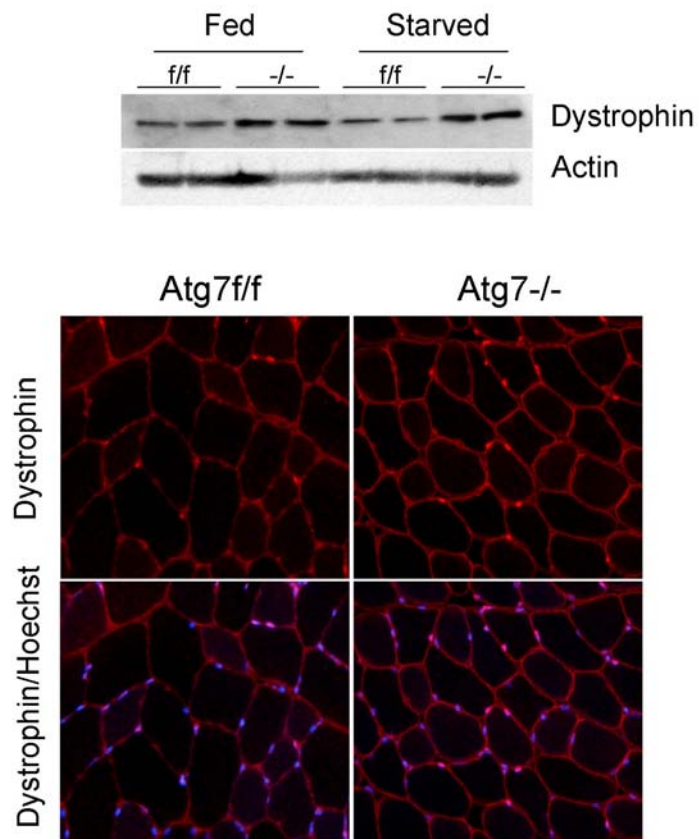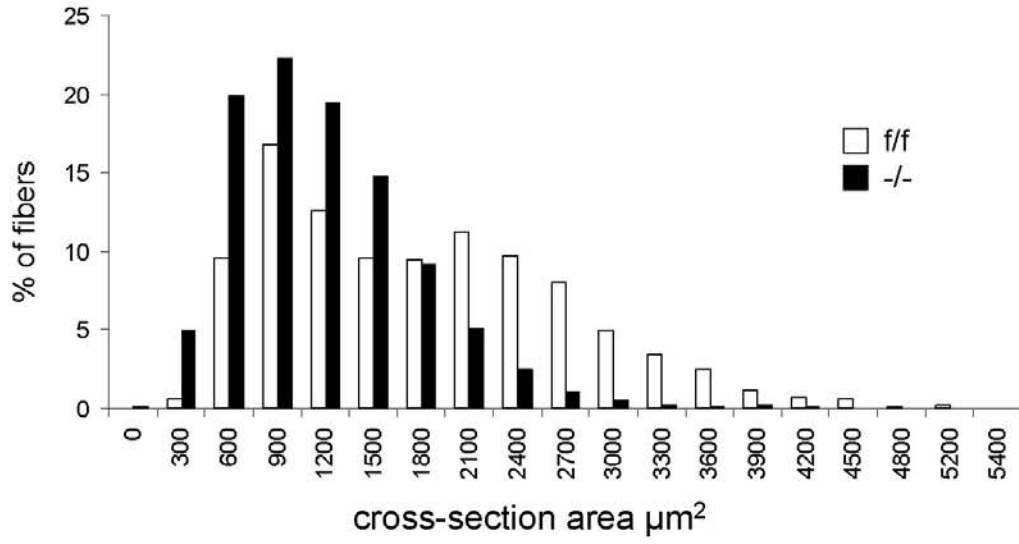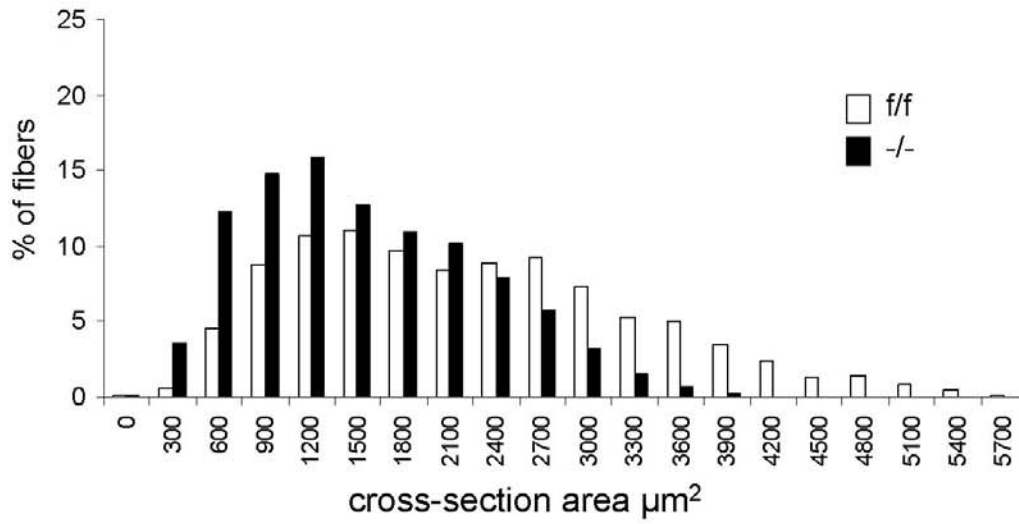
Figure S6

Figure S6. Dystrophin expression is not decreased in Atg7$^{-/-}$ muscles. Upper Panel: Immunoblot analysis of protein extracts from gastrocnemius muscles of fed or starved Atg7$^{f/f}$ and Atg7$^{-/-}$ mice. Lower Panel: immunostainig for anti-dystrophin revealed a normal localization of dystrophin in Atg7$^{f/f}$ and Atg7$^{-/-}$ TA muscles.
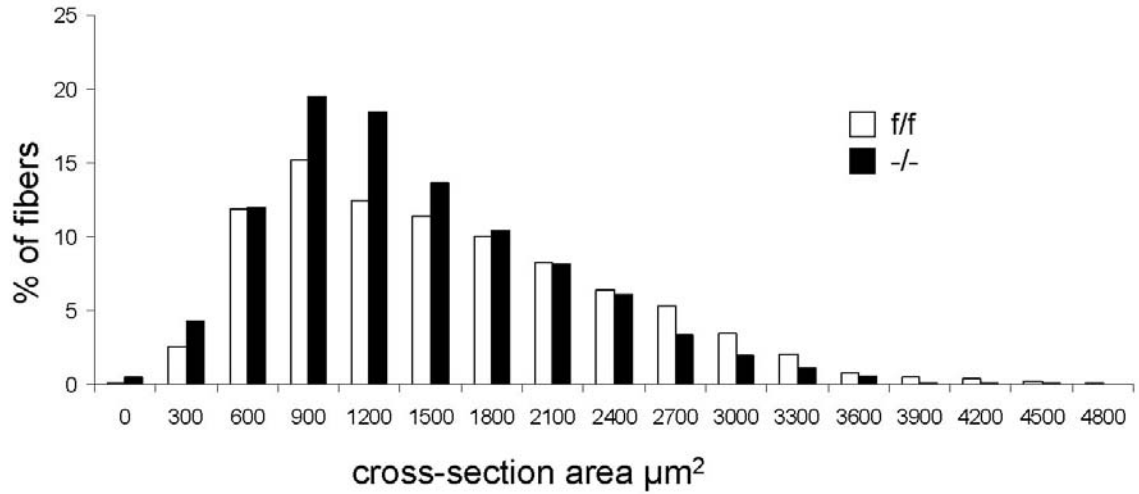
Figure S7

Female

Male

Figure S7. Frequency histograms showing the distribution of cross-sectional area (μm^2) of Figure 2B and Figure 4H.

Figure S8

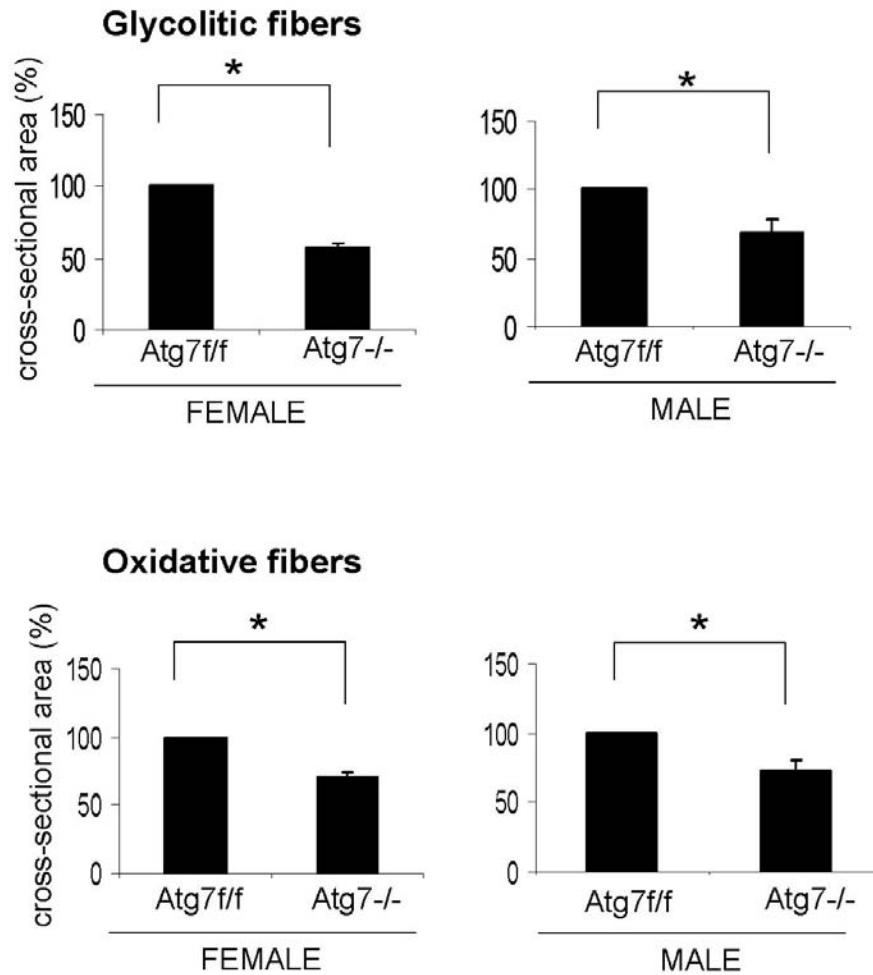## Glycolitic fibers

Oxidative fibers

Figure S8. The bar diagram represents the mean cross-sectional areas (μm^2) of glycolytic and oxidative fibers revealed by SDH staining of Atg7$^{f/f}$ and Atg7$^{-/-}$ muscles. Cryosections of TA muscles were stained for SDH, oxidative fibers appear dark blue while glycolitic fibers appear pale-white. At least 1000 fibers per muscle have been measured and at least four muscles for each group have been studied (*p<0.001), data are mean +/-s.e.m.
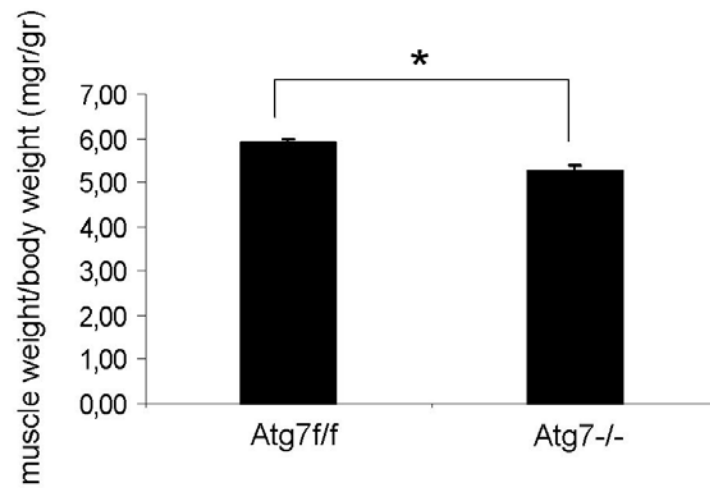
Figure S9

Figure S9. Muscle weight/body weight ratio. Four animals for each group were used. Gastrocnemius muscle weight was monitored, data are mean +/-s.e.m. (*p<0.05).
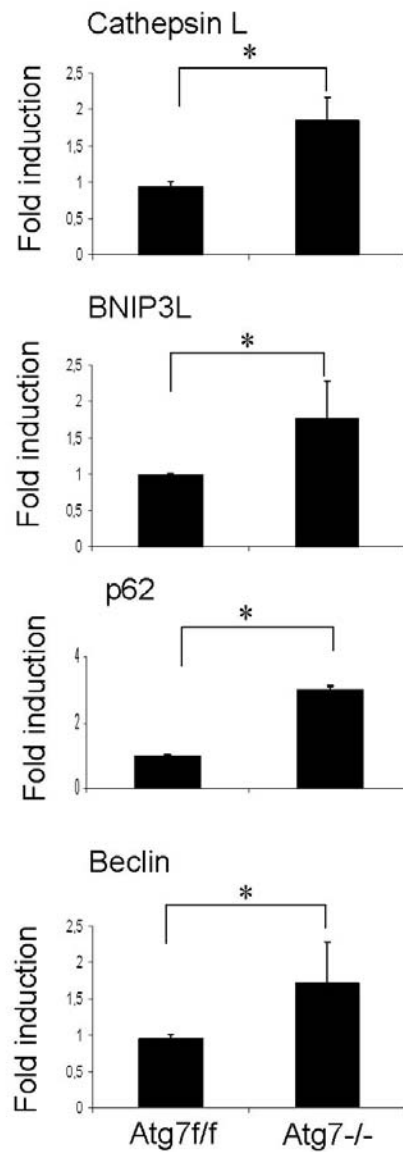
Figure S10

Figure S10. Enhanced up-regulation of the critical atrophy-related genes in Atg7$^{-/-}$ muscles. RNA was extracted from TA muscles and quantitative PCR analysis was performed in triplicates using specific oligonucleotides. Data were normalized to the β-actin content and expressed as fold increase over levels of Atg7$^{f/f}$ muscles, data are mean +/-s.e.m. (*p<0.05).

Figure S11
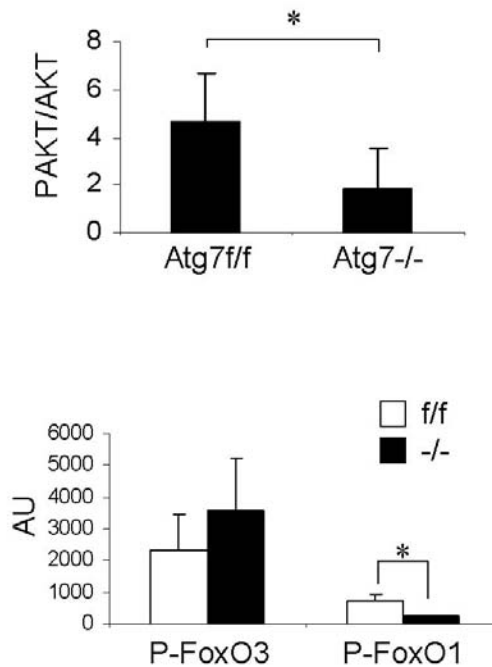
Figure S11. Akt and FoxO1 but not FoxO3 are dephosphrylated in Atg7$^{-/-}$ muscles. Muscle extracts of gastrocnemius muscles from three different mice for each group were immnublotted for P-AKT, AKT, P-FoxO1, P-FoxO3, P-S6 and P-4EBP1. Bands were quantified by densitometry (Gel-Pro Analyzer) and data were plotted as bar-graphs. Phosphorylation level of Akt and FoxO1 is significantly decreased. The mTOR downstream targets did not significantly differ between Atg7$^{-/-}$ and control (not shown). n=3, data are mean +/-s.e.m. (*p<0.05).

Figure S12
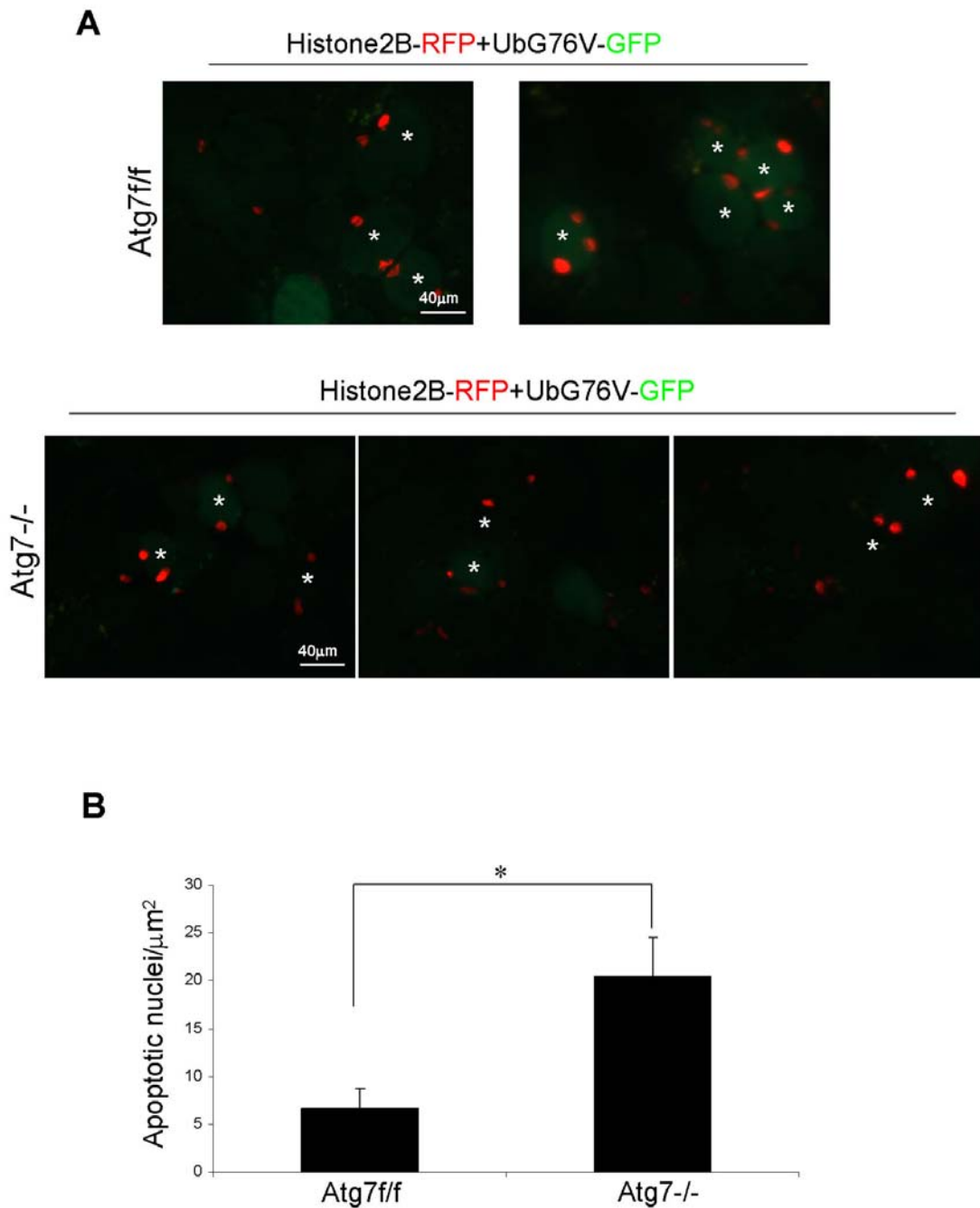
Figure S12. (A) Characterization of proteasome function in Atg7 deficient muscles by using an in vivo reporter assay. Adult TA muscles were cotransfected with Histone 2B-RFP and Ub^{G76V}-GFP, which is a ubiquitin-proteasome pathway activity reporter, and the level of fluorescence in transfected muscles was monitored. Transfected myofibers are revealed by the presence of red nuclei. Ub^{G76V}-GFP is normally degraded by the proteasome and therefore it is present at low levels, but accumulates quickly if proteasome activity is impaired. We have recently used this *in vivo* approach to show that proteasome inhibition does not affect

autophagosome formation (Mammucari et al., 2007). Indeed Atg7 null muscles show less fluorescence than control muscles confirming that proteasomal-dependent degradation is increased. Asterisks represent examples of transfected fibers. **(B)** Apoptotic nuclei are increased in Atg7$^{-/-}$ muscles. Apoptosis in gastrocnemius muscle were revealed by using the terminal deoxynucleotidyltransferase-mediated dUTP nick end labeling (DeadEnd Fluorometric TUNEL System (Promega)) as previously described (Dalla Libera et al., 2005). n=5, data are mean +/-s.e.m. (*p<0.05).

Figure S13

A Atg7f/f
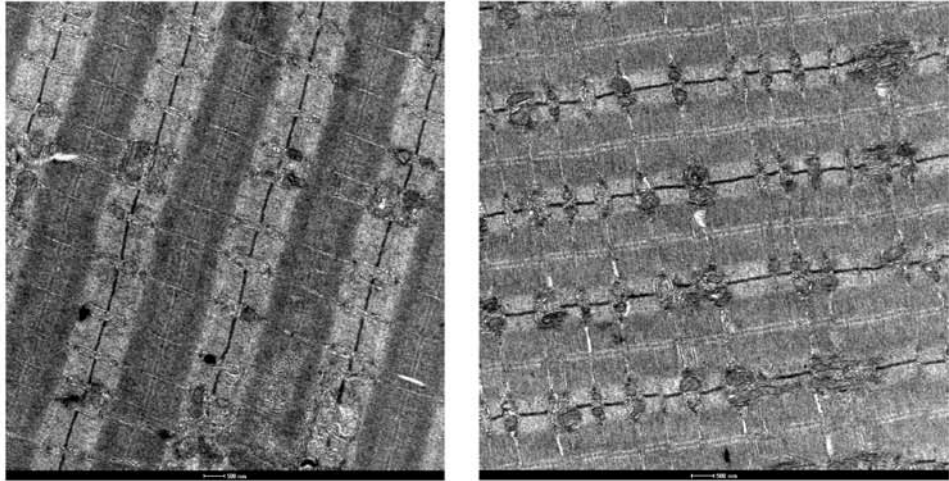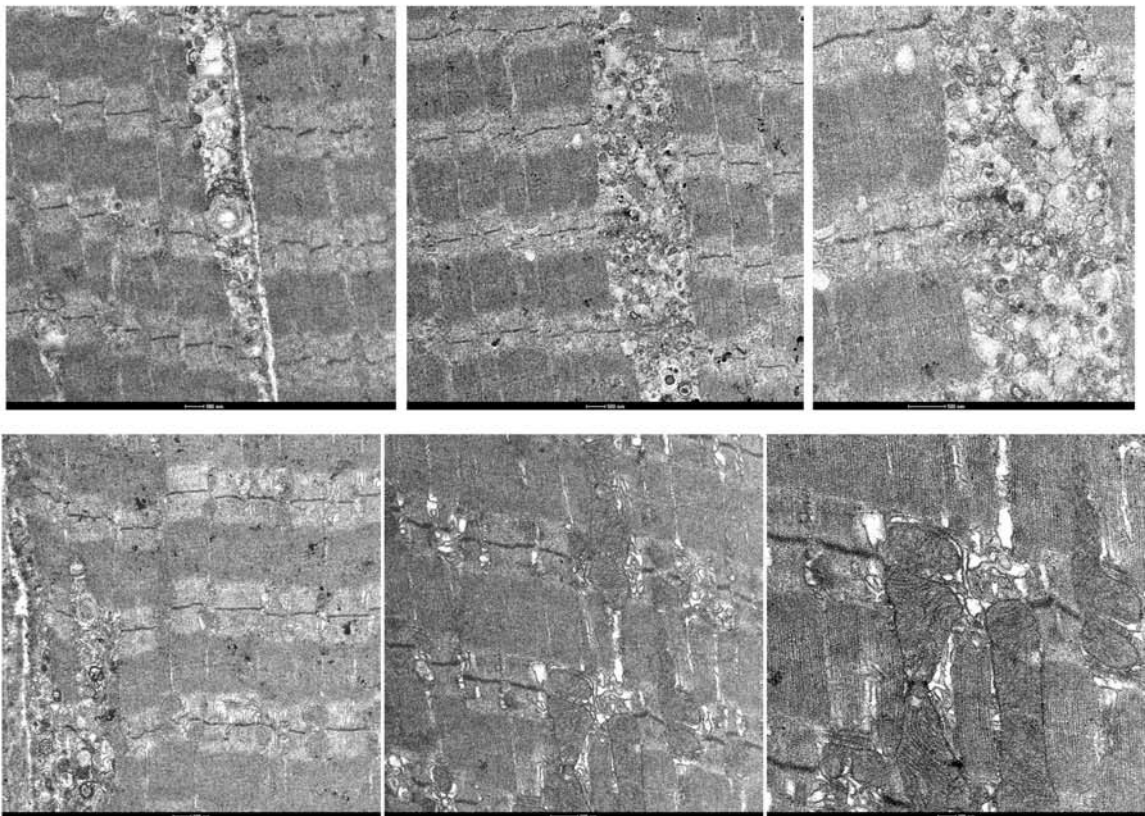
B Atg7-/-

Figure S13. (**A**) Electron micrographs of control Atg7$^{f/f}$ EDL muscles. (**B-C**) Several micrographs of Atg7 deficient EDL muscles which showed accumulation of membranes, abnormal mitochondria, alterations in alignment of sarcomeric proteins and dilated sarcoplasmic reticulum.

Figure S14

A
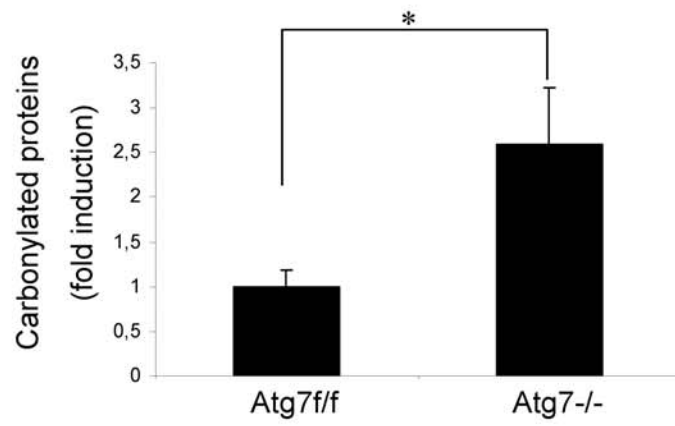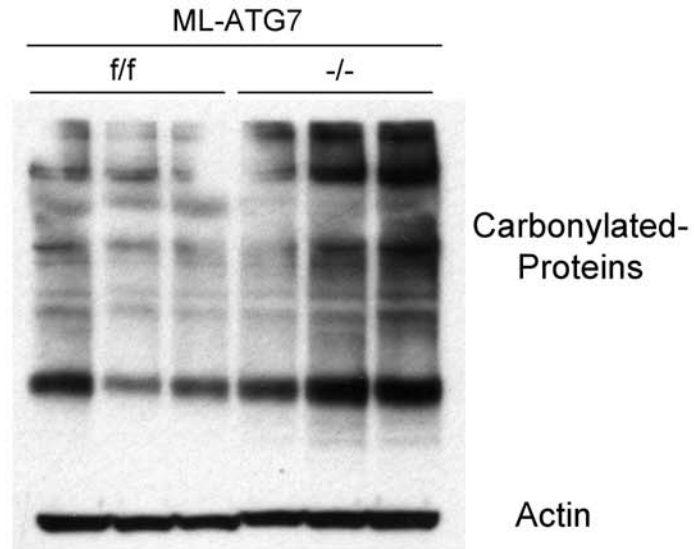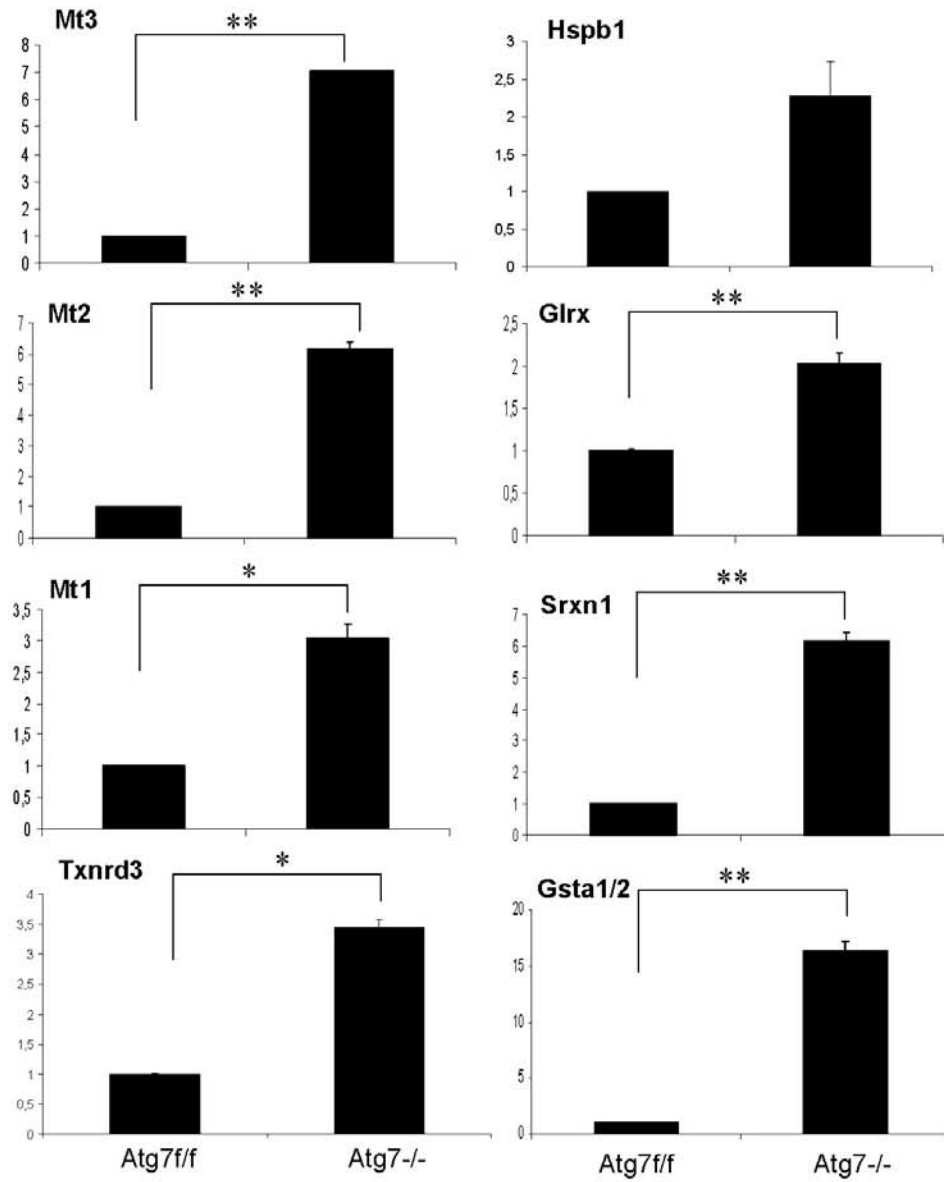
Figure S14

Figure S14

C

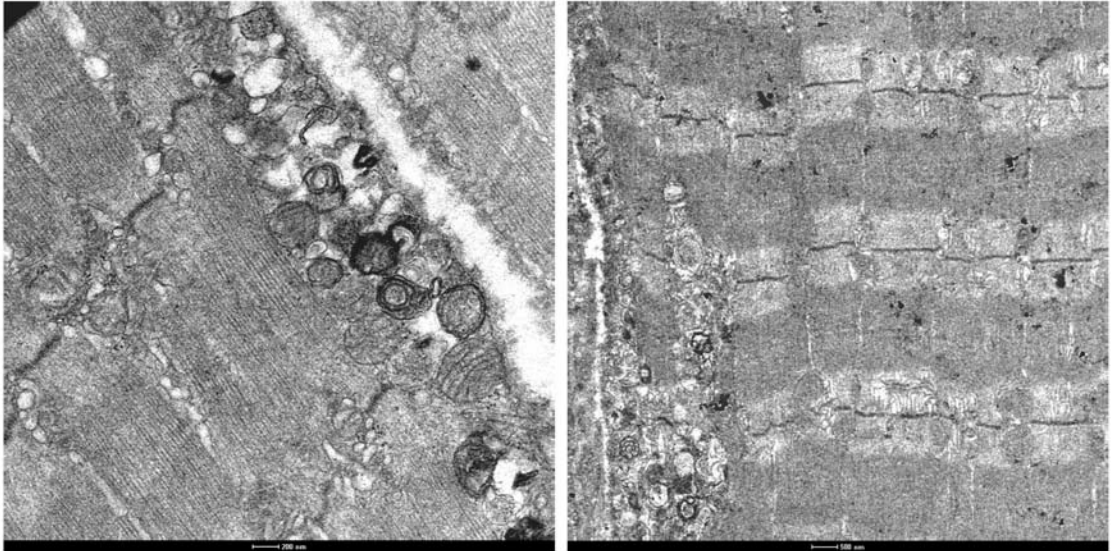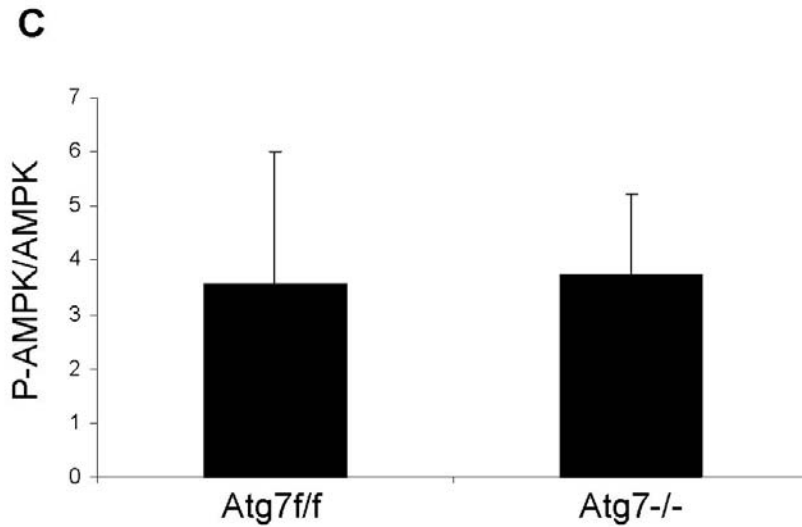**Figure S14.** **(A)** Carbonylated proteins are revealed by Oxyblot (Oxyblot Oxidized Protein Detection Kit, Millipore). A representative immunoblot for carbonylated proteins is depicted. Bar graph represents the mean of densitometric quantification of the carbonilated proteins, n=5, data are mean +/-s.e.m., * $p<0.05$. **(B)** Up-regulation of some genes involved in ROS scavenger in adult skeletal muscle. RNA was isolated from TA muscles. Real-time PCR was performed using the PCR Master Mix Applied Biosystem (ABI) and ready-made TaqMan expression assays. Expression values were normalized to β-actin expression. Data are mean +/-s.e.m. * $p<0.05$, ** $p<0.001$. Mt1: Metallothionein 1; Mt2: Metallothionein 2; Mt3: Metallothionein 3; Txnrd3: Thioredoxin reductase 3; Glrx: Glutaredoxin; Srxn1: Sulfiredoxin 1; Gsta1/2: Glutathione S-transferase, a1/a2; Hspb1: Hsp25. **(C)** Immunoblotting analysis for AMPK phosphorylation was performed on gastrocnemius muscles of Atg7^{-/-} and control mice. Densitometric quantification of PAMPK/AMPK ratio is shown as bar graph (n=5).Data are mean +/- s.e.m.

Figure S15
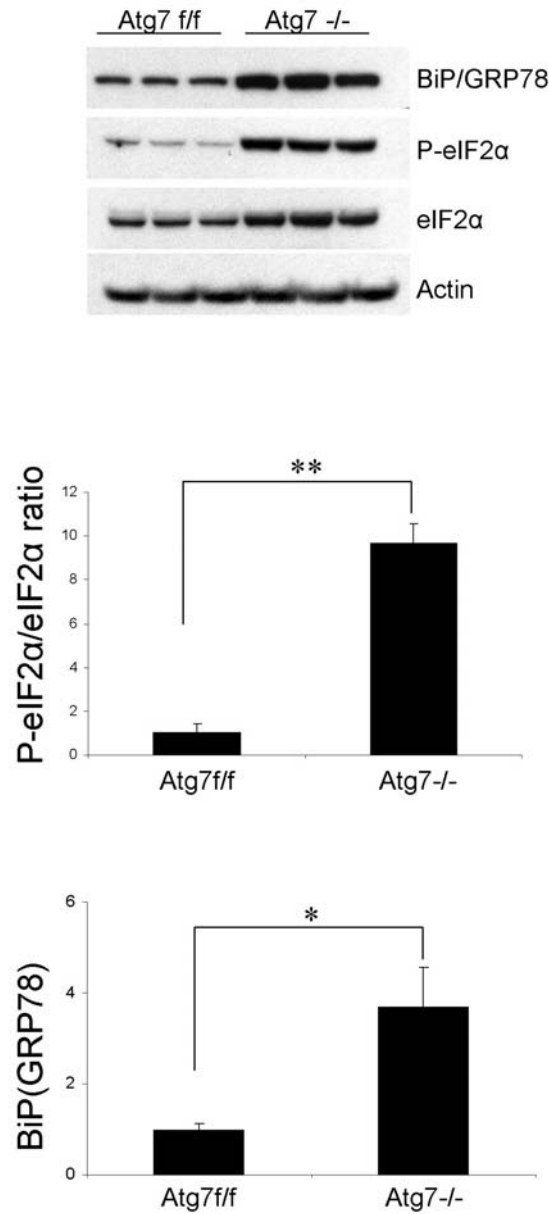
Figure S15. Inhibition of autophagy caused ER stress and unfolding protein response, revealed by phosphorylation of eIF2α and upregulation of BiP (GRP78). Protein extracts of gastrocnemius muscles were immunoblotted for BiP (GRP78), P-eIF2α and eIF2α and the bands were quantified by densitomentry. Bar graphs represent mean of densitometric quantification +/- sem (n=3, **p<0.01, *p<0.05)
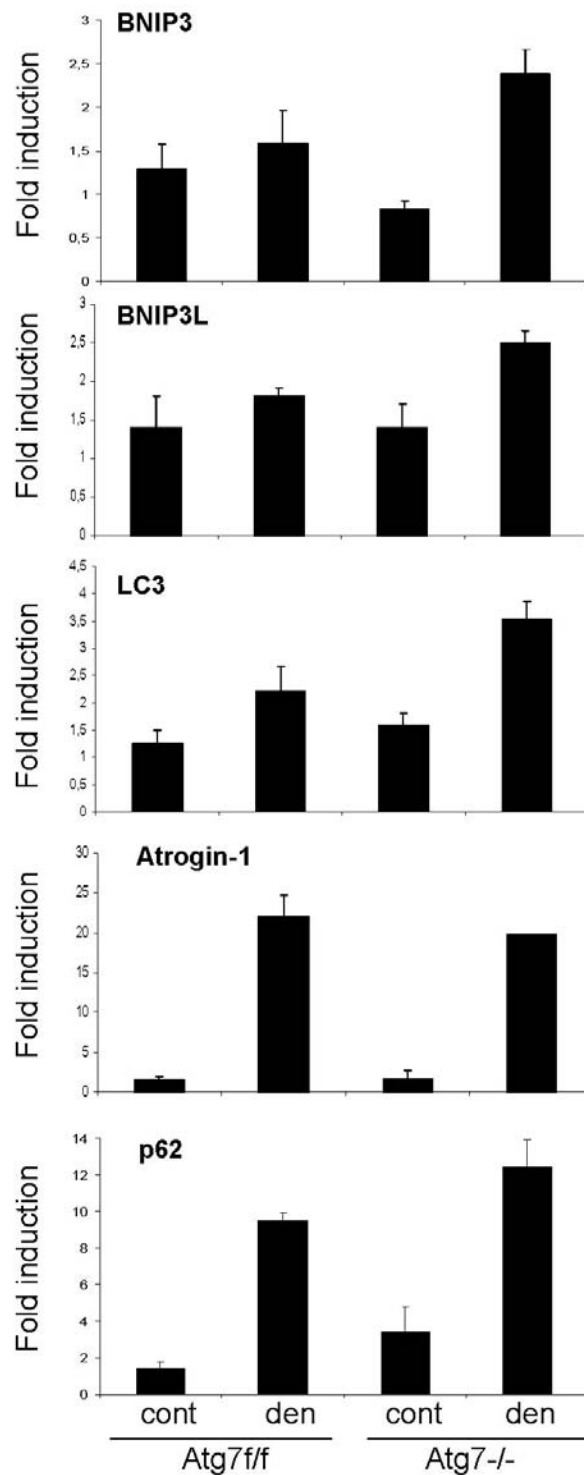
Figure S16. Expression of the critical atrophy-related genes was studied by Quantitative Real-Time PCR. RNA was extracted from TA of 3 days denervated muscles and quantitative PCR analysis was performed in triplicates, data are mean +/-s.e.m.

Figure S17
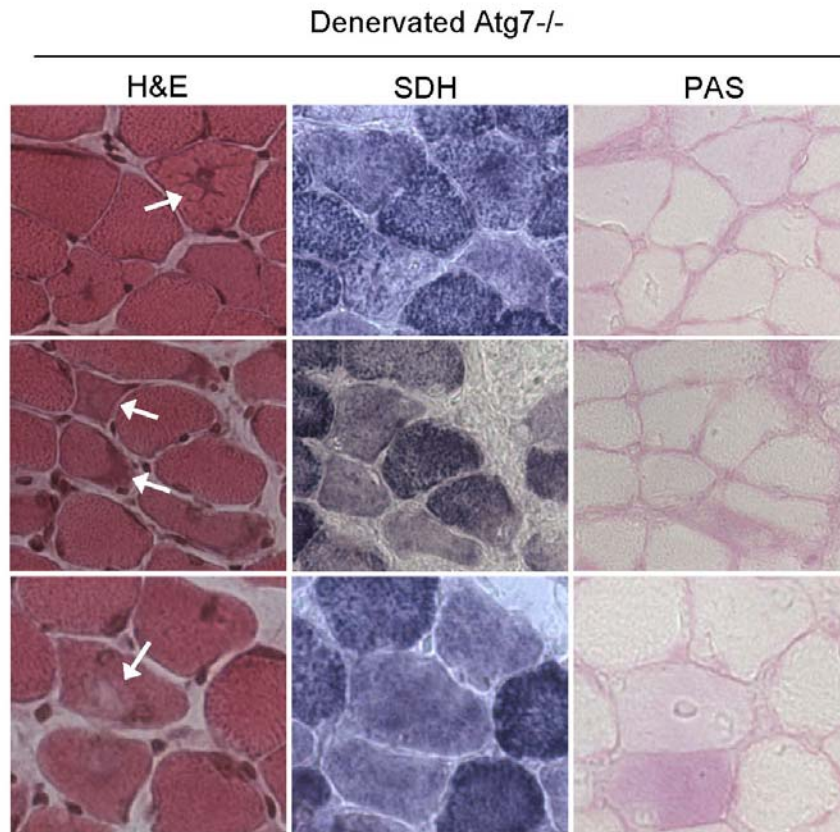
Figure S17. Morphological analyses on denervated Atg7$^{-/-}$ muscles. H&E staining showed the presence of haematoxylin positive inclusions and of vacuoles. SDH and PAS staining on serial sections confirmed the absence of glycogen accumulation and an alteration in mitochondria network.

Figure S18

Denervated Atg7-/-

| Anti-Ub | Anti-p62 | Merge |
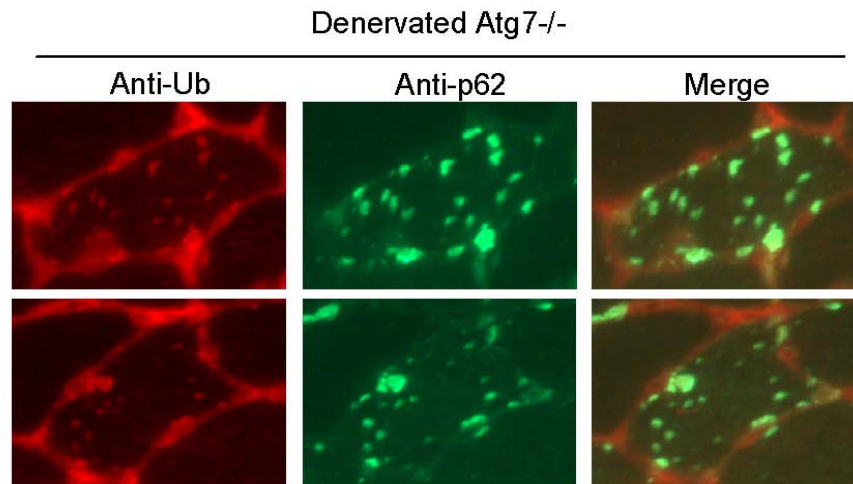
Figure S18. Double imunofluorescence staining reveals the colocalization of p62 and ubiquitin in denervated Atg7$^{-/-}$ myofibers. Protein aggregates were never detected in denervated muscles of Atg7$^{f/f}$ mice.
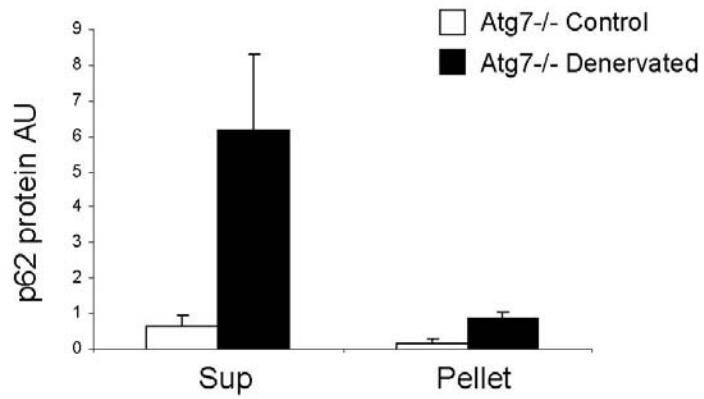
Figure S19

Figure S19. Quantification of p62 protein in detergent soluble and insoluble fractions of innervated and denervated Atg7$^{-/-}$ muscles depicted in Figure 3G. The p62 protein level is normalized for the appropriate loading control. Actin is the loading control for the insoluble fraction (pellet) while GAPDH is the loading control for the soluble fraction (Sup). Data are mean+/-s.e.m.

Figure S20
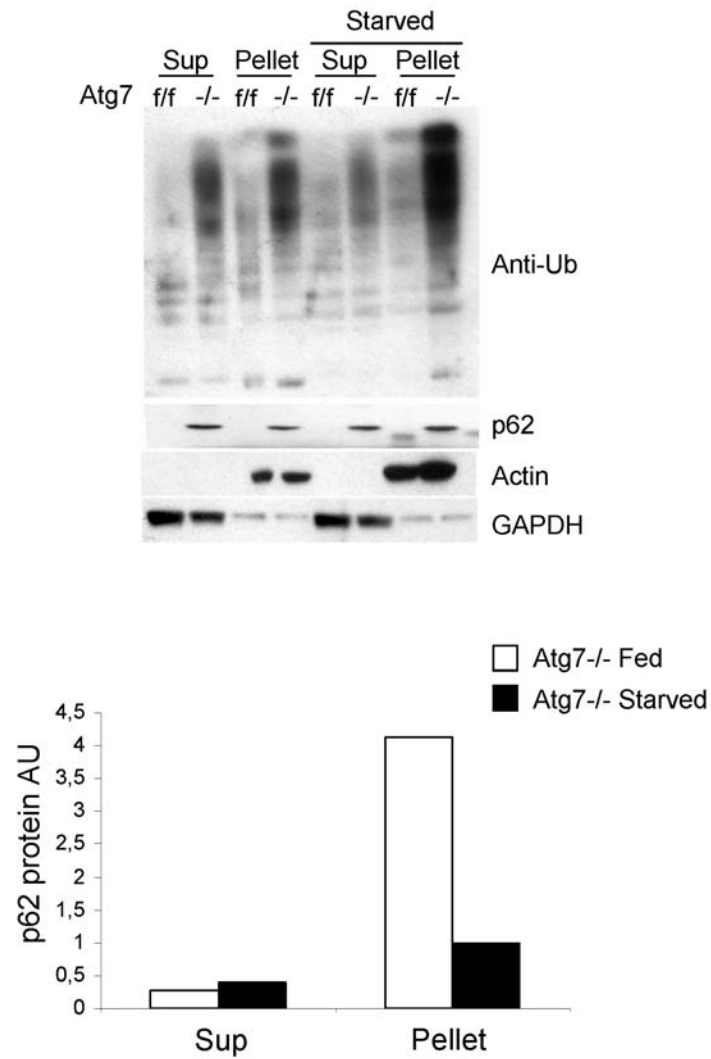
Figure S20. Immunoblotting for ubiquitinated proteins and for p62 of fed and starved muscles from Atg7$^{-/-}$ and control mice. Actin is the loading control for the insoluble fraction (pellet) while GAPDH is the loading control for the soluble fraction (Sup). Quantification of p62 protein in detergent soluble and insoluble fractions of fed and starved Atg7$^{-/-}$ muscles. The p62 protein level is normalized for the appropriate loading control.

Supplemental References

Bothe, G. W., Haspel, J. A., Smith, C. L., Wiener, H. H., and Burden, S. J. (2000). Selective expression of Cre recombinase in skeletal muscle fibers. Genesis *26*, 165-166.

Dalla Libera, L., Ravara, B., Gobbo, V., Danieli Betto, D., Germinario, E., Angelini, A., and Vescovo, G. (2005). Skeletal muscle myofibrillar protein oxidation in heart failure and the protective effect of Carvedilol. J Mol Cell Cardiol *38*, 803-807.

Komatsu, M., Waguri, S., Ueno, T., Iwata, J., Murata, S., Tanida, I., Ezaki, J., Mizushima, N., Ohsumi, Y., Uchiyama, Y.*, et al.* (2005). Impairment of starvation-induced and constitutive autophagy in Atg7-deficient mice. J Cell Biol *169*, 425-434.

Mammucari, C., Milan, G., Romanello, V., Masiero, E., Rudolf, R., Del Piccolo, P., Burden, S. J., Di Lisi, R., Sandri, C., Zhao, J.*, et al.* (2007). FoxO3 Controls Autophagy in Skeletal Muscle In Vivo. Cell Metab *6*, 458-471.

Mizushima, N., Yamamoto, A., Matsui, M., Yoshimori, T., and Ohsumi, Y. (2004). In vivo analysis of autophagy in response to nutrient starvation using transgenic mice expressing a fluorescent autophagosome marker. Mol Biol Cell *15*, 1101-1111.

Schuler, M., Ali, F., Metzger, E., Chambon, P., and Metzger, D. (2005). Temporally controlled targeted somatic mutagenesis in skeletal muscles of the mouse. Genesis *41*, 165-170.

MATERIALS AND METHODS (II PART)

Generation of muscle specific Atg7-MLC-1f conditional knockout mice

The generation of muscle specific Atg7 conditional knockout mice was achieved by bearing an Atg7 Flox allele transgenic mice (Komatsu *et al*., 2005) (Atg7$^{f/f}$) crossed with transgenic mice expressing *Cre-recombinase* under the control of a *Myosin Light Chain 1 fast* promoter (MLC-1f) (Bothe *et al*., 2000; Mammucari *et al*., 2007). In figure 1 it is shown the schematic representation of the generation of Atg7$^{f/f}$ conditional knockout mice.
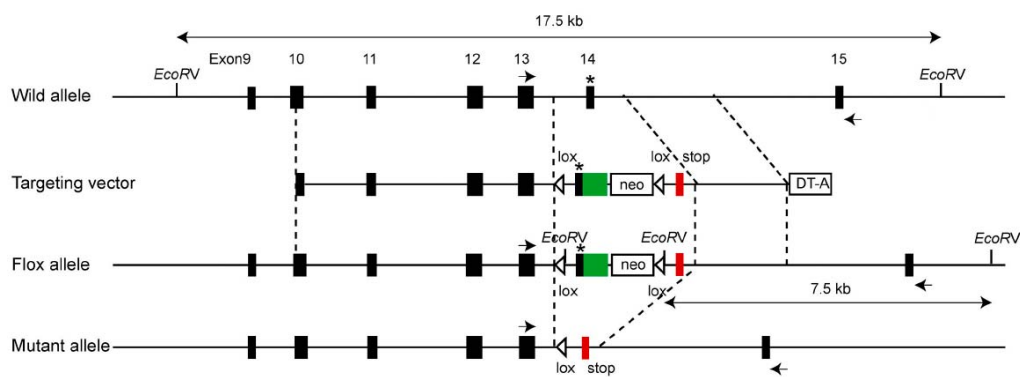
Figure 1: Generation of Atg7$^{f/f}$ mice. Schematic representation of the targeting vector and the targeted allele of Atg7 gene. The coding exons numbered in accordance with the initiation site as exon 1 are depicted by black boxes. Green and red boxes indicate Atg7 cDNA fragment (aa 1786–2097) and Atg7 cDNA fragment with stop codon (aa 1669–1698), respectively. The open triangles denote loxP sequence. Arrows indicate the positions of PCR primers. The asterisk denotes the essential cysteine residue on exon 14. EcoRV, EcoRV sites; neo, neomycin-resistant gene cassette; DT-A, diphtheria toxin gene (Komatsu *et al*., 2005).

The *Myosin Light Chain 1 fast* promoter (MLC-1f) (Figure 2) is expressed only in skeletal muscle during the embryonic development.

Figure 2: MLC-1f-Cre promoter: nls-Cre recombinase is associated with nuclear localization signalling.

In the following figure is represented the generation of muscle specific Atg7-MLC-1f conditional knockout mice.
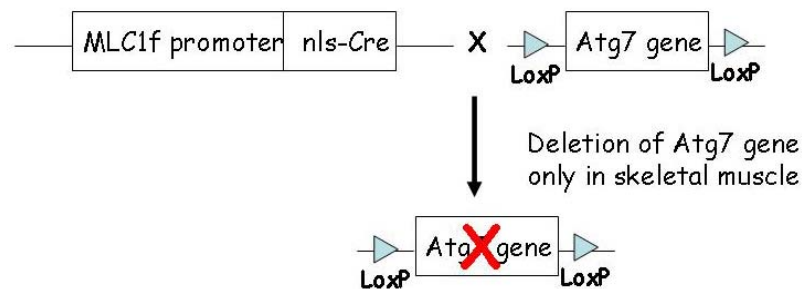
Genotyping of Atg-MLC-1f knockout mice

To genotype the knockout $Atg7^{f/f}$ –MLC-1f mice, we were used the toes of the animal.

<u>PCR for MLC1f-Cre</u>

The extraction of genomic DNA was made for MLC-1f with the following Lysis Buffer:

- Tris-HCL 1M pH 7.5,

- Proteinase K 10mg/mL (Invitrogen).

The samples were denaturated by incubation for 1 hour at 57° C and then the proteinase Kinase was inactivated at 100°C for 5 minutes. The DNA was ready for the PCR reaction using the following primers and program:

<u>Primers</u>:

NSP-780: CACCAGCCAGCTATCAACTCG
NSP-979: TTACATTGGTCCAGCCACCAG

Sample mix was prepared as:

Template DNA	2 μl
Primer NSP-780 (10 μM)	0.2 μl
Primer NSP-979 (10 μM)	0.2 μl
GoTaq Green master mix 2X (Promega)	10 μl
Water	
Total volume	20 μl

Program:

step 1:	94° C for 3 minutes
step 2:	94° C for 45 seconds
step 3	61° C for 30 seconds
step 4	72°C 1 minute
step 5:	go to step 2 for 40 times

Size band: 200 bp

PCR for Atg7$^{fl/fl}$

The extraction of genomic DNA was made for Atg7$^{fl/f}$with the following Lysis Buffer (Komatsu *et al.*, 2005):

Tris-HCL pH 8	50 mM
NaCl	0.1 M
EDTA	20 mM
SDS	1%
Proteinase K (Sigma)	25 mg/mL
Pronase E (Sigma)	100 mg/mL

The samples were denaturated by incubation at 55° C over-night. The DNA was ready for the PCR reaction using the following primers and program:

Primers:

Hind-Fw: TGGCTGCTACTTCTGCAATGATGT

Pst-Rv: CAGGACAGAGACCATCAGCTCCAC

Sample mix was prepared as:

Template DNA	1 μl (of a diluition 1/50)
Primer Hind-Fw (10 μM)	0.2 μl
Primer Pst-Rv (10 μM)	0.2 μl
GoTaq Green master mix 2X (Promega)	10 μl
Water	
Total volume	20 μl

Program:

step 1:	94° C for 5 minutes
step 2:	94° C for 45 seconds
step 3	58° C for 45 seconds
step 4	72°C 4 minutes
step 5	72°C 10 minutes
step 6:	go to step 2 for 35 times

Size band: 500 bp flox allele

       1.5 kb wild allele

Cre-mediated recombination was confirmed by PCR with genomic DNA from gastrocnemius muscles (Figure 3).
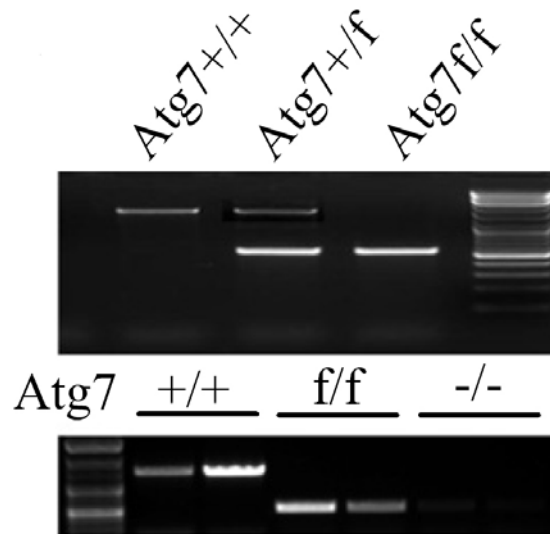
Figure 3: Upper panel, genotyping of the Atg7$^{f/f}$ mice. Lower panel, PCR analysis with genomic DNA from gastrocnemius muscle. One of the two PCR primers is inside the floxed region. Absence of a PCR product revealed an efficient Cre-mediated recombination of lox-P sites.

Generation of muscle specific Atg7-HSA inducible conditional knockout mice

Mice bearing an Atg7 Flox allele (Komatsu *et al.*, 2005) (Atg7$^{f/f}$) were crossed with transgenic mice expressing a *Cre-recombinase* fused with a modified estrogen receptor domain (*Cre-ER^{TM}*) driven by Human Skeletal Actin promoter (HSA) (Schuler *et al.*, 2005).

In normal condition, Atg7$^{f/f}$ is expressed in skeletal muscle before treatment with tamoxifen, but since it has a heat shock protein complex bound to a modified estrogen receptor domain, it cannot be phosphorylated and is therefore degraded rapidly. The deletion of site flox Atg7 was induced only by exogenous treatments with tamoxifen, which binds the estrogen receptor (Kroll *et al.*, 2003) (Figure 4). Tamoxifen-inducible *Cre-ER^{TM}* was activated by Intra Peritoneum injection of 5 µg Tamoxifen (Sigma) to 2 months old mice daily for one week. Atg7$^{f/f}$ but *Cre-ER^{TM}* negative mice have been treated with Tamoxifen as described above and have been used as controls. Muscles were collected two weeks after the last Tamoxifen injection.

A)
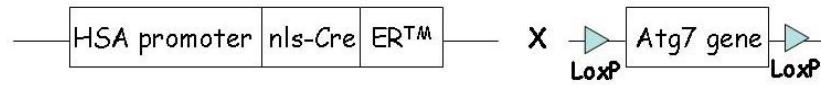
B)
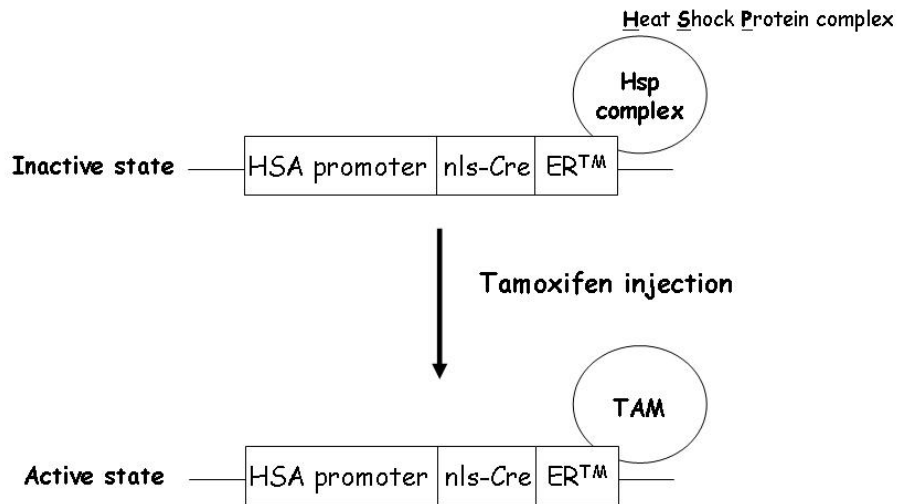
C) Deletion of Atg7 gene in skeletal muscle
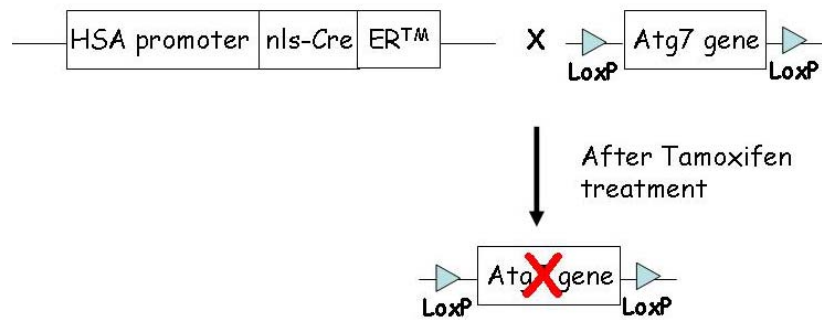
Figure 4: Schematic representation of Atg7 inducible conditional knockout mice. A) during normal condition, Atg7$^{f/f}$ is expressed in skeletal muscle and in other tissue. B) treatment with tamoxifen induces the Cre-recombinase.

The protocol for genotyping the inducible conditional knockout mice is the same of the MLC1f-Atg7 mice.

Mouse tibialis anterior muscle electroporation

Experiments were performed on adult Atg7-MLC-1f tibialis anterior (TA). The animals were anesthetized by an intraperitoneal injection of ketamine (75 mg/Kg) and xylazine (20 mg/Kg). The muscle was isolated through a small hindlimb incision, and 25 μg of plasmid DNA were injected along the muscle length. Electric pulses were then applied by two stainless steel spatula electrodes placed on each side of the isolated muscle belly (50 Volts/cm, 5 pulses, 200 ms intervals). Muscles were analyzed 8 days later. No gross or microscopic evidence for necrosis or inflammation as a result of the transfection procedure was noted (Sandri *et al.*, 2004 and Dona *et al.*, 2003).

Tibialis Anterior muscle were transfected with different plasmids:

- YFP-LC3 (Tanida *et al.*, 2004),
- Ub^{G76V}-GFP (Dantuma *et al.*, 2000),
- Histone 2B-RFP.

Cut of the sciatic nerve of Atg7-MLC-1f mice

The right hindlimbs of 3 months old Atg7 knockout mice were denervated cutting the sciatic nerve unilaterally. The animals were anesthetized by an intraperitoneal injection of ketamine (75 mg/Kg) and xylazine (20 mg/Kg). The sciatic nerve was unilaterally cut at the level of trochanter. About 0.5-1 cm of the peripheral nerve stump was removed and the proximal stump was sutured into a superficial muscle to avoid reinnervation and obtain a permanent denervation of the lower hindlimb. The mice was sacrificed 3 days after operation, for gene expression analyses, or after 14 days for biochemestry analyses.

Measurements of Muscle Force in vivo

Muscle force was measured in a living animal as previously described (Blaauw *et al.*, 2008).

Gastrocnemius muscle contractile performance was measured *in vivo* using a 305B muscle lever system (Aurora Scientific Inc.) in mice anaesthetized with a

mixture of Xilazine and Zoletil. Mice were placed on a thermostatically controlled table, the knee was kept stationary and the foot was firmly fixed to a footplate, which was connected to the shaft of the motor. Contraction was elicited by electrical stimulation of the sciatic nerve. Teflon-coated seven multi-stranded steel wires (AS 632, Cooner Sales, Chatsworth, CA, USA) were implanted with sutures on either side of the sciatic nerve proximally to the knee before its branching. At the distal ends of the two wires, the insulation was removed, while the proximal ends were connected to a stimulator (Grass S88). In order to avoid recruitment of the dorsal flexor muscles, the common peroneal nerve was cut. The torque developed during isometric contractions was measured at stepwise increasing stimulation frequency, with pauses of at least 30s between stimuli to avoid effects due to fatigue. Duration of the trains never exceeded 600ms. Force developed by plantar flexor muscles was calculated by dividing torque by the lever arm length (taken as 2.1 mm). Eccentric contractions were analysed to study muscle damage. Muscle lengthening was achieved by moving the foot backward at a velocity of 40mm/s while the gastrocnemius was stimulated with a frequency sufficient to induce full tetanic fusion (100 Hz). The footplate was moved 200ms after initiation of stimulation train, thus eccentric pull occurs during the isometric plateau of the tetanus. The range of movement during the pull was calculated to be 308, clearly inside physiological limits of movement for the foot. Total duration of tetanic stimulation was limited to 600ms, assuring no sag of force. This protocol was repeated 20 times taking the decrease in the isometric force plateau (before beginning of the stretch) as an indication for muscle damage, with pauses of 30 s.

Histology analysis and fiber size measurements

TA Cryosections , 10μm thick, were used to analyze tissue morphology with different methods:

Hematoxylin and Eosin stain (H&E)

Hematoxylin colors basophilic structures with blue-purple hue. The basophilic structures are usually the ones containing nucleic acids, such as the ribosome and

the chromatin-rich cell nucleus, and the cytoplasmc regions rich in RNA. Eosin colors eosinophilic tructures bright pink. The eosinophilic structures are generally composed of intracellular or extracellular protein.

The methods consist of:

Materials	Time
PFA 4%	10 minutes
3 washs in PBS	5 minutes each
Harris Hematoxylin (Sigma)	6 minutes
Wash in running tap water	3 minutes
Alcoholic acid	10 seconds
Wash in running tap water	3 minutes
Eosin Y Solution Alcoholic (Sigma	1 minute
DEHYDRATION	
Ethanol 70%	5 minutes
Ethanol 95%	2 minutes
Ethanol 100%	3 minutes
Xilen 1	5 minutes
Xilen 2	5 minutes
Mount with Entellan	

Succinate dehydrogenase (SDH)

The succinate dehydrogenase is an enzyme complex, bound to the inner mitochondrial membrane. The reaction gives a purple coloration in the oxidative fibers. The sections were incubated for 30 minutes at 37°C with SDH solution (0.2M sodium succinate (Sigma), 0.2M phspahte (Sigma) buffer ph 7.4 and 50mg of nitro blue tetrazolium (NBT - Sigma). After the incubation, the sections were washed 3 minutes with PBS and then mounted with Elvanol.

After SDH staining, fiber cross-sectional areas were measured, by using Image J 1.33u software (National Institutes of Health). All data are expressed as the mean SEM (error bars). Comparisons were made by using t test, with $P<0.05$ being considered statistically significant.

Periodic acid-Schiff (PAS)

This method is used to identify glycogen in tissues. The reaction of periodic acid selectively oxidizes the glucose residues, creates aldehydes that react with the Schiff reagent and creates a purple-magenta color. A suitable basic stain is often used as a counter stain. The sections were treated with:

Materials	Time
Fix in Carnoy's fixative	5 minutes
Wash in water	3 times
0.5% periodic acid	5 minutes
Wash in water	3 times
Schiff's solution (Sigma)	10 minutes
Wash in running tap water	10 minutes
Mount with Elvanol	

Immunohistochemistry analysis

Tibialis anterior (TA) muscle cryosections of 10μm thick, were processed for immunostaining.

p62 staining

Muscle cryosections were fixed with PFA 4%, treated with 0,1% Triton and incubated in blocking solution (0.5% BSA, 10% mouse serum in PBS) at RT for 10 minutes. Samples were then incubated with the primary antibody (Progen) (dilution 1:200) at 4°C over-night. Then the sections were washed with PBS three times for 5 minutes and incubated with the Guinea-pig-Cy2-conjugated secondary antibodies (dilution 1:800) at 37°C for 1hour. After the wash and incubation with dapi, slides were mounted with Elvanol.

Ubiquitin staining

Muscle cryosections were fixed with PFA 4%, treated with 0,1% Triton and incubated in blocking solution (0.5% BSA, 10% mouse serum in PBS) at RT for

10 minutes. After that the sample was incubated with the primary antibody (BIOMOL international) (dilution 1:500) at 4°C over-night. Then the sections were washed with PBS three times for 5 and incubated with the anti-muose-Cy3-conjugated secondary antibodies (dilution 1:500) at 37°C for 1hour. After the wash and incubation with dapi, slides were mounted with Elvanol.

Dystrophin staining

Cryosections were fixed with PFA 4%, treated with 0,1% Triton and incubated in blocking solution (0.5% BSA, 10% mouse serum in PBS) at RT for 10 minutes. After that the sample was incubated with the primary antibody (ABCAM) (diluition 1:200) at 4°C over-night. Then the sections were washed with PBS three times for 5 minutes and incubated with the anti-muose-Cy3-conjugated secondary antibodies (dilution 1:200) at 37°C for 1hour. After the wash and incubation with dapi, slides were mounted with Elvanol.

IgG staining

Cryosections were incubated in blocking solution (0.5% BSA, 10% goat serum in PBS) at RT for 10 minutes. after the sample was incubated with anti-muose-Cy3-conjugated secondary antibodies (dilution 1:200) at 37°C for 1hour. After the wash and incubation with dapi, slides were mounted with Elvanol.

Images were collected with an epifluorescence Leica DM5000B microscope equipped with a Leica DFC300-FX digital charge-coupled device camera by using Leica DC Viewer software.

Fluorescence microscopy and electron microscopy

Cryosections of muscles transfected with YFP-LC3 were examined in a fluorescence microscope as described (Mizushima *et al*., 2004). Images were collected with an epifluorescence Leica DM5000B microscope equipped with a Leica DFC300-FX digital charge-coupled device camera by using Leica DC Viewer software.

For electron microscopy, we used conventional fixation-embedding procedures based on glutaraldehyde-osmium fixation and Epon embedding.

Gene expression analyses

Quantitative Real-time PCR was performed with SYBR Green chemistry (Applied Biosystems). SYBR green is a fluorescent dye that intercalates into double-stranded DNA and produces a fluorescent signal. The Real-Time PCR Instrument allows real time detection of PCR products as they accumulate during PCR cycles and create an amplification plot, which is the plot of fluorescence signal versus cycle number. In the initial cycles of PCR, there is little change in fluorescence signal. This defines the baseline for the amplification plot. An increase in fluorescence above the baseline indicates the detection of accumulated PCR products. A fixed fluorescence threshold can be set above the baseline. The parameter Ct (threshold cycle) is defined as the fractional cycle number at which the fluorescence passes the fixed threshold. So the higher the initial amount of the sample, the sooner the accumulated product is detected in the PCR process as a significant increase in fluorescence, and the lower is the Ct value.

Quantification of the PCR products and determination of the level of expression

A relative quantification method were used to evaluate the differences in gene expression, as described by Pfaffl (Pfaffl, 2001). In this method, the expression of a gene is determined by the ratio between a test sample and a housekeeping gene. The relative expression ratio of a target gene is calculated based on the PCR efficiency (E) and the threshold cycle deviation (ΔCt) of unknown samples versus a control, and expressed in comparison to a reference gene.

The mathematical model used for relative expression is represented in this equation:

$$\text{Ratio} = \frac{(E_{target})^{\Delta Ct}}{(E_{reference})^{\Delta Ct}}$$

The internal gene reference used in our real time PCR was β-actin, whose abundance did not change under the experimental conditions.

Primer pairs design

Gene-specific primer pairs were selected with Primer3 software (http://frodo.wi.mit.edu/cgi-bin/primer3/primer3_www.cgi); sequences of distinct exons were chosen to avoid amplifying contaminant genomic DNA. Primer pairs were selected in a region close to the 3'-end of the transcript, and amplified fragments of 150-250bp in length. To avoid the amplification of contaminant genomic DNA, the target sequences were chosen on distinct exons, separated by a long (more than 1000bp) intron. The melting temperature was chosen to be of about 58-60° C.

The sequences of the primer pairs are listed in the Table 1:

	Forward primer	Reverse primer
MAP1-LC3b	cactgctctgtcttgtgtaggttg	tcgttgtgcctttattagtgcatc
Cathepsin L	gtggactgttctcacgctcaag	tccgtccttcgcttcatagg
Atrogin 1	gcaaacactgccacattctctc	cttgaggggaaagtgagacg
Murf1	acctgctggtggaaaacatc	cttcgtgttccttgcacatc
Bnip3	ttccactagcaccttctgatga	gaacaccgcatttacagaacaa
Bnip3l	ttggggcattttactaaccttg	tgcaggtgactggtggtactaa
p62	Cccagtgtcttggcattctt	agggaaagcagaggaagctc
b-actin	ctggctcctagcaccatgaagat	ggtggacagtgaggccaggat

Tabella 1: Sequence of primers used in Q-RT-PCR analyses.

Extraction of total RNA

Total RNA was isolated from TA using the *Promega SV Total Isolation kit.*

Synthesis of the first strand of cDNA

400ng of total RNA was reverse transcribed with SuperScript^{TM} III (Invitrogen) in the following reaction mix:

Random primer hexamers (50ng/μl random)   1μl

dNTPs 10 mM   1μl

H$_2$O Rnase-free   8.5μl

The samples were mixed by vortexing and briefly centrifuged and denaturated by incubation for 5 minutes at 65° C to prevent secondary structures of RNA.

Samples were incubated on ice for 2 minutes to allow the primers to align to the RNA; and the following components were added sequentially:

First strand buffer 5× (Invitrogen)	5μl
DTT 100mM	2μl
RNase Out (Invitrogen)	1μl
SuperScript^{TM} III (Invitrogen)	0.5μl

The volume was adjusted to 20ul with water.

The used reaction program was:

step1:	25°C for 10 minutes
step2:	42°C for 50 minutes
step3:	70°C for 15 minutes

At the end of the reaction, the volume of each samples was adjusted to 50ul with RNase free water.

Real-Time PCR reaction

1μl of diluted cDNAs were amplified in 10μl PCR reactions in a ABI Prism 7000 (Applied Biosystem) thermocycler, coupled with a ABI Prism 7000 Sequence Detection System (Applied Biosystems) in 96-wells plates (Micro Amp Optical, Applied Biosystems).

In each well 10ul Sample mix + 10ul reaction mix were added.

Sample mix was prepared as follows:

Template cDNA	1μl
H$_2$O Rnase-free	9μl
Total volume	10μl

The SYBR® Green qPCR (Qiagen) was used for the Real-Time PCR reaction as follows:

SYBR® Green qPCR (Qiagen)	10µl
Mix Primer forward /reverse 50mM	0.4µl
Total volume	10µl

The PCR cycle used for the Real-Time PCR was:

step 1:	95° C for 15 minutes
step2:	95° C for 25 seconds
step3	58° C for 1 minute
step4:	go to step 2 for 40 times

Gel Electrophoresis And Western Blot

Lysis and Protein extraction from gastrocnemius muscle

About 30 Sections of gastrocnemius muscles, 20μm thick each, were lysed with 100μl of Lysis Buffer containing:

Solution	Final Concentration
Tris pH 7.5	50 mM
NaCl	150mM
$MgCl_2$	10mM
DTT	0.5mM
EDTA	1mM
Glycerol	10%
SDS	2%
Triton X100	1%
Cocktail di inibitori di proteasi (Complete, Roche)	1X
PMSF	1mM
$NaVO_3$	1mM
NaF	5mM
β-glycerophosphate	3mM

After incubation at 70°C for 10 minutes and centrifugation at 13000rpm for 10 minutes at 4°C the surnatant protein concentration was measured using BCA[TM] protein assay kit (PIRCE) following the manufacturer's instructions.

In order to separate MYH isoforms we used polyacrylamide gel containing high glycerol concentration according to previously published protocol (Mizunoya *et al*., 2008).

Electrophoretic run of proteins

The extracted proteins from gastrocnemius muscle were solubizated in <u>Loading buffer</u> made for esch semple as following:

1X NuPAGE® LDS Sample Buffer (Invitrogen)   4µl

1X NuPAGE® Reducing Agent (Invitrogen)   2µl

The volume of each sample was brought to 20µl with 1% SDS. The samples were denaturated at 70 °C for 10 minutes. Samples were loaded on SDS 4-12% precast polyacrylamide gels (NuPAGE Novex-Bis-tris-gels) (Invitrogen). The electrophoresis was run in 1X MES Running buffer (Invitrogen) for 1hour and 30 minutes at 150V constant.

Transfer of the protein to the PVDF membrane

After the electrophoretic run, proteins were transferred from gels to PDVF membranes. The gel and the membrane were equilibrated in Transfer Buffer. The Transfer Buffer was prepared as follows:

    20X NuPAGE® Transfer buffer(Invitogen)   50ml

    10X NuPAGE® Antioxidant (Invitogen)   1ml

    20% Methanol (Sigma-Aldrich)   200ml

The volume was brought to 1l with distilled water. The transfer was obtained by applying a current of 400mA for 1 hour and 30 minutes at 4°C. To evaluate the efficiency of transfer, proteins were stained with Red Ponceau 1x (Sigma). The staining was easily reversed by washing with distilled water.

Incubation of the membrane with antibodies

Once the proteins were transferred on PVDF membranes, the membranes were saturated with <u>Blocking Buffer</u> (5% no fat milk powder solubilizated in TBS 1X with 0.1% TWEEN) for 1 hour at room temperature and were incubated overnight with various primary antibodies at 4°C . Then membranes were washed 3 times

with TBS 1X with 0.1% TWEEN at room temperature and incubated with secondary antibody-HRP Conjugate (Bio-Rad), for 1 hour at room temperature. Immunoreaction was revealed by ECL (Pierce) and followed by exposure to X-ray film (KODAK Sigma-Aldrich).

The following antibodies were used for immunoblotting analyses:

Antibody	Company
anti-Akt	Cell Signalling
anti-phospho-Akt (Ser473)	Cell Signalling
anti-phospho-4EBP1 (Thr37/46)	Cell Signalling
anti-phospho-4EBP1 (Ser65)	Cell Signalling
anti-4EBP1	Cell Signalling
anti-phospho-S6 (Ser240/244)	Cell Signalling
anti-S6	Cell Signalling
anti-AMPKα (Thr 172)	Cell Signalling
anti-AMPKα	Cell Signalling
anti-LC3	NanoTools
anti-p62	PROGEN
Anti-P-eIF2α (S51)	ABCAM
anti-eIF2α	ABCAM
anti-dystrophin (IHC)	ABCAM
anti-dystrophin (WB)	SIGMA
monoclonal anti-GAPDH	Sigma-Aldrich
monoclonal anti-dystrophin (clone MANDRA1)	Sigma-Aldrich
anti-BIP	BD (Becton Dickinson and Company)
anti-mono- and polyubiquinylated conjugates (clone FK2)	BIOMOL international.
Atg7 was a generous gift of Dr. T. Ueno	

All the peroxidase-conjugated secondary antibodies were from Bio-Rad.

Blots were stripped using Restore Western Blotting Stripping Buffer (Pierce) according to the manufacturer's instructions and reprobed if necessary.

Oxy-blot

To study the level of carbonylation of muscle proteins, caused by an increase in oxygen free radicals, we used the Oxyblot Protein Oxidation Detection Kit from Millipore.

The reagents supplied in the kit are:

10X 2,4-Dinitrophenylhydrazine (DNPH) Solution

Neutralization Solution

Mixture of Standard Proteins with attached DNP residues 75

1° Antibody: Rabbit Anti-DNP Antibody 4.0

2° Antibody: Goat Anti-Rabbit IgG (HRP-conjugated)

10X Derivatization-Control Solution

Cryosections of gastrocnemius muscles, 20μm thick, were lysed in lysis buffer with 50mM of DTT. The composition of the lysis buffer is similar to that used in Lysis and Protein extraction from gastrocnemius muscle. The samples were then incubated at 70°C for 10 minutes in termomix, and centrifuged at 1300rpm for 10 minutes at 4°C. The surnatant is derivatized with DNPH soltution and then neutralized. This way the samples were ready to be load.

Detergent-soluble and insoluble fraction

This method is used for the measure of the difference of quantity of ubiquitin-protein in the soluble and insoluble fraction. Detergent-soluble and insoluble fractions were obtained according to Hara (Hara *et al.*, 2006).

Frozen gastrocnemius muscles were powdered by pestle and mortar and lysed in a homogenyzation buffer containing:

Solution	Final concentration
Saccarose	250 mM
Tris-HCl pH 7.5	10 mM
NaCl	10 mM
MgCl$_2$	3 mM
proteasome inhibitor MG-132	20 μM
N-ethylmaleimide (NEM)	10 mM
TritonX100	1%
Cocktail di inibitori di proteasi (Complete, Roche)	1X
PMSF	1 mM
NaVO$_3$	1 mM
NaF	5 mM
β-glycerophosphate	3 mM

The samples were treated with Polytron PT 1200E one pulse for 5 sec. After the homogenyzation was over, samples were incubated on ice for 5 minutes and centrifuged at 2300rpm for 5 minutes at 4°C. The surnatant represents the soluble fraction.

To obtain the insoluble fraction, the pellet of the previous step was treated with a Lysis Buffer containing:

Solution	Final Concentration
Tris-HCl pH 7.5	50 mM
NaCl	150 mM
MgCl$_2$	10 mM
DTT	0.5 mM
EDTA	1 mM
Glycerol	10%
TritonX100	1%
SDS	1%
Cocktail di inibitori di proteasi (Complete, Roche)	1X
PMSF	1 mM
NaVO$_3$	1 mM
NaF	5 mM
β-glycerophosphate	3 mm

The samples were incubated on ice for 5 minutes, incubated at 70°C for 10 minutes in termomix and centrifuged at 6200rpm for 10 minutes at 4°C. In this case the surnatant represents the insoluble fraction.

At the end the different fractions were used for immunobloting (see above).

Creatine kinase assay

To evaluate the amount of creatine kinase present in the blood, samples of plasma were obtained using peri-orbital bleeding. By placing a piece of glass pipette of a small diameter behind the eye of the mouse and twisting gently till rupture of the vessel, around 100µl of blood were collected in a tube containing 2µl of 0,5M EDTA as anticoagulant. Creatine kinase content was measured by the accumulation of b-NADP using a kit from Sentinel Diagnostics.

TUNEL assay on muscle sections

The DeadEnd[TM] Fluorometric TUNEL System measures the fragmented DNA of apoptotic cells by catalytically incorporating fluorescein-12-dUTP(a) at 3′-OH DNA ends using the Terminal Deoxynucleotidyl Transferase Recombinant enzyme (rTdT). rTdT forms a polymeric tail using the principle of the TUNEL (TdT-mediated dUTP Nick-End Labeling) assay. The fluorescein-12-dUTPlabeled DNA can then either be visualized directly by fluorescence microscopy or quantified by flow cytometry.

Sections of gastrocnemius muscle were revealed by using the terminal deoxynucleotidyltransferase-mediated dUTP nick end labeling (DeadEnd Fluorometric TUNEL System (Promega) as previously described.

Statistical analysis

All data are expressed as means ± standard error (se). Differences between groups were assessed using Student's t test. Significance was defined as a value of $P < 0.05$ (95% confidence).

BIBLIOGRAPHY

Abeliovich H, Dunn WA Jr, Kim J, Klionsky DJ. (2000). Dissection of autophagosome biogenesis into distinct nucleation and expansion steps. J Cell Biol 151: 1025–1034.

Agarraberes F., Terlecky S. and Dice J.F. (1997). An intralysosomal hsp70 is required for a selective pathway of lysosomal protein degradation. J. Cell Biol. 272, 137.

Ahlberg J., Marzella L. and Glaumann H. (1982). Uptake and degradation of proteins by isolated rat liver lysosomes. Suggestion of a microautophagic pathway of proteolysis. Lab. Invest. 47, 523-532.

Anglade P, Vyas S, Hirsch EC, Agid Y. (1997). Apoptosis and autophagy in nigral neurons of patients with Parkinson's disease. Histol. Histopathol. 12: 25–31.

Askanas, V., and Engel, W.K. (2006). Inclusion-body myositis: a myodegenerative conformational disorder associated with Aβ, protein misfolding, and proteasome inhibition. Neurology 66, S39–S48.

Bechet, D., Tassa, A., Taillandier, D., Combaret, L., and Attaix, D. (2005). Lysosomal proteolysis in skeletal muscle. Int J Biochem Cell Biol 37, 2098-2114.

Birkenkamp, K. U., and Coffer, P. J. (2003). Regulation of cell survival and proliferation by the FoxO (Forkhead box, class O) subfamily of Forkhead transcription factors. Biochem Soc Trans 31, 292-297.

Bjørkøy G, Lamark T, Brech A, Outzen H, Perander M, Overvatn A, Stenmark H, Johansen T. (2005). p62/SQSTM1 forms protein aggregates degraded by autophagy and has a protective effect on huntingtin-induced cell death. J Cell Biol; 171:603-14.

Blaauw, B., Mammucari, C., Toniolo, L., Agatea, L., Abraham, R., Sandri, M., Reggiani, C., and Schiaffino, S. (2008). Akt activation prevents the force drop induced by eccentric contractions in dystrophin-deficient skeletal muscle. Hum. Mol. Genet. 17, 3686–3696.

Bodine, S. C., Latres, E., Baumhueter, S., Lai, V. K., Nunez, L., Clarke, B. A., Poueymirou, W. T., Panaro, F. J., Na, E., Dharmarajan, K. (2001a). Identification of ubiquitin ligases required for skeletal muscle atrophy. Science *294*, 1704-1708.

Borden, K. L. and P. S. Freemont (1996). The RING finger domain: a recent example of a sequence-structure family. Curr Opin Struct Biol 6(3): 395-401.

Bothe, G. W., Haspel, J. A., Smith, C. L., Wiener, H. H., and Burden, S. J. (2000). Selective expression of Cre recombinase in skeletal muscle fibers. Genesis 26, 165-166.

Brett A. McCray, J. Paul Taylor. (2008). The Role of Autophagy in Age-Related Neurodegeneration. Neurosignals. 16:75-84.

Brummelkamp, T.R., Bernards, R., and Agami, R. (2002). A system some proteolysis in a model of muscle wasting. for stable expression of short interfering RNAs in mammalian cells. Science 296, 550–553.

Brunet, A., Bonni, A., Zigmond, M. J., Lin, M. Z., Juo, P., Hu, L. S., Anderson, M. J., Arden, K. C., Blenis, J., and Greenberg, M. E. (1999). Akt promotes cell survival by phosphorylating and inhibiting a Forkhead transcription factor. Cell 96, 857-868.

Bursch, W., Hochegger, K., Torok, L., Marian, B., Ellinger, A., Hermann, R.S. (2000). Autophagic and apoptotic types of programmed cell death exhibit different fates of cytoskeletal filaments. J. Cell Sci. 113: 1189–1198.

Cai, D., Frantz, J. D., Tawa, N. E., Jr., Melendez, P. A., Oh, B. C., Lidov, H. G., Hasselgren, P. O., Frontera, W. R., Lee, J., Glass, D. J., and Shoelson, S. E. (2004). IKKbeta/NF-kappaB activation causes severe muscle wasting in mice. Cell 119, 285-298.

Chan, E.Y., Kir, S., Tooze, S.A. (2007). siRNA screening of the kinome identifies ULK1 as a multi-domain modulator of autophagy, J. Biol. Chem. 282 25464–25474.

Chiang H.-L. and Dice J.F. (1988). Peptide sequences that target proteins for enhanced degradation during serum withdrawal. J. Biol. Chem. 263, 6797-6805.

Codogno, P., Meijer, A.J. (*2005*) Autophagy and signaling: Their role in cell survival and cell death. Cell Death Differ. 12 *(*Suppl. 2) 1509–1518.

Crighton, D., Wilkinson, S., O'Prey, J., Syed, N., Smith, P., Harrison, P.R., Gasco, M., Garrone, O., Crook, T., Ryan, K.M. (2006) DRAM, a p53-induced modulator of autophagy, is critical for apoptosis. Cell 126:121–134.

Criollo, A., Maiuri, M.C., Tasdemir, E., Vitale, I., Fiebig, A.A., Andrews, D., Molgo, J., Diaz, J., Lavandero, S., Harper, F., et al. (2007). Regulation of autophagy by the inositol trisphosphate receptor. Cell Death Differ. 14, 1029–1039.

Cuervo A.M., Terlecky S.R., Dice J.F. and Knecht E. (1994). Selective binding and uptake of ribonuclease A and glyceraldehyde-3-phosphate dehydrogenase by isolated rat liver lysosomes. J. Biol. Chem. 269, 26374-26380.

Cuervo A.M. and Dice J.F. (1996). A receptor for the selective uptake and degradation of proteins by lysosomes. Science 273, 501-503.

Cuervo A.M., Dice J.F. and Knecht E. (1997). A population of rat liver lysosomes responsible for the selective uptake and degradation of cytosolic proteins. J. Biol. Chem. 272, 5606-5615.

Cuervo A.M., Gomes A.V., Barnes J.A. and Dice J.F. (2000). Selective degradation of annexins by chaperone-mediated autophagy. J. Biol. Chem. 275, 33329-33335.

Cuervo AM, Stefanis L, Fredenburg R, Lansbury PT, Sulzer D. (2004). Impaired degradation of mutant α-synuclein by chaperone-mediated autophagy. Science; 305:1292-5.

Cuervo, A.M. (2004). Autophagy: many paths to the same end. Mol. Cell. Biochem. 263, 55–72.

Daido, S., Kanzawa, T., Yamamoto, A., Takeuchi, H., Kondo, Y., Kondo, S. (2004) Pivotal role of the cell death factor BNIP3 in ceramide-induced autophagic cell death in malignant glioma cells. Cancer Res. 64:4286–4293.

Dantuma, NP., Lindsten, K., Glas, R., Jellne, M. and Masucci, MG. (2000). Short-lived green fluorescent proteins for quantifying ubiquitin/proteasome-dependent proteolysis in living cells. Nat Biotechnol.18: 538-43.

Demarchi, F., Bertoli, C., Copetti, T., Tanida, I., Brancolini, C., Eskelinen, E.-L., Schneider, C. (2006). Calpain is required for macroautophagy in mammalian cells. J. Cell Biol. 175:595–605.

Dice J.F. (1987). Molecular determinants of protein half-lives in eukaryotic cells. FASEB J. 1, 349-357.

Dice J.F. (1992). Selective degradation of cytosolic proteins by lysosomes. Ann. NY Acad. Sci. 674, 58-64.

Djavaheri-Mergny, M., Amelotti, M., Mathieu, J., Besancon, F., Bauvy, C., Souquere, S., Pierron, G., Codogno, P. (2006) NF-κB activation represses tumor necrosis factor-α-induced autophagy. J. Biol. Chem. 281:30373–30382

Dobrowolny, G., Aucello, M., Rizzuto, E., Beccafico, S., Mammucari, C., Bonconpagni, S., Belia, S., Wannenes, F., Nicoletti, C., Del Prete, Z., et al. (2008). Skeletal muscle is a primary target of SOD1G93A-mediated toxicity. Cell Metab. 8, 425–436.

Dona, M., Sandri, M., Rossini, K., Dell'Aica, I., Podhorska-Okolow, M., and Carraro, U. (2003). Functional in vivo gene transfer into the myofibers of adult skeletal muscle. Biochem Biophys Res Commun 312, 1132-1138.

Dunn, W.A., JR. 1990. Studies on the mechanisms of autophagy: formation of the autophagic vacuole. J. Cell Biol. 110: 1923–1933.

Eskelinen E-L. (2006). Roles of LAMP-1 and LAMP-2 in lysosome biogenesis and autophagy. Mol Aspects Med; 27:495-502.

Fukuda T, Ewan L, Bauer M, Mattaliano RJ, Zaal K, Ralston E, Plotz PH, Raben N. (2006). Dysfunction of endocytic and autophagic pathways in a lysosomal storage disease. Ann Neurol; 59:700-8.

Glabe, C. (2001) Intracellular mechanisms of amyloid accumulation and pathogenesis in Alzheimer's disease. J. Mol. Neurosci. 17, 137–145.

Glass, D. J. (2003). Molecular mechanisms modulating muscle mass. Trends Mol Med 9, 344-350.

Goldspink, G. (1999). Changes in muscle mass and phenotype and the expression of autocrine and systemic growth factors by muscle in response to stretch and overload. J Anat 194, 323-334.

Gomes, M. D., Lecker, S. H., Jagoe, R. T., Navon, A., and Goldberg, A. L. (2001). Atrogin-1, a muscle-specific F-box protein highly expressed during muscle atrophy. Proc Natl Acad Sci U S A 98, 14440-14445.

Gozuacik, D. and Kimchi, A. (2004). Autophagy as a cell death and tumor suppressor mechanism. Oncogene. 23 : 2891-2906.

Hara, T., Nakamura, K., Matsui, M., Yamamoto, A., Nakahara, Y., Suzuki-Migishima, R., Yokoyama, M., Mishima, K., Saito, I., Okano, H., and Mizushima, N. (2006). Suppression of basal autophagy in neural cells causes neurodegenerative disease in mice. Nature 441, 885–889.

Hoyer-Hansen, M., Bastholm, L., Szyniarowski, P., Campanella, M., Szabadkai, G., Farkas, T., Bianchi, K., Fehrenbacher, N., Elling, F., Rizzuto, R., (2007) Control of macroautophagy by calcium, calmodulin-dependent kinase kinase-β, and Bcl-2. Mol. Cell 25:193–205.

Hunter, R. B., Stevenson, E., Koncarevic, A., Mitchell-Felton, H., Essig, D. A., and Kandarian, S. C. (2002). Activation of an alternative NF-kappaB pathway in skeletal muscle during disuse atrophy. Faseb J 16, 529-538.

Hunter, R. B., and Kandarian, S. C. (2004). Disruption of either the Nfkb1 or the Bcl3 gene inhibits skeletal muscle atrophy. J Clin Invest 114, 1504-1511.

Ichimura Y, Kirisako T, Takao T, Satomi Y, Shimonishi Y, Ishihara N, Mizushima N, Tanida I, Kominami E, Ohsumi M, Noda T, Ohsumi Y. (2000). A ubiquitin-like system mediates protein lipidation. Nature 408: 488–492.

Ichimura, Y., Kominami, E., Tanaka, K. and Komatsu, M. (2008). Selective turnover of p62/A170/SQSTM1 by autophagy. Autophagy 4:8, 1063-1066.

Ichimura, Y., Kumanomidou, T., Sou, Y.S., Mizushima, T., Ezaki, J., Ueno, T., Kominami, E., Yamane, T., Tanaka, K., Komatsu, M. (2008). Structural basis for

sorting mechanism of p62 in selective autophagy, J. Biol. Chem. 283 22847–22857.

Jackson, P. K., and Eldridge, A. G. (2002). The SCF ubiquitin ligase: an extended look. Mol Cell 9, 923-925.

Kabeya Y, Mizushima N, Yamamoto A, Oshitani-Okamoto S, Ohsumi Y, Yoshimori T (2004) LC3, GABARAP and GATE16 localize to autophagosomal membrane depending on form-II formation. J Cell Sci 117: 2805–2812.

Kabeya, Y., Mizushima, N., Ueno, T., Yamamoto, A., Kirisako, T., Noda, T., Kominami, E., Ohsumi, Y., Yoshimori, T. (2000). LC3, a mammalian homologue of yeast Apg8p, is localized in autophagosome membranes after processing, EMBO J. 19 5720–5728.

Kalimo, H., Savontaus, M.L., Lang, H, Paljarvi, L., Sonninen, V., Dean, P.Bc, Katevuo, K. and Salminen, A. (1988). X-linked myopathy with excessive autophagy : a new hereditary muscle disease. Ann. Neurol. 23 : 258-265.

Kamada, Y., Funakoshi, T., Shintani, T., Nagano, K., Ohsumi, M., Ohsumi, Y. (2000). Tormediated induction of autophagy via an Apg1 protein kinase complex, J. Cell Biol. 150 1507–1513.

Kamura, T., Koepp, D. M., Conrad, M. N., Skowyra, D., Moreland, R. J., Iliopoulos, O., Lane, W. S., Kaelin, W. G., Jr., Elledge, S. J., Conaway, R. C., *et al.* (1999). Rbx1, a component of the VHL tumor suppressor complex and SCF ubiquitin ligase. Science *284*, 657-661.

Kim, J. and Klionsky, D.J. (2000). Autophagy, cytoplasm-to-vacuole targeting pathway, and pexophagy in yeast and mammalian cells. Annu. Rev. Biochem. 69: 303–42.

Kim J, Huang WP, Stromhaug PE, Klionsky DJ. (2002). Convergence of multiple autophagy and cytoplasm to vacuole targeting components to a perivacuolar membrane compartment prior to de novo vesicle formation. J Biol Chem 277: 763–773.

Kirisako T, Ichimura Y, Okada H, Kabeya Y, Mizushima N, Yoshimori T, Ohsumi M, Takao T, Noda T, Ohsumi Y (2000) The reversible modification

regulates the membrane-binding state of Apg8/Aut7 essential for autophagy and the cytoplasm to vacuole targeting pathway. J Cell Biol 151: 263–276.

Kirkegaard, K., Taylor, M.P. and Jackson, W.T. (2004). Cellular autophagy: surrender, avoidance and subversion by microorganisms. Nat. Rev. Microbiol. 2: 301–314.

Klionsky, D.J. and Emr, S.D. (2000). Autophagy as a regulated pathway of cellular degradation. Science 290: 1717–1721.

Klionsky, D. J., Cregg, J. M., Dunn, W. A., JR., Emr, S. D., Sakai, Y., Sandoval, I. V., Sibirny, A., Subramani, S., Thumm, M., Veenhuis, M. and Ohsumi, Y. (2003). A unified nomenclature for yeast autophagy-related genes. Dev Cell 5, 539–45.

Klionsky D.J., Geng. (2008). The Atg8 and Atg12 ubiquitin-like conjugation systems in macroautophagy. 'Protein Modifications: Beyond the Usual Suspects' Review Series. EMBO Rep. 9: 859–864.

Klionsky DJ, Abeliovich H, Agostinis P, Agrawal DK, Aliev G, Askew DS, Baba M, Baehrecke EH, Bahr BA, Ballabio A, Bamber BA, Bassham DC, Bergamini E, Bi X, Biard-Piechaczyk M, Blum JS, Bredesen DE, Brodsky JL, Brumell JH, Brunk UT, Bursch W, Camougrand N, Cebollero E, Cecconi F, Chen Y, Chin LS, Choi A, Chu CT, Chung J, Clarke PG, Clark RS, Clarke SG, Clave C, Cleveland JL, Codogno P, Colombo MI, Coto-Montes A, Cregg JM, Cuervo AM, Debnath J, Demarchi F, Dennis PB, Dennis PA, Deretic V, Devenish RJ, Di Sano F, Dice JF, Difiglia M, Dinesh-Kumar S, Distelhorst CW, Djavaheri-Mergny M, Dorsey FC, Droge W, Dron M, Dunn WA, Jr., Duszenko M, Eissa NT, Elazar Z, Esclatine A, Eskelinen EL, Fesus L, Finley KD, Fuentes JM, Fueyo J, Fujisaki K, Galliot B, Gao FB, Gewirtz DA, Gibson SB, Gohla A, Goldberg AL, Gonzalez R, Gonzalez-Estevez C, Gorski S, Gottlieb RA, Haussinger D, He YW, Heidenreich K, Hill JA, Hoyer-Hansen M, Hu X, Huang WP, Iwasaki A, Jaattela M, Jackson WT, Jiang X, Jin S, Johansen T, Jung JU, Kadowaki M, Kang C, Kelekar A, Kessel DH, Kiel JA, Kim HP, Kimchi A, Kinsella TJ, Kiselyov K, Kitamoto K, Knecht E, et al. (2008). Guidelines for the use and interpretation of assays for monitoring autophagy in higher eukaryotes. Autophagy 4: 151-175.

Kochl, R., Hu, X.W., Chan, E.Y., and Tooze, S.A. (2006). Microtubules facilitate autophagosome formation and fusion of autophagosomes with endosomes. Traffic 7, 129–145.

Komatsu, M., Tanida, I., Ueno, T., Ohsumi, M., Ohsumi, Y., Kominami, E. (2001). The C-terminal region of an Apg7p/Cvt2p is required for homodimerization and is essential for its E1 activity and E1-E2 complex formation. J Biol Chem 276: 9846–9854.

Komatsu, M., Waguri, S., Ueno, T., Iwata, J., Murata, S., Tanida, I., Ezaki, J., Mizushima, N., Ohsumi, Y., Uchiyama, Y., et al. (2005). Impairment of starvation-induced and constitutive autophagy in Atg7-deficient mice. J. Cell Biol. 169, 425–434.

Komatsu, M., Waguri, S., Chiba, T., Murata, S., Iwata, Jun-ichi., Tanida, I., eno, T., Koike, M., Uchiyama, Y., Kominami, E., and Tanaka, K. (2006). Loss of autophagy in the central nervous system causes neurodegeneration in mice. Nature 441, 880-884.

Komatsu, M., Ueno, T., Waguri, S., Uchiyama, Y., Kominami, E., Tanaka, K. (2007). Constitutive autophagy: vital role in clearance of unfavorable proteins in neurons, Cell Death Differ. 14 887–894.

Kouroku Y, Fujita E, Tanida I, Ueno T, Isoai A, Kumagai H, Ogawa S, Kaufman RJ, Kominami E, Momoi T. (2007). ER stress (PERK/eIF2alpha phosphorylation) mediates the polyglutamine-induced LC3 conversion, an essential step for autophagy formation. Cell Death Differ 14: 230–239.

Kroll, J., Cobo, P., and Sato, T. N. (2003). Versatile inducible activation system of Akt/PKB signaling pathway in mice. Genesis 35, 160-163.

Kuma A, Mizushima N, Ishihara N, Ohsumi Y (2002) Formation of the approximately 350-kDa Apg12–Apg5•Apg16 multimeric complex, mediated by Apg16 oligomerization, is essential for autophagy in yeast. J Biol Chem 277: 18619–18625.

Kuma, A., Hatano, M., Matsui, M., Yamamoto, A., Nakaya, H., Yoshimori, T., Ohsumi, Y., Tokuhisa, T., and Mizushima, N. (2004). The role of autophagy during the early neonatal starvation period. Nature *432*, 1032-1036.

Lecker, S. H., Jagoe, R. T., Gilbert, A., Gomes, M., Baracos, V., Bailey, J., Price, S. R., Mitch, W. E., And Goldberg, A. L. (2004). Multiple types of skeletal muscle atrophy involve a common program of changes in gene expression. FASEB J 18, 39-51.

Lecker, S. H., Goldberg, A. L., and Mitch, W. E. (2006a). Protein degradation by the ubiquitin-proteasome pathway in normal and disease states. J Am Soc Nephrol 17, 1807-1819.

Lecker, S.H., Goldberg, A.L., and Mitch, W.E. (2006). Protein degradation by the ubiquitin-proteasome pathway in normal and disease states. J. Am. Soc.Nephrol. 17, 1807–1819.

Levine, B. and Klionsky, D. J. (2004). Development by selfdigestion: molecular mechanisms and biological functions of autophagy. Dev Cell 6, 463–77.

Levine, B. and Kroemer, G. (2008). Autophagy in the pathogenesis of disease. Cell 132: 27-42.

Li, Y. P., and Reid, M. B. (2000). NF-kappaB mediates the protein loss induced by TNF-alpha in differentiated skeletal muscle myotubes. Am J Physiol Regul Integr Comp Physiol 279, R1165-1170.

Liang, C., Feng, P., Ku, B., Dotan, I., Canaani, D., Oh, B.H., Jung, J.U. (2006). Autophagic and tumour suppressor activity of a novel Beclin1-binding protein UVRAG. Nat. Cell Biol. 8:688–699.

Liang, J., Shao, S.H., Xu, Z.X., Hennessy, B., Ding, Z., Larrea, M., Kondo, S., Dumont, D.J., Gutterman, J.U., Walker, C.L., et al. (2007) The energy sensing LKB1–AMPK pathway regulates p27(kip1) phosphorylation mediating the decision to enter autophagy or apoptosis. Nat. Cell Biol. 9:218–224.

Liang, X.H., Kleeman, L.K., Jiang, H.H., Gordon, G., Goldman, J.E., Berry, G., Herman, B., Levine, B. (1998). Protection against fatal Sindbis virus encephalitis by Beclin, a novel Bcl-2-interacting protein. J. Virol. 72:8586–8596.

Liberski PP, Sikorska B, Bratosiewicz-Wasik J, Gajdusek DC, Brown P. (2004). Neuronal cell death in transmissible spongiform encephalopathies (prion diseases) revisited: from apoptosis to autophagy. Int. J. Biochem. CellBiol. 36: 2473–2490.

Luby-Phelps K., Ning, J. Fogerty G. and Besharse J.C. (2003). Visualization of identified GFP-expressing cells by light and electron microscopy, J. Histochem. Cytochem. 51: 271–274

Lum, J.J., Bauer, D.E., Kong, M., Harris, M.H., Li, C., Lindsten, T., and Thompson, C.B. (2005). Growth factor regulation of autophagy and cell survival in the absence of apoptosis. Cell 120, 237–248.

Lum, J.J., DeBerardinis, R.J., and Thompson, C.B. (2005). Autophagy in metazoans: cell survival in the land of plenty. Nat Rev Mol Cell Biol 6, 439-448.

Lunemann JD, Schmidt J, Dalakas MC, Münz C. (2007). Macroautophagy as a pathomechanism in sporadic inclusion body myositis. Autophagy; 3.

Lunemann, J.D., Schmidt, J., Schmid, D., Barthel, K., Wrede, A., Dalakas, M.C., and Munz, C. (2007). β-Amyloid is a substrate of autophagy in sporadic inclusion body myositis. Ann. Neurol. 61, 476–483.

Maiuri, M.C., Le Toumelin, G., Criollo, A., Rain, J.C., Gautier, F., Juin, P., Tasdemir, E., Pierron, G., Troulinaki, K., Tavernarakis, N., et al. (2007). Functional and physical interaction between Bcl-X(L) and a BH3-like domain in Beclin-1. EMBO J. 26:2527–2539.

Maiuri, M.C., Zalckvar, E., Kimchi, A., and Kroemer, G. (2007a). Self-eating and self-killing: crosstalk between autophagy and apoptosis. Nat. Rev. Mol. Cell Biol. 8, 741–752.

Mammucari, C., Milan, G., Romanello, V., Masiero, E., Rudolf, R., Del Piccolo, P., Burden, S.J., Di Lisi, R., Sandri, C., Zhao, J., et al. (2007). FoxO3 Controls Autophagy in Skeletal Muscle In Vivo. Cell Metab. 6, 458–471.

Maria Fimia, G., Stoykova, A., Romagnoli, A., Giunta, L., Di Bartolomeo, S., Nardacci, R., Corazzari, M., Fuoco, C., Ucar, A., Schwartz, P., et al. (2007). Ambra1 regulates autophagy and development of the nervous system. Nature 447:1121–1125.

Masiero E, Agatea L, Mammucari C, Blaauw B, Loro E, Komatsu M, Metzger D, Reggiani C, Schiaffino S, Sandri M. (2009). Autophagy is required to maintain muscle mass. Cell Metab. 10:507-15.

McCarthy, J. J., and Esser, K. A. (2007). Counterpoint: Satellite cell addition is not obligatory for skeletal muscle hypertrophy. J Appl Physiol 103, 1100-1102; discussion 1102-1103.

Meijer, A.J., Codogno, P. (2006). Signalling and autophagy regulation in health, aging and disease, Mol. Aspects Med. 27 411–425.

Meley, D., Bauvy, C., Houben-Weerts, J.H., Dubbelhuis, P.F., Helmond, M.T., Codogno, P., Meijer, A.J. (2006) AMP-activated protein kinase and the regulation of autophagic proteolysis. J. Biol. Chem. 281:34870–34879.

Mills, K.R., Reginato, M., Debnath, J., Queenan, B., Brugge, J.S. (2004) Tumor necrosis factor-related apoptosis-inducing ligand (TRAIL) is required for induction of autophagy during lumen formation in vitro. Proc. Natl. Acad. Sci. 101:3438–3443.

Mitchener J.S., Shelburne, J.D., Bradford. W.D., Hawkins H.K. (1976). Cellular autophagocytosis induced by deprivation of serum and amino acids in HeLa cells. Am. J. Pathol. 83: 485–491.

Mizunoya W, Wakamatsu J, Tatsumi R, Ikeuchi Y. (2008). Protocol for high-resolution separation of rodent myosin heavy chain isoforms in a mini-gel electrophoresis system. Anal Biochem. 377:111-3.

Mizushima N, Noda T, Yoshimori T, Tanaka Y, Ishii T, George MD, Klionsky DJ, Ohsumi M, Ohsumi Y (1998a) A protein conjugation system essential for autophagy. Nature 395: 395–398.

Mizushima N, Sugita H, Yoshimori T, Ohsumi Y (1998b) A new protein conjugation system in human. The counterpart of the yeast Apg12p conjugation system essential for autophagy. J Biol Chem 273: 33889–33892.

Mizushima N, Noda T, Ohsumi Y (1999) Apg16p is required for the function of the Apg12p–Apg5p conjugate in the yeast autophagy pathway. EMBO J 18: 3888–3896.

Mizushima N, Yamamoto A, Hatano M, Kobayashi Y, Kabeya Y, Suzuki K, Tokuhisa T, Ohsumi Y, Yoshimori T. (2001). Dissection of autophagosome

formation using Apg5-deficient mouse embryonic stem cells. J Cell Biol 152: 657–668.

Mizushima N, Yoshimori T, Ohsumi Y (2002) Mouse Apg10 as an Apg12-conjugating enzyme: analysis by the conjugation-mediated yeast two-hybrid method. FEBS Lett 532: 450–454.

Mizushima, N., Ohsumi, Y. And Yoshimori, T. (2002). Autophagosome formation in mammalian cells. Cell Struct. Funct. 27: 421–429.

Mizushima N, Kuma A, Kobayashi Y, Yamamoto A, Matsubae M, Takao T, Natsume T, Ohsumi Y, Yoshimori T (2003) Mouse Apg16L, a novel WD-repeat protein, targets to the autophagic isolation membrane with the Apg12–Apg5 conjugate. J Cell Sci 116: 1679–1688.

Mizushima, N., Yamamoto, A., Matsui, M., Yoshimori, T., and Ohsumi, Y. (2004). In vivo analysis of autophagy in response to nutrient starvation using transgenic mice expressing a fluorescent autophagosome marker. Mol Biol Cell *15*, 1101-1111.

Mizushima, N., Levine, B., Cuervo, A.M., and Klionsky, D.J. (2008). Autophagy fights disease through cellular self-digestion. Nature 451: 1069-1075.

Mordier, S., Deval, C., Bechet, D., Tassa, A., and Ferrara, M. (2000). Leucine limitation induces autophagy and activation of lysosomedependent proteolysis in C2C12 myotubes through a mammalian target of rapamycin-independent signaling pathway. J. Biol. Chem. 275, 29900–29906.

Moriyasu, Y., Ohsumi, Y. (1996) Autophagy in tobacco suspension-cultured cells in response to sucrose starvation. Plant Physiol. 111*:*1233–1241.

Moss, F. P., and Leblond, C. P. (1971). Satellite cells as the source of nuclei in muscles of growing rats. Anat Rec 170, 421-435.

Nagata E, Sawa A, Ross CA, Snyder SH. (2004) Autophagosome-like vacuole formation in Huntington's disease lymphoblasts. NeuroReport 15, 1325–1328.

Nakatogawa, H., Ichimura, Y., Ohsumi, Y. (2007). Atg8, a ubiquitin-like protein required for autophagosome formation, mediates membrane tethering and hemifusion, Cell 130 165–178.

Nezis IP, Simonsen A, Sagona AP, Finley K, Gaumer S, Contamine D, Rusten TE, Stenmark H, Brech A. (2008). The *Drosophila melanogaster* homologue of mammalian p62, is required for the formation of protein aggregates in adult brain. J Cell Biol; 180:1065-71.

Nishino I. (2006). Autophagic vacuolar myopathy. Semin Pediatr Neurol; 13:90-5.

Noda, T., Ohsumi, Y.(1998) Tor, a phosphatidylinositol kinase homologue, controls autophagy in yeast. J. Biol. Chem. 273:3963–3966.

Oberstein, A., Jeffrey, P.D., Shi, Y. (2007). Crystal structure of the Bcl-XL–Beclin 1 peptide complex: Beclin 1 is a novel BH3-only protein. J. Biol. Chem. 282:13123–13132.

Ohsumi, Y. (2001). Molecular dissection of autophagy: two ubiquitin-like systems, Nat. Rev. Mol. Cell Biol. 2 211–216.

Okamoto K, Hirai S, Iizuka T, Yanagisawa T, Watanabe M. (1991). Reexamination of granulovacuolar degeneration. Acta Neuropathol. (Berl.). 82: 340–345.

Passmore, L. A., and Barford, D. (2004). Getting into position: the catalytic mechanisms of protein ubiquitylation.. Biochem J 379, 513-525.

Pallafacchina, G., Calabria, E., Serrano, A. L., Kalhovde, J. M., and Schiaffino, S. (2002). A protein kinase B-dependent and rapamycin-sensitive pathway controls skeletal muscle growth but not fiber type specification. Proc Natl Acad Sci U S A 99, 9213-9218.

Pankiv S, Clausen TH, Lamark T, Brech A, Bruun JA, Outzen H, Øvervatn A, Bjørkøy G, Johansen T. (2007). p62/SQSTM1 binds directly to Atg8/LC3 to facilitate degradation of ubiquitinated protein aggregates by autophagy. J Biol Chem; 282:24131-45.

Pattingre, S., Tassa, A., Qu, X., Garuti, R., Liang, X.H., Mizushima, N., Packer, M., Schneider, M.D., Levine, B. (2005). Bcl-2 antiapoptotic proteins inhibit Beclin 1-dependent autophagy. Cell 122:927–939.

Penner, C. G., Gang, G., Wray, C., Fischer, J. E., and Hasselgren, P. O. (2001). The transcription factors NF-kappab and AP-1 are differentially regulated in skeletal muscle during sepsis. Biochem Biophys Res Commun 281, 1331-1336.

Periyasamy-Thandavan, S., Jiang, M., Schoenlein, P., and Dong, Z. (2009). Autophagy: molecular machinery, regulation, and implications for renal pathophysiology. Am J Physiol Renal Physiol 297: F244–F256.

Pette, D., and Heilmann, C. (1979). Some characteristics of sarcoplasmic reticulum in fast- and slow-twitch muscles. Biochem Soc Trans *7*, 765-767.

Pette, D., Henriksson, J., and Emmerich, M. (1979). Myofibrillar protein patterns of single fibres from human muscle. FEBS Lett 103, 152-155.

Pfaffl, M. W. (2001). A new mathematical model for relative quantification in real-time RT-PCR. Nucleic Acids Res 29, e45.

Price, S. R. (2003). Increased transcription of ubiquitin-proteasome system components: molecular responses associated with muscle atrophy. Int J Biochem Cell Biol 35, 617-628.

Punnonen, E.L., Autio, S., Marjomäki, V.S., Reunanen, H. (1992). Autophagy, cathepsin L transport, and acidification in cultured rat fibroblasts. J. Histochem. Cytochem. 40: 1579–1587.

Pyo, J.O., Jang, M.H., Kwon, Y.K., Lee, H.J., Jun, J.I., Woo, H.N., Cho, D.H., Choi, B., Lee, H., Kim, J.H., et al. (2005) Essential Roles of Atg5 and FADD in autophagic cell death: Dissection of autophagic cell death into vacuole formation and cell death. J. Biol. Chem. 280:20722–20729.

Raben N, Hill V, Shea L, Takikita S, Baum R, Mizushima N, Ralston E, Plotz P. (2008). Suppression of autophagy in skeletal muscle uncovers the accumulation of ubiquitinated proteins and their potential role in muscle damage in Pompe disease. Hum Mol Genet. 17: 3897-908.

Ravikumar B, Duden R, Rubinsztein DC. (2002) Aggregate-prone proteins with polyglutamine and polyalanine expansions are degraded by autophagy. Hum Mol Genet; 11:1107-17.

Ravikumar, B., Vacher, C., Berger, Z., Davies, J.E., Luo, S., Oroz, L.G., Scaravilli, F., Easton, D.F., Duden, R., O'Kane, C.J., et al. (2004). Inhibition of mTOR induces autophagy and reduces toxicity of polyglutamine expansions in fly and mouse models of Huntington disease. Nat. Genet. 36:585–595.

Reef, S., Zalckvar, E., Shifman, O., Bialik, S., Sabanay, H., Oren, M., Kimchi, A. (2006) A short mitochondrial form of p19ARF induces autophagy and caspase-independent cell death. Mol. Cell 22:463–475.

Reggiori, F. (2006). 1. Membrane origin for autophagy. Curr Top Dev Biol 74, 1–30.

Rehfeldt, C. (2007). In response to Point:Counterpoint: Satellite cell addition is/is not obligatory for skeletal muscle hypertrophy. J Appl Physiol 103, 1104.

Rubinsztein, D.C., Gestwicki, J.E., Murphy, L.O., and Klionsky, D.J. (2007). Potential therapeutic applications of autophagy. Nat. Rev. Drug Discov. 6, 304–312.

Sacheck J.M., Ohtsuka A., McLary S.C. and Goldberg A.L. (2004). IGF-I stimulates muscle growth by suppressing protein breakdown and expression of atrophy-related ubiquitin ligases, atrogin-1 and MuRF1. Am. J. Physiol. Endocrinol. Metab. 287: E591–E601.

Sandri, M., Sandri, C., Gilbert, A., Skurk, C., Calabria, E., Picard, A., Walsh, K., Schiaffino, S., Lecker, S.H., and Goldberg, A.L. (2004). Foxo transcription factors induce the atrophy-related ubiquitin ligase atrogin-1 and cause skeletal muscle atrophy. Cell 117, 399–412.

Sandri, M. (2008). Signaling in muscle atrophy and hypertrophy. Physiology (Bethesda) 23, 160-170.

Sandri, M. (2010). Autophagy in health and disease: 3. Autophagy Involvement in Muscle Atrophy. Am J Physiol Cell Physiol. (Articles in Press).

Sapp E, Schwarz C, Chase K, Bhide PG, Young AB, Penney J, Vonsattel JP, Aronin N, DiFiglia M. (1997) Huntingtin localization in brains of normal and Huntington's disease patients. Ann. Neurol. 42, 604–612.

Sarkar, S., Floto, R.A., Berger, Z., Imarisio, S., Cordenier, A., Pasco, M., Cook, L.J., Rubinsztein, D.C. (2005) Lithium induces autophagy by inhibiting inositol monophosphatase. J. Cell Biol. 170:1101–1111.

Sarkar, S., Davies, J.E., Huang, Z., Tunnacliffe, A., and Rubinsztein, D.C. (2007). Trehalose, a novel mTOR-independent autophagy enhancer, accelerates the clearance of mutant huntingtin and alpha-synuclein. J. Biol. Chem. 282, 5641–5652.

Sartorelli, V., and Fulco, M. (2004). Molecular and cellular determinants of skeletal muscle atrophy and hypertrophy. Sci STKE *2004*, re11.

Scherz-Shouval, R., Shvets, E., Fass, E., Shorer, H., Gil, L., Elazar, Z. (2007) Reactive oxygen species are essential for autophagy and specifically regulate the activity of Atg4. EMBO J. 26*:*1749–1760*.*

Schiaffino, S., and Hanzlikova, V. (1972a). Autophagic degradation of glycogen in skeletal muscles of the newborn rat. J Cell Biol *52*, 41-51.

Schiaffino S, Hanzlíková V. (1972b). Studies on the effect of denervation in developing muscle. II. The lysosomal system. J Ultrastruct Res 39: 1-14.

Schiaffino, S., and Reggiani, C. (1996). Molecular diversity of myofibrillar proteins: gene regulation and functional significance. Physiol Rev 76, 371-423.

Schiaffino, S., Sandri, M., and Murgia, M. (2007). Activity-Dependent Signaling Pathways Controlling Muscle Diversity and Plastici. Physiology *22*, 269-278.

Schuler, M., Ali, F., Metzger, E., Chambon, P., and Metzger, D. (2005). Temporally controlled targeted somatic mutagenesis in skeletal muscles of the mouse. Genesis 41, 165- 170.

Shintani T, Mizushima N, Ogawa Y, Matsuura A, Noda T, Ohsumi Y (1999) Apg10p, a novel protein-conjugating enzyme essential for autophagy in yeast. EMBO J 18: 5234–5241.

Shintani, T., and Klionsky, D.J. (2004). Autophagy in health and disease: a double-edged sword. Science 306, 990-995.

Stefanis L, Larsen KE, Rideout HJ, Sulzer D, Greene LA. (2001) Expression of A53T mutant but not wild-type a-synuclein in PC12 cells induces alterations of

the ubiquitindependent degradation system, loss of dopamine release, and autophagic cell death., and J. Neurosci. 21, 9549–9560.

Stefanis, L. (2005) Caspase-dependent and -independent neuronal death: two distinct pathways to neuronal injury. Neuroscientist 11, 50–62.

Stitt, T.N., Drujan, D., Clarke, B.A., Panaro, F., Timofeyva, Y., Kline, W.O., Gonzalez, M., Yancopoulos, G.D., and Glass, D.J. (2004). The IGF-1/PI3K/Akt pathway prevents expression of muscle atrophy-induced ubiquitin ligases by inhibiting FOXO transcription factors. Mol. Cell 14, 395–403.

Sugawara K, Suzuki NN, Fujioka Y, Mizushima N, Ohsumi Y, Inagaki F (2004) The crystal structure of microtubule-associated protein light chain 3, a mammalian homologue of Saccharomyces cerevisiae Atg8. Genes Cells 9: 611–618.

Suzuki K, Kirisako T, Kamada Y, Mizushima N, Noda T, Ohsumi Y. (2001). The pre-autophagosomal structure organized by concerted functions of APG genes is essential for autophagosome formation. EMBO J 20: 5971–5981.

Suzuki NN, Yoshimoto K, Fujioka Y, Ohsumi Y, Inagaki F (2005) The crystal structure of plant ATG12 and its biological implication in autophagy. Autophagy 1: 119–126.

Takeshige, K., Baba, M., Tsuboi, S., Noda, T., Ohsumi, Y. (1992). Autophagy in yeast emonstrated with proteinase-deficient mutants and conditions for its induction. J. Cell Biol. 119:301–311.

Tanaka Y, Guhde G, Suter A, Eskelinen E-L, Hartmann D, Lullmann-Rauch R, Janssen PM, Blanz J, von Figura K, Saftig P. (2000). Accumulation of autophagic vacuoles and cardiomyopathy in LAMP-2-deficient mice. Nature; 406:902-6.

Tanida I, Mizushima N, Kiyooka M, Ohsumi M, Ueno T, Ohsumi Y, Kominami E (1999) Apg7p/Cvt2p: A novel protein-activating enzyme essential for autophagy. Mol Biol Cell 10: 1367–1379.

Tanida I, Tanida-Miyake E, Ueno T, Kominami E (2001) The human homolog of Saccharomyces cerevisiae Apg7p is a protein-activating enzyme for multiple

substrates including human Apg12p, GAT E-16, GABARAP, and MAP-LC3. J Biol Chem 276: 1701–1706.

Tanida I, Tanida-Miyake E, Komatsu M, Ueno T, Kominami E. (2002). Human Apg3p/Aut1p homologue is an authentic E2 enzyme for multiple substrates, GATE-16, GABARAP, and MAP-LC3, and facilitates the conjugation of hApg12p to hApg5p. J Biol Chem 277: 13739–13744.

Tanida I, Komatsu M, Ueno T, Kominami E. (2003). GATE-16 and GABARAP are authentic modifiers mediated by Apg7 and Apg3. Biochem Biophys Res Commun 300: 637–644.

Tanida, I., Ueno, T. and Kominam, E. (2004). LC3 conjugation system in mammalian autophagy. Int J Biochem Cell Biol. 36: 2503-18.

Tanida, I., Ueno, T., and Kominami, E. (2004a). Human light chain 3/MAP1LC3B is cleaved at its carboxyl-terminal Met121 to expose Gly120 for lipidation and targeting to autophagosomal membranes. J Biol Chem 279: 47704-47710.

Tanida, I., Ueno, T., and Kominami, E. (2004b).LC3 conjugation system in mammalian autophagy. Int J Biochem Cell Biol 36: 2503-2518.

Tanida I, Sou YS, Minematsu-Ikeguchi N, Ueno T, Kominami E. (2006) Atg8L/Apg8L is the fourth mammalian modifier of mammalian Atg8 conjugation mediated by human Atg4B, Atg7 and Atg3. FEBS J 273: 2553–2562.

Temiz, P., Weihl, C.C., and Pestronk, A. (2009). Inflammatory myopathies with mitochondrial pathology and protein aggregates. J. Neurol. Sci. 278, 25–29.

Terlecky S.R. and Dice J.F. (1993). Polypeptide import and degradation by isolated lysosomes. J. Biol. Chem. 268, 23490-23495.

Terman A, Brunk UT. (2005) Autophagy in cardiac myocyte homeostasis, aging, and pathology. Cardiovasc Res; 68:355-65.

Thorburn, J., Moore, F., Rao, A., Barclay, W.W., Thomas, L.R., Grant, K.W., Cramer, S.D., Thorburn, A. (2005) Selective inactivation of a Fas-associated death domain protein (FADD)-dependent apoptosis and autophagy pathway in immortal epithelial cells. Mol. Biol. Cell 16:1189–1199.

Tothova J., Blaauw B., Pallafacchina G., Rudolf R., Argentini C., Reggiani C. and Schiaffino S. (2006). NFATc1 nucleocytoplasmic shuttling is controlled by nerve activity in skeletal muscle, J. Cell Sci. 119: 1604–1611

Waddell, D. S., Baehr, L. M., van den Brandt, J., Johnsen, S. A., Reichardt, H. M., Furlow, J. D., and Bodine, S. C. (2008b). The glucocorticoid receptor and FOXO1 synergistically activate the skeletal muscle atrophy-associated MuRF1 gene. Am J Physiol Endocrinol Metab 295, E785-797.

Wang, X., Blagden, C., Fan, J., Nowak, S.J., Taniuchi, I., Littman, D.R., and Burden, S.J. (2005). Runx1 prevents wasting, myofibrillar disorganization, and autophagy of skeletal muscle. Genes Dev. 19, 1715–1722.

Webb JL, Ravikumar B, Atkins J, Skepper JN, Rubinsztein DC. (2003) Alpha-synuclein is degraded by both autophagy and the proteasome. J. Biol. Chem. 278, 25009–25013.

Williamson, D. L., Kimball, S. R., and Jefferson, L. S. (2005). Acute treatment with TNF-alpha attenuates insulin-stimulated protein synthesis in cultures of C2C12 myotubes through a MEK1-sensitive mechanism. Am J Physiol Endocrinol Metab 289, E95-104.

Xiong, Y., Contento, A.L., Nguyen, P.Q., Bassham, D.C. (2007b). Degradation of oxidized proteins by autophagy during oxidative stress in Arabidopsis. Plant Physiol. 143:291–299.

Yamada Y, Suzuki NN , Hanada T, Ichimura Y, Kumeta H, Fujioka Y, Ohsumi Y , Inagaki F (2007) The crystal structure of Atg3, an autophagy-related ubiquitin carrier protein (E2) enzyme that mediates Atg8 lipidation. J Biol Chem 282: 8036–8043.

Yamamoto, A., Cremona, M.L., and Rothman, J.E. (2006). Autophagymediated clearance of huntingtin aggregates triggered by the insulinsignaling pathway. J. Cell Biol. 172, 719–731.

Yoshimoto, K., Hanaoka, H., Sato, S., Kato, T., Tabata, S., Noda, T., Ohsumi, Y.(2004) Processing of ATG8s, ubiquitin-like proteins, and their deconjugation by ATG4s are essential for plant autophagy. Plant Cell 16:2967–2983.

Young, A.R., Chan, E.Y., Hu, X.W., Kochl, R., Crawshaw, S.G., High, S., Hailey, D.W., Lippincott-Schwartz, J., Tooze, S.A. (2006). Starvation and ULK1-dependent cycling of mammalian Atg9 between the TGN and endosomes, J. Cell Sci. 119 3888–3900.

Yu WH, Cuervo AM, Kumar A, Peterhoff CM, Schmidt SD, Lee JH, Mohan PS, Mercken M, Farmery MR, Tjernberg LO, Jiang Y, Duff K, Uchiyama Y, Naslund J, Mathews PM, Cataldo AM, Nixon RA. (2005). Macroautophagy—a novel β-amyloid peptide-generating pathway activated in Alzheimer's disease. J Cell Biol; 171:87-98.

Zhao, J., Brault, J.J., Schild, A., Cao, P., Sandri, M., Schiaffino, S., Lecker, S.H., and Goldberg, A.L. (2007). FoxO3 coordinately activates protein degradation by the autophagic/lysosomal and proteasomal pathways in atrophying muscle cells. Cell Metab. 6,